FUNCTIONAL AND POSITIONAL CANDIDATE GENE STUDIES OF LATE-ONSET ALZHEIMER'S DISEASE

By

Denise Harold

Thesis submitted in fulfilment of the requirements for the degree of Doctor of Philosophy

Department of Psychological Medicine
School of Medicine
Cardiff University

2004

ProQuest LLC
789 East Eisenhower Parkway
P.O. Box 1346
Ann Arbor, MI 48106-1346

For Graham

TABLE OF CONTENTS

ACKNOWLEDGEMENTS

First and foremost I would like to thank my two supervisors, Dr. Malcolm Liddell and Prof. Mike Owen for giving me the opportunity to do a PhD in the department. Your help and support has always been very much appreciated. I would also like to thank Dr. Lesley Jones, Prof. Julie Williams and Prof. Mick O'Donovan for all their advice in Monday morning meetings. For helping to clarify the mud that is statistics, thank you to Valentina Moskvina. Thanks to Tim Peirce for all of his work on *CHAT*. Thanks also to the Alzheimer's team, particularly Dragana Turic, Luke Jehu and Melanie Dunstan for contributing to the work here, but also just for being nice people! Cheers to all members of Psych Med past and present. For providing me with a distraction from the dreaded thesis I have to thank my friends and family. Hopefully I'll actually get to see them now. Last but not least, thanks to Thom Yorke and the lads, for their music to write theses by.

ABBREVIATIONS

A	adenine
aa	amino acid
Aβ	amyloid-β
ACh	acetylcholine
AChE	acetylcholinesterase
ACN	acetonitrile
AD	Alzheimer's disease
ADAM	a disintegrin and metalloprotease
AICD	amyloid precursor protein intracellular domain
ALOX5	5-lipoxygenase
ApoE	apolipoprotein E
APP	amyloid precursor protein
ASP	affected sibling pair
A2M	α2-macroglobulin
BLAST	basic local alignment search tool
bp	base pair
C	cytosine
CAMDEX	Cambridge mental disorders of the elderly examination
CCD	charge-couple device
CDAD	clinically diagnosed Alzheimer's disease patient group
cDNA	complementary DNA
CERAD	consortium to establish a registry for Alzheimer's disease
ChAT	choline acetyltransferase
cM	centimorgan
°C	degrees Celsius
ddH_2O	distilled deionised water
del	deletion
DHPLC	denaturing high performance liquid chromatography
DKK1	dickkopf homologue 1
DNA	deoxyribonucleic acid
DNAJC12	DnaJ homologue, subfamily C, member 12
dNTP	deoxynucleotide triphosphate
EDTA	ethylenediaminetetraacetic acid
EOAD	early onset Alzheimer's disease
ER	endoplasmic reticulum
Exo	exonuclease I
g	gram
G	guanine
het	heterozygote
indel	insertion/deletion
ins	insertion
kDa	kilodalton
LD	linkage disequilibrium
LOAD	late onset Alzheimer's disease
LRP	low-density lipoprotein receptor related protein
Mb	megabase pairs
MCI	mild cognitive impairment
mg	milligram

$MgCl_2$	magnesium chloride
min	minute
µl	microlitre
µM	micromolar
ml	millilitre
MLS	multipoint LOD score
mM	millimolar
MMSE	mini mental state examination
Mr	relative molecular mass
MRC	medical research council
mRNA	messenger ribonucleic acid
M	molar
nb	nucleus basalis
NCBI	national center for biotechnology information
NFT	neurofibrillary tangle
ng	nanogram
NICD	notch intracellular domain
NINCDS- ADRDA	national institute of neurological and communicative disorders and stroke and the Alzheimer's disease and related disorders association
nm	nanometre
NSAID	non-steroidal anti-inflammatory drug
PCR	polymerase chain reaction
PHF	paired helical filament
PMAD	post-mortem confirmed Alzheimer's disease patient group
PS	presenilin
RFLP	restriction fragment length polymorphism
rpm	revolutions per minute
RT	reverse transcription
s	second
SAP	shrimp alkaline phosphatase
SD	standard deviation
SEC24C	SEC24 related gene family, member C
SGPL1	sphingosine-1-phosphate lyase 1
SIRT1	silent mating type information regulation 2 homologue 1
SLC18A3	solute carrier family 18, member 3
SNP	single nucleotide polymorphism
SP	senile plaque
T	thymine
TBE	tris-borate EDTA
TEAA	triethylammonium acetate
U	unit
UBE2D1	ubiquitin-conjugating enzyme E2D 1
UK	United Kingdom
UTR	untranslated region
UV	ultraviolet
VAChT	vesicular acetylcholine transporter
VNTR	variable number of tandem repeats
w/v	weight per volume

SUMMARY

Alzheimer's disease is a neurodegenerative disorder characterised by progressive memory impairment, a decline in language function and a variety of behavioural symptoms. The majority of AD cases have an age at onset above 65 years and exhibit no clear pattern of inheritance. The only known genetic risk factor for this late onset AD, LOAD, is the ε4 allele of the apolipoprotein E gene on chromosome 19. There is significant evidence of linkage to LOAD on chromosome 10q21-23. Therefore, nine candidate genes that map to this region were examined as susceptibility loci for the disease. In addition, a purely functional candidate, ADAM12, was examined on the basis of its homology to α-secretase enzymes. 58,752 base pairs of genomic sequence were screened by DHPLC, covering all exons, intron-exon boundaries and putative promoter regions, and 89 polymorphisms were detected. An additional 25 SNPs were identified from a SNP database. A two-stage strategy was employed. Variants were initially tested for association with LOAD by genotyping them in a small case-control sample, either in DNA pools or individually. Polymorphisms showing a significant difference between cases and controls were carried forward to the second stage and individually genotyped in a larger sample. A number of SNPs initially gave a positive result but after individual genotyping in a larger sample only 2 SNPs in the ADAM12 gene showed evidence for association with LOAD. As a large number of polymorphisms were examined, this may be a false positive finding, but this gene certainly warrants further investigation.

1. INTRODUCTION

"Shame on the soul, to falter on the road of life while the body still endures."
Marcus Aurelius, Meditations, 2nd Century AD

"Old age is no place for sissies."
Bette Davis, 1908-1989

1.1 History

At a meeting in Munich in 1906, the German neurologist Alois Alzheimer described to his colleagues the case of housewife Auguste D. and her "peculiar disease of the cerebral cortex" (translated in Wilkins & Brody, 1969[1]). Alzheimer had observed the Frau from her initial hospitalisation at age 51, until her death four and a half years later. She had an impaired memory, was disoriented in time and place, suffered from persecutory delusions and auditory hallucinations and displayed language abnormalities. At autopsy, a generally atrophic brain without macroscopic lesions was observed. Microscopic study revealed cortical cell loss, neurofibrillary tangles and neuritic plaques throughout the cortex. Alzheimer's description was accepted as a 'new' disorder and was named Alzheimer's disease (AD) in 1910 by Emil Kraepelin. This term was initially restricted to rare cases of 'presenile dementia', such as that of Auguste D., with onset occurring before the age of 65. It became apparent after the work of Blessed and colleagues[2] however, that the 'presenile dementia' was pathologically and symptomatologically identical to the late-onset form of the disease (age at onset >65 years) that we are unfortunately so familiar with today.

1.2 Symptoms of AD

1.2.1 Cognitive Symptoms

Memory impairment is the classical presenting symptom for AD. Patients forget such things as names, appointments, conversations and places. They have trouble paying attention, they lose their way, they misplace objects like car keys, or the car itself. All of these problems of recent memory (the ability to encode new information and store it for later recall) get progressively worse and lead to disorientation in time and space. The retrieval of old remote memories is relatively preserved in the early stages, but as the disease advances these memories too are progressively lost in a reverse chronological fashion, such that the patient seems to live in the ever more distant past. Accompanying the losses in memories of personal events (episodic memory), there are also losses in semantic memory (facts and vocabulary) and visuospatial memory (remembering pictures or faces).

The earliest deficits in language production present as word-finding difficulties, which progress to poor naming of objects (anomia). Initially patients can compensate for this problem using circumlocution (literally 'talking around it'). For example, Auguste D., unable to name a cup, referred to it as a 'milk-pourer'. Word-list generation (*e.g.* listing animals that begin with the letter 'A') is impaired, as is comprehension of others' speech. Expression of language shows syntactical errors and simplification of sentence structure. Verbal paraphasias (substituting a meaning-related word for the intended one) occur and become progressively less related to the target word as the disease advances. Speech production may remain fluent but progressively makes less sense (fluent aphasia). In late AD, incomplete sentences and rambling patterns replace coherent speech. Reiterative speech disturbances can

occur such as the tendency to repeat the words of others (echolalia), the tendency to repeat one's own words (palilalia) and the repetition of the final syllable of a word (logoclonia). Eventually, mutism may occur.

Agnosia is the failure to correctly interpret a sensory input in the presence of an intact sensory system. AD patients commonly develop visual agnosia, whereby they can see an object but can't recognise it or identify it incorrectly. For example, a patient may mistake a toothbrush for a hairbrush and attempt to use it accordingly. A particularly distressing form of agnosia is prosapagnosia, where the patient fails to recognise familiar faces. Some individuals also develop 'mirror sign' and fail to recognise their own mirror image.

Visuospatial awareness is impaired early in AD. Patients get lost easily in unfamiliar surroundings, lose their way while driving, and eventually become disorientated in their own homes. Impaired spatial awareness is exemplified by clock drawing tasks, which are particularly sensitive to disruption in AD (see Figure 1.1).

Apraxia is the inability to carry out learned motor acts despite intact motor and sensory systems. AD patients commonly develop ideomotor apraxia and ideational apraxia. Ideomotor apraxia is a disturbance of voluntary movement in which a person cannot translate an idea or thought into the performance of simple motor acts. Ideational apraxia is a disturbance of voluntary movement in which a person misuses objects because he/she has difficulty identifying the concept or purpose behind those objects. Apraxia reduces the ability of the patient to perform many activities of daily living such as getting dressed or cooking a meal.

Subtle frontal-executive impairments occur early in AD and lead to difficulties in planning, problem solving, abstractions, judgement and reasoning.

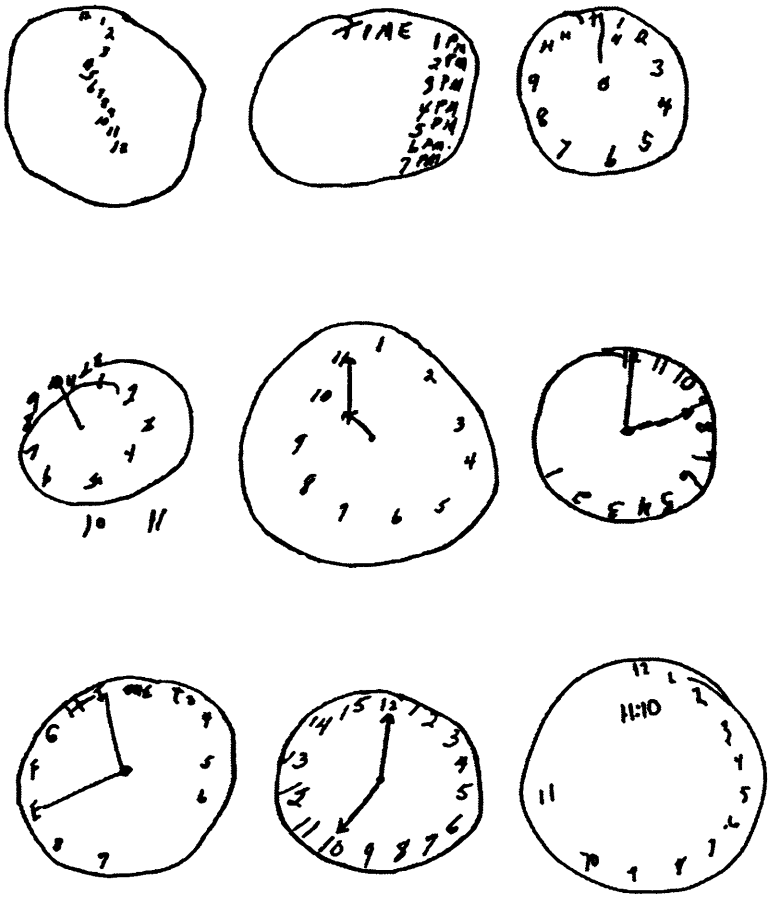

Figure 1.1 Abnormal clock drawings in AD patients. The task is to draw the face of a numbered clock and to indicate the hands at ten minutes past eleven. Taken from Mendez Ashla, 2000[3].

1.2.2 Non-Cognitive Symptoms

As indicated in the case of Auguste D., delusions and hallucinations can be a feature of AD. The delusions of AD patients are understandable as an attempt to comprehend their situation, and are remarkably similar between individuals. Delusions are generally paranoid in nature; patients suspect that objects have been stolen, that they are being imprisoned, that an intruder has been in the house or that

the caregiver is an impostor. Hallucinations are less common than delusions and are more likely to be visual than auditory in nature. Common hallucinations include dead relatives coming to visit.

Apathy is apparent early in the clinical course with diminished interest and reduced concern. Agitation becomes increasingly common as the illness advances and is a frequent precipitant of nursing home placement. Other behavioural symptoms include aggression, anxiety, depression, insomnia, and wandering.

Physical symptoms tend to occur late in the disease. Non-specific changes occur in both gait and balance and myoclonic jerks and other seizures may develop. Loss of sphincter control is a frequent accompaniment of dementia and urinary incontinence is found in the majority of cases of severe AD. Weight loss is also pronounced and may be an intrinsic feature of the disease process or secondary to the progressive impairments, which can result in an inadequate consumption of food and fluids.

There is currently thought to be a transitional state between normal ageing and AD, termed mild cognitive impairment (MCI). MCI is defined as impairment in memory only, with other cognitive functions spared. Approximately 15% of patients with MCI will progress to AD within a year, or up to 70% in 4-5 years[4, 5], compared to a 1-2% conversion rate in age-matched normal controls[6]. The mean survival after symptom onset for AD is 10.3 years but may range from 2 to more than 20 years[7]. Most patients evolve through several typical stages and these are summarised in Table 1.1. The most common causes of death are aspiration pneumonia and sepsis associated with urinary tract infections or infection of decubitus ulcers.

Table 1.1 Principal clinical findings in each stage of Alzheimer's disease (adapted from Mendez and Cummings, 2003[8]).

Preclinical Stage I: 1-3 years
Memory: new learning defective, remote recall mildly impaired
Perception: topographic disorientation, poor complex constructions
Language: poor word-list generation, mild anomia, empty circumloculatory speech
Behaviour: indifference, occasional irritability, sadness or delusions

Stage II: 2-10 years
Memory: recent and remote recall more severely impaired
Perception: poor constructions, spatial disorientation, and visual agnosia
Language: fluent aphasia, anomia, paraphasia, poor comprehension
Other cognitive: apraxia and acalculia
Behavioural: indifference or irritability, sadness and delusions in some
Motor system: restlessness, pacing

Stage III: 8-12 years
Cognitive functions: severely deteriorated
Speech: echolalia, palilalia, logoclonia, dysarthria, terminal mutism
Motor: limb rigidity, flexion posture, urinary and faecal incontinence

1.3 Neuropathology of AD

1.3.1 Senile Plaques and Neurofibrillary Tangles

The neuropathological hallmarks of AD are senile plaques (SPs) and neurofibrillary tangles (NFTs). It is not the presence of SPs and NFTs that is indicative of disease, for both are found in the brains of healthy, aged individuals. Rather it is the density of these lesions, particularly in the limbic and association cortices, that signifies disease.

Senile plaques consist of extracellular deposits of β-amyloid (Aβ) peptides, proteolytic derivatives of the amyloid precursor protein (APP). When these plaques are associated with swollen, distorted neuronal processes, they are called neuritic plaques. Two species of fibrillar Aβ, 40 and 42 amino acids long ($A\beta_{40}$ and $A\beta_{42}$ respectively), are found in neuritic plaques. The slightly more hydrophobic form,

$A\beta_{42}$, is particularly prone to aggregation[9]. The neurites often contain paired helical filaments (indistinguishable to those of NFTs), normal glial processes and abnormal organelles. Microglia are found within and adjacent to the central amyloid core and astrocytes are found at the plaque periphery. In addition to amyloid fibrils, neuritic plaques include α2-macroglobulin (A2M), α1-antichymotrypsin, apolipoprotein E (ApoE) and low-density lipoprotein receptor related protein (LRP) among other components. The morphology of a neuritic plaque is shown in Figure 1.2A.

Only a subset of all Aβ deposits in the AD brain is associated with neuritic plaques. Many of the plaques found in limbic and association cortices and almost all of those found in areas of the brain not typically associated with AD, do not have a fibrillar, compacted centre, nor are they associated with neuritic dystrophy or glial changes. These diffuse plaques are comprised primarily of $A\beta_{42}$, with little or no $A\beta_{40}$ and are believed to represent immature lesions that are precursors to neuritic plaques. Lending support to this theory is the fact that often only diffuse plaques are found in limbic and association cortices of healthy, aged brains. In addition, patients with Down's syndrome often display diffuse deposits as early as their teenage years but do not show neuritic plaques until some two decades later, a time at which they first display abundant neurofibrillary tangles in limbic and association cortices[10].

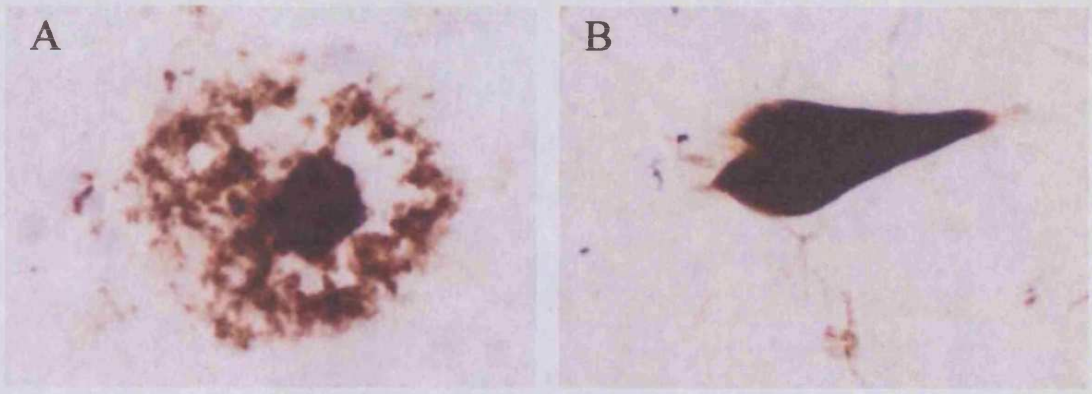

Figure 1.2 Morphology of neuritic plaques and neurofibrillary tangles. A. Neuritic plaque (labelled with a monoclonal antibody for human amyloid peptide using diaminobenzidine combined with haematoxylin counterstain, ×2500 magnification). B. Neurofibrillary tangle (Gallyas stain, ×2500 magnification). Taken from Cummings and Cole, 2002[11].

Neurofibrillary tangles are relatively insoluble, intracellular aggregates composed of paired helical filaments (PHFs) that occupy the cell body and may extend into the dendrites but do not occur in the axon. PHFs consist of protofilaments arranged to form a tubule and contain abnormally phosphorylated microtubule-associated τ protein. Phosphate groups are attached and removed from τ in a dynamic process that regulates the ability of the protein to facilitate the assembly and stabilisation of microtubules. In AD, the τ protein accumulates an excess number of phosphate groups and becomes dysfunctional, dissociating from the microtubule and resulting in the destabilisation and disrupted assembly of this important cytoskeletal component of the intracellular transport system[12, 13]. Neurofibrillary tangles lead to the death of the nerve cells in which they occur (although nerve cell death also occurs in regions with few tangles). These lesions are not unique to AD and occur in other neurodegenerative disorders, including the frontotemporal dementias, corticobasal degeneration, progressive supranuclear palsy and dementia pugilistica; as previously mentioned, a small number are also found in normal ageing.

SPs and NFTs are regionally specific, occurring predominantly in the hippocampus, entorhinal cortex, and association areas of the neocortex (see Figure 1.3). The cognitive phenotype of AD reflects the location of these lesions. Hippocampal dysfunction has been related to the memory impairment suffered by patients with AD. Dysfunction of the left posterior association cortex produces fluent aphasia and involvement of the right posterior association cortex leads to the visuospatial dysfunction typical of patients with AD[14].

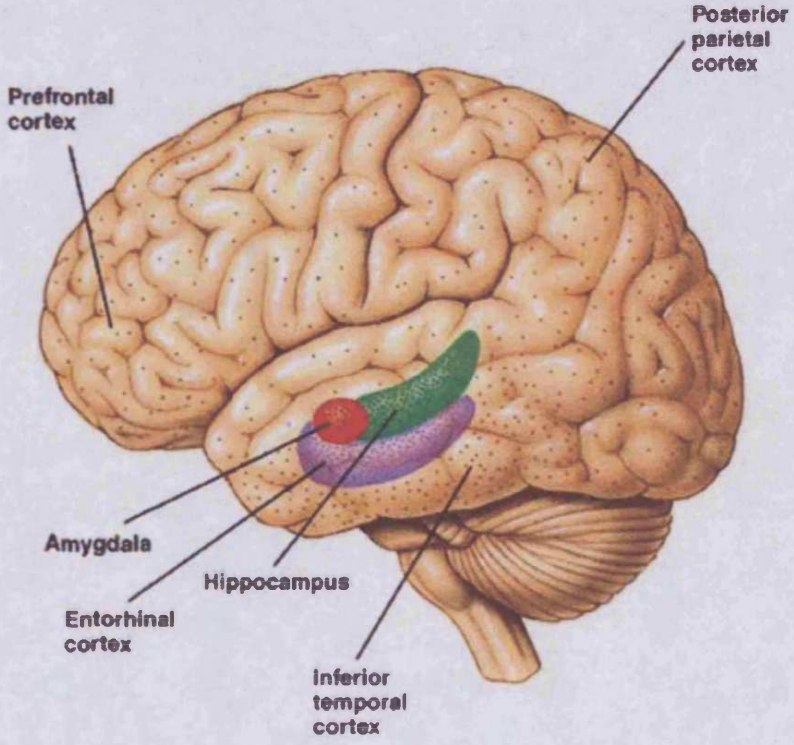

Figure 1.3 Distribution of senile plaques and neurofibrillary tangles in the brain. The larger the number of dots and the closer they are to each other, indicates how heavily an area is affected by plaques and tangles. Taken from http://www.driesen.com.

1.3.2 Other Neuropathological Hallmarks of AD

In addition to plaques and tangles, granulovacuolar degeneration and amyloid angiopathy are evident in the brains of AD patients. Granulovacuolar degeneration is highly selective for the pyramidal neurons of the hippocampus. Vacuoles are present in the cytoplasm of these cells, with each vacuole containing a single dense granule. Several vacuoles may occur within the same cell body. Amyloid angiopathy refers to the deposition of fibrillar amyloid in small arterioles, venules and capillaries within the cerebral cortex. The amyloid appears to principally be the $A\beta_{40}$ species[15].

There is significant neuronal loss in AD. Degeneration of the basal forebrain cholinergic system is a classic feature of AD and has been correlated with the depth of dementia, at least in late stages of the disease (further discussed in Chapter 3). In addition, neuronal loss or atrophy in the locus ceruleus and raphe nuclei of the brainstem leads to deficits in noradrenergic and serotonergic transmitters respectively[16].

1.4 Diagnosis of AD

The diagnosis of AD has been standardised with criteria developed by the Work Group of the National Institute of Neurologic and Communicative Disorders and Stroke and the Alzheimer's Disease and Associated Disorders Association (NINCDS-ADRDA)[17]. These criteria (listed in Table 1.2) have three levels of certainty for an AD diagnosis: definite AD, probable AD, and possible AD. Criteria for probable AD require the gradual onset and progression of deficits in memory and at least one other area of cognition in an alert patient when other disorders that might account for dementia are absent. The probable AD diagnosis requires basic cognitive

testing, *e.g.* the Mini-Mental State Examination (MMSE)[18] to demonstrate the deficits and some confirmation of these by other neuropsychological tests. Criteria for possible AD allow for variations in the onset, presentation, or course of AD and for the presence of another potentially dementing disorder that is believed not to be primarily responsible for the dementia. The definitive diagnosis of AD requires examination of the brain and demonstration of more neurofibrillary tangles and neuritic plaques, particularly in the cerebral cortex, than expected for the patient's age. The use of NINCDS-ADRDA clinical criteria yields greater than 90% sensitivity in diagnosing AD, but a less than 70% accuracy rate in the specific diagnosis of AD indicates that these criteria do not fare so well in excluding other pathologies that might be contributing to the syndrome of dementia[19].

Table 1.2 NINCDS-ADRDA criteria (taken from McKhann *et al.*, 1984[17]).

I. The criteria for the clinical diagnosis of PROBABLE AD include:
• Dementia established by clinical examination and documented by the Mini-Mental Test, Blessed Dementia Scale, or some similar examination, and confirmed by neuropsychological tests;
• Deficits in two or more areas of cognition;
• Progressive worsening of memory and other cognitive functions;
• No disturbance of consciousness;
• Onset between ages 40 and 90, most often after age 65;
• Absence of systemic disorders or other brain diseases that in and of themselves could account for the progressive deficits in memory and cognition

II. The diagnosis of PROBABLE AD is supported by:
• Progressive deterioration of specific cognitive functions such as language (aphasia), motor skills (apraxia), and perception (agnosia);
• Impaired activities of daily living and altered patterns of behaviour;
• Family history of similar disorders, particularly if confirmed neuropathologically;
• Laboratory results of:
– normal lumbar puncture as evaluated by standard techniques;
– normal pattern or non-specific changes in EEG such as increased slow-wave activity;
– evidence of cerebral atrophy on CT with progression documented by serial observation

III. Other clinical features consistent with the diagnosis of PROBABLE AD, after exclusion of causes of dementia other than AD, include:
• Plateaus in the course of progression of the illness;
• Associated symptoms of depression, insomnia, incontinence, delusions, illusions, hallucinations, catastrophic verbal, emotional, or physical outbursts, sexual disorders, and weight loss;
• Other neurologic abnormalities in some patients, especially with more advanced disease and including motor signs such as increased muscle tone, myoclonus, or gait disorder;
• Seizures in advanced disease;
• CT normal for age

IV. Features that make the diagnosis of PROBABLE AD uncertain or unlikely include:
• Sudden, apoplectic onset;
• Focal neurologic findings such as hemiparesis, sensory loss, visual field deficits, and incoordination early in the course of the illness;
• Seizures or gait disturbances at the onset or very early in the course of the illness

V. Clinical diagnosis of POSSIBLE AD:
• May be made on the basis of the dementia syndrome, in the absence of other neurologic, psychiatric, or systemic disorders sufficient to cause dementia, and in the presence of variations in the onset, in the presentation, or in the clinical course;
• May be made in the presence of a second systemic or brain disorder sufficient to produce dementia, which is not considered to be *the* cause of the dementia;
• Should be used in research studies when a single, gradually progressive severe cognitive deficit is identified in the absence of other identifiable cause

VI. Criteria for diagnosis of DEFINITE AD are:
• The clinical criteria for probable AD and
• Histopathologic evidence obtained from a biopsy or autopsy

1.5 Prevalence of Dementia

The Alzheimer's Society estimates that over 750,000 people in the UK suffer from dementia (41,800 in Wales). It is estimated that by 2010 there will be approximately 840,000 people with dementia in the UK and this is expected to rise to over 1.5 million people by 2050. As AD accounts for 55% of all dementia, we can expect this disease to place a huge burden on society, in terms of both care and cost.

1.6 Risk Factors

A risk factor can be defined as any environmental exposure, personal characteristic, or event that affects the probability of developing a given condition, and may have causal implications. The most powerful risk factor for AD is advancing age. Lobo *et al.* (2000)[20] pooled data from eleven European population-based studies, comparing the age- and sex-specific prevalence of AD. The age-standardised prevalence of AD was 4.4% in individuals aged 65 years or more, but the prevalence increases almost exponentially with increasing age (see Table 1.3).

Table 1.3 Prevalence rates (%) for AD estimated from a pooling of data from European studies by Lobo *et al.* (2000)[20]

Age group	Males	Females
65-69	0.6	0.7
70-74	1.5	2.3
75-79	1.8	4.3
80-84	6.3	8.4
85-89	8.8	14.2
90+	17.6	23.6

As indicated by Table 1.3, AD is more prevalent in women than men. In fact, AD affects women almost 1.5 times as often as men and remains more common in women even after adjusting for greater longevity among women and shorter disease survival among men[21, 22].

Several studies have found that previous head injury is a risk factor for AD. A meta-analysis of early case-control studies found that a history of head trauma with loss of consciousness was 80% more common in Alzheimer's disease cases than in normal controls[23].

A low level of education has been associated with a higher incidence of dementia or AD[24]. Although this could be confounded by factors such as impaired nutrition, increased years of education may reflect greater cognitive capacity and consequently more cerebral reserve. The results of the 'Nun Study' by Snowdon and colleagues[25] highlighted the possible influence of cerebral reserve on the emergence of AD. This study assessed the verbal ability of a group of elderly nuns by analysing the autobiographies they had written as young adults. On examination of their brains *post mortem*, it was discovered that all those with confirmed Alzheimer's disease had low verbal ability.

Epidemiological retrospective studies have been conducted to determine the risk of developing AD among patients receiving anti-inflammatory drugs. A meta-analysis of observational studies examining the role of non-steroidal anti-inflammatory drug (NSAID) use in preventing AD, determined that the pooled relative risk of Alzheimer's disease among users of NSAIDs was 0.72. The risk was 0.95 among short-term users (< 1 month), 0.83 among intermediate-term users (mostly < 24 months) and 0.27 among long-term users (mostly > 24 months)[26]. The effect of NSAIDs may be mediated through their impact on inflammatory processes that occur in neuritic plaques.

Another class of drugs reported to have a protective effect against AD are the cholesterol-lowering HMG-CoA reductase inhibitors, also termed statins. Two retrospective clinical studies have indicated that the risk of developing AD is approximately 70% lower in patients taking statins[27, 28].

Genetic factors have significant involvement in AD and these will be discussed in detail in the following sections.

1.7 Heritability of AD

There is considerable evidence that familial factors play an important role in the aetiology of AD. For example, it has long been known that there is a markedly increased cumulative risk of dementia among first-degree relatives of individuals with AD. In a re-analysis of seven case-control studies, first-degree relatives of AD patients had a 3.5-fold increase in risk for developing AD[29]. This relative risk decreased with increasing age at onset of the proband, but even by age 80 years a statistically significant 2.6-fold increase in risk for first-degree relatives was observed.

That a disease shows familial aggregation however, does not necessarily mean that it has a genetic component; the higher incidence of the disorder may simply be the result of shared family environment. Twin studies are commonly undertaken to distinguish between the effects of genetic and environmental factors, based on the differences in concordance rates observed between monozygotic (MZ) and dizygotic (DZ) twins. A number of AD twin studies have been performed in the past. A study summarising the data of three twin studies showed concordance rates of 80% in

monozygotic twin pairs and 35% in dizygotic twins, resulting in a heritability estimate of 0.84[30].

1.8 Molecular Genetics of AD

AD has been traditionally divided into late-onset cases (LOAD), with an age at onset greater than 60-65 years and early-onset cases (EOAD), with age at onset below this cut-off. A small proportion of the already uncommon early-onset cases appear to segregate in an autosomal dominant manner. In a population-based study in the city of Rouen, Campion *et al.* (1999)[31] calculated the prevalence of EOAD to be 41.2 per 100,000 individuals at risk and the prevalence of autosomal dominant EOAD to be 5.3 per 100,000 individuals at risk (12.9% of EOAD). The inheritance pattern of the more common late-onset form of the disease, which accounts for more than 95% of all AD cases[32], appears to be much more complex.

Numerous studies have been conducted in an attempt to uncover the pathogenic mutations and susceptibility alleles involved in AD, but before describing them, an introduction to current disease gene discovery techniques is apt.

1.8.1 Disease Gene Discovery Methods

1.8.1.1 Linkage Analysis

Typically, the starting point in determining the genetic factors involved in a disease has been linkage analysis, which tests for cosegregation of a genetic marker and disease phenotype within many independent families or over many generations in an extended pedigree. In this way markers that are physically linked to the disease locus are identified in chromosomal segments common to all the affected members

of a family. Of course, issues such as diagnostic misclassification and locus heterogeneity will reduce the power of a study to detect linkage.

Classic linkage analysis, which involves the specification of a genetic model, is a powerful method for detecting loci segregating in a Mendelian fashion. However for complex diseases, where the mode of transmission is unknown, non-parametric linkage analysis is more appropriate (although less powerful). While the former method follows the cosegregation of markers and disease over a number of generations in large, multiplex families, the latter method examines allele sharing in affected relatives, usually affected sib-pairs.

Chromosomal abnormalities that have been associated with the disease may target a study to a particular chromosome, but otherwise linkage is usually performed on a genome-wide scale. Such screens typically employ 300-600 microsatellite markers (corresponding to marker-to-marker intervals of 10 cM and 5 cM, respectively). Samples should be of sufficient size to detect the expected effect size, although in reality prohibitively large samples may be required to detect small effects[33]. As such, most linkage studies are only capable of detecting loci with moderate to large effects.

The data obtained from a linkage study can be assessed according to standards devised by Lander and Kruglyak[34], who proposed guidelines for identifying results that are statistically significant as well as those that warrant further investigation despite not reaching formal statistical significance. While achieving a 'significant' result according to these guidelines is grounds for proceeding to examine the linked

region, a region showing 'suggestive linkage' should first be replicated prior to examination.

1.8.1.2 Association Studies

Once a critical region has been identified by linkage, it is necessary to identify the variant in the region that causes or increases susceptibility to the disease in question. A popular method used to attempt this is the association study, which simply looks for a significant difference in marker allele frequencies between a group of disease afflicted cases and unaffected controls. Disease-marker association can be explained by two genetic mechanisms: direct association, and indirect association due to linkage disequilibrium (LD). In direct association, the marker allele itself is functionally involved in the disease risk. Linkage disequilibrium stems from a marker locus sufficiently close to the disease locus that association of the two loci has not yet been eroded in the population by recombination. A marker allele may also appear to be associated with a disease if cases and controls are not ethnically comparable. In such a situation, differences in allele frequency will emerge at all loci that differentiate these groups whether the alleles are causally related to disease or not. It is therefore vital to ensure cases and controls are well matched for ethnicity (and indeed other possible confounding factors). One strategy that has been employed is the use of unaffected family members as controls, such as parents or siblings. However, parents may not be available for late-onset diseases such as LOAD and using siblings results in a loss of power, as they are over-matched to the cases. Therefore, using well chosen unrelated controls may be the best option. Another issue regarding study design is sample size. Fortunately, association studies

have more power to detect small effect sizes compared with linkage and so appropriate sample sizes are more attainable[33].

The critical region identified by a linkage study is usually tens of megabase pairs long and likely to contain large numbers of genes and sequence variants. The task therefore of identifying the causal variant is no small feat. Depending on how much is known about the pathogenesis of the disease, there may be a glaringly obvious candidate gene (or genes), in which case it may be pertinent to initially examine variants in these genes. Alternatively, a more systematic LD mapping approach may be taken, whereby a number of evenly spaced markers across the critical region are tested for association with the disease. The polymorphic markers to be genotyped in either strategy may need to be detected experimentally, or as is increasingly the case, previously identified markers may already be described in polymorphism databases such as dbSNP (http://www.ncbi.nlm.nih.gov/SNP/index.html). The labour and cost involved in genotyping large numbers of markers can be reduced by DNA pooling, so that allele frequencies are compared in a small number of pools rather than a large number of individuals. This has the added advantage of using less DNA than typing individuals, thereby elongating the life of the sample.

1.8.2 Discovery of Genes Involved in AD

The methods described above have been successfully used to identify four genes involved in the pathogenesis of AD. Mutations in three of these appear to individually cause the rare, autosomal dominant form of the disease. A common variant in the fourth gene acts as a susceptibility factor for the late-onset form of the disease, as well as reducing age at onset in both early and late forms.

1.8.2.1 Amyloid Precursor Protein

Middle-aged individuals with Down Syndrome (trisomy 21) commonly develop the clinical features of AD and invariably present with the neuropathological hallmarks of the disease at autopsy[35, 36]. This provided a good indicator for the presence of an AD gene on chromosome 21. Indeed, the first positive AD genetic linkage was discovered between a locus on chromosome 21q and autosomal dominant EOAD[37]. In subsequent analyses, some families with autosomal dominant EOAD failed to show linkage to chromosome 21 markers which cast doubt on the initial positive linkage finding. As we now know, locus heterogeneity exists within autosomal dominant EOAD and Goate and colleagues (1991)[38] went on to discover a point mutation in the amyloid precursor protein (*APP*) gene in a family showing linkage on chromosome 21. Since then, a number of pathogenic mutations have been identified in autosomal dominant EOAD families: there are currently 16 *APP* mutations listed in the Alzheimer Disease & Frontotemporal Dementia Mutation Database (http://www.molgen.ua.ac.be/ADMutations/default.cfm).

1.8.2.2 Presenilins

As it was evident that *APP* mutations did not account for all cases of autosomal dominant EOAD, the search for further pathogenic loci continued. In 1992 a locus on the long arm of chromosome 14 was detected by linkage analysis and a few years later a gene, named *presenilin 1* (*PSEN1*), was identified and isolated by a positional cloning strategy[39, 40]. Similarly, evidence for a locus on chromosome 1q was reported in several kindreds known as the Volga-German families, a group of related kindreds of German-Russian origin with multiple cases of autosomal dominant early-onset AD[41]. Subsequently, the *presenilin 2* gene (*PSEN2*) was identified based on its

homology to *PSEN1*[42, 43]. 136 *PSEN1* pathogenic mutations are listed in the Alzheimer Disease & Frontotemporal Dementia Mutation Database; 10 *PSEN2* pathogenic mutations are listed.

APP and *PSEN1* mutations lead to autosomal dominant AD with early onset (age 45-60) and rapid progression (death in 6-8 years). Mutations in *PSEN2* also produce autosomal dominant AD but with a more variable age at onset[14]. Further autosomal dominant AD cases exist for which a pathogenic mutation has not been identified[44].

1.8.2.3 Apolipoprotein E

Successes in linkage analysis have not been restricted to autosomal dominant EOAD families. Late-onset families have also been examined, leading to the identification of a linkage region for LOAD on chromosome 19[45]. Subsequent studies identified an association between variation at the *apolipoprotein E* (*APOE*) gene on chromosome 19q13.2 with LOAD[46]. There are three major isoforms of apoE: E2, E3 and E4, which differ from each other by one or two amino acids. These isoforms are coded for by alleles ε2, ε3 and ε4 respectively. Numerous studies have consistently found an increased risk of LOAD in carriers of the ε4 allele, whereas the ε2 allele appears to have a protective effect. Warwick Daw and colleagues (2000)[47] have estimated that *APOE* genotype can make a difference of ≤17 years in age at onset of AD, and presence of the ε4 allele is also associated with an earlier expression of clinical symptoms in carriers of specific *APP*[48] or *PSEN1* mutations[49]. It should be stressed however that the ε4 allele is a risk factor for LOAD and is neither necessary nor sufficient to cause the disease.

1.8.3 Pathogenesis of AD

1.8.3.1 APP Processing

The amyloid precursor protein, APP, and related family members amyloid precursor like protein-1 and -2 (APLP-1 and -2) are homologous type I transmembrane proteins[50]. APP is ubiquitously expressed and contains a large extracellular region, a transmembrane domain and a small cytoplasmic tail. Alternative splicing of the *APP* gene on chromosome 21 results in at least eight isoforms of the protein[51], but the predominant isoforms are APP695, APP751 and APP770, containing 695, 751 and 770 amino acids respectively. APP695, the isoform primarily expressed in CNS neurons, differs from APP751 and APP770 in that it lacks a Kunitz proteinase inhibitor (KPI) domain found in the other two isoforms. APP is synthesised in the endoplasmic reticulum and undergoes several post-translational modifications including N-glycosylation, O-glycosylation and tyrosyl-sulphation in the Golgi apparatus. This mature form of APP is transported to the cell surface via the secretory pathway. APP is also endocytosed from the cell surface and processed in the endosomal–lysosomal pathway[52-57].

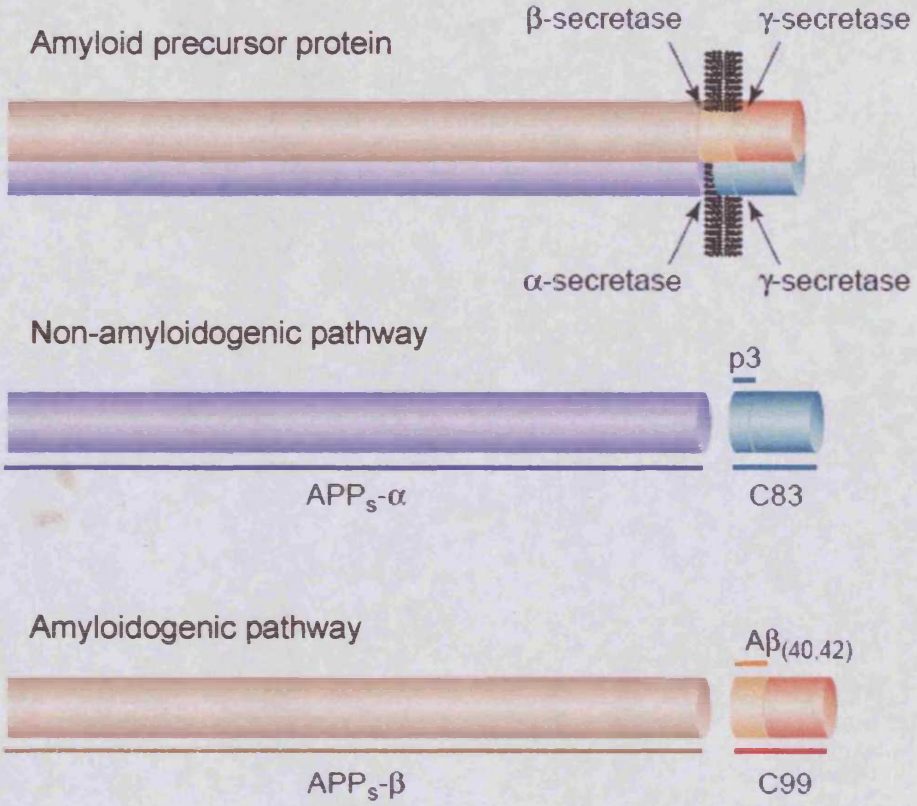

Figure 1.4. Normal processing of APP involves cleavage predominantly by the α-secretase, which cuts APP in the middle of the β-amyloid sequence, thus precluding the formation of Aβ. The C83 fragment is subsequently cleaved by γ-secretase. Alternatively, cleavage of APP by β- and γ-secretase results in the formation of $A\beta_{40}$ or $A\beta_{42}$ depending on the site of γ-secretase cleavage. Adapted from Chapman *et al.*, 2001[58].

APP is processed via two proteolytic pathways involving the secretases α-, β- and γ-secretase and these pathways are illustrated in Figure 1.4. In the 'non-amyloidogenic' pathway, APP is cleaved by α-secretase, which cuts within the Aβ domain and thus precludes Aβ peptide generation. Following the release of the soluble extracellular α-N-terminal fragment (α-APPs), the C-terminal APP fragment (C83) undergoes γ-cleavage, leading to the generation of the p3 peptide. Alternatively, in the amyloidogenic pathway APP is cleaved by β-secretase to generate soluble extracellular β-N-terminal fragment (β-APPs) and the C-terminal APP fragment,

C99. Subsequent cleavage of C99 by γ-secretase results in the formation of the Aβ peptide.

α-Secretase cleavage of APP occurs between residues Lys16 and Leu17 of the Aβ sequence (see Figure 1.5) and is the predominant pathway of APP metabolism in most cells[59]. This occurs in both a constitutive manner and as a result of stimulation by regulatory factors (*e.g.* activation of protein kinase C by phorbol esters is able to upregulate the α-cleavage pathway). The subcellular localisation of α-cleavage is unclear. Immunocytochemical analysis has indicated that α-cleavage occurs within the endoplasmic reticulum and various compartments within the trans-Golgi apparatus[60]. In addition, there is α-secretase activity at the cell membrane[61, 62]. This is possibly due to the presence of distinct enzymes with similar functions. Indeed, three members of the ADAMs family of proteins have been demonstrated to have α-secretase activity. ADAMs are multidomain proteins and some members have been implicated in ectodomain shedding via a metalloprotease domain[63]. Experiments conducted on embryonic fibroblasts derived from mice with a knockout of the TNFα converting enzyme, TACE (also known as ADAM17) show that phorbol esters-mediated release of α-APPs is completely blocked by the loss of the protease[64]. However, constitutive α-secretase activity is not affected by disruption of the *TACE* gene. Similarly, coexpression of ADAM9 with APP in COS cells leads to an increase in production of α-APPs upon phorbol ester treatment of the cells, above that seen in the absence of transfected ADAM9[65]. ADAM10 has been implicated in both the constitutive and protein kinase C-regulated α-secretase pathways[66, 67]. A significant decrease of platelet ADAM10 levels has been observed in AD patients together with a similar decrease in α-APPs in both thrombin-activated platelets and CSF[68].

Moreover, in an AD mouse model that overexpresses mutated human APP (V717I) in neurons and therefore leads to Aβ deposition and memory deficits, overexpression of ADAM10 increased the secretion of α-APPs, reduced the formation of Aβ peptides and alleviated cognitive deficits[69]. Therefore, it is possible that several ADAMs may have partially overlapping α-secretase activities.

The enzyme responsible for β-secretase cleavage has been cloned and is called BACE1, for β-site APP cleaving enzyme[70-74]. BACE1 is a type 1 transmembrane protein, containing two active site motifs with a conserved sequence, similar to aspartyl proteases. Like many proteases, BACE1 is synthesised as a zymogen. After cleavage of a prodomain that maintains the enzyme in a latent form, BACE1 is targeted through the secretory pathway to the plasma membrane and clusters within lipid rafts[75]. APP processing by BACE1 also occurs preferentially within lipid rafts[75]. Like APP, BACE1 can be internalised in endosomes, which may be the preferential site of BACE1 activity due to its acidic pH[76]. Studies in *BACE1* knockout mice provide strong evidence that BACE1 is the major β-secretase in brain. Knockout of the *BACE1* gene completely impairs the β-secretase cleavage of APP and abolishes the generation of Aβ[77]. These mice develop normally and show no phenotypic alterations despite lacking the primary β-secretase activity in brain[78]. BACE1 can cleave APP either at Asp1 of the Aβ sequence or at Glu11 (the β and β' cleavage site respectively) although the functional significance of this heterogeneity is unclear[79]. A homologous enzyme to BACE1 has been identified. BACE2 is 51% identical to BACE1 although it is apparently not significantly (if at all) involved in Aβ generation as it is only expressed at very low levels in the brain[80]. *In vitro* assays with peptide substrates demonstrate that BACE2 can cleave APP at the β-secretase

site[81, 82]. However, it also cleaves between Phe19-Phe20 and Phe20-Ala21 within the Aβ peptide, resulting in increased secretion of α-APPs and P3-like products and reduced production of Aβ species[81].

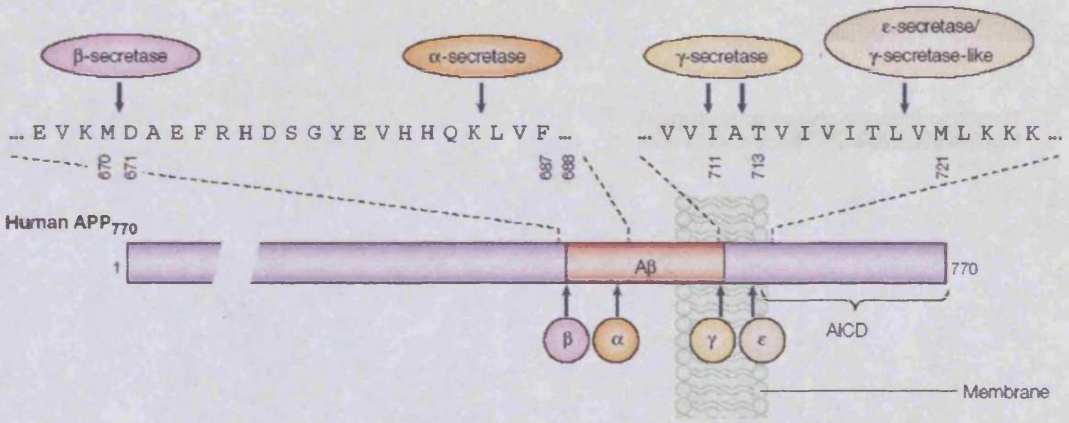

Figure 1.5. Proteolytic cleavage sites in APP. The amino-acid sequences surrounding and within the transmembrane domains of APP are shown together with the sites of cleavage that occur during the processing of the molecule. Adapted from Sisodia & St George-Hyslop, 2002[83].

γ-Secretase is unusual in that it cleaves APP within the membrane bilayer, which was previously thought to be biochemically impossible[84]. It is however reminiscent of the intramembrane proteolysis of Notch, which is cleaved during development in a presenilin-dependent fashion, thereby releasing a fragment (called the Notch intracellular domain; NICD) that activates the transcription of genes involved in cell-fate determination[85, 86].

Presenilin 1 and 2 (PS1 and PS2) are ubiquitously expressed proteins, comprising eight membrane-spanning regions with cytoplasmic orientation for both the N- and C-termini[87, 88]. They share 76% homology, with the area of highest variability being in the N-terminal region and the large cytoplasmic loop between transmembrane domains 6 and 7[43]. Both presenilins undergo endoproteolytic cleavage within this

large loop[89]. The resulting N- and C-terminal fragments remain associated[90] and this association seems to be critical for presenilin function[91]. The presenilins were implicated in γ-secretase function when it was found that a *PS1* knockout severely reduced Aβ generation[92]. When the *PS2* gene was eliminated as well, no Aβ generation was observed at all[93, 94]. Moreover, experiments using several γ-secretase inhibitors have shown that they specifically bind to the presenilin N- or C-terminal fragments and inhibit the γ-secretase activity[95, 96]. The presenilins contain two functionally important aspartate residues within transmembrane domains 6 and 7 that appear to be necessary for normal γ-secretase activity. When either, or both, of these residues are mutated in PS1, Aβ and P3 production are greatly reduced with a concomitant increase in the levels of APP C-terminal fragments[93, 97, 98]. Presenilins alone are not sufficient for γ-cleavage. Instead, γ-secretase activity is associated with a high molecular weight PS-containing complex[90, 91, 99]. Biochemical purification of this complex led to the identification of the type I transmembrane glycoprotein, nicastrin[100]. A genetic screen of *Caenorhabditis elegans* revealed two genes, *aph-1* and *pen-2*, each encoding multipass transmembrane proteins that interact strongly with the presenilin orthologue, sel-12 and the nicastrin orthologue aph-2[101]. When all four components were expressed together in *Saccharomyces cerevisiae*, an organism that lacks any endogenous γ-secretase activity, fully active γ-secretase was reconstituted[102]. The interaction of the γ-secretase components is depicted in Figure 1.6.

In addition to the cleavage sites already mentioned, an additional ε-cleavage site exists. This ε-site occurs at a position distal to the Aβ 40/42 γ-secretase sites and is located close to the inner leaflet of the membrane bilayer[103]. Proteolysis at this site

results in the formation of an APP intracellular domain (AICD) that is believed to be involved in nuclear signalling[104]. Cleavage at the ε-site is presenilin-dependent and can be inhibited by treatment with γ-secretase inhibitors and is therefore probably γ-secretase mediated[105].

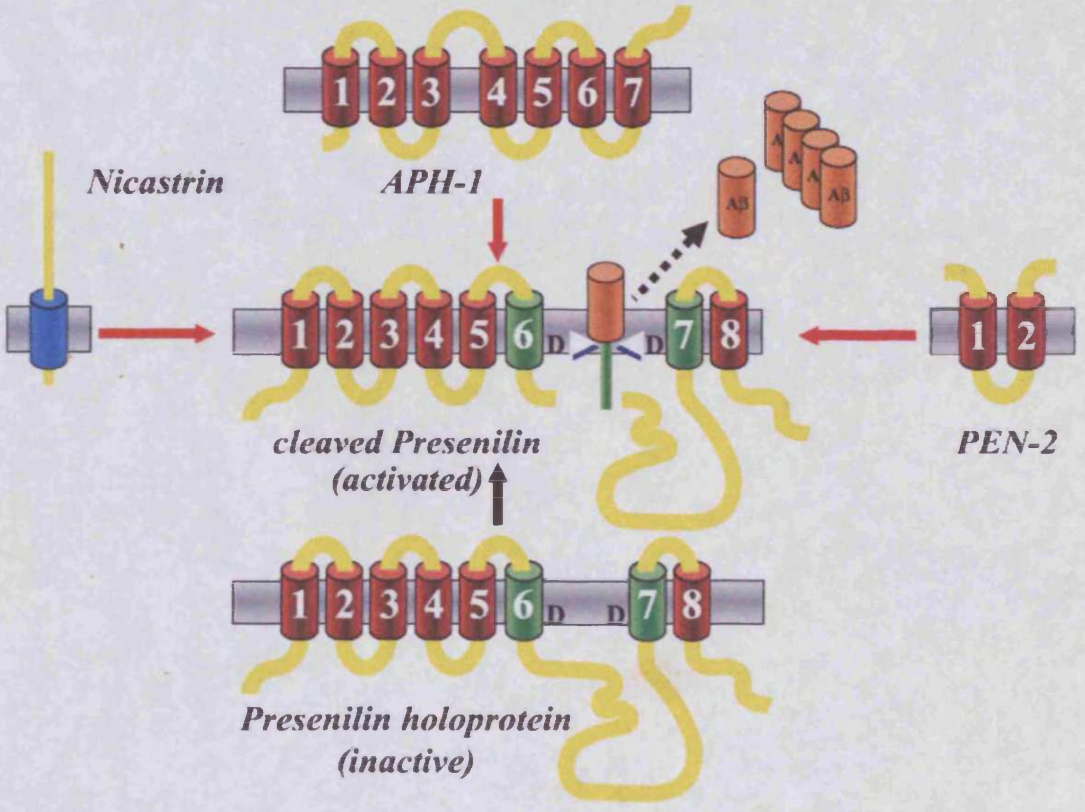

Figure 1.6. Presenilins are cleaved to form the physiologically active N- and C-terminal fragments. Additional cofactors are required to form the fully active γ-secretase complex. These factors include APH-1, Nicastrin and PEN-2. These four proteins act as a native protease, liberating Aβ into the extracellular space following β-cleavage. Taken from Aguzzi & Haass, 2003[106].

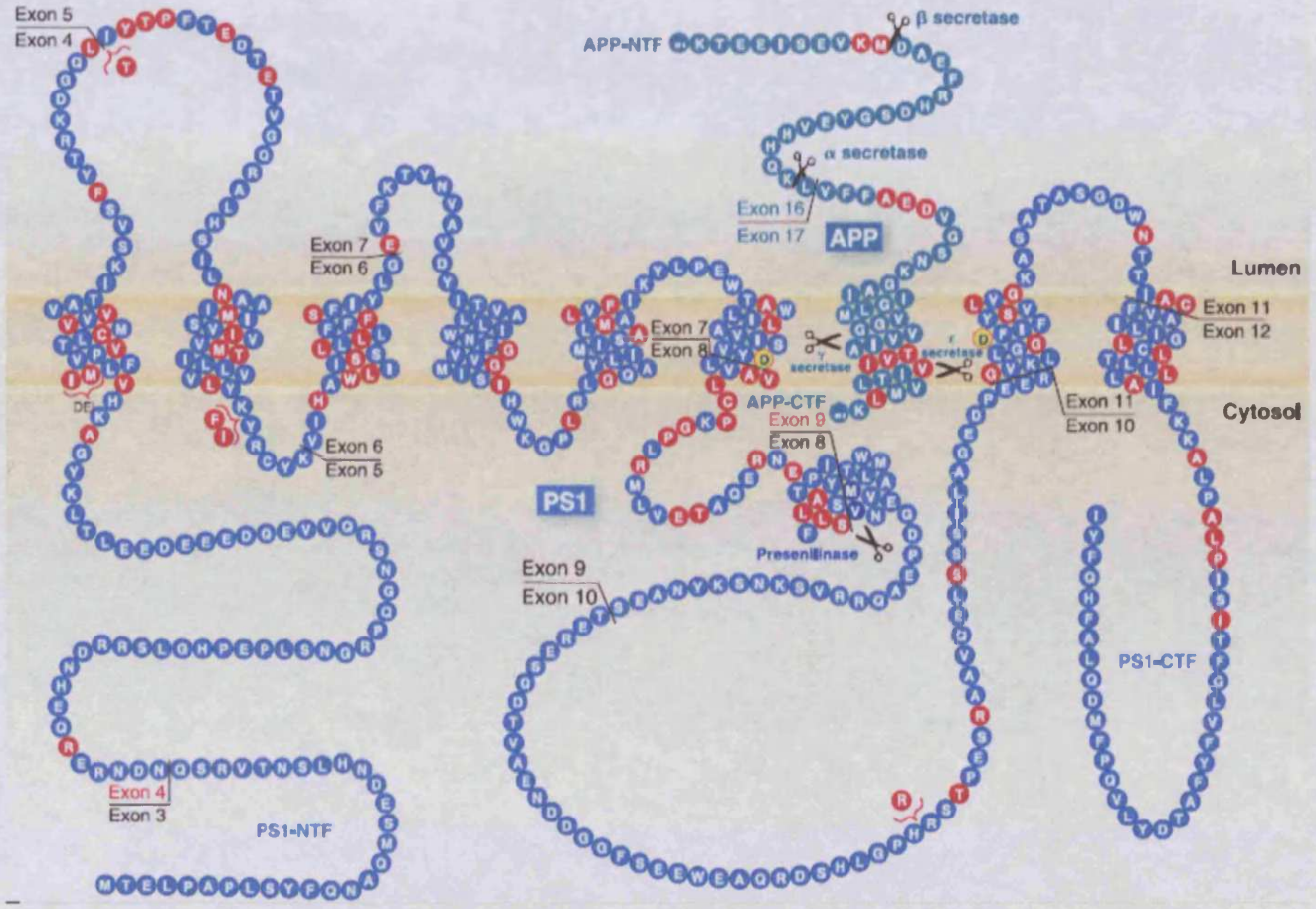

Figure 1.7. APP processing. The entire amino acid sequence of PS1 (blue circles) and a portion of the COOH-terminal sequence of APP (green circles) are shown. Some of the mutations in each molecule known to cause autosomal dominant AD are also shown (depicted in red). Taken from Hardy and Selkoe 2002[107].

1.8.3.2 Mutations in *APP*, *PS1* and *PS2*

Alteration of APP processing appears to be the mechanism by which autosomal dominant mutations in the *APP* and *presenilin* genes cause AD. In APP, pathogenic mutations are found in exons 16 and 17, clustered around the β- and γ-secretase sites (see Figure 1.7). The effects of these mutations have been elucidated somewhat by cell culture studies. For example, a double mutation at amino acids 670 and 671 from Lys–Met to Asp–Leu (the 'Swedish' mutation) that lies upstream of the β-cleavage site results in a five- to eight-fold increase in the formation of both $A\beta_{40}$ and $A\beta_{42}$[108]. Mutations at amino acid 717, such as the 'London' mutation (Val→Ile) and the 'Indiana' mutation (Val→Phe), lie close to the γ-secretase site and results in a more than two-fold increase of the more insoluble $A\beta_{42}$, which rapidly aggregates to form amyloid depositions[109]. Mutations in the presenilin genes are predominantly located in the highly conserved transmembrane domains and are presumed to distort the precise conformation of the molecule within the membrane. The effect of these mutations again appears to be the enhanced production of $A\beta_{42}$[98, 110]. Therefore, in these families, the cause of AD appears to be a direct result of increased levels of Aβ, with $A\beta_{42}$ in particular, associated with neurotoxicity.

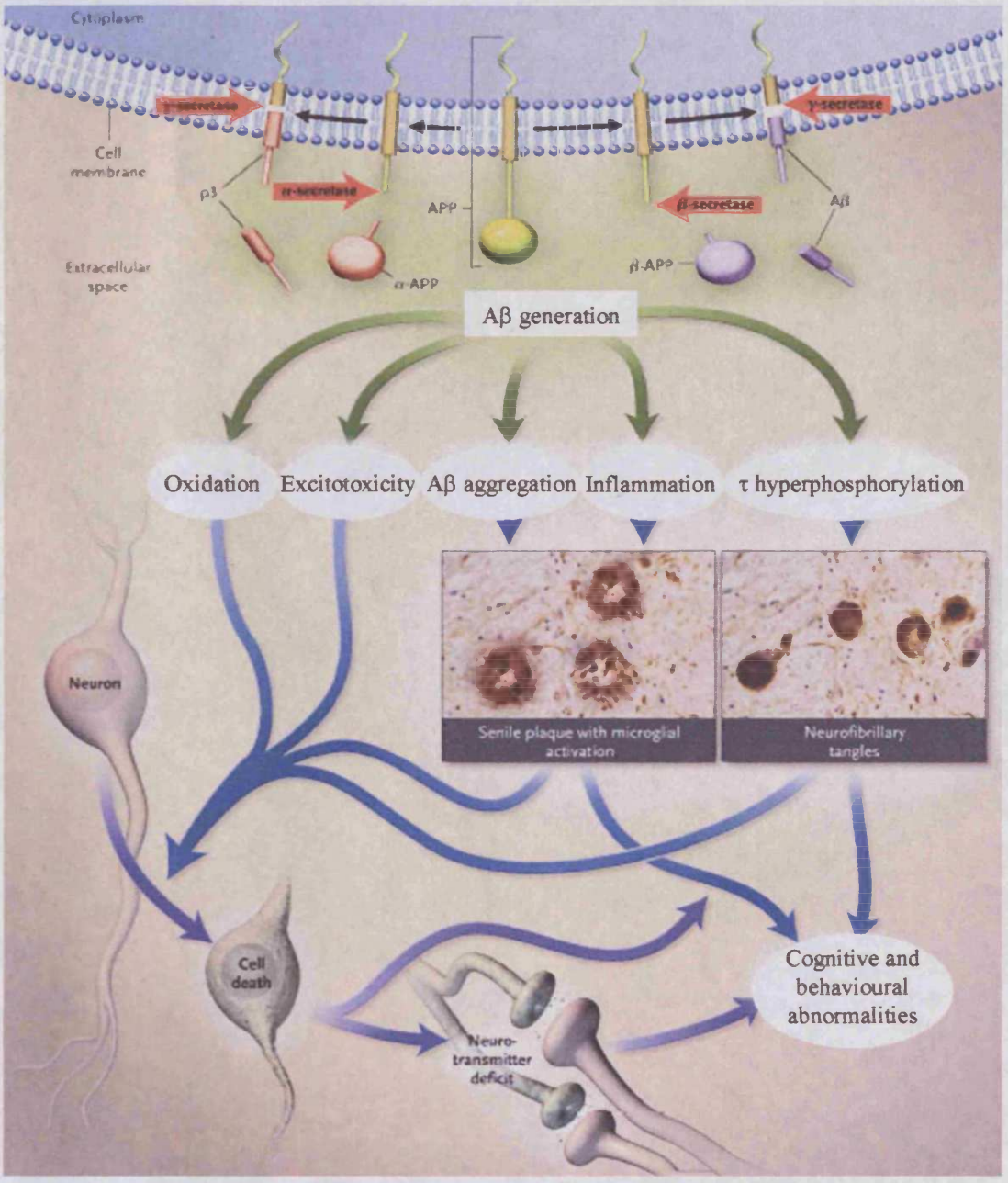

Figure 1.8. Putative Amyloid Cascade. The amyloid cascade progresses from the generation of the Aβ peptide from the amyloid precursor protein, through multiple secondary steps, to cell death. Adapted from Cummings 2004[111].

1.8.3.3 Aβ and the Amyloid Cascade Hypothesis

The discovery of the aforementioned mutations and their mechanism of action led to the formulation of the amyloid cascade hypothesis, which postulates that elevated levels of Aβ result in the oligomerisation, fibrillogenesis and aggregation of the

peptide. This is thought to initiate a cascade of injurious events, including free radical production, glial activation and direct neuronal damage (see Figure 1.8). Soluble Aβ oligomers are themselves a neurotoxic species prior to deposition in senile plaques[112]. They can lead to the generation of hydroxyl ions and oxidative injury of phospholipid membranes, and this loss of membrane integrity leads to cell death[113]. Aβ may also exert toxicity through influences on calcium channels, exaggerating calcium influx and initiating cell death pathways. Although controversial, the hyperphosphorylation of τ is believed to be a downstream consequence of increased Aβ levels and results in neurofibrillary tangles and cell death. The aggregation of Aβ in plaques precipitates microglial activation and the inflammatory response that surrounds the extracellular lesions. These reactive changes may further compromise brain function. The combination of plaques, tangles, neuronal loss and neurotransmitter deficits result in AD. The generation of transgenic mice that overexpress human APP carrying autosomal dominant mutations has lent support to the hypothesis that Aβ is central to AD. These mice produce an age-dependent increase in Aβ, develop deposits resembling senile plaques in the brain regions most heavily affected in AD and demonstrate spatial memory deficits[114-121]. Dystrophic neurites in plaque vicinity, heavy astrogliosis and microglia activation are also observed. A brief summary of the primary APP-based transgenic mouse models is given in Table 1.4. Although neurodegeneration is not observed to a degree anywhere near that seen in human AD, there is loss of synaptophysin staining in aged PDAPP mice[115], a modest loss of neurons in the APP23 mice[122] and an even smaller, though statistically significant, neuronal loss in the hippocampus of Tg2576 mice[123]. It is perhaps notable that none of the APP or APP/PS mice show evidence of neurofibrillary tangles, a fact often cited in

arguments against the amyloid cascade hypothesis, as discussed in the following section.

Mice	Transgene (mutation)	Phenotype					
		DP	AP	Glia	NFT	ND	Cog
NSEAPP	APP751 (no mutation)	+	-	-	-	-	+
PDAPP	APP (V717F)	+	+	+	-	-	+
Tg2576	APP695 (K670N, M671L)	+	+	+	-	-	+
APP23	APP751 (K670N, M671L)	+	+	+	-	+	+
PSAPP	APP695 (K670N, M671L) + PS1 (M146L)	+	+	+	-	-	+
CRND8	APP695 (K670N, M671L + V717F)	+	+	+	-	?	+
JNPL3	TAU (P301L)	-	-	+	+	?	?
TAPP	TAU (P301L) + APP695 (K670N, M671L)	+	+	+	+	?	?

Table 1.4. Summary of the primary APP-based transgenic models of Alzheimer's disease. Phenotype: DP=diffuse plaques; AP=amyloid plaques; Glia=gliosis (astrogliosis and microgliosis); NFT=neurofibrillary tangles; ND=neurodegeneration; Cog=cognitive impairment. Adapted from Higgins and Jacobsen, 2003[124].

1.8.3.4 τ and the Amyloid Cascade Hypothesis

As described earlier, neurofibrillary tangles are relatively insoluble, intracellular aggregates composed of paired helical filaments (PHFs). These PHFs consist of protofilaments arranged to form a tubule and contain hyperphosphorylated microtubule-associated τ protein. The gene encoding human τ is located on chromosome 17q21, where it occupies over 100kb and contains at least 16 exons. The τ gene is alternatively spliced, resulting in the production of different isoforms. In the central nervous system, alternative splicing of exons 2, 3, and 10 results in the appearance of six τ isoforms. Because exon 10 codes for one of the regions involved in binding to microtubules, alternative splicing of exon 10 produces τ isoforms, with either three or four tubulin/microtubule binding regions[125].

Some researchers believe that τ (as opposed to Aβ) is central to AD. The τ hypothesis emphasises the role of this protein and the consequent neurofibrillary tangles in producing cell loss and dementia and postulates that τ pathology is independent of amyloid pathology. One argument in favour of the τ hypothesis is the fact that the number of NFTs appears to correlate well with neuronal loss and the severity of dementia in AD, which is not the case for SPs[126]. However, as previously mentioned, there is evidence to indicate that soluble Aβ oligomers are neurotoxic[112] and therefore can induce neuronal death before the appearance of SPs. Indeed, young APP transgenic mice show altered synaptic morphology and electrophysiological changes well before the microscopic appearance of Aβ deposits[127, 128]. Because such mice show steadily rising total Aβ levels in the brain before plaques develop[129], Aβ oligomers could be responsible.

That mutations in the τ gene can lead to NFTs and dementia (frontotemporal dementia with parkinsonism linked to chromosome 17; FTDP-17) has also been used to argue the primacy of τ in AD[130]. However the same fact can be used against the hypothesis, as no amyloid is deposited in these individuals. Therefore while mutations in *APP* or APP processing genes result in a pathology of both plaques and tangles, mutations in τ can only produce the latter. Why NFTs and neuronal loss are not observed in APP-only transgenic mice is unclear, but may be a result of species differences. However, double transgenic mice have been generated (TAPP; see Table 1.4), overexpressing mutated τ and APP. Whereas the Aβ pathology in the double transgenic animals is not different from that observed in single APP transgenic mice (Tg2576), PHF formation is largely accelerated compared with mice overexpressing only mutated τ[121]. This argues strongly in favour of an upstream role

of Aβ in the generation of NFTs. It is possible then, that tangles occurring in the course of normal ageing are pathologically augmented by the initiation of aberrant amyloid metabolism. Therefore, while the presence of τ pathology in AD is no doubt deleterious, there are likely to be parallel molecular changes not dependent on τ that also contribute to neuronal dysfunction.

1.8.3.5 ApoE and the Amyloid Cascade Hypothesis

ApoE is one of the major apolipoproteins in the plasma and the principal cholesterol carrier protein in the brain. The ε4 allele has been consistently found to be associated with LOAD. One copy of the ε4 allele increases the risk of AD three-fold whereas two copies of the allele increase the risk eight-fold[131]. Several studies have reported that amyloid plaque density is correlated to *APOE* genotype in a gene dosage-dependent manner, with *APOE* ε4 homozygous subjects demonstrating significantly increased plaque density compared with *APOE* ε3/ε4 heterozygotes or *APOE* ε3 homozygous patients[132-139].

Studies in PDAPP mice suggest that apoE contributes to the deposition of Aβ. Disruption of the *APOE* gene in these mice inhibited the accumulation of Aβ in immunoreactive deposits[140]. Moreover, amyloid deposition was found to be strictly dependent on apoE expression levels in a dose-dependent manner. The absence of apoE appeared to affect the extracellular accumulation, but not the synthesis, of Aβ[141]. Therefore, the *APOE* ε4 allele may act by enhancing the deposition or decreasing the clearance of Aβ, adding further weight to the hypothesis that Aβ is central to AD pathogenesis.

1.8.4 Finding New Genes for LOAD

Not all causative mutations have been identified for autosomal dominant EOAD and identification of these rare mutations may help us further elucidate the pathogenesis of AD. But discovering the susceptibility alleles for LOAD is perhaps of more global importance. The *APOE* ε4 allele is neither necessary nor sufficient to cause disease and as 50% of LOAD cases carry no ε4 alleles, there must be additional risk factors[142]. Therefore, a number of linkage and association studies of LOAD have been performed and these are described below.

1.8.4.1 Linkage Analysis in LOAD

1.8.4.1.1 Chromosome 10

Perhaps the strongest evidence for linkage to LOAD lies on chromosome 10. Our department and collaborators have performed a two-stage genome screen to search for novel risk factors for LOAD[143-145]. The first stage involved genotyping 292 affected sibling pairs (ASPs) at approximately 20cM intervals throughout the genome. In the second stage, 451 ASPs (which included the original 292) were genotyped with an additional 91 markers in the sixteen regions where the multipoint lod score (logarithm of the odds ratio for linkage/no linkage) was greater than 1 in stage 1. The strongest (and only significant) evidence for linkage was on chromosome 10, with a multipoint lod score (MLS) of 3.9. This linkage region spans approximately 42cM, from D10S1426 (59 cM, 30.5Mb, 10p11.23) to D10S2327 (101 cM, 80.1Mb, 10q22.3) and is illustrated in Figure 1.9.

Evidence pointing to the same region on chromosome 10q was found in an independent sample of late-onset extended pedigrees that were selected based on

probands with extremely high plasma values of $A\beta_{42}$. Plasma $A\beta_{42}$ levels are elevated in both LOAD individuals and their cognitively normal relatives. Therefore Ertekin-Taner *et al.* (2000)[146] used plasma $A\beta_{42}$ levels as a surrogate trait and performed linkage analysis on extended AD pedigrees. Strongest linkage (a MLS of 3.93) was detected between markers D10S1227 and D10S1211, which coincides with the region giving maximum signal in our study (see Figure 1.9).

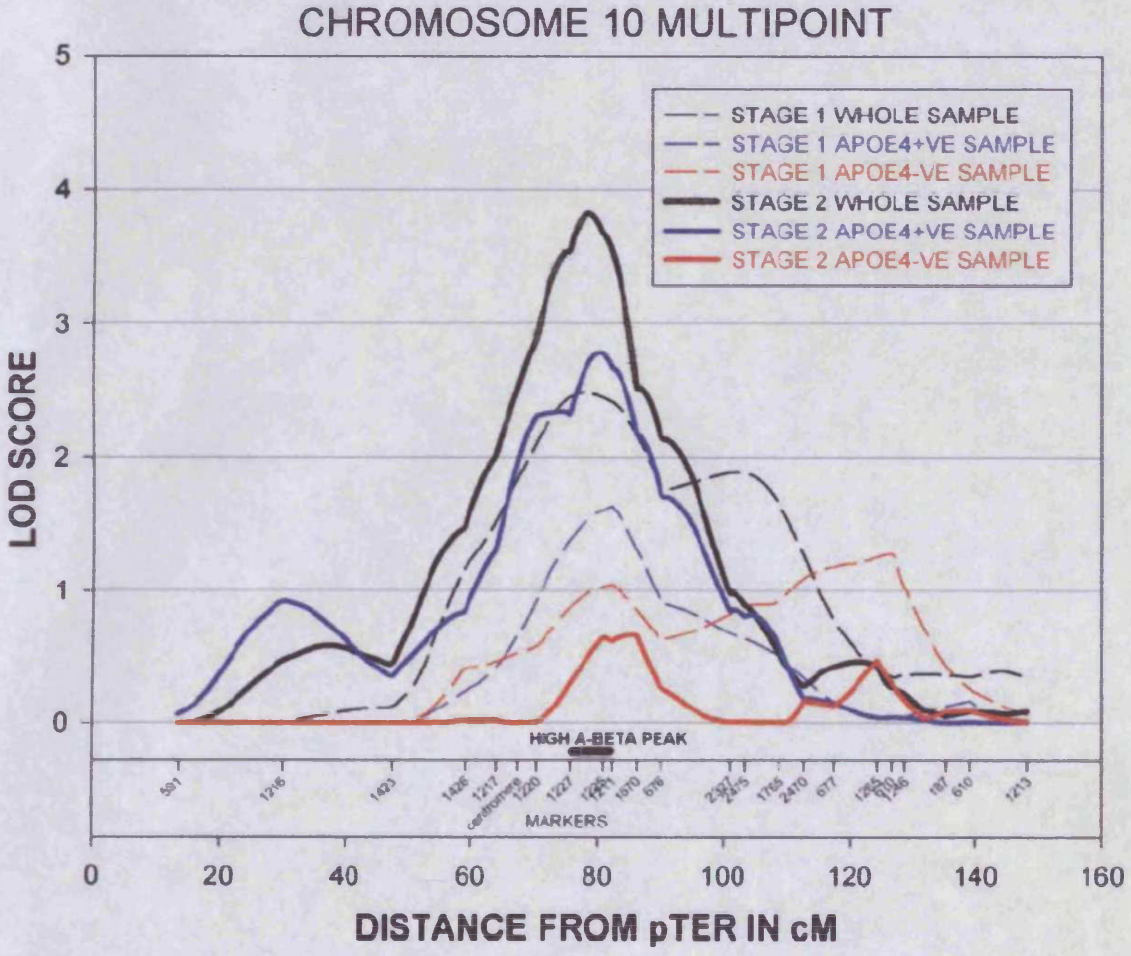

Figure 1.9. Chromosome 10 multipoint map for LOAD by Myers *et al.* (2000)[144]. Multipoint linkage analyses were carried out on the whole sample (429 pairs), on pairs where both siblings had at least one APOE4 allele (APOE4+ve; 262 pairs), and on pairs where neither sibling had an APOE4 allele (APOE4-ve; 83 pairs). The region of linkage for high plasma $A\beta_{42}$ from the Ertekin-Taner *et al.* (2000)[146] report is also shown.

Recently, Wijsman *et al.* (2004)[147] have employed a Bayesian Markov chain-Monte Carlo method to allow multipoint linkage analysis under oligogenic trait models in LOAD pedigrees. Age at onset (AAO) was used as the phenotype because the method of analysis used has been implemented only for continuous traits, but AAO is a measure of severity that is also a surrogate for AD and there is evidence for a genetic basis for AAO[47, 148, 149]. They found modest corroboratory evidence for a locus on chromosome 10 at a location similar to that previously identified, specifically at marker D10S1652 (81cM).

Evidence for linkage has also been found at a more telomeric region of chromosome 10q. Bertram *et al.* (2000)[150] tested seven markers on chromosome 10q within a 47cM region flanking the gene encoding the insulin-degrading enzyme (IDE), which is believed to play a role in the degradation of Aβ. The data were analysed using parametric and nonparametric methods in the whole sample (1426 subjects from 435 multiplex AD families) and in a subset of families with late-onset AD. There was some overlap in this sample with that used in our two-stage screen. However, in LOAD families these researchers found the strongest signals for markers D10S583 (115cM), D10S1710 (124cM) and D10S1671 (127cM), approximately 40cM distal to our main peak.

Similarly, Li *et al.* (2002)[151] performed a genome screen in an overlapping sample of 449 families affected with AD, using age at onset as a quantitative trait. They found evidence for suggestive linkage near marker D10S1237 (135cM). It is unclear whether the various peaks on chromosome 10q represent linkage to one or two underlying loci. However, signals from so many studies, even though not all are

independent, do at least raise confidence that this region contains one or more susceptibility loci.

1.8.4.1.2 Chromosome 12

Chromosome 10q is not the only region to be implicated by linkage studies of LOAD. For example, evidence for a late-onset AD locus has been found on chromosome 12. In a two-stage genome-wide screen, Pericak-Vance *et al.* (1997)[152] observed linkage to chromosome 12 in a 32cM region between markers D12S373 (36cM) and D12S390 (68cM), with a peak MLS of 3.5. Scott *et al.* (2000)[153] further refined the linkage of Pericak-Vance and colleagues by analysing additional markers in the same sample. They performed several different analyses in order to control for family size, presence of the *APOE* ε4 allele and presence of dementia with Lewy bodies. The highest LOD score was observed in the ε4-negative subset of families, at the edge of the original peak near D12S1632 (72cM).

Attempts to replicate the initial findings of Pericak-Vance *et al.* have been inconsistent. Rogaeva *et al.* (1998)[154] have reported additional evidence for a locus on chromosome 12, although their linkage was concentrated at either end of the Pericak-Vance interval, with the strongest linkage being located near D12S390 (68cM). However, in an independent and larger set of patients, the previous findings could not be replicated and a different region on chromosome 12p, close to the α2-macroglobulin gene (*A2M*) showed suggestive evidence of linkage[155]. Most of the evidence came from affected pairs where neither member had an ε4 allele.

The results from all of these studies are collated in Figure 1.10. It should be noted that in our genome screen[145], the maximum MLS for chromosome 12 (located 23cM from pter), was also in the ε4-negative stratum. Although an MLS of 1.4 did not even pass the threshold for suggestive linkage, this section of the study was quite underpowered due to the small numbers of ε4-negative sibling pairs.

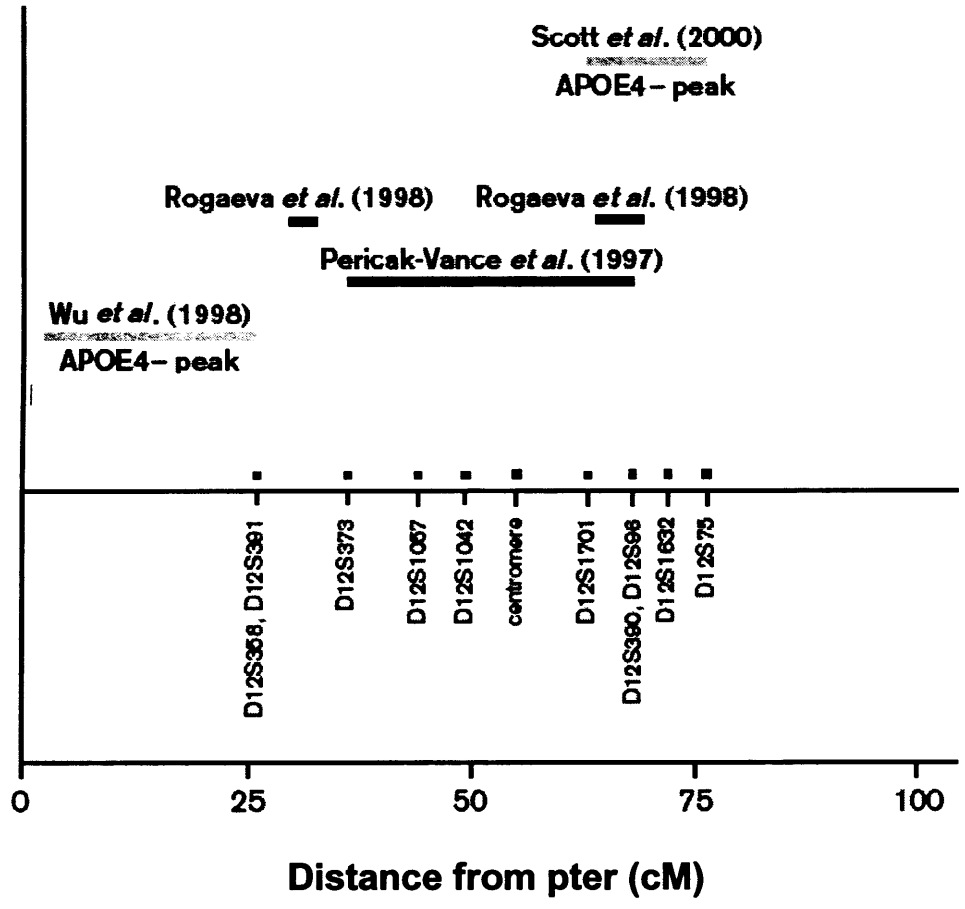

Figure 1.10. Locations of peak regions on chromosome 12 from several studies. Adapted from Myers and Goate (2001)[156].

1.8.4.1.3 Chromosome 9

In 2000, Pericak-Vance and colleagues re-screened the genome in 466 LOAD families (730 ASPs)[157]. Their most significant linkage (MLS=4.31) was obtained on chromosome 9p with marker D9S741 in a subset of autopsy confirmed LOAD

families. Scott *et al.* (2003)[158] applied ordered-subset analysis to the Pericak-Vance data to identify loci with increased evidence for linkage (relative to the overall sample) in subsets of families defined by mean and minimum ages at onset. The LOD score in the chromosome 9p region increased to 4.6 at D9S741 in 334 families with minimum age at onset between 60 and 75 years. Interestingly, Myers and colleagues (2002)[145] largest peak on chromosome 9 is with this same marker (MLS=1.7), although it should be noted that as much as 80% of the sample overlaps with that of Pericak-Vance.

1.8.4.1.4 Other Chromosomal Loci

Olson and colleagues have reanalysed the data generated by our genome screen[143, 145] using a covariate-based ASP linkage method. They found the *APP* region on chromosome 21q to be strongly linked to ASPs of the oldest current age (lod score=5.54) who lack *APOE* ε4 alleles[159]. Similarly, the likelihood of linkage increases on chromosome 20p to a lod score of 4.1 with increasing current age and with increasing number of ε2 alleles and decreasing number of ε4 alleles[160]. A two-locus model provided evidence of strong epistasis between chromosome 20p and the *APP* region on chromosome 21, limited to patients who were of an older age and lacked ε4 alleles. The authors suggested that the development and/or rate of progression of AD in such families is influenced by the presence of high risk alleles at both loci, which probably interact biologically to increase susceptibility to a very-late-onset form of AD.

Various other loci have been identified. Scott *et al.* (2003)[158] detected regions on chromosome 2q34 in a subset of families with early-onset AD and 15q22 in families

with AD of very late onset (≥79 years). Chromosome 19q13 has been frequently reported to show evidence for linkage[145,147,157,160, 161], which is assumed to correspond to the *APOE* gene. Wijsman *et al.* (2004)[147] also identified strong evidence of a second LOAD gene on chromosome 19p13.2, which is distinct from *APOE* on 19q.

Identification of chromosomal regions bearing susceptibility loci for LOAD is vital and the linkage reports mentioned above have been the basis for numerous candidate gene studies.

1.8.4.2 Candidate Gene Studies in LOAD

Despite the large number of candidate gene studies that have been undertaken to date and the number of positive associations reported, no single finding has been consistently replicated to the degree of the APOE ε4 association with AD. For example, the *insulin-degrading enzyme* (*IDE*) gene is a good LOAD candidate, based on both its position in a region of linkage on chromosome 10[150, 151] and on the functional involvement of the enzyme in the degradation of Aβ[162]. While there are three positive reports of association between variants in this gene and LOAD[163-165], there are also two negative reports[166, 167]. Similarly, the gene encoding the serum protease inhibitor α2-macroglobulin, *A2M*, is a good candidate gene as it maps to a region of suggestive linkage on chromosome 12p[155], the protein has been implicated in AD on the basis of its ability to mediate the clearance and degradation of Aβ[168], and it is also a component of senile plaques. However, initial positive reports of association between variation in this gene and LOAD[169, 170] have been followed by negative findings and a lack of replication by independent groups[171-178].

Unfortunately, such apparently contradictory findings are common in both LOAD and many other complex diseases.

There are a number of factors that might explain these inconsistent reports. For example, an initial finding of association may be a type I error, *i.e.* a false positive. Population stratification is commonly cited as a reason for false positive association, although it has rarely been demonstrated as the culprit[179] and is not an issue when family-based samples are employed (*e.g.* in the positive *A2M* finding of Blacker and colleagues[169]). Nevertheless, for population-based samples, it is vital to match cases and controls for possible confounding factors.

It is of course possible that the positive result is just a chance finding. Given a significance level of α=0.05, then there is a 1 in 20 chance of rejecting the null hypothesis when it is in fact true. Taking into account the copious number of LOAD association studies performed worldwide, it is to be expected that a percentage will report 'significant' findings, where no association exists.

However, researchers must take care not to inflate these chance findings, by adjusting the significance thresholds appropriately whenever they perform multiple statistical tests on the same dataset. The degree to which to correct for multiple testing is a source of much debate, with many researchers of the mind that Bonferroni's correction (which approximates to dividing the required significance level, *e.g.* 0.05, by the number of independent null hypotheses being tested) is overly conservative. Indeed, type I errors cannot decrease without inflating type II errors (the probability of accepting the null hypothesis when the alternative is true) and a

false negative is just as erroneous as a false positive. Therefore, researchers must try and find a balance between the two. This is probably best achieved by a combination of cautious reporting of initial positive findings and a reliance on replication before accepting an association as definitive.

There are a number of reasons why a candidate gene study may fail to detect association, when variation at that locus does in fact cause susceptibility to the disease. A likely cause is that the study is insufficiently powered to detect the effect size. For example, for a risk allele with a frequency of 20% and an odds ratio of 2, 85 cases and 85 controls are required to achieve 80% power to detect this effect. If the same risk allele had a smaller odds ratio of 1.5, then 266 cases and 266 controls are required for 80% power. It is therefore likely that many of the smaller studies that have been performed in the past have been underpowered (at least for detecting small odds ratios).

The calculations above assume that either the susceptibility allele itself is being tested, or a marker allele in complete LD with the susceptibility allele. If this is not the case, then power is reduced. While there are several measures of LD, the square of the correlation coefficient, r^2, is considered the most appropriate. To have the same power to detect the association between the disease and the marker locus, the sample size must be increased by roughly $1/r^2$ when compared with the sample size for detecting association with the susceptibility locus itself[180, 181]. Therefore, a study with an apparently good sample size may fail to detect association of a true susceptibility gene with the disease if 'inappropriate' markers are used.

Choice of markers is not an issue for replication studies. In these cases, it should only be necessary to genotype the marker or markers that have been reported to be associated with the disease. However, power is again relevant here. A replication study should take into account the reported effect size and then determine if the replication sample has sufficient power to detect this effect. If the sample size is too small, then failure to replicate could be a result of type II error rather than type I error in the initial report. Other reasons why a study may fail to replicate a reported association are 1) the two studies are examining different populations and genetic heterogeneity exists between the different groups; 2) biases varies between the two studies; 3) the original finding was a false positive.

It is therefore important for a candidate gene study to employ a sufficiently powered sample (that has been well matched for possible confounding factors) and an appropriate choice of markers, if it hopes to minimise the type I and II error rate.

1.9 Aim of this Study

The aim of the research presented within this thesis was to detect a novel locus or loci conferring susceptibility to late-onset Alzheimer's disease. A candidate gene approach was taken, examining both positional candidates within a region of reported linkage on chromosome 10q and a purely functional candidate, also on chromosome 10q but not in an identified linkage region. All candidate genes were screened for sequence variants and in some cases database SNPs were also employed. Variants were tested for association with LOAD by genotyping them in case-control samples, either in DNA pools, individually or both.

2. MATERIALS AND METHODS

2.1 DNA Samples

Genomic DNA derived from LOAD patients and unaffected control individuals was used for mutation screening and association analyses. Three independent case-control samples were employed in the course of this project and will be referred to as the Cardiff, Belfast and MRC samples. The DNA in the Cardiff and Belfast samples was depleted early in the project and so the majority of studies use the MRC sample. The sample used for a particular study will be indicated in the relevant chapter.

2.1.1 Cardiff Sample

The Cardiff sample consisted of 133 LOAD patients and 135 controls. The cases were composed of both a clinically diagnosed patient group (CDAD; n=99) and a post-mortem confirmed patient group (PMAD; n=34). Both the case and control groups were Caucasians of UK origin. The 99 patients within the CDAD group had been diagnosed as having probable AD according to the National Institute of Neurological and Communicative Disorders and Stroke (NINCDS) and the Alzheimer's Disease and Related Disorders Association (ADRDA)[17] criteria with an age at onset ≥60 years. The patients were recruited from elderly care homes, local psychogeriatric hospitals or were the probands of multiply affected families. The average age at onset was 72.5 years (SD=6.5) and 47% were male. The PMAD group consisted of 34 confirmed AD cases provided by the MRC brain bank. All members of this group fulfilled CERAD[182] neuropathological criteria for definite AD. The average age at onset of this group was 74.0 years (SD=6.4) and 38% were male. The age-matched control group had an average age at collection of 78.1 years (SD=7.2)

and 43.7% were male. Controls were screened for cognitive decline using the Mini Mental State Examination (MMSE)[18] and a cut off score of 28 was adopted.

2.1.2 Belfast Sample

The Belfast sample consisted of 242 LOAD patients and 235 controls. Patients and controls were Caucasian, and at least their parents and grandparents had been born in Northern Ireland. All participants with a strong family history of dementia, greater than one first degree relative, were excluded. Blood samples from patients were obtained through the Memory Clinic, Belfast City Hospital and by referral from the Alzheimer's Disease Society. The mean age of patients was 75.4 years (SD=8.1) and 38% were men. Patients were subjected to a structured interview and physical examination. Diagnosis of probable Alzheimer's disease was arrived at by two experienced clinicians by use of the NINCDS-ADRDA. Where possible, a computed tomography scan was done to aid diagnosis. 235 volunteers who were age-matched to the AD patients were recruited as controls. The mean age was 74.7 years (SD=8.1) and 31% were men. Assessment of controls included a full medical history and a physical examination. Cognitive function was assessed with the MMSE. Those with a score of at least 28 were included in the study.

2.1.3 MRC Sample

For the MRC sample, clinical data and DNA samples were collected from 546 individuals (26% males) with Alzheimer's disease and 546 control subjects (26% males). Age at onset ranged from 60 to 92 years (mean=75.45 years, SD=6.485). Controls were matched for age (mean=76.30 years, SD=6.257), gender and ethnicity. The sample was recruited from both community and hospital settings and the

assessment was by structured interview including scales shown to be reliable and valid in similar contexts. The assessment battery used has demonstrated a positive predictive value (PPV) for NINCDS-ADRDA clinical diagnosis against the non-exclusive presence CERAD criteria for AD pathology of 0.92[183]. The standardised information from this assessment battery is used to form a diagnosis of probable AD according to NINCDS-ADRDA criteria.

Scales used include: 1) The MMSE; 2) The Cambridge Mental Disorders of the Elderly Examination (CAMDEX)[184]; 3) The Blessed Dementia Scale[2]; 4) The Bristol Activities of Daily Living Scale[185]; 5) The Behavioural Pathology in Alzheimer's Disease Rating Scale[186]; 6) Webster Rating Scale[187]; 7) Global Deterioration Scale[186]; 8) Cornell Scale for Depression in Dementia[188] and 9) the Neuropsychiatric Inventory[189]. The interview includes information from both the carer and the patient and all subjects had an age at onset greater than or equal to 60 years. To reduce potential genetic heterogeneity and population stratification, only individuals with grandparents of UK nationality were selected. Exclusion criteria included the presence of any other dementia, delirium, or other illnesses likely to significantly reduce cognitive function.

Controls were selected in two ways. Spouse controls were selected on the basis of the participation of their AD partner. Controls were also collected from general practices in the same areas as the AD patients. Controls were 60 years or above, of UK origin and had a normal level of cognitive functioning. Controls were screened for cognitive decline using the MMSE and again a cut off score of 28 was adopted. Assessment also included a section of the Cambridge Mental Disorders of the

Elderly Examination and the Geriatric Depression Scale[190]. Exclusion criteria included the presence of dementia, depression, delirium or other illnesses likely to significantly reduce cognitive function.

2.1.4 Mutation Screening Sample

A sample consisting of 14 LOAD patients diagnosed according to NINCDS-ADRDA criteria was employed when screening for polymorphisms. The average age at onset was 80.8 years (SD=6.3) and 7% were male.

2.1.5 Creation of DNA Pools

2.1.5.1 MRC Pools

A subset of the MRC sample, 186 cases and 186 age- and sex-matched controls, was used to create DNA pools for genotyping purposes. The average age at onset of cases was 74.34 (SD=6.461) and 25% were male. The average age at collection of controls was 75.42 (SD=6.535) and 25% were male. These samples were divided into two case pools of 96 and 90 individuals and two control pools of 96 and 90 individuals. The concentration of the DNA samples used to construct pools was measured using the PicoGreen dsDNA Quantitation Reagent (Invitrogen, Paisley) in a Fluoroskan Ascent fluorimeter (Labsystems, Cambridge). The samples were diluted to a final concentration of 6ng/μl and equal amounts of DNA were mixed to form the pools. These pools will be referred to as the MRC pools.

The MRC pools were validated prior to use. For this purpose, two SNPs (*CHAT* 1803 C>T and *CHAT* 1882 G>A) were genotyped both in the MRC pools and individually in the 186 cases and 186 controls that made up the pools. For pooled analysis, the

extension primers (see Section 2.8.1) employed were the 37-mers 5'-TCCCTCACTCCGTTGGTGGAGGGAAAGGAATGCATGC-3' for *CHAT* 1803 C>T and 5'-AAGGGTAAGACCATACCTACTGTGCTCAGTGCTTCAT-3' for *CHAT* 1882 G>A. The PCR fragment (ChAT xS) on which primer extension was performed (for both SNPs) is described in Chapter 3. Similarly, details of the individual genotyping assays can be found in Chapter 3. Individual and pooled genotyping data are given in Table 2.1 below. Estimation of differences between cases and control pools (Δ) was extremely accurate, with the mean error for Δ of 0.785%. In the course of the research presented within this thesis, a number of other SNPs were genotyped both in pools and individually. The data thus obtained was used to calculate a better estimate of pooling error, and these results can be found in Appendix A.

SNP	% Major Allele in Cases		% Major Allele in Controls		% Difference between Cases and Controls (Δ)		Error (%)
	Pools	**Real**	**Pools**	**Real**	**Pools**	**Real**	
CHAT 1803 C>T	88.44	84.14	87.37	83.33	1.08	0.81	0.27
CHAT 1882 G>A	74.50	74.73	70.97	69.89	3.54	4.84	1.30
Average							**0.785**

Table 2.1. Accuracy of estimating allele frequencies in DNA pools. The estimated allele frequencies in pools, together with the corresponding real allele frequency (as determined from individual genotyping) in 186 cases and 186 control samples are presented for each SNP. Δ: Difference in allele frequencies between cases and controls. Error: error of pooling defined as the discrepancy between the Δ obtained by pooled and individual genotyping. The estimate of error assumes that individual genotyping is 100% accurate.

2.1.5.2 WashU Pools

In addition, a set of pools for replication purposes was kindly supplied by our collaborator Alison Goate in Washington University. These 'WashU' pools were comprised of 270 Caucasian LOAD cases and 270 Caucasian controls. Both cases and controls were divided into three pools of 90 individuals. The average age at onset

of cases was 75.83 (SD=6.863) and 35% were male. The average age at last assessment of controls was 79.37 (SD=7.012) and 36% were male. The WashU series was part of the Washington University Alzheimer's Disease Research Center (ADRC) patient registry. Cases have a clinical diagnosis of dementia of the Alzheimer's type according to NINCDS-ADRDA criteria with a minimum age at onset of 60 years. Non-demented controls have a full neuropsychological and clinical interview and are assessed in the same manner as the cases. Both cases and controls were recruited from the Greater St. Louis metropolitan area. As I did not have access to the individual samples that made up the WashU pools I was unable to validate them.

2.1.6 DNA Extraction

High molecular weight genomic DNA was extracted from either whole blood, transformed lymphoblasts or from sections of post-mortem brain tissue following standard laboratory procedures. The approximate DNA concentration of each sample was subsequently assessed by spectrophotometer readings of a 1:20 dilution of DNA aliquots. Samples were then stored at -20°C until required.

(Note: I was not involved in diagnosis and collection of samples, extraction of DNA or construction of pools).

2.2 Characterisation of Candidate Genes

As a result of the human genome project, there is now likely to be a large amount of information available on any randomly chosen gene. This information is publicly available on the Internet at sites such as Ensembl (http://www.ensembl.org/) and

LocusLink (http://www.ncbi.nlm.nih.gov/LocusLink/index.html). As such, these sites were a starting point for all research on the candidate genes in this project.

The cDNA sequence for each gene was obtained from the GenBank database at NCBI (http://www.ncbi.nlm.nih.gov). Determination of intron/exon boundaries was based on alignment of the cDNA sequences with genomic clone sequences, using BLAST sequence homology searches (http://www.ncbi.nlm.nih.gov/blast/Blast.cgi). Genomic and cDNA sequence was subsequently imported into Sequencher™ (Gene Codes, Michigan, USA), a sequence analysis program, where they could be annotated and used as a reference for future research.

2.3 Polymerase Chain Reaction

The polymerase chain reaction (PCR) is a standard *in vitro* method that enables the rapid production of large quantities of a target sequence from total genomic DNA and is a prerequisite for many of the methods used in this project. PCR requires single stranded oligonucleotide primers complementary to the sequence flanking the region to be amplified. PCR fragments spanning exons, untranslated regions (UTRs) and limited 5' flanking regions were designed using Primer 3.0 (http://www-genome.wi.mit.edu/cgi-bin/primer/primer3_www.cgi). Primers were synthesised by Sigma-Genosys (Haverhill).

Amplification was performed under standard conditions of 1X PCR buffer (Qiagen, Crawley), 1.5 mM $MgCl_2$, 250 μM dNTPs, 0.5 μM of each primer, 0.3 units Hot Star Taq (Qiagen) and 18 ng genomic DNA in a 12 μl reaction. 1X Q-solution (Qiagen)

was occasionally used to amplify a GC rich sequence and I will indicate where this is the case. A typical individual reaction mix is shown below.

Reagent	Volume	Final Concentration/Amount
5X Q-solution (optional)	2.4µl	1X
10X Buffer (containing 15mM $MgCl_2$)	1.2µl	Buffer=1X; $MgCl_2$=1.5mM
2.5mM dNTPs	1.2µl	250 µM
10µM Sense Primer	0.6µl	0.5 µM
10µM Anti-sense Primer	0.6µl	0.5 µM
Hot Star Taq (5U/µl)	0.06µl	0.3 U
Genomic DNA (6ng/µl)	3.0µl	18ng
ddH_2O	Variable	

Table 2.2. Typical PCR reagents volumes and concentrations.

PCR optimisation was achieved by initially amplifying a fragment at a range of annealing temperatures and subsequently selecting the one that generated the best results. Cycling was conducted in a MJ Tetrad (MJ Research) with an initial denaturation of 94°C for 15min, followed by 35 cycles of 94°C for 30s, appropriate annealing temperature for 30s and 72°C for 45s with a final extension step of 72°C for 10 min. Synthesis of appropriately sized PCR products was confirmed by electrophoresis on agarose gels.

2.4 Agarose Gel Electrophoresis

Gels allow separation and identification of nucleic acids based on charge migration. Migration of nucleic acid molecules in an electric field is determined by size and conformation, allowing nucleic fragments of different sizes to be separated. In this project horizontal agarose gel electrophoresis was performed to a) check a PCR

reaction was successful or b) obtain genotype data from a RFLP analysis or a VNTR polymorphism. The concentration of agarose used for the gel depends primarily on the size of the DNA fragments to be analysed. For checking PCR, a 1.5% w/v gel was used. For RFLP analysis, where fragments of different size must be resolved, 2.5-3% w/v gels were used. Gels were prepared by melting the appropriate amount of agarose in 100ml 0.5X TBE buffer (National Diagnostics, Hull). The molten gel was allowed to cool slightly before adding 2.5µl of 10mg/ml ethidium bromide and was then poured into a gel-casting tray and well former combs were inserted. The gel was allowed to set, the combs removed and was then placed into an electrophoresis tank filled with 0.5X TBE buffer. Loading buffer was made from 5ml Glycerol (Sigma, Dorset), 0.03g Bromophenol Blue (Sigma), 0.03g Xylenecyanol (Sigma), 200µl 1M Tris-HCl pH 8.0 and 4.8ml dH2O. Samples were mixed with 2µl gel loading buffer, were loaded into the wells of the gel and then electrophoresed at approximately 100 volts for 0.5-2.5 hours. Gels were visualised under an UV transilluminator fitted with a Polaroid camera.

2.5 Post-PCR Purification

Several techniques that use PCR products as a template require those products to be purified of unincorporated primers and dNTPs. To achieve this, 1U each of exonuclease I (Amersham, Buckinghamshire) and shrimp alkaline phosphatase (Amersham) were added to 12µl PCR product, incubated (in a MJ Tetrad) at 37°C for 1 hour and then heated to 80°C for an additional 15 min to inactivate the two enzymes. The exonuclease I removes residual single-stranded primers and any extraneous single-stranded DNA produced by the PCR while the shrimp alkaline phosphatase removes the remaining dNTPs.

2.6 Denaturing High Performance Liquid Chromatography

In order to screen PCR fragments for polymorphisms, denaturing high performance liquid chromatography (DHPLC) was performed. This is an automated technology based on the separation of heteroduplex PCR products from their corresponding homoduplexes on an ion-pair reversed-phase liquid chromatography system. The hydrophobic stationary phase consists of alkylated nonporous poly(styrene/divinylbenzene) particles and the mobile phase consists of triethylammonium acetate (TEAA) and acetonitrile (ACN). The column is maintained at a set temperature to partially denature DNA molecules. Under these conditions, heteroduplexes attributable to mismatch pairing will form weaker interactions with the hydrophobic matrix. With a linear acetonitrile gradient, the heteroduplexes will therefore be eluted earlier than the homoduplexes. Samples containing a heterozygous mutation form both homoduplexes and heteroduplexes, and (theoretically) at least two peaks are observed. In reality, resolution is not optimal and it is more common to see one peak with a 'shoulder'. Samples that give a single peak could be either wild type or could contain a homozygous mutation.

2.6.1 Heteroduplex Formation

For each fragment, the 14 DNA samples of the mutation screening sample were PCR amplified. To form heteroduplexes, PCR products were heated to 94 °C and then gradually reannealed by cooling at a rate of 1°C/min for 40min.

2.6.2 Analysis Parameters

Optimal temperatures and corresponding eluent gradients for each PCR fragment were selected using DHPLC Melt (http://insertion.stanford.edu/melt.html). To ensure

maximum sensitivity, in addition to the temperature suggested by the software (n°C), each fragment was also run at n+2°C.

2.6.3 DHPLC Analysis

DHPLC analysis was carried out using the WAVE™ DNA Fragment Analysis System (Transgenomic). 5µl heteroduplexed PCR product was injected onto a DNASep™ column. Hetero- and homoduplexes were then eluted with a linear acetonitrile gradient formed by mixing buffer A (0.1M TEAA, pH 7.0) and buffer B (0.1M TEAA, pH 7.0, containing 25% ACN) at a constant flow rate of 0.9 ml/min. DNA was detected at 260nm. The analytical gradient was 4min long and buffer B was increased at 2%/min. For each fragment, the initial and final concentrations of buffer B were adjusted to obtain a retention time between 3 and 5 min. Between samples, the column was cleaned with 100% buffer B for 30s and equilibrated at starting conditions for 2 min. When all samples had been processed, the resultant chromatograms were compared, with a shift in trace pattern indicative of a heteroduplex.

2.7 DNA Sequencing

Polymorphisms detected by DHPLC were confirmed and characterised by fluorescent dye-terminator cycle sequencing, based on the chain-termination dideoxynucleotide method of Sanger and co-workers[191]. This method involves the synthesis of a DNA strand by a DNA polymerase using a single stranded template. Chain elongation occurs at the 3′ end of a primer and the deoxynucleotide added to the extension product is selected by base-pair matching to the template. When a dideoxynucleotide (ddNTP) is incorporated at the 3′ end of the growing chain, chain

elongation is terminated selectively at A, C, G, or T because the chain lacks a 3′-hydroxyl group. When a mixture of dNTPs and ddNTPs are used, polymerisation will be terminated randomly at each possible site. Each ddNTP base is tagged with a different fluorescent dye (see Table 2.3), which emits light at a characteristic wavelength, thus the identity of the dye corresponds to the final base on that fragment. All four colours and therefore all four bases can be detected and distinguished in a single capillary injection of a DNA sequencer. When the DNA fragments reach a detector window in the capillary, a laser excites the fluorescent dye labels. Emitted fluorescence from the dyes is collected by a cooled, charge-coupled device (CCD) camera at particular wavelength bands and stored as digital signals for processing. Sequencing analysis software interprets the result, calling the bases from the fluorescence intensity at each data point.

ddNTP	Dye Label	Colour of Analysed Data
A	dR6G	Green
C	dROX	Blue
G	dR110	Black
T	dTAMRA	Red

Table 2.3. Fluorescent ddNTPs used in DNA sequencing.

2.7.1 Sequencing Reaction

PCR products were initially purified as described in Section 2.5. Sequencing reactions were then performed using the Big Dye Terminator (v2.0) Cycle Sequencing kit (Applied Biosystems) in a total volume of 10µl. Two reactions were performed for each PCR product; one using the PCR sense primer and one using the PCR anti-sense primer. The reaction mix and thermocycling conditions are detailed below.

Reaction mix

Terminator mix	4µl
Primer (3.2µM)	1µl
Purified PCR product	5µl

Thermocycling conditions

96°C	2min	
96°C	30sec	X 25 cycles
55°C	15sec	
60°C	4min	

2.7.2 Post-Sequencing Purification

To generate high quality DNA sequence data, unincorporated dye terminators, salt and any other small molecule contaminants must be removed from sequencing product prior to electrophoresis. This was achieved by gel filtration, using Sephadex G-50 Fine resin (Sigma) loaded MultiScreen HV filtration plates (Millipore, Tyne and Wear). Dry Sephadex G-50 was added to the 96 wells of the filtration plate using a Column Loader (Millipore). 300 µl of ddH_2O was added to each well to swell the resin and the plate was let stand at room temperature for 3 hours. When required, the filtration plate was placed on top of a 96-well plate and spun in a centrifuge at 2500 rpm for 5 min to remove excess water and pack the columns. Individual sequencing products were diluted with 10µl ddH_2O and were then added to the centre of individual columns. The filtration plate was placed on top of a fresh 96-well plate

and again spun at 2500 rpm for 5 min. The eluted sequencing products were dried in a speed vacuum.

2.7.3 Sample Electrophoresis

Purified sequencing products were resuspended in 10μl Hi-Di Formamide (Applied Biosystems, Cheshire) and were subsequently electrophoresed on an ABI PRISM® 3100 Genetic Analyzer using a 36cm capillary array and POP-6™ polymer. The resultant data was analysed with Sequence Analysis software (version 3.7) before being imported into Sequencher™ to identify polymorphisms.

2.8 Genotyping

Where possible, all SNPs identified were typed in pools and/or individually in an association sample. Two different genotyping methods were employed: primer extension using the ABI PRISM® SNaPshot™ Multiplex Kit (Applied Biosystems) and restriction fragment length polymorphism (RFLP) analysis.

2.8.1 SNaPshot Genotyping

The chemistry of the SNaPshot™ Multiplex Kit is based on the dideoxy single-base extension of an unlabelled oligonucleotide primer (or primers). Each primer binds to a complementary template (*i.e.* PCR product) immediately adjacent to the SNP of interest, in the presence of fluorescently labelled ddNTPs and DNA Polymerase. The polymerase extends the primer by one nucleotide, adding a single ddNTP to its 3′ end. Hence the identity of the base at the polymorphic position can be identified. The fluorescent dyes are assigned to the individual ddNTPs as shown in Table 2.4.

ddNTP	Dye Label	Colour of Analysed Data
A	dR6G	Green
C	dTAMRA	Black
G	dR110	Blue
T	dROX	Red

Table 2.4. Fluorescent ddNTPs used in SNaPshot genotyping.

2.8.1.1 Extension Primer Design

Since primer extension does not permit any flexibility with respect to the location of the 3′ end of the primer, it is important to assess the sequence flanking the SNP. The extension primers used here were designed using software designed by Dobril Ivanov (http://m034.pc.uwcm.ac.uk/FP_Primer.html). This software assesses the secondary structure of the PCR product and the accessibility of the SNP, in order to determine whether to use a primer complementary to the sense or anti-sense DNA strand.

2.8.1.2 Genotyping in DNA pools

Each DNA pool sample, as well as an individual sample heterozygous for the SNP of interest was PCR amplified in duplicate. PCR products were subsequently purified as described in Section 2.5. For optimisation purposes, a test primer extension reaction was initially performed on just one of the samples by combining 2μl purified PCR product with 2.5μl SNaPshot kit, 2.5μl buffer (200mM Tris-HCl, 5mM $MgCl_2$), 1μl 0.5μM extension primer and 2μl ddH_2O. The reaction mix was incubated at 94°C for 2 min and then was subject to 25 cycles of 94°C for 5s, 43°C for 5s and 60°C for 5s. To prevent unincorporated fluorescent ddNTPs obscuring the primer extension products during electrophoresis, the reactions were treated with 1 U shrimp alkaline phosphatase at 37°C for 1 hour followed by 15min at 80°C. Aliquots of 1μl

SNaPshot product and 9μl Hi-Di formamide were combined in a 96-well plate, which was loaded onto an ABI PRISM® 3100 Genetic Analyzer. Reactions were electrophoresed on a 36-cm capillary array using POP4 polymer. Electrophoresis data were processed using Genescan Analysis version 3.7 (Applied Biosystems). Peak heights of the allele-specific extended primers were determined by using Genotyper version 2.5 (Applied Biosystems). As Genescan Analysis is unable to accurately quantify fluorescence signals above 6000 units it is important to optimise reactions so as to generate peak heights between 2000 and 4000 fluorescence units. After measuring the height of the peak of the extension product in the test reaction, the concentration of the extension primer for the required peak height is simply calculated as $Y'/(Y/X)$ where, Y' is the required peak height (*e.g.* 3000), Y is the initial peak height and X is the initial primer concentration (*e.g.* 0.5μM)[192]. Primer extension was then performed on all samples using the optimised primer concentration. The allele frequency in each pool was determined as the mean of the two primer extension assays performed for each PCR replicate, corrected for the degree of unequal allelic representation detected in a heterozygote as described below.

2.8.1.3 Correction for Unequal Allelic Detection

For a biallelic marker, the primer extension products for each allele are not equally represented. Possible explanations include differential PCR amplification of alleles[193] and differential efficiencies of the incorporation of the ddNTPs for each allele-specific reaction[194]. An additional explanation is the unequal emission energies of the different fluorescent dyes[192]. In order to allow for unequal representation of alleles, the estimated allele frequencies from pools were corrected by using the mean of the

ratios obtained from two analyses of a heterozygote as given by the equation: Frequency of allele $A = A/(A+kB)$ where A and B are the peak heights of the primer extension products representing alleles A and B in pools and k is the mean of two replicates of A/B ratios observed in a heterozygote[195].

2.8.1.4 Troubleshooting in SNaPshot Genotyping

As mentioned previously, an optimisation step was initially performed to calculate the required concentration of the extension primer, but this step was also used to assess the suitability of the primer for genotyping analysis. A negative control (lacking DNA template) was always run concurrently. If extraneous peaks were observed in the test reaction, then the experiment was repeated using fresh exonuclease I and shrimp alkaline phosphatase in the purification stages, to ensure adequate removal of PCR primers, dNTPs and fluorescent ddNTPs. However, when extraneous peaks were also observed in the negative control, then this was likely due to extension primer hairpin extension or extension primer dimer extension, and where possible, an alternative extension primer was designed. In the pooled analysis, the allele frequency in each pool was determined as the mean of the two primer extension assays performed for each PCR replicate. Had a large discrepancy been observed between the peak height ratios of two replicates, then the entire experiment would have been repeated from the PCR stage. However, replicates gave remarkably consistent results throughout, with in general no more than a 1% difference observed between the two samples. This suggests that not much variation is introduced at the PCR stage and the use of replicates may only be required to detect errors introduced by factors such as inaccurate pipetting, PCR dropouts *etc.*

2.8.2 Restriction Fragment Length Polymorphism (RFLP) Genotyping

For biallelic SNPs requiring individual genotyping, a restriction enzyme was chosen that could distinguish between the two alleles when an appropriate PCR amplimer was digested and electrophoresed on an agarose gel. Where no natural restriction site existed, it was necessary to create a site by primer-generated mutagenesis. With an assay designed, the required association sample was amplified by PCR as previously described. Products were then digested for 16 hours with 5 units of restriction enzyme in the presence of the appropriate restriction buffer (as supplied by the manufacturer of the enzyme) and 1X BSA, if required, at the appropriate temperature. Digested products were electrophoresed on 2.5%-3.0% agarose gels.

2.8.2.1 *APOE* Genotyping

The MRC association sample was *APOE* genotyped by Luke Jehu. As this data was used in the ADAM12 study (Chapter 5), the protocol for APOE genotyping will be described here. PCR primers were 5'-TCCAAGGAGCTGCAGGCGGCGC-3' (sense) and 5'-ACAGAATTCGCCCCGGCCTGGTACACTGCC-3' (antisense) to generate a 227bp fragment. Amplification was performed using 1X PCR buffer (Qiagen), 1X Q-solution (Qiagen), 1.5 mM $MgCl_2$, 250 μM dNTPs, 0.5 μM of each primer, 0.3 units Taq (Qiagen) and 18 ng genomic DNA in a 12 μl reaction. Cycling was conducted in a MJ Tetrad (MJ Research) with an initial denaturation of 94°C for 3min, followed by 35 cycles of 94°C for 30s, 66°C for 30s and 72°C for 1 min with a final extension step of 72°C for 10 min. PCR products were then digested for 16 hours with 5 units of *Hha* I in the presence of the appropriate restriction buffer (as supplied by the manufacturer of the enzyme) and 1X BSA at 37°C. Digested products were electrophoresed on 3.0% agarose gels. The expected genotype patterns

are displayed in Figure 2.1. The tables below display the distribution of *APOE* genotypes in the MRC sample. The ε4 allele, which is reasonably common in the general population, has a substantial effect size (OR=3.9).

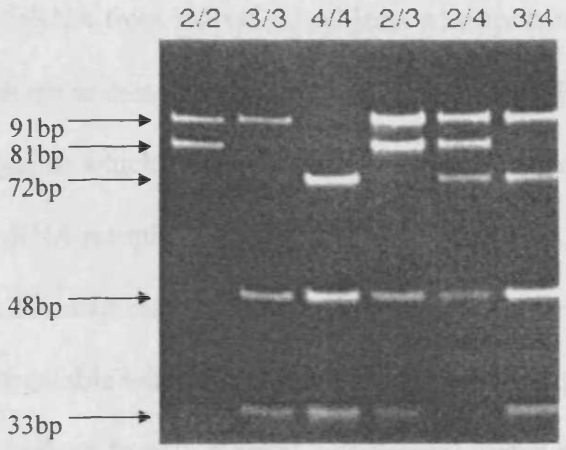

Figure 2.1. Examples of *APOE* genotypes. A gel is shown after electrophoresis of *Hha* I fragments from an ε2/ε2 homozygote, ε3/ε3 homozygote, ε4/ε4 homozygote, ε2/ε3 heterozygote, ε2/ε4 heterozygote and ε3/ε4 heterozygote. The fragment sizes are shown to the left of the gel. Note that three fragments common to each genotype are not observed due to their small size (21bp, 18bp and 16bp).

APOE	**ε Genotype**						***P***
	2/2	**2/3**	**2/4**	**3/3**	**3/4**	**4/4**	
Patients	2 (0.004)	24 (0.04)	26 (0.05)	176 (0.32)	244 (0.45)	71 (0.13)	
Controls	2 (0.004)	79 (0.15)	11 (0.02)	324 (0.60)	115 (0.21)	11 (0.02)	**0.0000**

Table 2.5. Association of *APOE* genotype with LOAD in the MRC sample of 546 cases and 546 controls. Genotype counts and frequencies are shown.

APOE	**ε Allele**			**Odds Ratio for ε4 allele (95% C.I.)**	***P***
	2	**3**	**4**		
Patients	54 (0.05)	620 (0.57)	412 (0.38)	3.8659	
Controls	94 (0.09)	842 (0.78)	148 (0.14)	(3.1263-4.7804)	**0.0000**

Table 2.6. Association of *APOE* genotype with LOAD in the MRC sample of 546 cases and 546 controls. Allele counts and frequencies are shown.

2.9 Allele Specific Expression

To investigate potential *cis*-acting influences on gene expression, it is possible to use SNPs within an expressed sequence as a tag for mRNA transcribed from each chromosomal allele. It is then possible to apply quantitative methods of allele discrimination to mRNA from individual subjects who are heterozygous for the marker polymorphism to measure relative allelic expression. Each allele serves as an internal control against which expression of the other allele can be measured within each individual mRNA sample, thereby enabling detection of genuine *cis*-acting phenomena that affect expression, while controlling for *trans*-acting confounders[196]. 60 samples were available with which to investigate allelic expression. *Post-mortem* brain tissue derived from frontal, parietal, or temporal cortex of these 60 unrelated, anonymous human adults was obtained from three sources (The MRC London Neurodegenerative Diseases Brain Bank, United Kingdom; The Stanley Medical Research Institute Brain Bank, Bethesda; The Karolinska Institute, Stockholm). Subjects were drawn principally from psychiatric control groups. From each individual, approximately 500 mg of tissue was processed for genomic DNA, by use of standard phenol/chloroform procedures and approximately 300–500 mg of tissue was processed for total RNA, by use of the RNAwiz isolation reagent (Ambion, Huntingdon). Total RNA was treated with DNAse prior to reverse transcription (RT), which was performed by use of the RETROscript kit (Ambion). DNA/RNA extraction and reverse transcription was kindly performed by Nick Bray.

These samples were amplified by use of primers that were based on single exonic sequence, capable of amplifying either cDNA or genomic DNA. Genomic DNA from all subjects was initially genotyped to identify heterozygotes for the marker

polymorphism. The corresponding cDNA samples were assayed twice as two separate RT reactions alongside the corresponding genomic DNA samples. The same analytic conditions were used for genomic DNA and cDNA to enable use of the average of the ratios observed from genomic DNA (as a perfect 1:1 ratio of the two alleles) to correct allelic ratios obtained from cDNA analyses for any inequalities in allelic representation specific to each assay[195]. When a difference in allelic expression was observed, this entire process was repeated to confirm the initial observation.

Allelic representation was measured by use of the SNaPshot™ primer extension method described previously. Peak heights of allele-specific extended primers were determined by the use of Genotyper version 2.5 (Applied Biosystems). The ratio of cDNA peak heights, corrected by use of the average genomic ratio from all heterozygous samples, was used to calculate relative expression of the two alleles in each individual sample.

2.10 Statistical Analyses

For the DHPLC mutation screening set, power was calculated using the equation: $1-(1-f)^n$, where f = allele frequency and n = number of chromosomes examined. Therefore, a screening set of 28 chromosomes (14 individuals) has 95% power to detect an allele with a frequency of 10%. Power and sample size requirements for case-control samples were calculated using the Power Calculator at the UCLA department of statistics website (http://calculators.stat.ucla.edu/powercalc). Pearson's $\chi 2$ and Fisher's exact test were used to analyse SNP associations using the Simple Interactive Statistical Analysis website (http://home.clara.net/sisa); Fisher's exact test

was used for analyses where one or more cell had a count of <5. Odds ratios and 95% confidence intervals were also calculated using the Simple Interactive Statistical Analysis website. All polymorphisms typed individually were tested for deviation from Hardy-Weinberg equilibrium using an updated version of the HW program written by Peter McGuffin and Peter Holmans (update by Marian Hamshere). Haplotypic association was tested using EHPLUS with PMPLUS implemented to obtain empirical significance levels[197]. The EHPLUS software was modified by Marian Hamshere and Valentina Moskvina. The square of the correlation coefficient (r^2) was used to determine the levels of linkage disequilibrium between polymorphisms. This was also calculated using the modified EHPLUS program. Meta-analyses were carried out using the Woolf program written by Peter McGuffin. Heterogeneity between studies was assessed with a $\chi 2$ test.

3. INVOLVEMENT OF THE CHOLINERGIC GENE LOCUS IN LOAD

3.1 ChAT and VAChT

Choline acetyltransferase, ChAT, is the enzyme responsible for the synthesis of the neurotransmitter acetylcholine (ACh), which mediates cholinergic neuron communication. ACh is synthesised in the cytoplasm of cholinergic nerve terminals and is then translocated into synaptic vesicles by the action of the vesicular acetylcholine transporter, VAChT. After exocytotic release from the nerve terminal, ACh can bind to two classes of ACh receptor (AChR), muscarinic and nicotinic AChRs. ACh is hydrolysed to produce choline by the action of acetylcholinesterase (AChE). This process is displayed in Figure 3.1 (p.69).

3.1.1 The Cholinergic Gene Locus

The genes encoding ChAT and VAChT, *CHAT* and *SLC18A3* respectively, are expressed from the same locus on chromosome 10q11.2, referred to as the cholinergic gene locus. The genomic organisation of these two functionally related genes is unusual in that the entire *SLC18A3* gene lies within the first intron of *CHAT* in the same transcriptional orientation, implying that the two genes may be coregulated to some extent. Indeed, coordinated upregulation of *CHAT* and *SLC18A3* transcripts by various extracellular factors such as leukaemia inhibitory factor, ciliary neurotrophic factor, retinoic acid, cAMP, glucocorticoids and nerve growth factor has been demonstrated[198-204]. The single *CHAT* gene produces multiple transcripts as a result of alternative splicing. Five isoforms of ChAT mRNA have been identified to date, termed R, N1, N2, S and M. All five mRNAs translate into a 69-kDa form of the enzyme, with the M and S transcripts also encoding 82- and 74-kDa proteins

respectively, because of the presence of two translation initiation sites in these transcripts[205, 206].

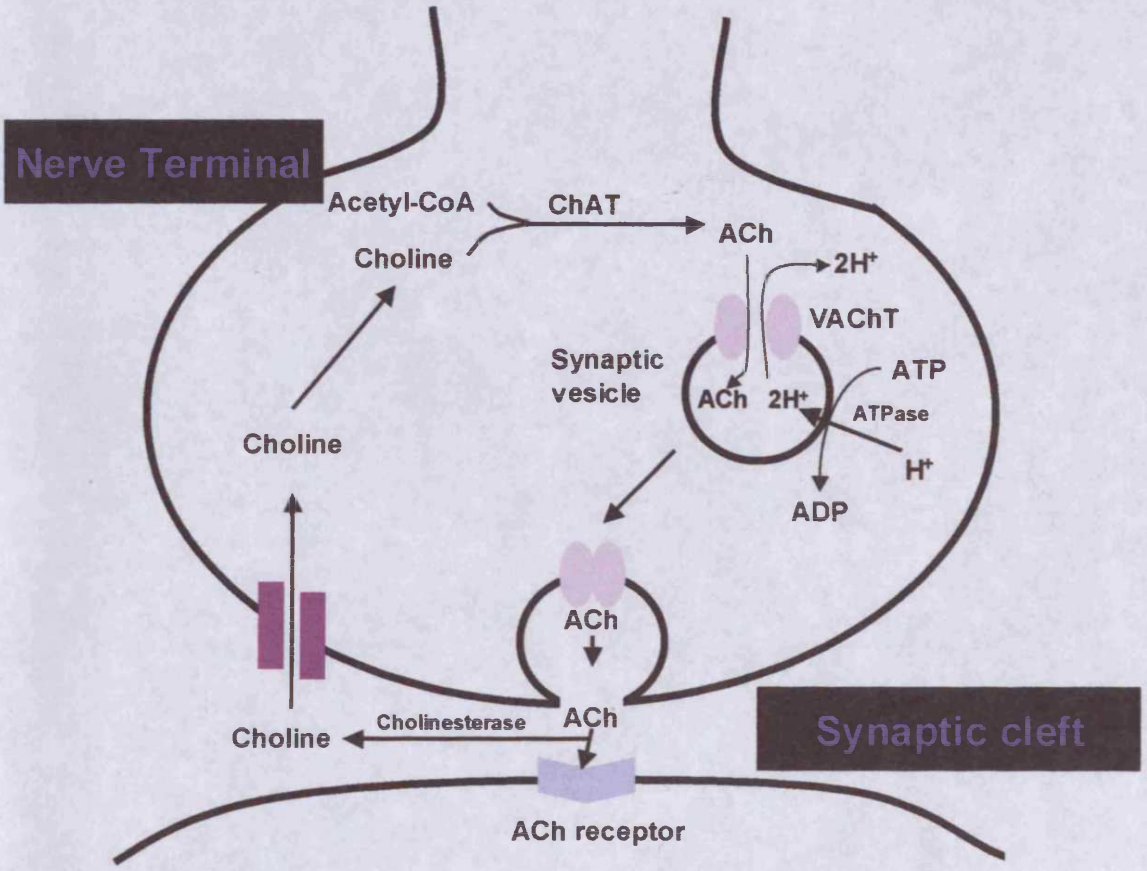

Figure 3.1. The synthesis of ACh. Choline is transported into the nerve terminal by a high affinity choline transporter. ACh is synthesised from choline and acetylcoenzyme A by ChAT and is then transported into the synaptic vesicle by VAChT, which uses the electrochemical gradient generated by a proton ATPase to exchange two protons by one ACh molecule. After exocytotic release from the nerve terminal, some ACh molecules are hydrolysed by AChE before they bind to the AChR and the remaining ACh molecules are hydrolysed by AChE after dissociation from AChR.

3.1.2 Subcellular Localisation of ChAT and VAChT

The ChAT enzyme exists in at least two forms in cholinergic nerve terminals; a soluble form (80-90% of the total enzyme activity) and a non-ionically membrane bound form (10-20%)[207]. The nature of the membrane association and significance of this enzyme pool are unknown. The 82-kDa form of ChAT contains two functional nuclear localisation signal (NLS) motifs, resulting in this isoform having a predominantly nuclear subcellular distribution[208]. The subcellular localisation of the 74-kDa form of ChAT has not been determined. The 69-kDa form of ChAT is a nucleocytoplasmic shuttling protein with a predominantly cytoplasmic localisation determined by a functional NLS and an unidentified putative nuclear export signal[209]. VAChT is predominantly, if not only, present in synaptic vesicles[210, 211].

3.1.3 Cholinergic Neurons

Cholinergic neurons are distributed widely throughout the central and peripheral nervous systems where they are involved in motor function, the autonomic nervous system and various integrative brain functions such as learning and memory[212]. They are aggregated in eight major groups: Ch1-Ch8[213]. In the human brain, cholinergic neurons are detected in the medial septal nucleus (Ch1), nucleus of the diagonal band of Broca (Ch2 and Ch3), the basal nucleus of Meynert (Ch4), the caudate nucleus, the putamen, the nucleus accumbens, the pedunculopontine tegmental nucleus (Ch5), the laterodorsal tegmental nucleus (Ch6), the medial habenular nucleus (Ch7), the parabigeminal nucleus (Ch8), some cranial nerve nuclei and the anterior horn of the spinal cord[213]. These pathways are displayed in Figure 3.2 (p.71).

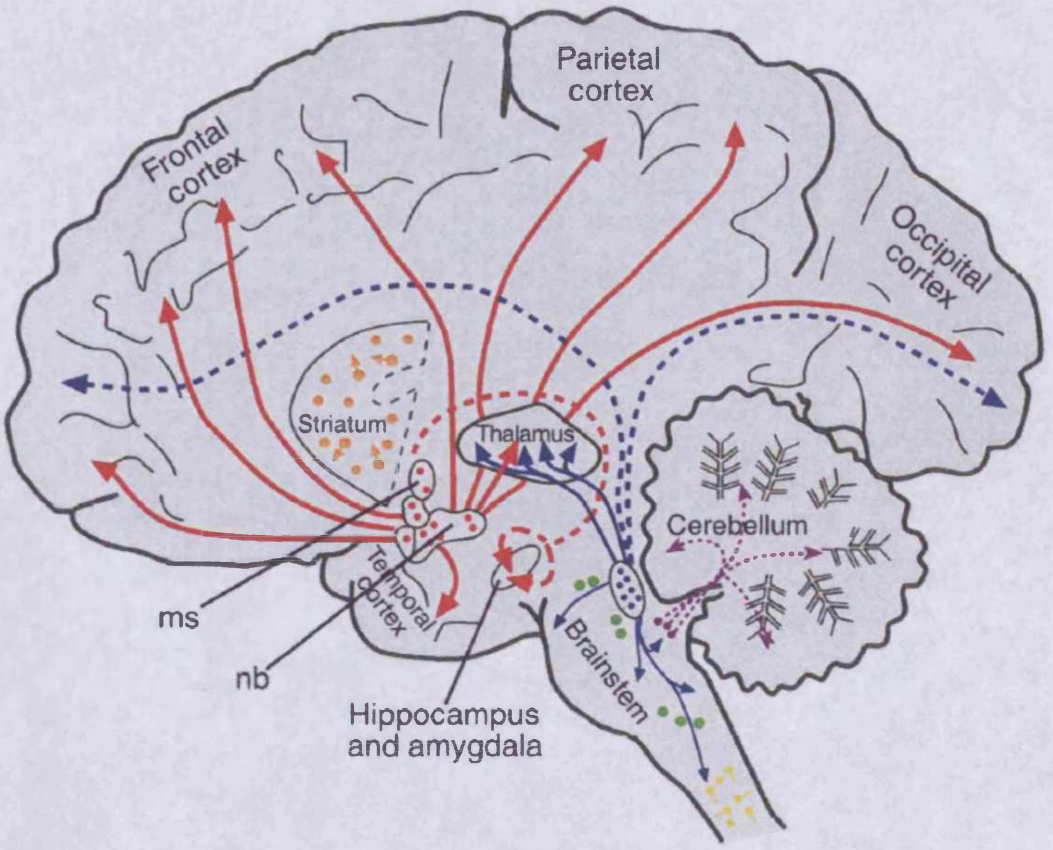

Figure 3.2. Cholinergic systems in the human brain. Two major pathways project widely to different brain areas: basal-forebrain cholinergic neurons [red, including the nucleus basalis (nb) and medial septal nucleus (ms)] and pedunculopontine–lateral dorsal tegmental neurons (blue). Other cholinergic neurons include striatal interneurons (orange), cranial-nerve nuclei (green circles), vestibular nuclei (purple); and spinal cord preganglionic and motoneurons (yellow). Taken from Perry *et al.*, 1999[214].

3.1.4 The Cholinergic Hypothesis

The "cholinergic hypothesis of geriatric memory dysfunction" was formulated twenty-two years ago and postulates that a loss of cholinergic function in the central nervous system contributes significantly to the cognitive decline associated with advanced age and AD[215]. This hypothesis is based on several lines of evidence. In 1974, Drachman and Leavitt[216] observed that scopolamine, a muscarinic receptor antagonist, could induce amnesia in young healthy human subjects comparable with that seen in (nondemented) elderly individuals. These deficits could be reversed by

acetylcholinesterase inhibitors. A number of subsequent reports have found that systemic administration of cholinergic receptor antagonists interferes with performance on a variety of memory tasks in both rodents and non-human primates[217-220]. Additional evidence supporting the cholinergic hypothesis came from three biochemical studies reporting that the brains of patients with severe AD exhibit a significant loss of ChAT activity, which is apparently correlated with the degree of cognitive impairment[221-223]. The loss in ChAT activity is generally consistent with a reduction in the number of basal forebrain cholinergic neurons[224-226]. Dysfunction of the basal forebrain cholinergic neurons that innervate the cerebral cortex and hippocampus is now a well-established feature of AD and results in a decrease in ChAT and AChE in these terminal fields[227-229]. These basal forebrain cholinergic neurons appear to be significantly more vulnerable than even the nearby neostriatal cholinergic neurons[230]. Decline in ChAT activity has been positively correlated with psychometric, clinical and pathological (density of senile plaques, neuritic plaques and neurofibrillary tangles) indexes of dementia severity[229, 231-233]. On the basis of this collective evidence, drugs that potentiate central cholinergic function (*e.g.* AChE inhibitors) have been developed and have thus far proven to be the most effective forms of therapeutic treatment against the disease. However, it should be noted that such cholinomimetic replacement strategies have only met with limited success in alleviating the cognitive deficits in AD[234, 235].

There have been some challenges to the validity of the cholinergic hypothesis on the basis of recent reports using AChE or ChAT assays, which indicate that there is little or no loss of enzyme activity in the brains of patients diagnosed with mild cognitive impairment and/or mild AD[236, 237]. These studies propose that the cholinergic deficit

occurs only late in the disease. However, neither ChAT nor AChE are rate-limiting enzymes for synthesis and degradation of ACh and the actual functional state of the cholinergic system may not be reflected well by these markers. A number of factors could be compromised in cholinergic neurons before changes in these enzymes would be observed, some of which are discussed below.

3.1.5 The Nature of Cholinergic Dysfunction in AD

It has been reported that there are alterations in nicotinic AChR expression levels (predominantly α4 nicotinic receptors) in AD brain regions such as the hippocampus and cortex[238-240]. [^{11}C]Nicotine-based PET studies indicate that nicotinic receptor deficits are an early phenomenon in AD and suggest that cortical nicotinic receptor deficits significantly correlate with the level of cognitive impairment[241]. It has also been shown that α7 nicotinic AChRs, which are known to be involved in numerous processes, including neurotransmitter release[242], long-term potentiation[243, 244] and learning[245, 246], can serve as high-affinity binding sites for Aβ peptides[247]. Moreover, Aβ peptides can block the functional interaction of nicotinic agonists with their receptors on hippocampal neurons[248].

Most studies suggest that there are no differences in the number of muscarinic receptors between Alzheimer and control brains[249, 250]. However, there is some evidence for a disruption of the coupling between the muscarinic M1 receptors, their G-proteins and second messenger systems[250-252]. A number of *in vitro* studies have shown that activation of the M1 muscarinic receptor stimulates the non-amyloidogenic, α-secretase pathway of APP processing, resulting in elevated α-APPs and decreased Aβ levels[59, 253-256]. M1 agonists also decrease τ protein

phosphorylation *in vitro* and *in vivo*[257, 258]. Therefore, a disruption in M1 signalling may lead to increased Aβ levels and phosphorylation of τ with a concurrent loss of the synaptotrophic α-APPs.

There is a large amount of evidence indicating that Aβ can negatively regulate various steps in the synthesis and release of ACh from basal forebrain cholinergic neurons[259-264]. Indeed, low concentrations of Aβ reduced the high-affinity choline uptake (the rate-limiting step in ACh synthesis) and acetylcholine release in slices from rat hippocampus and cortex, but not from striatum. In contrast, Aβ had no effect on ChAT activity in hippocampal or cortical slice preparations[259, 260].

Cholinergic neurons are highly dependent upon nerve growth factor (NGF) for their function[265-268] and use high-affinity tyrosine receptor kinase A (trkA) and low-affinity (p75) receptors for signalling. The importance of NGF in the brain has been underlined by the work of Capsoni and colleagues (2000)[269], who have generated a transgenic mouse that expresses a neutralizing monoclonal antibody against NGF. In aged mice, brain pathology exhibits remarkable similarities to the pathology seen in progressive AD, including amyloid plaques, hyperphosphorylated τ, abnormalities of the neuronal cytoskeleton reminiscent of tangles and marked cholinergic neuron degeneration. In individuals with AD, there is typically a marked loss of high-affinity trkA receptors, which correlates with a loss of cholinergic neurons[270-272]. In basal forebrain cholinergic neuron target regions, including the hippocampus, NGF protein and expression levels are normal or increased[273-278] but NGF levels in the basal forebrain nuclei are reduced[279, 280]. Together, these data suggest that retrograde transport of NGF from target regions is impaired in AD.

Therefore, cholinergic dysfunction and Aβ deposition interact in a complex manner. A hypothetical model is proposed: in AD, cholinergic neurotransmission is negatively affected by a loss of α4 nAChRs and disruption of M1 AChR signalling. Aβ can also have a detrimental effect on cholinergic neurotransmission by blocking α7 nAChR signalling and reducing high-affinity choline uptake and ACh release. Reduced cholinergic activity can in turn lead to increased τ phosphorylation and enhanced Aβ production via disrupted M1 signally and therefore a feedback loop is initiated. A loss of the synaptotrophic α-APPs contributes to cholinergic degeneration. This leads to a loss of the high affinity NGF trkA receptors, which exacerbates cholinergic hypofunction via dysfunctional neurotrophin support. This model therefore encompasses many of the characteristic features of AD: cholinergic degeneration, enhanced Aβ production and increased τ phosphorylation.

Considering their key roles in cholinergic neurotransmission, the products of the cholinergic gene locus are good candidates for involvement in the pathogenesis in AD. As the cholinergic gene locus maps to 50.7Mb on chromosome 10, within a region showing substantial evidence for a susceptibility gene for LOAD[144, 146], these genes are excellent functional and positional candidates for influencing susceptibility to LOAD.

In order to test whether allelic variation in *CHAT* and *SLC18A3* confers susceptibility to LOAD, these two genes were screened for sequence variants, which were subsequently examined in LOAD case-control samples from the UK.

Much of the SNP discovery work on the *CHAT* gene was performed by Tim Peirce, an undergraduate placement student working under my supervision. The genotyping of all polymorphisms was a joint effort.

3.2 Materials and Methods

Described here are the specific methods used to study the cholinergic gene locus. More detailed descriptions of subject groups and methods are described in Chapter 2.

3.2.1 Subjects

The mutation screening sample consisted of 14 UK Caucasian patients, with age at onset >65 years. For the association study, the Cardiff sample comprising 133 UK Caucasian AD patients (age at onset 72.9±6.5 years) and 135 age-matched controls (age at collection 78.1±7.2 years) was employed. Two additional association samples were used for replication purposes; a subset of the MRC sample consisting of 135 UK Caucasian AD patients (age at onset 74.3±6.2 years) and 135 age- and sex-matched controls (age at collection 75.3±6.4 years) and the Belfast sample consisting of 242 Northern Irish Caucasian AD patients (age at onset 75.4±8.1 years) and 235 age-matched controls (age at collection 74.7±8.1 years). All patients were diagnosed according to NINCDS-ADRDA criteria[17]. Cognitive function of controls was assessed using the mini mental-state exam (MMSE)[18]. Only those with a score of at least 28 were included in the study.

3.2.2 Collection of Gene Sequences

The *CHAT* gene exists as five splice variants; M, N1, N2, R and S. The *SLC18A3* gene is located within the first intron of the R variant of *CHAT* and is itself

uninterrupted by introns (see Figure 3.3, p.83). The cDNA sequence for each splice variant/gene was obtained from the GenBank database at NCBI (http://www.ncbi.nlm.nih.gov). The specific cDNA accession numbers are as follows: M *CHAT* = NM_020549.2; N1 *CHAT* = NM_020985.1; N2 *CHAT* = NM_020986.1; R *CHAT* = NM_020984.1; S *CHAT* = AF305908.2; *SLC18A3* = NM_003055.1). Determination of coding sequences, untranslated regions (UTRs) and intronic regions was based on alignment of the cDNA sequences against genomic sequence available from the UCSC Genome Bioinformatics Site (http://genome.ucsc.edu), using BLAST sequence homology searches.

3.2.3 Polymerase Chain Reaction (PCR)

PCR fragments spanning exons, UTRs and limited 5' flanking regions were designed using Primer 3.0 (http://www-genome.wi.mit.edu/cgi-bin/primer/primer3_www.cgi). Primer sequences are listed in Table 3.1 (p.79). PCR amplification was performed under standard conditions of 1X PCR buffer (Qiagen), 1.5 mM $MgCl_2$, 250 μM dNTPs, 0.5 μM of each primer, 0.6 units Hot Star Taq (Qiagen) and 48 ng genomic DNA in a 24 μl reaction. Cycling was conducted in a MJ Tetrad (MJ Research) with an initial denaturation of 94°C for 15min, followed by 35 cycles of 94°C for 30s, optimal annealing temperature for 30s (see Table 3.1, p.79) and 72°C for 45s with a final extension step of 72°C for 10 min. Synthesis of appropriately sized PCR products was confirmed by electrophoresis on 1.5% agarose gels. In the case of one fragment, (ChAT xM; see Table 3.1, p.79), the fragment size (1007bp) was too large for DHPLC. Therefore PCR products from each individual in the mutation screening set were digested with the enzyme *Sma* I to generate two smaller fragments of 600 and 407bp. These fragments were separated by agarose gel electrophoresis, followed

by gel extraction using the QIAquick Gel Extraction kit (Qiagen) according to the manufacturers instructions. Separated fragments were resuspended in PCR buffer prior to DHPLC.

Fragment name	Spanning	Sense Primer Sequence (5'→3')	Antisense Primer Sequence (5'→3')	Size (bp)	Annealing Temperature (°C)
ChAT R Prom	5'Flanking region of R variant (*CHAT*)	GGGAGACTCACCTTCCTTCTG	AGTCACAATGCCCACCTAGC	668	64
ChAT xR	Exon R (*CHAT*)	CTGGAAGAGAGACGCAAACC	GTGGGCTCTGGAGTGACTGT	356	64
VAChT Prom	5'Flanking region of *SLC18A3* gene	GTCGGCTCTTGCCTCCTC	GAGTCGGAGAAAGGGTTGG	560	62
VAChT 1	Part of *SLC18A3* exon	GCATTAGCATGAGCGACGTA	CACAGCCTCCGACAGCTT	603	60
VAChT 2	Part of *SLC18A3* exon	GACAGCCTCCCCGAAGTC	GCTCAAGGGGTTCACTAGCA	525	64
VAChT 3	Part of *SLC18A3* exon	GAAGATCGGGGTGCTGTTT	GGCAATGTAGGGGTCTAGCA	511	64
VAChT 4	Part of *SLC18A3* exon	GTGGGCACTCCCATCCAC	CTCAAAGCCCAGCGAGTG	516	64
VAChT 5	Part of *SLC18A3* exon	ATCTCCTATTCGGTGGCCTA	GGATATGGAACGGGTCACAG	492	64
VAChT 6	Part of *SLC18A3* exon	CTAGCATCCCCACTCCTCCT	GGACTTGGAGACCCAGTTCA	468	64
ChAT N PROM	5'Flanking region of N variant (*CHAT*)	AGCCTGCATCTGTCTGTCCT	CTTTCTCAAAGGCCTCAACG	513	60
ChAT xN	Exon N (*CHAT*)	GCCCAGGATAGACCCTCTTT	ATCCCACACTCGCATCTCTC	401	62
ChAT M Prom	5'Flanking region of M variant (*CHAT*)	CTCAGCATTTCCCAGTCACC	CAGGGTCGCCTGTGTGTTAG	519	64
ChAT xM	Exon M (*CHAT*)	CGCAGTCCTTAAGCATCCTC	GGGCCAAGTGAAGTGAGAAC	*1007	60
ChAT E1 Prom	Putative cis-acting regulatory regions	CTGCCTTAGTCTGGGGAGAG	ACCTGACCTTGTCCTTGCTG	553	64
ChAT E2 Prom	Putative cis-acting regulatory regions	CCCCAACTGCAAAGTGAAAG	CTAGTCGGAGGGTCCTTGG	551	62
ChAT xS	Exon S (*CHAT*)	TGCCTGGAACCCAATAGATAAG	CTCCCAATTAGCCCAGATGC	238	60
ChAT x5	Exon 5 (*CHAT*)	TCAGCACGTACAGGTGGAAG	ATTTCCTTGGCACCCTGAG	497	55
ChAT x6	Exon 6 (*CHAT*)	GGGACAGAGCACAATGAGGT	CCTTCTGCCCTGTCTTTGTC	499	59
ChAT x7	Exon 7 (*CHAT*)	AAGCTCCTGGCACATACCTG	GTGTCCATTCCACTGCAAGA	504	59
ChAT x8	Exon 8 (*CHAT*)	AGTGCAGGAACCACATCTGA	GATCAAGGAAGGATGGTGCT	501	62
ChAT x9	Exon 9 (*CHAT*)	CCATGATGATGCAGTTCTGG	GGCAACTGGTGGAGAGACAT	493	62
ChAT x10	Exon 10 (*CHAT*)	GTGGAATCCAGCACAGTCAA	GCTCCCACACTATGGCTGAT	471	59
ChAT x11	Exon 11 (*CHAT*)	TTCTGGCTGGTCCAGAGATT	CCTGGGTCTTGTTGTGATCC	503	59
ChAT x12	Exon 12 (*CHAT*)	TGACTGCCGTAAATCTGCTG	ATTCTCAGGCCACTGCAATC	502	60
ChAT x13	Exon 13 (*CHAT*)	AGCAAGGTTATTTCCCCAGA	GATTTTGGTGGCCTCTCTGA	503	58
ChAT x14	Exon 14 (*CHAT*)	CCCAGTTCAGTCTGCTCCTC	TAGTCCTGGCCTGGTTTGTC	488	60
ChAT x15	Exon 15 (*CHAT*)	GGTTTAAAAGGCTGCTTGGA	CCCCGGGTGTATATAAGCAA	482	60
ChAT x16	Exon 16 (*CHAT*)	TTCCCCTCACAGTTGACTCC	CAGTGAGGCTGCTGTGGTT	500	59
ChAT x17	Exon 17 (*CHAT*)	CATGGTAGAGCGGTCAGTCC	CCAAGCCTGGTCAGTAAACC	495	59
ChAT x18	Exon 18 (*CHAT*)	CCCAGGTGGAAAACAGAGAA	CTCCTAACACTCCGGCTCTG	520	60

Table 3.1. Details of *CHAT* and *SLC18A3* PCR assays for the purpose of DHPLC, including PCR primers, annealing temperatures and size of amplimers.
*This fragment was digested into two smaller fragments (600 and 407bp) with *Sma* I. These smaller fragments were separated and analysed individually.

3.2.4 Denaturing High Performance Liquid Chromatography (DHPLC)

The search for polymorphisms was performed by DHPLC scanning on the Wave™ DNA Fragment Analysis System (Transgenomic). The 14 screening samples were amplified as described above, except the final extension in the PCR protocol was followed by denaturation at 94°C for 5min and then cooling to 54°C over 40min, to allow heteroduplex formation. Column temperature and acetonitrile gradient were determined with the DHPLC Melt program (http://insertion.stanford.edu/melt1.html). To ensure maximum sensitivity, in addition to the (highest) temperature suggested by the software (n°C), each fragment was also run at n+2°C. The resultant chromatograms were compared, with a shift in trace pattern indicative of a heteroduplex. An example of a DHPLC trace is displayed at the end of this chapter (Figure 3.4).

3.2.5 DNA Sequencing

For fragments that displayed a heteroduplex peak, the PCR products of one heterozygous and one homozygous sample were incubated at 37°C with 1 unit each of shrimp alkaline phosphatase and exonuclease I to remove unincorporated primers and dNTPs. Purified products were then bidirectionally sequenced on an ABI 3100 Genetic Analyzer (Applied Biosystems) using the Big Dye Terminator (v2.0) Cycle Sequencing kit (Applied Biosystems). Sequence traces were subsequently exported to the Sequencher™ program in order to characterise polymorphisms. Sequence chromatograms for all SNPs identified are displayed at the end of this chapter (Figures 3.5 to 3.21).

3.2.6 Genotyping

SNPs: Where a natural restriction site existed that could distinguish between the two alleles of a SNP, a restriction fragment length polymorphism (RFLP) assay was designed, using the original PCR primers. Where no natural site existed, an artificial restriction site was created by primer-generated mutagenesis (see Table 3.3, p.85). For each RFLP assay, the Cardiff association sample was PCR amplified, then digested with 5 units of the appropriate restriction enzyme (see Table 3.3, p.85). Digested products were electrophoresed on 2.5-3% agarose gels.

VNTR: The VNTR was typed by PCR amplification followed by visualisation on a 1.5% agarose gel.

Examples of the expected profile for each genotype of a polymorphism are shown at the end of this chapter (Figures 3.5 to 3.21).

3.2.7 Statistical Analyses

All SNPs were tested for deviation from Hardy-Weinberg equilibrium independently in each population using an updated version of the HW program written by Peter McGuffin and Peter Holmans (update by Marian Hamshere). Pearson's $\chi 2$ and Fisher's exact test were used to analyse SNP associations using the Simple Interactive Statistical Analysis pages (http://home.clara.net/sisa). Fisher's exact test was used for analyses where one or more cell had a count of <5. The VNTR was tested for association with LOAD using CLUMP[281]. Haplotypic association was tested using EHPLUS with PMPLUS implemented to obtain empirical significance levels[197]. The EHPLUS software was modified by Marian Hamshere and Valentina Moskvina. The square of the correlation coefficient (r^2) was used to determine the

levels of linkage disequilibrium between SNPs. This was also performed using the modified EHPLUS program. Meta-analyses were carried out using the Woolf program written by Peter McGuffin. Heterogeneity between studies was assessed with a $\chi 2$ test.

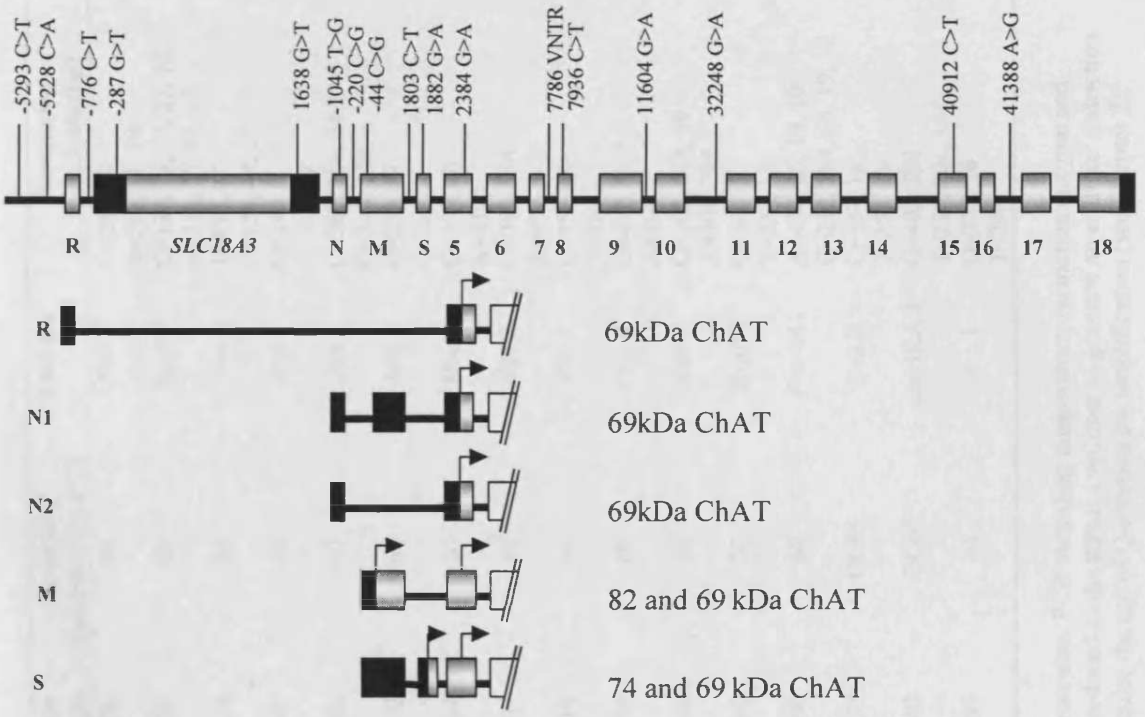

Figure 3.3. Genomic structure of the *CHAT* and *SLC18A3* genes and the 17 identified polymorphisms. Dark shading indicates untranslated regions. Arrows indicate translational start sites. For *CHAT*, nucleotide numbers start from the translational start site of the 82-kDA splice variant (M) of the gene. Similarly, numbering starts from the translational start site of *SLC18A3* for variants detected in this gene.

Variant	Location	Variant Sequence Information	dbSNP Identity	Typing Assay
CHAT				
-5293 C>T	198bp upstream exon R	GGGTGGGGGG**Y**ACAATGGGAG	rs733722	RFLP
-5228 C>A	133bp upstream exon R	TGGGAAGGCT**M**CCCTCTGACT		RFLP
-1045 T>G	Exon N (5'UTR)	AGTAGGAGCC**K**AGCATTCCGG	rs3729496	RFLP*
-220 C>G	40bp upstream exon M	AGACCCAACC**S**TCTCCAGGAT	rs3810948	RFLP*
-44 C>G	Exon M (5'UTR)	GGTAGATTCT**S**GGGGCCGGGA		RFLP
1803 C>T	31bp upstream exon S	CATTCACCCA**Y**GCATGCATTC		RFLP*
1882 G>A	Exon S (Asp→Asn)	GGAATGCAGA**R**ATGAAGCACT	rs1880676	RFLP*
2384 G>A	Exon 5 (Ala→Thr)	CCGTAAGATG**R**CAGCAAAAAC	rs3810950	RFLP
7786 VNTR	57-122bp upstream exon 8	See text		PCR sizing
7936 C>T	Exon 8 (Leu→Phe)	CTCTGGTGTA**Y**TCAGCTACAA	rs868750	RFLP
11604 G>A	140bp downstream exon 9	TCCAAAGTGG**R**GCCCCTACTT	rs2377871	RFLP
32248 G>A	68bp upstream exon 11	GCCCTGTGTG**R**GGCTCTGAGG		RFLP
40912 C>T	Exon 15 (His→His)	GCAGGCTCCA**Y**CGAAGACTGG		RFLP*
41388 A>G	129bp downstream exon 16	TGGCAAGGCC**R**CTTCACCACT		RFLP
SLC18A3				
-776 C>T	336bp upstream *SLC18A3*	GCTGCCGCGC**Y**CCCTTCCCCA	rs885835	RFLP*
-287 G>T	5'UTR	GGCGAAGTGC**K**CCCAGTCTCC	rs2377879	RFLP
1638 G>T	3'UTR	ACCGCCTTGG**K**TCAAGGGGGC	rs2269338	RFLP*

Table 3.2. Details of the 17 polymorphisms identified in the *CHAT* and *SLC18A3* genes. * indicates that a restriction site was artificially created by primer generated mutagenesis. RFLP =Restriction Fragment Length Polymorphism; PCR= Polymerase Chain Reaction.

Gene	SNP Name	RFLP Sense Primer (5'→3')	RFLP Antisense Primer (5'→3')	Size (bp)	Annealing Temperature (°C)	Enzyme	Restriction Fragments (bp)
CHAT	-5293 C>T	TCTAATGAGTACGTGGCAGAGC	CTGGATGGCACATGGAACC	296	64	*Rsa* I	C=286, 10 T=195, 91, 10
CHAT	-5228 C>A	TCTAATGAGTACGTGGCAGAGC	CTGGATGGCACATGGAACC	296	64	*Nla* IV	C=137, 79, 37, 27, 16 A=216, 37, 27, 16
CHAT	-1045 T>G	GCTTTGAGAAAGGAGTAGGAcCC	ATCCCACACTCGCATCTCTC	215	60	*Ava* I	T=173, 42 G=152, 42, 21
CHAT	-220 C>G	CCATCAGGATTGTCCCAAGT	CTGCTGCTGAATCCTGGAGc	240	60	*Msp* I	C=240 G=218, 22
CHAT	-44 C>G	CCATCAGGATTGTCCCAAGT	TCCTCCCTCCTCTCTCTTCC	508	60	*Ava* I	C=360, 114, 34 G=360, 148
CHAT	1803 C>T	GGAGGGAAAGGAATGCAcGC	CTCTCCCCAGACTAAGGCAGGT	252	60	*Mlu* I	C=235, 17 T=252
CHAT	1882 G>A	ACCTACTGTGCTCAGTGCTTgAT	CTAGGTCACAACGCCTCCAG	219	60	*Mbo* I	G=199, 20 A=219
CHAT	2384 G>A	TCAGCACGTACAGGTGGAAG	ATTTCCTTGGCACCCTGAG	497	60	*Bbv* I	G=263, 234 A=497
CHAT	7936 C>T	CTGGGAGGAAGGGCTCAG	TCAAGGAAGGATGGTGCTTG	316	60	*Rsa* I	C=252, 64 T=316
CHAT	11604 G>A	CCATGATGATGCAGTTCTGG	GGCAACTGGTGGAGAGACAT	493	60	*Dra* II	G=450, 42, 1 A=493
CHAT	32248 G>A	TTCTGGCTGGTCCAGAGATT	CCTGGGTCTTGTTGTGATCC	503	60	*Ban* II	G=308, 145, 50 A=308, 195
CHAT	40912 C>T	TAGGTGGGCACCAGTCaTCG	CCCCGGGTGTATATAAGCAA	246	60	*Bsp*D I	C=246 T=228, 18
CHAT	41388 A>G	TTCCCCTCACAGTTGACTCC	CAGTGAGGCTGCTGTGGTT	500	60	*Fnu*4H I	A=406, 65, 19, 10 G=212, 194, 65, 19, 10
SLC18A3	-776 C>T	GTCGGCTCTTGCCTCCTC	CGAGGAACCGGCTGCCGgGC	375	GC65	*Dra* II	C=357, 18 T=375
SLC18A3	-287 G>T	GCATTAGCATGAGCGACGTA	CACAGCCTCCGACAGCTT	603	GC60	*Bsi*HKA I	G=402, 201 T=254, 201, 148
SLC18A3	1638 G>T	AGCCCACCCAACCGCCTcGG	GAGCAATGGAAGGAAGGACA	293	64	*Ava* I	G=277, 16 T=293

Table 3.3. Assay details of *CHAT* and *SLC18A3* RFLP genotyping assays, including RFLP primers, amplimer size, PCR annealing temperature, restriction enzyme and expected RFLP fragment sizes. A lower case letter in the RFLP primer indicates the 'mismatched base' introduced to the RFLP amplimer to generate an artificial restriction site (see Chapter 2). Annealing temperatures preceded by 'GC' indicate that amplimers are GC-rich and require the use of Q-solution for amplification (see Chapter 2).

3.3 Results

3.3.1 Polymorphisms Identified

A total of seventeen polymorphisms were identified in *CHAT* and *SLC18A3* (Figure 3.3 and Table 3.2, p.83). All but one of the sequence variants were SNPs. Three were non-synonymous coding SNPs; a D7N polymorphism in the S exon of *CHAT* (1882 G>A), an A120T polymorphism in exon 5 of *CHAT* (2384 G>A) and a L243F polymorphism in exon 8 of *CHAT* (7936 C>T). One further exonic SNP was detected but this did not change the protein sequence (40912 C>T, H547H). Five SNPs were detected in regions 5' to translation in *CHAT* and two of these were in the UTRs of the alternatively spliced 5' exons M and N. The remaining four SNPs were intronic. In addition a 66bp variable number tandem repeat (VNTR) was also identified in intron 7 of *CHAT*, containing 1 to 4 copies of the sequence 5'-AAG GGA GGG AAG AGG AAG GAG ATG GAA GGA AGA GGG AAG GAG GGA GGG GAG GCA GAA GGG AGG GAG-3'. In *SLC18A3*, three SNPs were detected: one in the 5'upstream sequence, one in the 5' UTR and one in the 3'UTR.

3.3.2 Association Analysis

Unless otherwise indicated, polymorphisms were in Hardy-Weinberg equilibrium (HWE). All polymorphisms identified were tested for association with LOAD in the Cardiff sample of 133 cases and 135 age-matched controls. As the sample size was relatively small, it was decided *a priori* to genotype any SNP displaying an association with a P value ≤ 0.1000 in the replication samples and two SNPs fulfilled these criteria, *CHAT* 1882G>A and *CHAT* 11604G>A (see Table 3.4, p.87).

Variant	Genotype			*P*	Allele		*P*
CHAT							
-5293 C>T	**C/C**	**C/T**	**T/T**		**C**	**T**	
Patients	88	35	7		211 (0.81)	49 (0.19)	
Controls	76	34	7	0.9008	186 (0.79)	48 (0.21)	0.6414
-5228 C>A	**C/C**	**C/A**	**A/A**		**C**	**A**	
Patients	94	4	0		192 (0.98)	4 (0.02)	
Controls	99	3	0	0.6608	201 (0.99)	3 (0.01)	0.4780
-1045 T>G	**T/T**	**T/G**	**G/G**		**T**	**G**	
Patients	75	41	6		191 (0.78)	53 (0.22)	
Controls	59	39	10	0.3471	157 (0.73)	59 (0.27)	0.1630
-220 C>G	**C/C**	**C/G**	**G/G**		**C**	**G**	
Patients	95	21	2		211 (0.89)	25 (0.11)	
Controls	95	14	2	0.5523	204 (0.92)	18 (0.08)	0.3621
-44 C>G	**C/C**	**C/G**	**G/G**		**C**	**G**	
Patients	80	43	6		203 (0.79)	55 (0.21)	
Controls	65	42	10	0.3710	172 (0.74)	62 (0.26)	0.1779
1803 C>T	**C/C**	**C/T**	**T/T**		**C**	**T**	
Patients	50	17	1		117 (0.86)	19 (0.14)	
Controls	67	18	2	0.7746	152 (0.87)	22 (0.13)	0.7321
1882 G>A	**G/G**	**G/A**	**A/A**		**G**	**A**	
Patients	34	25	9		93 (0.68)	43 (0.32)	
Controls	49	33	3	**0.0826**	131 (0.77)	39 (0.23)	**0.0886**
2384 G>A	**G/G**	**G/A**	**A/A**		**G**	**A**	
Patients	69	51	11		189 (0.72)	73 (0.28)	
Controls	65	47	6	0.5834	177 (0.75)	59 (0.25)	0.4698
7786VNTR	**1/2**	**2/2**	**2/3**	**2/4**	**3/3**	**1**	**2**	**3**	**4**	
Patients	4	103	14	1	1	4	225	16	1	
Controls	2	82	9	0	2	0.8143	2	175	13	0	0.9472
7936 C>T	**C/C**	**C/T**	**T/T**		**C**	**T**	
Patients	106	12	0		224 (0.95)	12 (0.05)	
Controls	97	16	0	0.3530	210 (0.93)	16 (0.07)	0.3690
11604 G>A	**G/G**	**G/A**	**A/A**		**G**	**A**	
Patients	72	39	8		183 (0.77)	55 (0.23)	
Controls	83	31	2	**0.0721**	197 (0.85)	35 (0.15)	**0.0270**
32248 G>A	**G/G**	**G/A**	**A/A**		**G**	**A**	
Patients*	114	10	2		238 (0.94)	14 (0.06)	
Controls	99	16	1	0.3064	214 (0.92)	18 (0.08)	0.3298
40912 C>T	**C/C**	**C/T**	**T/T**		**C**	**T**	
Patients	101	14	1		216 (0.93)	16 (0.07)	
Controls	89	19	2	0.4294	197 (0.90)	23 (0.10)	0.1781
41388 A>G	**A/A**	**A/G**	**G/G**		**A**	**G**	
Patients	39	56	35		134 (0.52)	126 (0.48)	
Controls	26	60	32	0.3171	112 (0.47)	124 (0.53)	0.3639
SLC18A3							
-776 C>T	**C/C**	**C/T**	**T/T**		**C**	**T**	
Patients	70	19	3		159 (0.86)	25 (0.14)	
Controls	72	23	2	0.7877	167 (0.86)	27 (0.14)	0.9256
-287 G>T	**G/G**	**G/T**	**T/T**		**G**	**T**	
Patients	121	8	0		250 (0.97)	8 (0.03)	
Controls	102	9	1	0.4757	213 (0.95)	11 (0.05)	0.3084
1638 G>T	**G/G**	**G/T**	**T/T**		**G**	**T**	
Patients	91	27	1		209 (0.88)	29 (0.12)	
Controls	88	25	1	0.9900	201 (0.88)	27 (0.12)	0.9094

Table 3.4. Genotype and allelic association for the 17 sequence variants detected in *CHAT* and *SLC18A3* in the Cardiff sample. * Genotypes not in Hardy-Weinberg equilibrium. *P* values in bold are those that gave evidence of possible association and were carried forward for further analysis.

For the SNP 11604 G>A in intron 9 of the *CHAT* gene, the A allele appeared to be more common in LOAD patients than in controls (P=0.0270). This SNP was genotyped in the two additional case-control samples, MRC and Belfast (Table 3.5 below). In neither the MRC (P=0.1099) nor Belfast (P=0.4343) samples was a significant difference found between allele distributions in patients and controls, suggesting that the initial positive finding is a type I error. Indeed, combining data from all three samples in a meta-analysis revealed no evidence for association of this SNP with LOAD (P= 0.2283). There was no significant heterogeneity between samples (P= 0.0589).

11604 G>A		**Genotype**			***P***	**Allele**		***P***
		G/G	**G/A**	**A/A**		**G**	**A**	
Cardiff	Patients	72	39	8	0.0721	183 (0.77)	55 (0.23)	**0.0270**
	Controls	83	31	2		197 (0.85)	35 (0.15)	
MRC	Patients	88	42	5	0.4090	218 (0.81)	52 (0.19)	0.1099
	Controls	95	33	3		223 (0.85)	39 (0.15)	
Belfast	Patients	129	75	5	0.6655	333 (0.80)	85 (0.20)	0.4343
	Controls	130	84	8		344 (0.77)	100 (0.23)	

Table 3.5. Association of the 11604 G>A polymorphism in *CHAT* intron 9 with LOAD. *P* values <0.05 are indicated in bold.

For the non-synonymous SNP 1882 G>A in the S exon of the *CHAT* gene, there was a trend to an excess of A/A homozygotes in the LOAD patients compared to controls in the Cardiff sample (genotypic P= 0.0826). The Cardiff sample showed that 1882 G>A and 2384 G>A were in complete LD (r^2=1; see Tables 3.11 and 3.12, p.97-98), although fewer genotypes were obtained for 1882G>A than for 2384G>A due to depletion of DNA stocks from the Cardiff sample; this accounts for the discrepancy in the genotype number in Table 3.4 (p.87). 2384G>A was not significant in the Cardiff sample and so presumably 1882 G>A would not have been either, had

genotype data been attainable for the full sample. However, as non-synonymous coding SNPs, we decided to genotype 1882 G>A and 2384G>A in the other case-control samples. Complete LD was again observed between 1882 G>A and 2384G>A in the MRC sample and we therefore typed only the former in the Belfast sample. Table 3.6 (p.90) shows that in the MRC sample there was no evidence of association (genotypic P=0.6952), but in the Belfast sample there was significantly more A/A homozygotes in patients compared with controls (P=0.0307 genotypic). This is partly due to the small number of A/A genotypes observed in the control sample, which is out of HWE (P=0.0160). This trend to increased A/A genotypes in cases is not apparent at all in the MRC sample.

Combining all three samples in a meta-analysis revealed no genotypic (G/- Vs A/A; P=0.1135) or allelic association (P=0.2397) using 2384G>A in Cardiff (as it is in complete LD with 1882 G>A but has more genotyping data) and 1882G>A in MRC and Belfast. There was no significant heterogeneity between studies (P=0.1389 for G/- Vs A/A genotypes, and P=0.1838 for G Vs A).

In a recent report, Mubumbila *et al.* (2002)[282] found a very significant association of the 2384G>A SNP with AD in their sample of 122 LOAD cases and 112 controls collected in France and Germany (P<0.0005 allelic and genotypic; see Table 3.6, p.90). Their genotype frequencies are substantially different to those observed in any of our samples, with much higher numbers of minor allele homozygotes in both cases (34.4% Vs 6.7%) and controls (12.5% Vs 3.9%), although this is a similar trend to that observed in the Belfast sample, with increased numbers of minor allele homozygotes in the patients compared with controls. Both the case and control

genotypes in their analysis are markedly out of HWE (cases P=0.0000; controls P=0.0110). We cannot determine the reasons for this, but it may reflect age effects, the combination of two populations (French/German) with different genotype frequencies, or genotyping error. The significant association observed in this sample might therefore be an artefact.

Indeed, in an independent study Schwarz *et al.* (2003)[283] attempted to replicate this association in a sample of 172 LOAD cases and 143 controls collected in Germany (Table 3.6 below). They found no association of the A/A genotype with LOAD and notably the genotype/allele frequencies observed in their sample are much more similar to those found in our study.

SNP/ Sample		Genotype			*P* genotypic	*P* G/- Vs A/A	Allele		*P* allelic
		GG	GA	AA			G	A	
1882 G>A	Patients	34	25	9	0.0826	**0.0264**	93 (0.68)	43 (0.32)	0.0886
Cardiff	Controls	49	33	3			131 (0.77)	39 (0.23)	
2384 G>A	Patients	69	51	11	0.5834	0.3007	189 (0.72)	73 (0.28)	0.4698
Cardiff	Controls	65	47	6			177 (0.75)	59 (0.25)	
1882 G>A	Patients	71	56	8	0.6952	0.8021	198 (0.73)	72 (0.27)	0.4439
MRC	Controls	64	62	9			190 (0.70)	80 (0.30)	
2384 G>A	Patients	71	56	8	0.6952	0.8021	198 (0.73)	72 (0.27)	0.4439
MRC	Controls	64	62	9			190 (0.70)	80 (0.30)	
1882 G>A	Patients	105	77	12	**0.0307**	**0.0110**	287 (0.74)	101 (0.26)	0.0551
Belfast	Controls	127	79	3*			333 (0.80)	85 (0.20)	
2384 G>A	Patients	48	32	42*	**0.0003**	**0.0000**	128 (0.52)	116 (0.48)	**0.0000**
Mubumbila	Controls	64	34	14*			162 (0.72)	62 (0.28)	
2384 G>A	Patients	100	66	6	0.6493	0.3665	266 (0.77)	78 (0.23)	0.7441
Schwarz	Controls	83	52	8			218 (0.76)	68 (0.24)	

Table 3.6. Association of the non-synonymous *CHAT* SNPs 1882 G>A/2384 G>A (which are in complete LD) with LOAD. Data combined in the meta-analysis are shown in red. *P* values <0.05 are indicated in bold. The data of Mubumbila *et al.* (2002)[282] and Schwarz *et al.* (2003)[283] are also presented for comparison. *Genotypes not in Hardy-Weinberg equilibrium.

We also genotyped the non-synonymous SNP 7936 C>T, in order to investigate whether there was any association of the amino acid change in the two additional

samples (Table 3.7 below). No significant difference was observed in genotypic or allelic frequencies between cases and controls in any sample. Similarly, no association was observed when the data was combined in a meta-analysis (P=0.5413). Again, there was no significant heterogeneity between studies (P=0.2034).

7936 C>T		Genotype			*P*	Allele		*P*
		CC	CT	TT		C	T	
Cardiff	Patients	106	12	0	0.3530	224 (0.95)	12 (0.05)	0.3690
	Controls	97	16	0		210 (0.93)	16 (0.07)	
MRC	Patients	116	18	1	0.3946	250 (0.93)	20 (0.07)	0.2248
	Controls	120	13	0		253 (0.95)	13 (0.05)	
Belfast	Patients	156	25	0	0.3949	337 (0.93)	25 (0.07)	0.2518
	Controls	161	34	1		356 (0.91)	36 (0.09)	

Table 3.7. Association of the non-synonymous 7936 C>T SNP in *CHAT* exon 8 with LOAD.

3.3.3 Haplotype Association

Analysis of haplotype association with LOAD was performed for all possible 2-marker haplotypes using genotyping data generated from the Cardiff sample for the sixteen SNPs (Table 3.8, p.93). Single SNP associations that became more significant when combined in haplotypes in the Cardiff sample were analysed in the MRC sample. The other SNPs for which there was individual genotype data from the MRC sample were also analysed in two-marker haplotypes. Several associations were identified in the Cardiff sample, but appeared to reflect the false positive association of 11604 G>A with LOAD (Table 3.8, p.93) and none of these replicated in the MRC sample (Table 3.10, p.95). Apart from the 11604G>A combinations, -776 C>T and 40912 C>T displayed a significant 2-marker haplotype association (P=0.037) in the Cardiff sample, although neither were significant by themselves. Again, this did not replicate in the MRC sample (P=0.329).

	-5228 C>A	-776 C>T	-287 G>T	1638 G>T	-1045 T>G	-220 C>G	-44 C>G	1803 C>T	1882 G>A	2384 G>A	7936 C>T	11604 G>A	32248 G>A	40912 C>T	41388 A>G
-5293 C>T	0.704	0.346	0.740	0.912	0.386	0.833	0.628	0.908	0.540	0.902	0.295	**0.042**	0.517	0.313	0.846
-5228 C>A		0.972	0.438	0.889	0.097	0.694	0.410	0.930	0.126	0.360	0.255	0.404	0.515	0.096	0.824
-776 C>T			0.428	0.992	0.704	0.771	0.737	0.971	0.685	0.983	0.974	0.642	0.560	**0.037**	0.409
-287 G>T				0.649	0.353	0.234	0.334	0.444	0.108	0.590	0.270	0.066	0.679	0.426	0.268
1638 G>T					0.085	0.533	0.069	0.617	0.247	0.563	0.525	**0.011**	0.578	0.198	0.242
-1045 T>G						0.081	0.400	0.113	0.136	0.433	0.380	**0.033**	0.442	0.221	0.352
-220 C>G							0.061	0.913	0.413	0.488	0.191	**0.018**	0.399	0.084	0.468
-44 C>G								0.157	0.109	0.429	0.386	**0.039**	0.373	0.320	0.387
1803 C>T									0.215	0.247	0.066	0.344	0.963	0.542	0.565
1882 G>A										0.113	0.197	0.216	0.206	0.550	0.207
2384 G>A											0.532	**0.034**	0.597	0.481	0.700
7936 C>T												0.108	0.133	0.188	0.558
11604 G>A													0.082	0.077	0.096
32248 G>A														0.287	0.513
40912 C>T															0.179

Table 3.8. 2-marker SNP haplotype associations in the Cardiff sample. *P* values <0.05 are indicated in bold.

SNP	Genotype			*P*	Allele		*P*
CHAT							
-5293 C>T Cardiff	**C/C**	**C/T**	**T/T**		**C**	**T**	
Patients	88	35	7		211 (0.81)	49 (0.19)	
Controls	76	34	7	0.9008	186 (0.79)	48 (0.21)	0.6414
-5293 C>T MRC	**C/C**	**C/T**	**T/T**		**C**	**T**	
Patients	65	46	6		176 (0.75)	58 (0.25)	
Controls	69	45	3	0.5682	183 (0.78)	51 (0.22)	0.4439
-1045 T>G Cardiff	**T/T**	**T/G**	**G/G**		**T**	**G**	
Patients	75	41	6		191 (0.78)	53 (0.22)	
Controls	59	39	10	0.3471	157 (0.73)	59 (0.27)	0.1630
-1045 T>G MRC	**T/T**	**T/G**	**G/G**		**T**	**G**	
Patients	72	31	9*		175 (0.78)	49 (0.22)	
Controls	73	37	4	0.2949	183 (0.80)	45 (0.20)	0.5754
-220 C>G Cardiff	**C/C**	**C/G**	**G/G**		**C**	**G**	
Patients	95	21	2		211 (0.89)	25 (0.11)	
Controls	95	14	2	0.5523	204 (0.92)	18 (0.08)	0.3621
-220 C>G MRC	**C/C**	**C/G**	**G/G**		**C**	**G**	
Patients	103	31	1		237 (0.88)	33 (0.12)	
Controls	109	24	0	0.3595	242 (0.91)	24 (0.09)	0.2295
-44 C>G Cardiff	**C/C**	**C/G**	**G/G**		**C**	**G**	
Patients	80	43	6		203 (0.79)	55 (0.21)	
Controls	65	42	10	0.3710	172 (0.74)	62 (0.26)	0.1779
-44 C>G MRC	**C/C**	**C/G**	**G/G**		**C**	**G**	
Patients	76	32	9*		184 (0.79)	50 (0.21)	
Controls	75	36	4	0.3416	186 (0.81)	44 (0.19)	0.5488
40912 C>T Cardiff	**C/C**	**C/T**	**T/T**		**C**	**T**	
Patients	101	14	1		216 (0.93)	16 (0.07)	
Controls	89	19	2	0.4294	197 (0.90)	23 (0.10)	0.1781
40912 C>T MRC	**C/C**	**C/T**	**T/T**		**C**	**T**	
Patients	107	25	2		239 (0.89)	29 (0.11)	
Controls	109	23	0	0.3522	241 (0.91)	23 (0.09)	0.4128
SLC18A3							
-776 C>T Cardiff	**C/C**	**C/T**	**T/T**		**C**	**T**	
Patients	70	19	3		159 (0.86)	25 (0.14)	
Controls	72	23	2	0.7877	167 (0.86)	27 (0.14)	0.9256
-776 C>T MRC	**C/C**	**C/T**	**T/T**		**C**	**T**	
Patients	99	30	3		228 (0.86)	36 (0.14)	
Controls	93	35	2	0.6849	221 (0.85)	39 (0.15)	0.6558
1638 G>T Cardiff	**G/G**	**G/T**	**T/T**		**G**	**T**	
Patients	91	27	1		209 (0.88)	29 (0.12)	
Controls	88	25	1	0.9900	201 (0.88)	27 (0.12)	0.9094
1638 G>T MRC	**G/G**	**G/T**	**T/T**		**G**	**T**	
Patients	74	22	1		170 (0.88)	24 (0.12)	
Controls	81	24	1	0.9979	186 (0.88)	26 (0.12)	0.9738

Table 3.9. SNPs genotyped in the MRC sample in an attempt to replicate 2-marker haplotype associations observed in the Cardiff sample. Cardiff genotype data is also shown for comparison. * Genotypes not in Hardy-Weinberg equilibrium.

	-776 C>T	1638 G>T	-1045 T>G	-220 C>G	-44 C>G	1882 G>A	7936 C>T	11604 G>A	40912 C>T
-5293 C>T	0.595	0.714	0.654	0.696	0.630	0.489	0.507	0.521	0.563
-776 C>T		0.897	0.616	0.416	0.690	0.625	0.183	0.397	0.329
1638 G>T			0.478	0.154	0.267	0.168	0.739	0.581	0.215
-1045 T>G				0.443	0.426	0.543	0.291	0.632	0.389
-220 C>G					0.518	0.339	0.349	0.084	0.421
-44 C>G						0.420	0.282	0.595	0.459
1882 G>A							0.350	0.640	0.561
7936 C>T								0.388	0.501
11604 G>A									0.466

Table 3.10. 2-marker SNP haplotype associations in the MRC sample.

3.3.4 Linkage Disequilibrium

Levels of linkage disequilibrium (LD) across the 56kb cholinergic gene locus are generally low (Tables 3.11 and 3.12, p.97-98). LD analysis was performed separately for the Cardiff case and control samples and the results were consistent between the two samples. Only two SNPs were found to be in complete LD in the Cardiff sample and these were the coding SNPs, 1882G>A and 2384G>A which are 500bp apart. High LD was also observed between –44 C>G and –1045 T>G, 1001bp apart. These two SNPs lie within the only observed region of conserved LD in this gene, that between SNPs 1638 G>T and 1803 C>T, (but even in this region, levels of LD are generally quite low).

Cases	-5228 C>A	-776 C>T	-287 G>T	1638 G>T	-1045 T>G	-220 C>G	-44 C>G	1803 C>T	1882 G>A	2384 G>A	7936 C>T	11604 G>A	32248 G>A	40912 C>T	41388 A>G
-5293 C>T	0.002	0.003	0.001	0.003	0.006	0.003	0.006	0.003	0.038	0.009	0.001	0.090	0.001	0.007	0.003
-5228 C>A		0.029	0.151	0.004	0.003	0.009	0.000	0.014	0.000	0.000	0.000	0.060	0.014	0.040	0.001
-776 C>T			0.002	0.009	0.051	0.003	0.049	0.000	0.035	0.023	0.010	0.021	0.004	0.011	0.007
-287 G>T				0.003	0.127	0.003	0.120	0.006	0.016	0.012	0.001	0.004	0.029	0.004	0.029
1638 G>T					0.375	0.724	0.371	0.716	0.060	0.052	0.010	0.041	0.037	0.002	0.000
-1045 T>G						0.440	0.976	0.396	0.120	0.109	0.188	0.047	0.007	0.001	0.001
-220 C>G							0.402	0.719	0.048	0.043	0.016	0.037	0.006	0.008	0.001
-44 C>G								0.420	0.114	0.105	0.194	0.043	0.007	0.001	0.001
1803 C>T									0.006	0.009	0.102	0.048	0.013	0.018	0.009
1882 G>A										1.000	0.010	0.083	0.033	0.018	0.000
2384 G>A											0.020	0.087	0.001	0.014	0.000
7936 C>T												0.000	0.007	0.003	0.028
11604 G>A													0.015	0.020	0.030
32248 G>A														0.352	0.013
40912 C>T															0.070

Table 3.11. Intermarker linkage disequilibrium values in LOAD cases as measured by r^2.

Controls	-5228 C>A	-776 C>T	-287 G>T	1638 G>T	-1045 T>G	-220 C>G	-44 C>G	1803 C>T	1882 G>A	2384 G>A	7936 C>T	11604 G>A	32248 G>A	40912 C>T	41388 A>G
-5293 C>T	0.005	0.001	0.001	0.003	0.033	0.002	0.004	0.004	0.009	0.006	0.072	0.033	0.002	0.002	0.017
-5228 C>A		0.056	0.114	0.000	0.000	0.001	0.000	0.014	0.000	0.000	0.021	0.001	0.000	0.003	0.000
-776 C>T			0.011	0.025	0.066	0.017	0.067	0.017	0.032	0.010	0.016	0.030	0.051	0.098	0.069
-287 G>T				0.000	0.163	0.001	0.135	0.010	0.025	0.017	0.004	0.008	0.025	0.001	0.000
1638 G>T					0.091	0.421	0.094	0.365	0.011	0.005	0.000	0.050	0.018	0.053	0.048
-1045 T>G						0.212	0.943	0.186	0.146	0.125	0.225	0.000	0.002	0.017	0.025
-220 C>G							0.219	0.745	0.034	0.026	0.005	0.013	0.031	0.034	0.004
-44 C>G								0.178	0.145	0.123	0.179	0.000	0.002	0.003	0.009
1803 C>T									0.045	0.041	0.012	0.009	0.028	0.006	0.000
1882 G>A										1.000	0.022	0.034	0.002	0.001	0.000
2384 G>A											0.028	0.015	0.002	0.001	0.002
7936 C>T												0.003	0.007	0.009	0.075
11604 G>A													0.013	0.018	0.005
32248 G>A														0.201	0.012
40912 C>T															0.128

Table 3.12. Intermarker linkage disequilibrium values in controls as measured by r^2.

3.4 Discussion

In our study, Tim Peirce and I detected and analysed seventeen sequence variants within the *CHAT/SLC18A3* complex of genes. The average intermarker distance was approximately 3kb. Of the seventeen variants we detected by DHPLC, ten had been or were subsequently reported in SNP databases and one of the coding SNPs was independently reported by Mubumbila *et al.* (2002)[282]. Prior to this study, the only polymorphisms identified at the cholinergic gene locus were the database SNPs and a series of rare mutations that cause a recessive congenital myasthenic syndrome[206]. Three of the SNPs reported in the present study caused coding changes in ChAT but any effect these coding changes may have on ChAT activity is unknown.

We found no substantial evidence for association of any polymorphism in the cholinergic gene locus with LOAD. The marginal evidence for association of 1882G>A in the Belfast sample probably arises from the deviation of control genotypes from Hardy-Weinberg equilibrium. Repeated genotyping of the 1882G>A in this sample gave the same result, suggesting the deviation from HWE is not due to laboratory error. Although there are several explanations for departure from HWE (including chance), the finding in our study might possibly reflect selection, as our control samples are all older than the case samples.

Mubumbila *et al.*[282] found a very significant association of the 2384G>A SNP with AD in their sample of 122 LOAD cases and 112 controls collected in France and Germany. This SNP is in complete LD with 1882G>A. However, their genotype frequencies are substantially different to those observed in any of our samples and both the case and control genotypes in their analysis are markedly out of HWE (cases

P=0.0000; controls P=0.0110). Possible reasons for the deviation are factors such as genotyping errors, population stratification, selection and chance. If we assume that the study of Mubumbila *et al.* represents a true association, our sample has power of greater than 99% to detect such an association. It is therefore surprising that we found no association in our total (successfully typed) sample of 460 LOAD cases and 462 controls. Neither did Schwarz *et al.* (2003)[283] replicate this association in an independent study.

The two-marker haplotype association analysis revealed some significant results, most of which arose in combination with the 11604G>A SNP which was the only significant SNP in the Cardiff case-control sample at the $P<0.05$ level. None of the significant results replicated in the second sample (Table 3.10, p.95), which suggests that the apparent associations were the result of chance. Thus we conclude there is no 2-marker haplotype association of the *CHAT* or *SLC18A3* genes with LOAD.

Although the cholinergic gene locus is an obvious candidate as a locus functionally and positionally implicated in AD, the detailed genetic study presented here indicates that variations in *CHAT* and *SLC18A3* are unlikely to be involved in the primary pathogenesis of late-onset AD. The cholinergic gene locus has a complicated structure and it is possible that the variants we have detected do affect regulation of these genes, but that this in itself does not contribute to the genetic susceptibility to LOAD. Moreover, it remains possible that rare polymorphisms exist which do affect susceptibility to AD, but the effects on ChAT activity might be expected to be subtle, given that abolition or reduction of activity of the ChAT enzyme is reported to cause myasthenic syndromes rather than dementia[206]. However, such rare polymorphisms would not account for late-onset AD in more than a small proportion of the

population and could not therefore account for the linkage data on chromosome 10[144]. As a final caveat, the weak LD across the gene means we cannot exclude the possibility that there are variants (rare or common) associated with AD in regulatory elements outside the regions of the gene we have screened which are not in strong LD with any of the SNPs we have genotyped. The detection of such alleles, particularly where they are of low frequency, poses a formidable challenge for molecular genetic studies.

3.5 Examples of Experimental Data

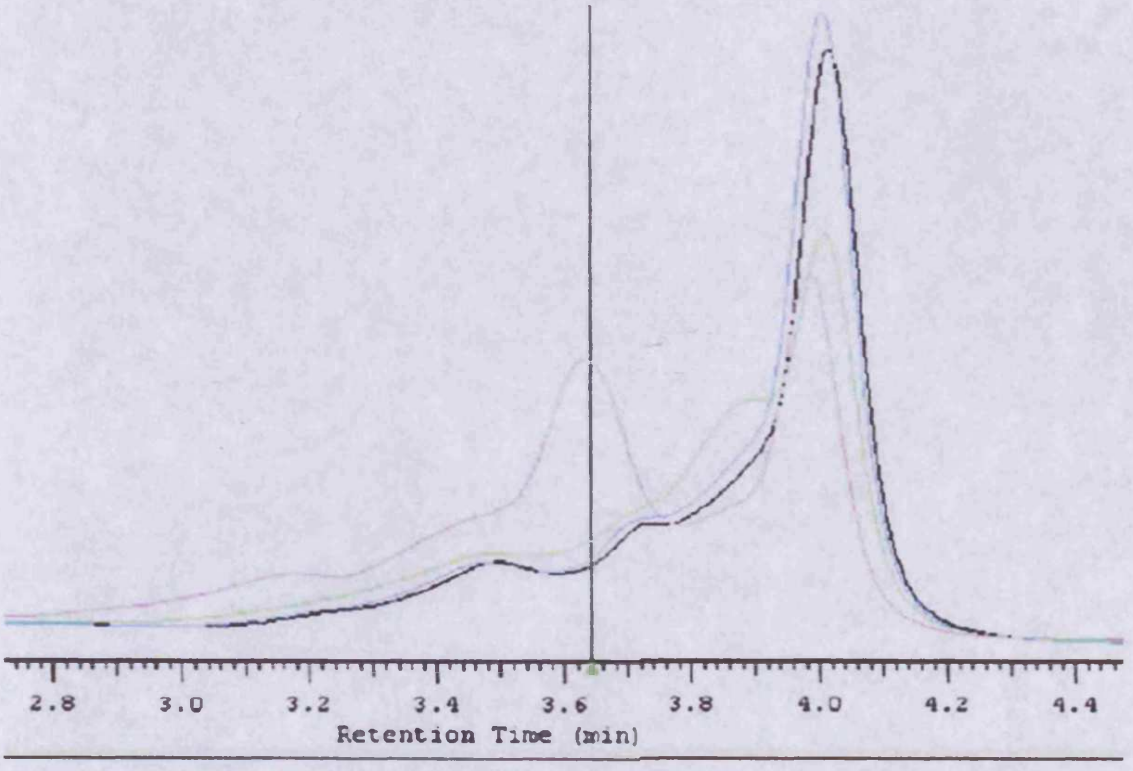

Figure 3.4. DHPLC traces from four individuals amplified for the ChAT xS fragment. The black and blue traces indicate homozygous individuals. The green trace represents an individual heterozygous for the *CHAT* SNP 1803 C>T and the pink trace represents an individual heterozygous for the *CHAT* SNP 1882 G>A.

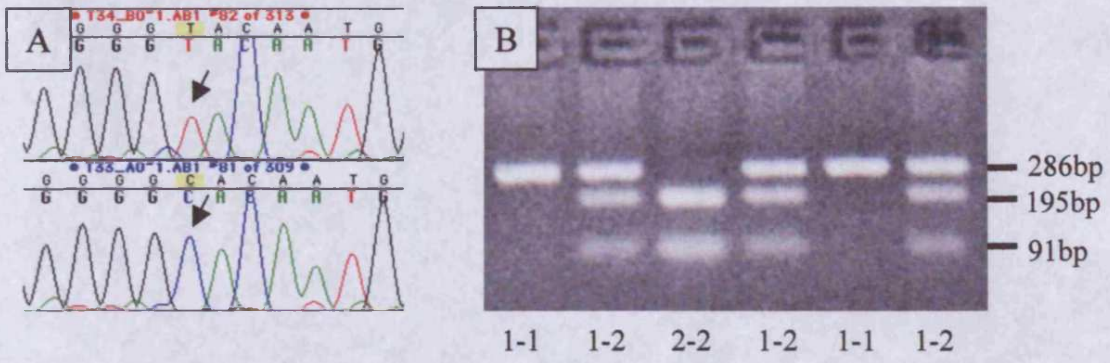

Figure 3.5 A) Sequence chromatograms for the *CHAT* SNP –5293 C>T (rs733722) showing a T/T homozygote in the upper panel and a C/C homozygote in the lower panel. **B)** RFLP fragments generated by the –5293 C>T *Rsa* I assay. Individuals homozygous for the C allele (1-1) were defined by the presence of two bands of size 286bp and 10bp. Individuals homozygous for the T allele (2-2) were defined by the presence of three bands of size 195bp, 91bp and 10bp. C/T heterozygotes (1-2) displayed four bands of size 286bp, 195bp, 91bp and 10bp. Note that the 10bp band has run off the gel due to the small size.

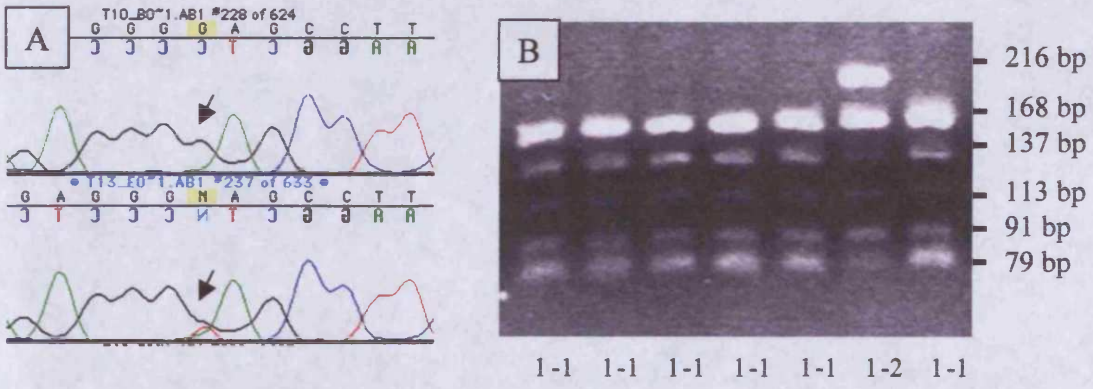

Figure 3.6 A) Sequence chromatograms in the reverse orientation for the *CHAT* SNP -5228 C>A showing a C/C (G/G) homozygote in the upper panel and an A/C (G/T) heterozygote in the lower panel. **B)** RFLP fragments generated by the -5228 C>A *Nla* IV assay. Individuals homozygous for the C allele (1-1) were defined by the presence of six bands of size 216bp, 168bp, 113bp, 91bp, 43bp and 37bp. Individuals homozygous for the A allele (2-2) were defined by the presence of seven bands of size 168bp, 137bp, 113bp, 91bp, 79bp, 43bp and 37bp. A/C heterozygotes (1-2) displayed bands of size 216bp, 168bp, 137bp, 113bp, 91bp, 79bp, 43bp, and 37bp. Note that the bands of size 43bp and 37bp ran off the gel due to their small size.

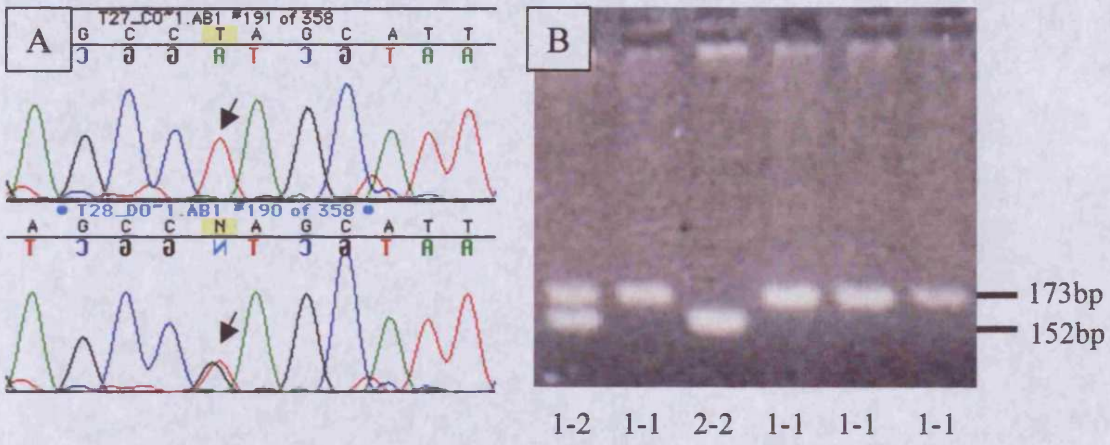

Figure 3.7 A) Sequence chromatograms for the *CHAT* SNP -1045 T>G (rs3729496) showing a T/T homozygote in the upper panel and a G/T heterozygote in the lower panel. **B)** RFLP fragments generated by the -1045 T>G *Ava* I assay. Individuals homozygous for the T allele (1-1) were defined by the presence of two bands of size 173bp and 42bp. Individuals homozygous for the G allele (2-2) were defined by the presence of three bands of size 152bp, 42bp and 21bp. G/T heterozygotes (1-2) displayed four bands of size 173bp, 152bp, 42bp and 21bp. Note that the 42 bp and 21bp bands have run off the gel due to their small size.

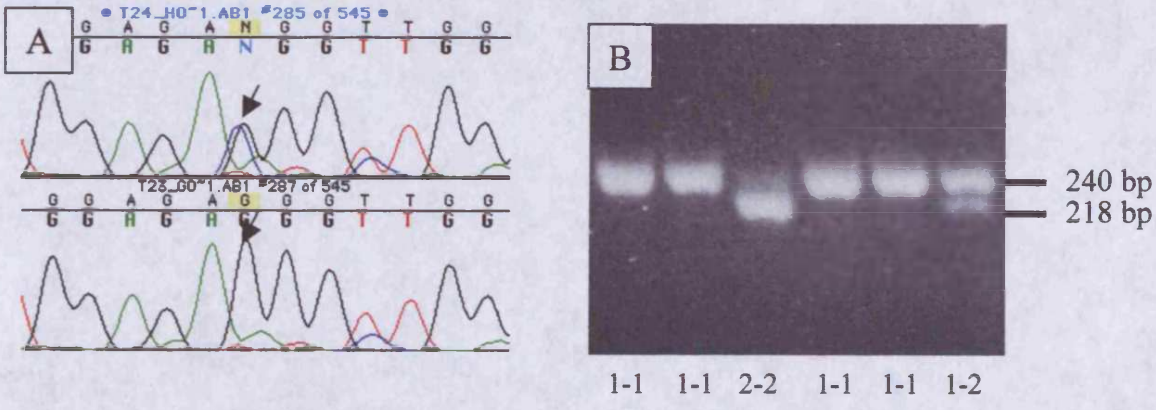

Figure 3.8 A) Sequence chromatograms in the reverse orientation for the *CHAT* SNP -220 C>G (rs3810948) showing a C/G heterozygote in the upper panel and a C/C (G/G) homozygote in the lower panel. **B)** RFLP fragments generated by the -220 C>G *Msp* I assay. Individuals homozygous for the C allele (1-1) were defined by the presence of one band of size 240bp. Individuals homozygous for the G allele (2-2) were defined by the presence of two bands of size 218bp and 22bp. C/G heterozygotes (1-2) displayed bands of size 240bp, 218bp and 22bp. Note that the band of size 22bp ran off the gel due to the small size.

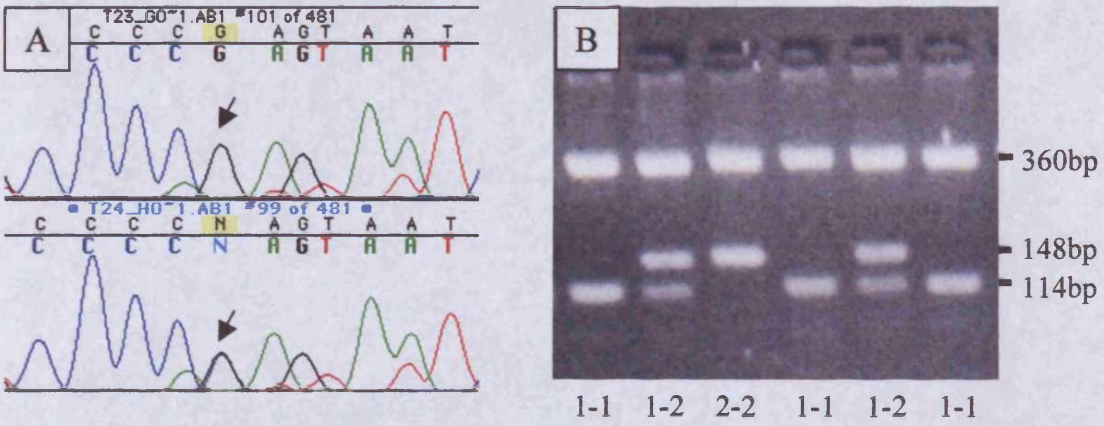

Figure 3.9 A) Sequence chromatograms in the reverse orientation for the *CHAT* SNP -44 C>G showing a C/C (G/G) homozygote in the upper panel and a C/G heterozygote in the lower panel. **B)** RFLP fragments generated by the -44 C>G *Ava* I assay. Individuals homozygous for the C allele (1-1) were defined by the presence of three bands of size 360bp, 114bp and 34bp. Individuals homozygous for the G allele (2-2) were defined by the presence of two bands of size 360bp and 148bp. G/C heterozygotes (1-2) displayed four bands of size 360bp, 148bp, 114bp and 34bp. Note that the 34bp band ran off the gel due to the small size.

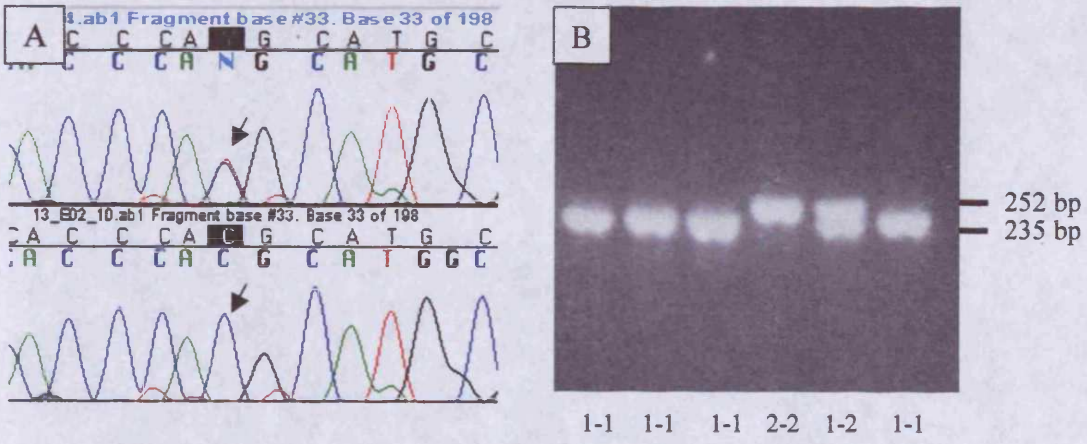

Figure 3.10 A) Sequence chromatograms for the *CHAT* SNP 1803 C>T showing a C/T heterozygote in the upper panel and a C/C homozygote in the lower panel. **B)** RFLP fragments generated by the 1803 C>T *Mlu* I assay. Individuals homozygous for the C allele (1-1) were defined by the presence of two bands of size 235bp and 17bp. Individuals homozygous for the T allele (2-2) were defined by the presence of one band of size 252bp. C/T heterozygotes (1-2) displayed bands of size 252bp, 235bp and 17bp. Note that the band of size 17bp ran off the gel due to the small size.

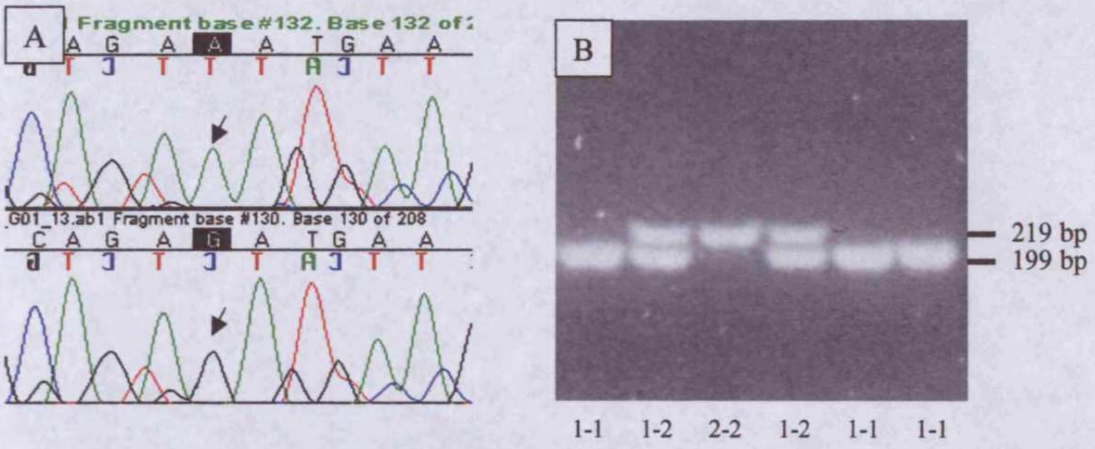

Figure 3.11 A) Sequence chromatograms for the *CHAT* SNP 1882 G>A (rs1880676) showing an A/A homozygote in the upper panel and a G/G homozygote in the lower panel. **B)** RFLP fragments generated by the 1882 G>A *Mbo* I assay. Individuals homozygous for the G allele (1-1) were defined by the presence of two bands of size 199bp and 20bp. Individuals homozygous for the A allele (2-2) were defined by the presence of one band of size 219bp. A/G heterozygotes (1-2) displayed bands of size 219bp, 199bp and 20bp. Note that the band of size 20bp ran off the gel due to the small size.

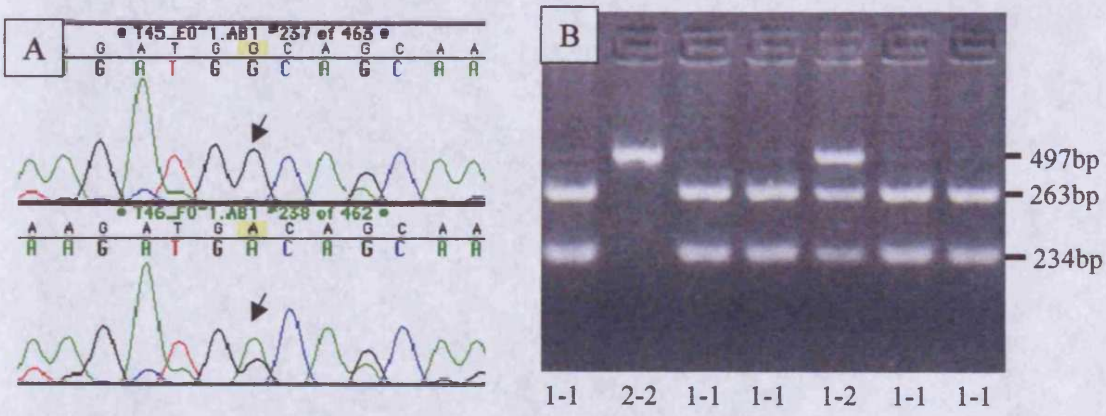

Figure 3.12 A) Sequence chromatograms for the *CHAT* SNP 2384 G>A (rs3810950) showing a G/G homozygote in the upper panel and an A/G heterozygote in the lower panel. **B)** RFLP fragments generated by the 2384 G>A *Bbv* I assay. Individuals homozygous for the G allele (1-1) were defined by the presence of two bands of size 263bp and 234bp. Individuals homozygous for the A allele (2-2) were defined by the presence of a single band of size 497bp. A/G heterozygotes (1-2) displayed three bands of size 497bp, 263bp and 234bp.

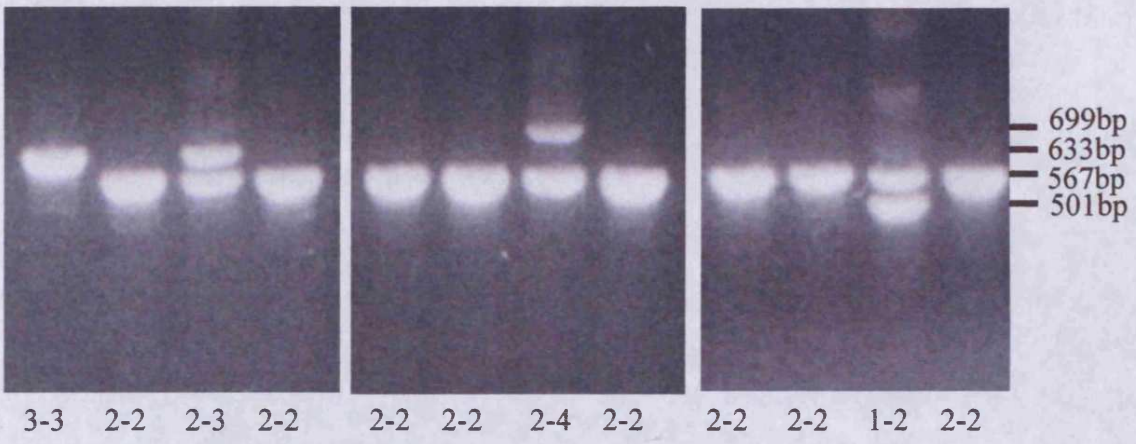

Figure 3.13. The *CHAT* 7786 VNTR, genotyped by PCR of the ChAT x8 fragment. Alleles with one repeat (1) give a band of 501bp; alleles with two repeats (2) give a band of 567bp; alleles with three repeats (3) give a band of 633bp and alleles with four repeats (4) give a band of 699bp.

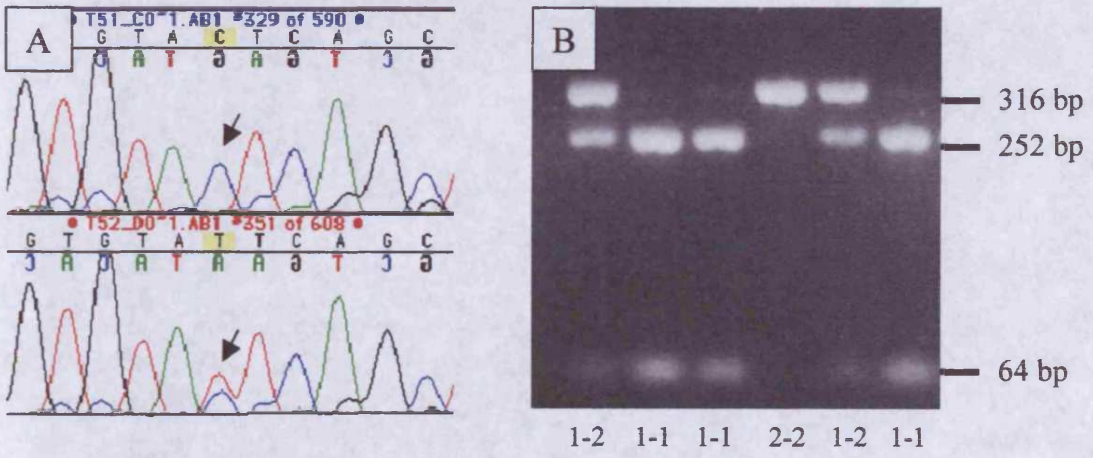

Figure 3.14 A) Sequence chromatograms for the *CHAT* SNP 7936 C>T (rs868750) showing a C/C homozygote in the upper panel and a C/T heterozygote in the lower panel. **B)** RFLP fragments generated by the 7936 C>T *Rsa* I assay. Individuals homozygous for the C allele (1-1) were defined by the presence of two bands of size 252bp and 64bp. Individuals homozygous for the T allele (2-2) were defined by the presence of a single band of size 316bp. C/T heterozygotes (1-2) displayed three bands of size 316bp, 252bp and 64bp.

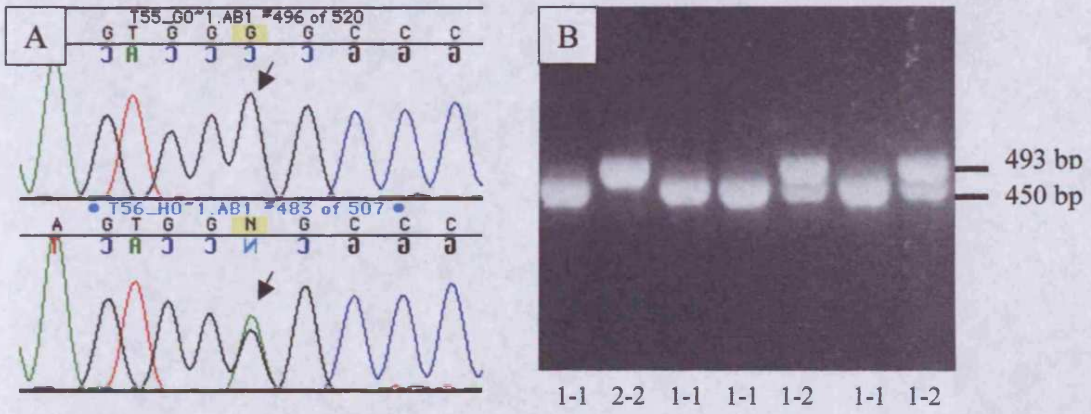

Figure 3.15 A) Sequence chromatograms for the *CHAT* SNP 11604 G>A (rs2377871) showing a G/G homozygote in the upper panel and an A/G heterozygote in the lower panel. **B)** RFLP fragments generated by the 11604 G>A *Dra* II assay. Individuals homozygous for the G allele (1-1) were defined by the presence of three bands of size 450bp, 42bp and 1bp. Individuals homozygous for the A allele (2-2) were defined by the presence of a single band of size 493bp. A/G heterozygotes (1-2) displayed four bands of size 493bp, 450bp, 42bp and 1bp. Note that the 42bp and 1bp bands have run off the gel due to their small size.

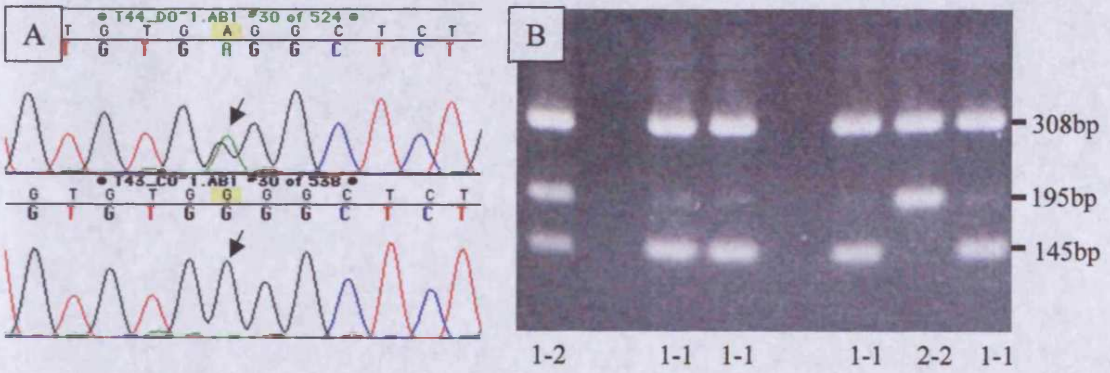

Figure 3.16 A) Sequence chromatograms for the *CHAT* SNP 32248 G>A showing an A/G heterozygote in the upper panel and a G/G homozygote in the lower panel. **B)** RFLP fragments generated by the 32248 G>A *Ban* II assay. Individuals homozygous for the G allele (1-1) were defined by the presence of three bands of size 308bp, 145bp and 50bp. Individuals homozygous for the A allele (2-2) were defined by the presence of two bands of size 308bp and 195bp. A/G heterozygotes (1-2) displayed four bands of size 308bp, 195bp, 145bp and 50bp. Note that the 50bp band ran off the gel due to the small size.

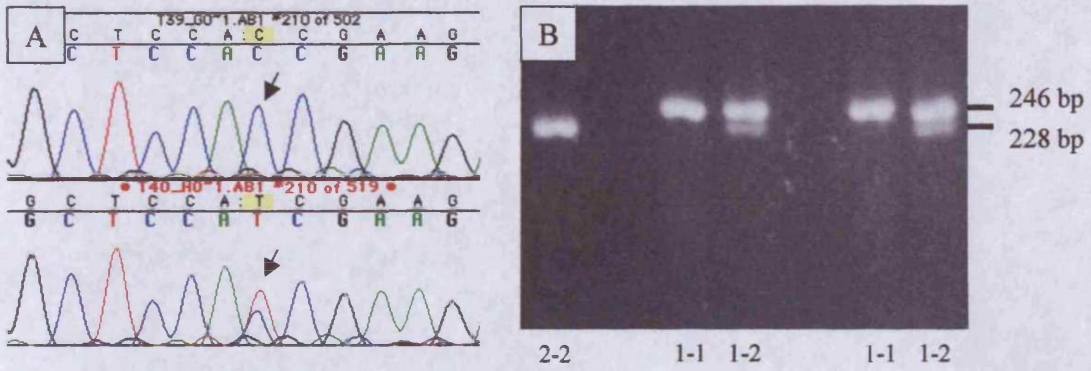

Figure 3.17 A) Sequence chromatograms for the *CHAT* SNP 40912 C>T showing a C/C homozygote in the upper panel and a C/T heterozygote in the lower panel. **B)** RFLP fragments generated by the 40912 C>T *Bsp* DI assay. Individuals homozygous for the C allele (1-1) were defined by the presence of one band of size 246bp. Individuals homozygous for the T allele (2-2) were defined by the presence of two bands of size 228bp and 18bp. C/T heterozygotes (1-2) displayed three bands of size 246bp, 228bp and 18bp. Note that the 18bp band ran off the gel due to the small size.

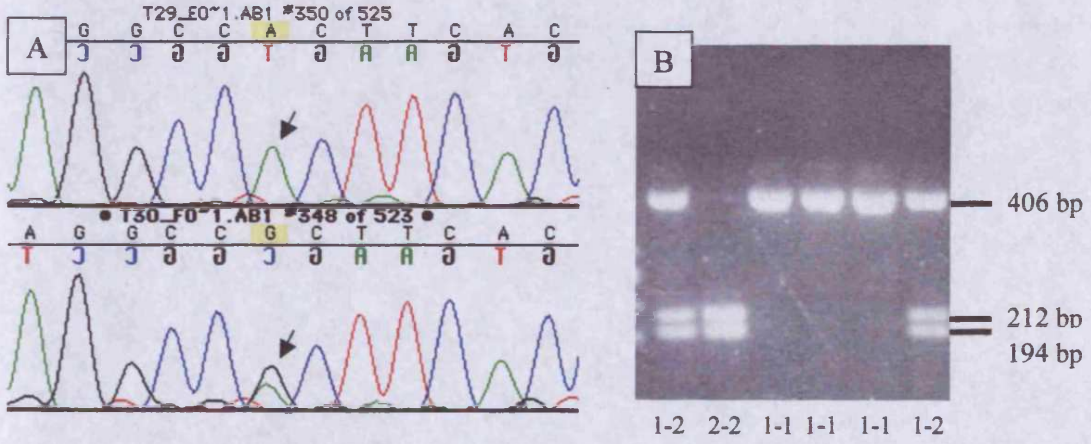

Figure 3.18 A) Sequence chromatograms for the *CHAT* SNP 41388 A>G showing an A/A homozygote in the upper panel and an A/G heterozygote in the lower panel. **B)** RFLP fragments generated by the 41388 A>G *Fnu* 4HI assay. Individuals homozygous for the A allele (1-1) were defined by the presence of four bands of size 406bp, 65bp, 19bp and 10bp. Individuals homozygous for the G allele (2-2) were defined by the presence of five bands of size 212bp, 194bp, 65bp, 19bp and 10bp. A/G heterozygotes (1-2) displayed six bands of size 406bp, 212bp, 194bp, 65bp, 19bp and 10bp. Note that the 65bp, 19bp and 10bp bands ran off the gel due to their small size.

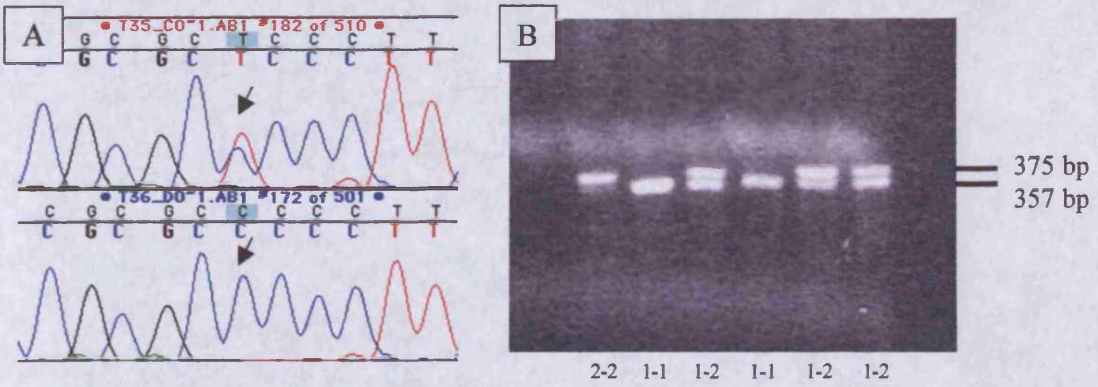

Figure 3.19 A) Sequence chromatograms for the *SLC18A3* SNP -776 C>T (rs885835) showing a C/T heterozygote in the upper panel and a C/C homozygote in the lower panel. **B)** RFLP fragments generated by the -776 C>T *Dra* II assay. Individuals homozygous for the C allele (1-1) were defined by the presence of two bands of size 357bp and 18bp. Individuals homozygous for the T allele (2-2) were defined by the presence of one band of size 375bp. C/T heterozygotes (1-2) displayed three bands of size 375bp, 357bp and 18bp. Note that the 18bp band ran off the gel due to the small size.

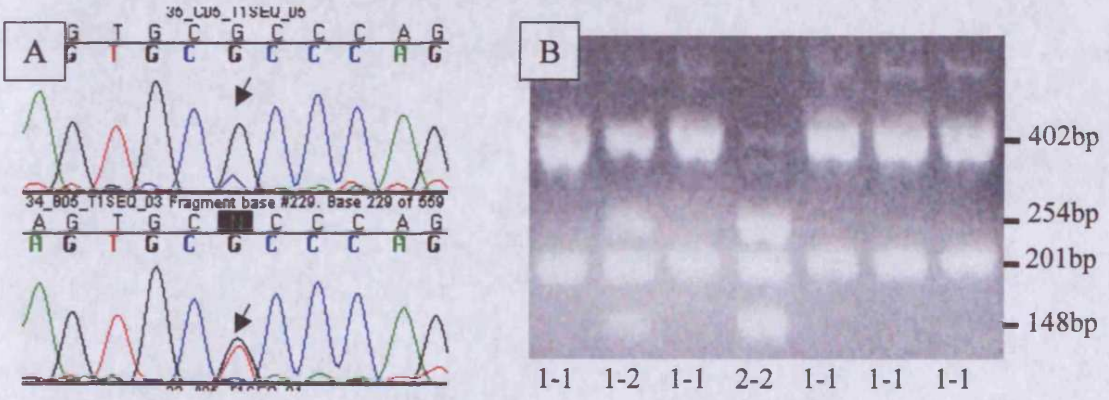

Figure 3.20 A) Sequence chromatograms for the *SLC18A3* SNP -287 G>T (rs2377879) showing a G/G homozygote in the upper panel and a G/T heterozygote in the lower panel. **B)** RFLP fragments generated by the -287 G>T *Bsi*HKA I assay. Individuals homozygous for the G allele (1-1) were defined by the presence of two bands of size 402bp and 201bp. Individuals homozygous for the T allele (2-2) were defined by the presence of three bands of size 254bp, 201bp and 148bp. G/T heterozygotes (1-2) displayed four bands of size 402bp, 254bp, 201bp and 148bp.

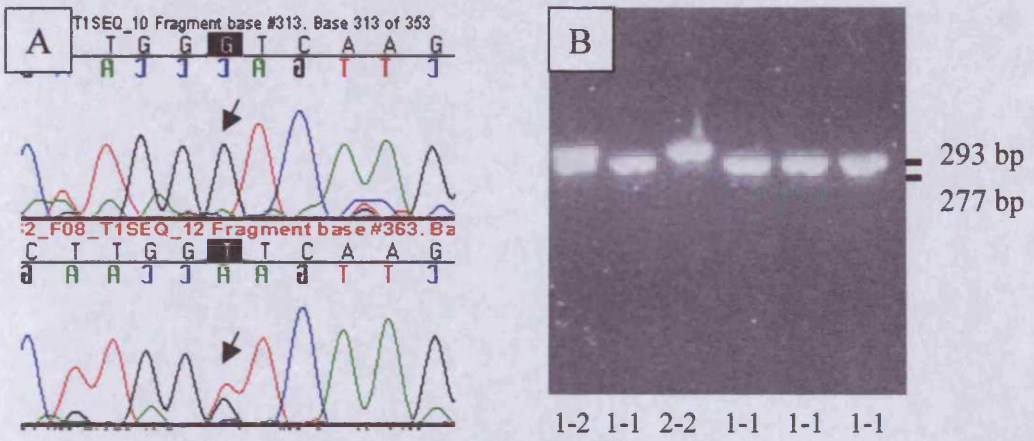

Figure 3.21 A) Sequence chromatograms for the *SLC18A3* SNP 1638 G>T (rs2269338) showing a G/G homozygote in the upper panel and a G/T heterozygote in the lower panel. **B)** RFLP fragments generated by the 1638 G>T *Ava* I assay. Individuals homozygous for the G allele (1-1) were defined by the presence of two bands of size 277bp and 16bp. Individuals homozygous for the T allele (2-2) were defined by the presence of one band of size 293bp. G/T heterozygotes (1-2) displayed three bands of size 293bp, 277bp and 16bp. Note that the 16bp band ran off the gel due to the small size.

4. CHROMOSOME 10: POSITIONAL CANDIDATES FOR LOAD

4.1 Chromosome 10 and LOAD

As described in Chapter 1, there is strong evidence for the presence of a LOAD susceptibility gene on chromosome 10. Our department and collaborators have performed a two-stage genome screen to search for novel risk factors for LOAD[143-145]. The strongest evidence for linkage was on chromosome 10, with a multipoint lod score (MLS) of 3.9, which is significant according to Lander and Kruglyak guidelines[34]. This peak was greater than that observed for chromosome 19 (MLS=1.3), attributed to *APOE*. Further support was observed in an independent quantitative trait loci (QTL) study of plasma levels of $A\beta_{42}$, showing significant linkage directly under the peak we observed[146]. It is therefore reasonable to hypothesise that this chromosome 10 locus is a major risk factor for LOAD. Our linkage peak covers a 42cM region on chromosome 10 and is defined by microsatellite markers D10S1426 (59 cM, 30.5Mb, 10p11.23) and D10S2327 (101 cM, 80.1Mb, 10q22.3) and contains 219 known genes according to Ensembl (http://www.ensembl.org). In addition to the *CHAT* and *SLC18A3* genes described in the previous chapter, seven further genes that map to this region were selected as candidates for involvement in LOAD; *ALOX5*, *DKK1*, *UBE2D1*, *DNAJC12*, *SIRT1*, *SGPL1* and *SEC24C*. Although the proteins encoded by some of these genes may seem of more functional relevance to LOAD than others, the primary reason for selection of all seven candidates was the fact that they map to the linkage region. The positions of each gene on chromosome 10 are indicated in Figure 4.1 (p.113) and a brief description of each candidate is given below.

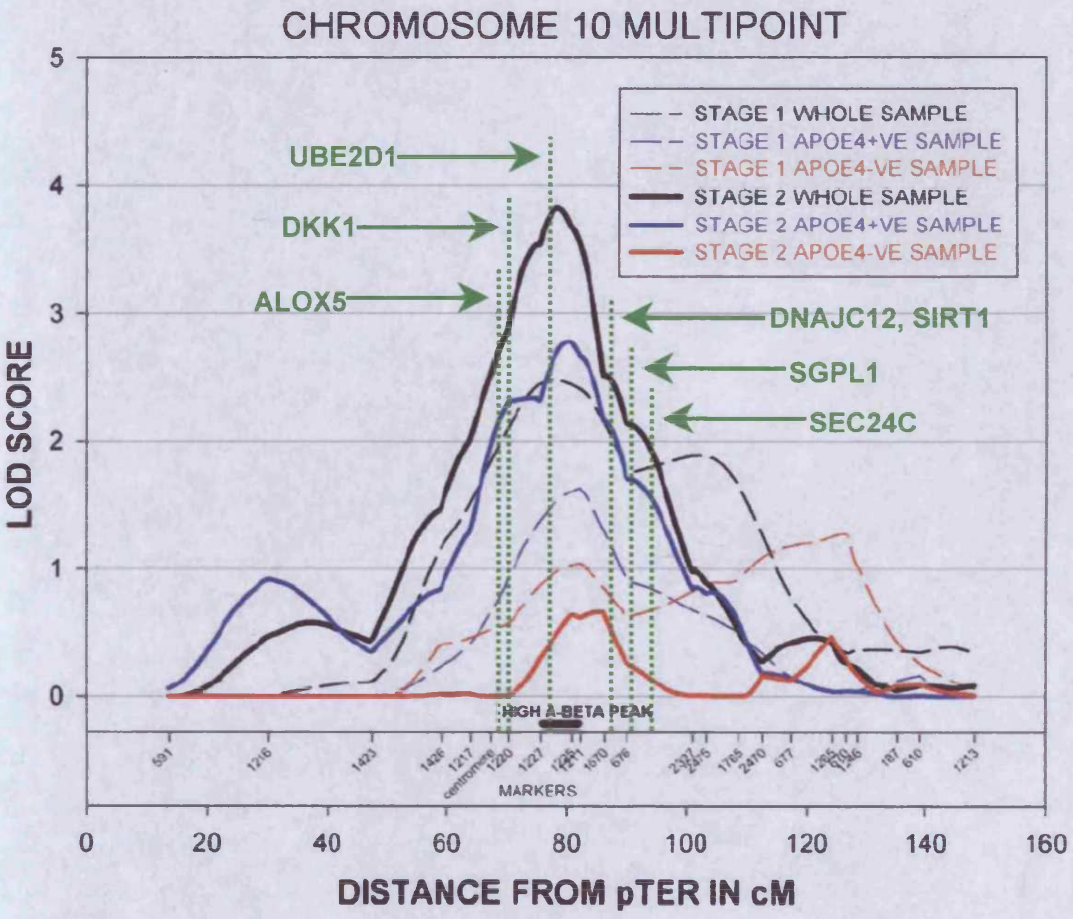

Figure 4.1. Chromosome 10 multipoint map for LOAD by Myers *et al.* (2000)[144] including the positions of the seven candidate genes examined. The region of linkage for high plasma $A\beta_{42}$ from the Ertekin-Taner *et al.* (2000)[146] report is also shown.

4.1.1 ALOX5

5-lipoxygenase (ALOX5) is the first committed enzyme in the biosynthetic pathway leading to the formation of leukotrienes from arachidonic acid. Both 5-lipoxygenase and cyclooxygenase (COX) use arachidonic acid as their common substrate, but whereas the ALOX5 pathway generates inflammatory leukotrienes, the COX pathway generates inflammatory prostaglandins. Leukotrienes and prostaglandins belong to a family of biologically active molecules called eicosanoids[284].

The human *ALOX5* gene is located on chromosome 10q11.2 at approximately 45Mb (according to UCSC version hg16), contains fourteen exons and spans 71875bp. In the 5' flanking region of the gene, both positive and negative regulatory regions as well as a transcription factor-binding region have been identified[285]. Expression of ALOX5 has been observed in neurons, especially in the cortex and in hippocampal pyramidal cells[286-288] and significant changes in ALOX5 activity/expression have been correlated with ageing[289, 290]. Given that inflammatory processes have been implicated in the pathophysiology of AD[291,292] and that retrospective, epidemiological studies have shown that long-term use of anti-inflammatory drugs such as NSAIDs is associated with a decreased risk of developing AD[293-296], ALOX5 is a plausible functional as well as positional candidate for involvement in Alzheimer's disease.

4.1.2 DKK1

Dkk1, a member of the Dickkopf family, is an antagonist of the Wnt signalling pathway[297,298]. Members of the Wnt family interact with frizzled, a seven-transmembrane receptor and the co-receptor lipoprotein-related proteins, LRP-5 and -6[299-303]. Activation of frizzled recruits the cytoplasmic bridging molecule, dishevelled, so as to inhibit glycogen synthetase kinase 3β (GSK-3β). Inhibition of GSK-3β decreases phosphorylation of β-catenin, preventing its degradation by the ubiquitin-mediated pathway[304, 305]. Unphosphorylated β-catenin accumulates in the cytoplasm and translocates to the nucleus, where it can associate with members of the LEF/TCF (T cell-specific transcription factor 1) family and become a transcriptional transactivator[306]. Dkk1 inhibits Wnt signalling by binding to LRP-5/6 and to the associated protein kremen, which results in the dissociation of LRP-5/6

from frizzled thereby preventing the formation of a functional Wnt receptor complex[300, 302, 307-309]. Inhibition of Wnt signalling has at least two consequences that might be relevant to AD pathology: (1) the enhanced phosphorylation of τ by GSK-3β [310]and (2) the degradation of β-catenin, which is known to interact with presenilin 1[311].

The human *DKK1* gene is located on chromosome 10q11.2 at approximately 53.4Mb, contains four exons and spans 3062bp.

4.1.3 UBE2D1

The ubiquitin-proteasomal pathway (UPP) is involved in many cellular processes, such as the cell cycle, apoptosis, endocytosis, and ATP-dependent proteasomal breakdown of proteins[312]. The UPP plays a prominent role in the detoxification and targeting of damaged proteins for degradation. Ubiquitinated proteins are found at increased levels in neurodegenerative diseases including AD[313] suggesting that the degree of protein damage has exceeded the capacity of the UPP to clear it, or that the efficiency of the UPP is in some way impaired. At least three classes of enzymes are involved in the conjugation of ubiquitin to proteins. Ubiquitin is first activated by ubiquitin-activating enzyme (E1) in the presence of ATP. Next, the activated ubiquitin is transferred to ubiquitin-conjugating enzyme (E2). E2 enzymes either by themselves or in combination with E3 enzymes (ubiquitin protein ligases) then transfer polyubiquitin chains to target proteins. The polyubiquitin chain is then recognised by the proteasome and degraded in an ATP-dependent manner[312].

UBE2D1 is a member of the E2 ubiquitin-conjugating enzymes and is involved in the iron-dependent ubiquitination of the hypoxia-inducible factor (HIF) by the von Hippel-Lindau tumour suppressor (pVHL) E3 ligase complex[314]. It is also significantly upregulated in the liver of iron-overloaded patients with hereditary haemochromatosis[315]. The human *UBE2D1* gene is located on chromosome 10q11.2-q21 at approximately 59.4Mb, contains seven exons and spans 35770bp.

4.1.4 DNAJC12

Molecular chaperones comprise several highly conserved families of related proteins, many of which are also heat shock proteins (Hsp). Chaperones of the Hsp70 family are highly versatile proteins involved in a large variety of processes, ranging from folding of newly synthesised proteins to facilitation of proteolytic degradation of unstable proteins[316-318]. Hsp40/DnaJ partner proteins directly interact with the Hsp70 proteins cooperatively to perform the chaperone function. Many Hsp40/DnaJ proteins have four domains: an N-terminal J domain which is believed to mediate interaction with Hsp70 protein; a glycine/phenylalanine (G/F)-rich domain; a central repeat region (CRR) and a weakly conserved C-terminal domain. The J domain-only proteins, which include DNAJC12, refer to members of a subclass of the Hsp40/DnaJ family that possess the J domain, but lack the G/F-rich domain and CRR[319]. The involvement of Hsp in several neurodegenerative diseases such as Parkinson's disease and Huntington's disease has been documented[320-323] suggesting a possible role for DNAJC12 in AD.

The human *DNAJC12* gene is located on chromosome 10q22.1 at approximately 68.9Mb and encodes two different isoforms, A and B. Variant A has five exons and

spans 41510bp. Variant B has three exons, spans 26972bp and differs in part of exon 3 and the 3' UTR with respect to variant A.

4.1.5 SIRT1

In *Saccharomyces cerevisiae*, the silent information regulator 2 (Sir2), which encodes an NAD-dependent protein deacetylase, functions in gene silencing, heterochromatin formation, DNA repair and suppression of DNA recombination[324-326]. Sir2 is a limiting component of yeast longevity. Cells lacking Sir2 have a reduced replicative life span and cells with an extra copy of *SIR2* display a much longer life span than wild type[327]. This extension probably results from a hypersilencing in the rDNA, which reduces recombination and the production of extrachromosomal rDNA circles, a known cause of senescence in ageing mother cells[328]. In *Caenorhabditis elegans*, increased dosage of the worm *sir-2.1* gene also extends the lifespan of worms beyond the wild-type[329] and the nearest human homologue SIRT1 has been shown to inhibit apoptosis through deacetylation of p53[330, 331]. These findings suggest that Sir2 and its homologues have a conserved role in the regulation of survival at both the cellular and organismal levels[332].

The human *SIRT1* gene is located on chromosome 10q22.1 at 69Mb, contains nine exons and spans 33716bp.

4.1.6 SGPL1

Sphingosine-1-phosphate lyase, SGPL1, catalyses the last step in sphingolipid breakdown[333]. The enzyme cleaves phosphorylated sphingoid bases (PSBs) into fatty aldehydes and phosphoethanolamine[334]. SGPL1 has one hydrophobic transmembrane

region near its amino terminus and a conserved pyridoxal-dependent decarboxylase domain that contains several essential cysteine residues[334].

In general, the prevalent sphingolipids of cells are the complex sphingolipids: phosphosphingolipids such as sphingomyelins and glycosphingolipids such as ganglioside GM1. Complex sphingolipids are found in all eukaryotes and some prokaryotes and viruses, mainly as components of the plasma membrane and related organelles. Some categories of sphingolipids spontaneously aggregate (in conjunction with cholesterol) to form liquid-ordered microdomains termed " lipid rafts"[335]. Lipid rafts are dynamic assemblies of proteins and lipids that float freely within the liquid-disordered bilayer of cellular membranes but can also cluster to form larger, ordered platforms. Cholesterol acts as a spacer between the hydrocarbon chains of the sphingolipids and functions as a dynamic glue that keeps the raft assembly together[336]. Removal of raft cholesterol leads to dissociation of most proteins from rafts and renders them non-functional[337]. There are three types of membrane proteins: those that are mainly found in the rafts, those that are present in the liquid-disordered phase, and those that move in and out of rafts[337]. The β-secretase, BACE1, is a constitutive raft resident[336]. Lipid rafts function by separating and condensing molecules, such that they can exert their function in concert. For example, they have been proposed to regulate APP processing by favouring the clustering of APP and BACE1[75]. Several studies have also reported a physical association of Aβ with GM1, the major galacto-shingolipid in lipid rafts[338, 339]. This association facilitates the aggregation of soluble Aβ in the form of amyloid fibrils[340].

The human *SGPL1* gene is located on chromosome 10q21 at approximately 71.9Mb, contains fifteen exons and spans 64151bp.

4.1.7 SEC24C

Exit of soluble and membrane proteins from the yeast endoplasmic reticulum occurs in vesicles covered with the COPII coat, which consists of the proteins Sec23p, Sec24p, Sec13p and Sec31p, and the small GTPase Sar1p[341-345]. The Sec23p–Sec24p complex is probably the component responsible for cargo recognition[346, 347]. The COPII pathway has a mammalian counterpart and most of the COPII components have been identified, including a human orthologue of Sec24p, SEC24C[348]. Since the secretase activities that process APP are localised in different intracellular compartments, it is possible that membrane transport is a factor in the pathogenesis of AD.

The human *SEC24C* gene is located on chromosome 10q22.3 at approximately 74.8Mb, contains 23 exons and spans 27787bp.

These seven candidate genes have been screened for sequence variants by denaturing high performance liquid chromatography (DHPLC). All polymorphisms detected were tested for association with LOAD in DNA pools of 186 LOAD cases and 186 age- and sex-matched controls.

4.2 Materials and Methods

Described here are the specific methods used to study these seven genes. More detailed descriptions of subject groups and methods are described in Chapter 2.

4.2.1 Subjects

The mutation screening sample consisted of 14 UK Caucasian patients, with age at onset >65 years. All SNPs identified were tested for association with LOAD in the MRC pools comprised of 186 UK Caucasian AD patients (age at onset 74.34 ± 6.461 years) and 186 age- and sex-matched controls (age at collection 75.42 ± 6.535 years). SNPs for which pooled genotyping showed significant (P<0.1) differences between cases and controls were individually genotyped in a subset of the MRC sample comprising 405 UK Caucasian AD patients (age at onset 75.54 ± 6.669 years) and 405 age- and sex-matched controls (age at collection 76.25 ± 6.407 years). The samples that made up the pools were included in the sample that underwent individual genotyping. All patients were diagnosed according to NINCDS-ADRDA criteria[17]. Cognitive function of controls was assessed using the mini mental-state exam (MMSE)[18]. Only those with a score of at least 28 were included in the study.

4.2.2 Collection of Gene Sequences

The cDNA sequence(s) for each gene was obtained from the GenBank database at NCBI (http://www.ncbi.nlm.nih.gov). Determination of coding sequences, untranslated regions (UTRs) and intronic regions was based on alignment of the cDNA sequences with genomic clone sequences, using BLAST sequence homology searches.

4.2.3 Polymerase Chain Reaction (PCR)

PCR fragments spanning exons, UTRs and limited 5' flanking regions were designed using Primer 3.0 (http://www-genome.wi.mit.edu/cgi-bin/primer/primer3_www.cgi). Primer sequences for each gene are listed in the appropriate section. PCR amplification was performed under standard conditions of 1X PCR buffer (Qiagen), 1.5 mM $MgCl_2$, 250 μM dNTPs, 0.5 μM of each primer, 0.6 units Hot Star Taq (Qiagen) and 48 ng genomic DNA in a 24 μl reaction. Cycling was conducted in a MJ Tetrad (MJ Research) with an initial denaturation of 94°C for 15min, followed by 35 cycles of 94°C for 30s, optimal annealing temperature for 30s and 72°C for 45s with a final extension step of 72°C for 10 min. Synthesis of appropriately sized PCR products was confirmed by electrophoresis on 2% agarose gels.

4.2.4 Denaturing High Performance Liquid Chromatography (DHPLC)

The search for polymorphisms was performed by DHPLC scanning on the Wave™ DNA Fragment Analysis System (Transgenomic). The 14 screening samples were amplified as described above, except the final extension in the PCR protocol was followed by denaturation at 94°C for 5min and then cooling to 54°C over 40min, to allow heteroduplex formation. Column temperature and acetonitrile gradient were determined with the DHPLC Melt program (http://insertion.stanford.edu/melt1.html). To ensure maximum sensitivity, in addition to the (highest) temperature suggested by the software (n°C), each fragment was also run at n+2°C. The resultant chromatograms were compared, with a shift in trace pattern indicative of a heteroduplex. An example of a DHPLC trace is displayed at the end of this chapter (Figure 4.9).

4.2.5 DNA Sequencing

For fragments that displayed a heteroduplex peak, the PCR products of one heterozygous and one homozygous sample were incubated at 37°C with 1 unit each of shrimp alkaline phosphatase and exonuclease I to remove unincorporated primers and dNTPs. Purified products were then bidirectionally sequenced on an ABI 3100 Genetic Analyzer (Applied Biosystems) using the Big Dye Terminator (v2.0) Cycle Sequencing kit (Applied Biosystems). Sequence traces were subsequently exported to the Sequencher™ program in order to characterise polymorphisms. Sequence chromatograms for all polymorphisms identified are displayed at the end of this chapter (Figures 4.10 to 4.61).

4.2.6 Genotyping

4.2.6.1 Pooled Genotyping

Each SNP was typed in pools by primer extension, using the ABI SNaPshot™ Multiplex kit. Extension primers were designed to be 15-40 nucleotides long and directly adjacent to the polymorphism. For a particular SNP, each pool was PCR amplified in duplicate. An individual DNA sample, heterozygous for each SNP was also amplified. Samples were then purified by incubation with 1 unit each of exonuclease I and shrimp alkaline phosphatase at 37°C for 1 hour. Primer extension was then performed according to SNaPshot™ kit instructions and products electrophoresed on the ABI 3100 Genetic Analyser. The resultant data was analysed using Genotyper® 2.5 and the calculated peak height ratios from each replicate were averaged. An example of the traces generated in pooled genotyping by the primer extension method is displayed at the end of this chapter (Figure 4.62). I genotyped all SNPs except for the eight identified in the *SIRT1* gene (which were genotyped by

Luke Jehu) and the five SNPs identified in the *SEC24C* gene (which were genotyped by Dragana Turic). Three insertion/deletion (indel) polymorphisms were identified in the course of this study. All three polymorphisms were genotyped in pools by Melanie Dunstan using a PCR sizing method. Amplimers spanning the indel of interest are amplified with one fluorescently labelled and one unlabelled primer. Products are electrophoresed on an ABI 377 DNA Sequencer. The resultant data is analysed using Genotyper® 2.5.

4.2.6.2 Individual Genotyping

Any SNP showing an association in pools at the α=0.1 level was typed individually in the aforementioned MRC association sample subset, consisting of 405 LOAD cases and 405 age- and sex-matched controls. Where a natural restriction site existed that could distinguish between the two alleles of a SNP, a restriction fragment length polymorphism (RFLP) assay was designed, using the original PCR primers. Where no natural site existed, an artificial restriction site was created by primer-generated mutagenesis. For each RFLP assay, the MRC association sample subset was PCR amplified, then digested with 5 units of the appropriate restriction enzyme. Digested products were electrophoresed on 2.5-3% agarose gels. Examples of the expected profile for each genotype of an individually typed SNP are shown at the end of this chapter (Figures 4.63 to 4.64).

4.2.7 Statistical Analyses

$\chi 2$ and Fisher's exact test were used to analyse SNP associations using the Simple Interactive Statistical Analysis pages (http://home.clara.net/sisa); Fisher's exact test was used for analyses where one or more cell had a count of <5. All polymorphisms

typed individually were tested for deviation from Hardy-Weinberg equilibrium using an updated version of the HW program written by Peter McGuffin and Peter Holmans (update by Marian Hamshere).

4.3 Results

4.3.1 ALOX5

Determination of the exons and intron/exon boundaries was based on alignment of the cDNA sequence NM_000698.1 against genomic sequence available from the UCSC Genome Bioinformatics Site (http://genome.ucsc.edu). PCR primers and assay details can be found in Table 4.1 (p.125). Extension primers are listed in Table 4.2 (p.126). Nine SNPs were identified in the *ALOX5* gene: one coding synonymous SNP T90T (8323 G>A), two 3'UTR SNPs (71772 C>A and 71776 A>G), two 5'flanking region SNPs (-1700 G>A and -557 T>C) and four intronic SNPs (268 G>A, 8172 C>T, 66971 A>G and 68965 G>A). These SNPs are shown in Figure 4.2 and Table 4.2 (p.126). Six SNPs were successfully genotyped in the MRC pools comprised of 186 cases and 186 age- and sex-matched controls. Of the three that failed, two (268 G>A and 8323 G>A) had successfully designed assays but the minor allele frequencies were too low to be reliably estimated from pools. The estimated allele frequencies and counts calculated for each successfully typed SNP are shown in Table 4.3 (p.127). There were no significant differences observed in the allele frequencies of any of the SNPs between cases and controls.

Fragment name	Spanning	Sense Primer Sequence (5'→3')	Antisense Primer Sequence (5'→3')	Size (bp)	Annealing Temperature (°C)
ALOX5 NRR1	Negative regulatory region 1	AAAGAACAGCGTTGGTGGAT	CAAATTCATTGTGTTGCATGTG	255	58
ALOX5 NRR2	Negative regulatory region 2	ACCACTGGCCATCTCTGG	CTCCTCAGCGAGGTGTCTG	455	62
ALOX5 PRR	Positive regulatory region	TTAGCCGAGATCAATACACGC	GGGTGTGGAGAAGGTTTCG	154	56
ALOX5 TFBR	Transcription factor binding region	AGGAACAGACACCTCGCTGAGGAGAG	GAGCAGCGAGCGCCGGGAGCCTCGGC	272	GC64
ALOX5 x1	5'UTR and exon 1	AGGAGGCTGCGGCGCTAGA	AGTTCTGCCCTCCCTGACA	383	GC57
ALOX5 x2	Exon 2	CTCCAGAACAAAGGCTCAGG	ACTTTCGGTTCTTGGGAAGC	306	62
ALOX5 x3	Exon 3	GGCCATACACTGTGGAAAGG	GAGGGAAGCCTGAACACTTG	256	62
ALOX5 x4	Exon 4	AGGAAAGGAGTGAGGGTTCC	TCTCCCTGTGTAACATCGTCTG	304	62
ALOX5 x5	Exon 5	GTTGTGAGGACCCCTGAGAG	TCAGACAGGAGAGCAGCATC	261	62
ALOX5 x6	Exon 6	GGCTGCCCTCTACTCAGAGC	CTGGCTTCCACCTGACAGAC	281	62
ALOX5 x7	Exon 7	CTGCTGAGCCTGATTTGGAC	TGGATCGCAGAGGACTGAG	240	62
ALOX5 x8	Exon 8	CTCCAGGCTCTTCTGATTCC	TCTCAGATGCCCTCCCATAG	386	57
ALOX5 x9	Exon 9	GCCTCCAGCACTTATTCAGC	CAGGCTGGGCTCTTCCAG	298	62
ALOX5 x10	Exon 10	TTCCTCAGGGATGGGTCTG	CCGCCCCAGGTAGTCAGG	315	58
ALOX5 x11	Exon 11	AGTCCCAGCGTCCGTGAG	TGAGGCCCAGTCCCTGAG	376	GC57
ALOX5 x12	Exon 12	TGGGGTCCTCAGGGACTG	GTCCGAGGGTGCAGTACG	243	62
ALOX5 x13	Exon 13	GAAAGAGGATGGACGGACTG	AGGCTGAGGAACCGCTTAAC	357	62
ALOX5 x14A	Exon 14 and part of 3'UTR	ACACGGGTAGTGGATTGACC	GCAGTTCCCTGAAGATCAAAG	383	62
ALOX5 x14B	Part of 3'UTR	CTTGGCAGTCACATCTCTTCC	ATGGCAGTGAGCTGTTTGG	398	62

Table 4.1. Details of *ALOX5* PCR assays, including PCR primers, annealing temperatures and size of amplimers. Annealing temperatures preceded by 'GC' indicate that amplimers are GC-rich and require the use of Q-solution for amplification (see Chapter 2).

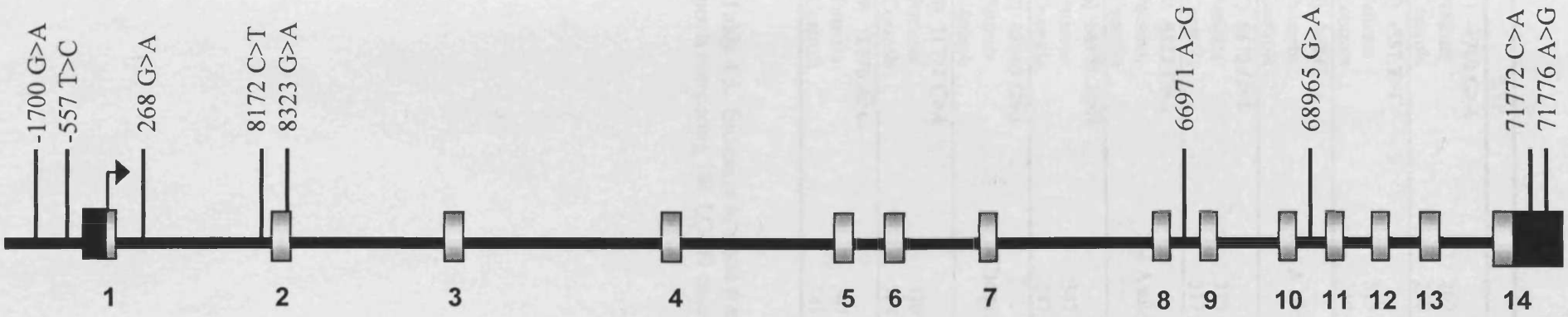

Figure 4.2. Diagram of the *ALOX5* gene (not to scale), indicating the positions of identified polymorphisms. For numbering of polymorphisms, +1 indicates 'A' of ATG translation start codon. Grey blocks indicate coding sequence, black blocks indicate untranslated regions.

SNP No.	SNP Name	Location	SNP Flanking Sequence	Fragment	Extension Primer (5'→3')	Expected Allele Peaks
1	-1700 G>A	1657bp upstream exon 1	TTACAGATCA**R**TGGACTAGAA	ALOX5 NRR1	TGTATAGCATGTACATTACAGATCA	A (Green) & G (Blue)
2	-557 T>C	516bp upstream exon 1	AGGAAGCCCT**Y**CTGATTCTCT	ALOX5 NRR2	GCGACCCATGAGAGAATCAG	A (Green) & G (Blue)
3	268 G>A	118bp downstream exon 1	GGACAGGACT**R**GGGGTGTCCA	ALOX5 x1	GCGGCCCGGACAGGACT	A (Green) & G (Blue)
4	8172 C>T	32bp upstream exon 2	CAGGAGACCA**Y**GCATGGCCTG	ALOX5 x2	AACAAAGGCTCAGGAGACCA	C (Black) & T (Red)
5	8323 G>A	Exon 2 (Thr→Thr)	CGCTGAAGAC**R**CCCCACGGGG	ALOX5 x2	GAAGTACATCACGCTGAAGAC	A (Green) & G (Blue)
6	66971 A>G	94bp upstream exon 9	GCATCATCCT**R**TAGGGCAGGC	ALOX5 x9	CACCCAGGCCTGCCCTA	C (Black) & T (Red)
7	68965 G>A	28bp downstream exon 10	GGTGGTCCTG**R**GGGAGGAGCC	ALOX5 x10	GGGTCCCGGCTCCTCCC	C (Black) & T (Red)
8	71772 C>A	3'UTR	ATAGTAGGTA**M**CCARTTCAAT	ALOX5 x14B	CAATTCCTTGCACATAGTAGGTA	A (Green) & C (Black)
9	71776 A>G	3'UTR	TAGGTAMCCA**R**TTCAATTACT	ALOX5 x14B	CTTGCACATAGTAGGTAMCCA	A (Green) & G (Blue)

Table 4.2. List of polymorphisms identified in the *ALOX5* gene, including the location of the polymorphism relative to the coding sequence, flanking sequence of the polymorphism, the extension primer used for SNaPshot and the expected allele peaks in the primer extension assay.

SNP	Allele		*P*
1) -1700 G>A	**G**	**A**	
Patients	262 (0.70)	110 (0.30)	
Controls	259 (0.70)	113 (0.30)	0.8102
2) -557 T>C	**T**	**C**	
Patients	315 (0.85)	57 (0.15)	
Controls	310 (0.83)	62 (0.17)	0.6180
3) 268 G>A			
Patients	The A allele was too rare to be detected in pools.		
Controls			
4) 8172 C>T	**C**	**T**	
Patients	323 (0.87)	49 (0.13)	
Controls	317 (0.85)	55 (0.15)	0.5258
5) 8323 G>A			
Patients	The A allele was too rare to be detected in pools.		
Controls			
6) 66971 A>G	**A**	**G**	
Patients	347 (0.93)	25 (0.07)	
Controls	347 (0.93)	25 (0.07)	1.0000
7) 68965 G>A			
Patients	The primer extension reaction could not be optimised.		
Controls			
8) 71772 C>A	**C**	**A**	
Patients	310 (0.83)	62 (0.17)	
Controls	309 (0.83)	63 (0.17)	0.9218
9) 71776 A>G	**A**	**G**	
Patients	347 (0.93)	25 (0.07)	
Controls	341 (0.92)	31 (0.08)	0.4044

Table 4.3. Estimates of allele frequencies and counts of *ALOX5* polymorphisms in DNA pools comparing 186 LOAD cases with 186 age- and sex-matched controls.

4.3.2 DKK1

Determination of the exons and intron/exon boundaries was based on alignment of the cDNA sequence XM_005730.4 against genomic sequence available from the UCSC Genome Bioinformatics Site (http://genome.ucsc.edu). PCR primers and assay details can be found in Table 4.4 (p.129). Extension primers are listed in Table 4.5 (p.129). RFLP primers and assay details are listed in Table 4.6 (p.130). Six SNPs were identified in the *DKK1* gene: one coding synonymous SNP A106A (560 G>A), three 5'flanking region SNPs (-621 C>G, -446 G>C and -294 Ins C) and two intronic SNPs (463 C>T and 2074 G>A). These SNPs are shown in Table 4.5 (p.129) and Figure 4.3 (p.130). Four SNPs were successfully genotyped in the MRC pools. Both SNPs that failed (-446 G>C and –294 Ins C) had successfully designed assays but the minor allele frequencies were too low to be reliably estimated from pools. The estimated allele frequencies and counts calculated for each successfully typed SNP are shown in Table 4.7 (p.131). For the intronic SNP 463 C>T, the C allele was significantly more frequent in cases than controls (P=0.0210). Therefore this SNP was genotyped individually in 405 cases and 405 age- and sex-matched controls (see Table 4.8, p.131). Although the association was again observed in the cases and controls that made up the pools (see Appendix A), in the enlarged sample the frequency of the C allele was similar in cases and controls (94% and 93% respectively; P=0.2299).

Fragment name	Spanning	Sense Primer Sequence (5'→3')	Antisense Primer Sequence (5'→3')	Size (bp)	Annealing Temperature (°C)
DKK1 PROM	5' Flanking region	GAGGAGGGCAACTGAAGGAC	CCCTGCGGTCCCAGAGTC	626	62
DKK1 x1	5'UTR and exon 1	GCACGTTCTACTCCCTCGTC	TTTGTTGTCTCCCTCCCAAG	548	60
DKK1 x2	Exon 2	ATAGACGCTCAAAGGCTGGA	GGTTTTGGAGAGGTGGACAG	325	60
DKK1 x3	Exon 3	GACCGGAGACAAACAGAACC	GGCATAACAGACTGCCACTG	370	60
DKK1 x4A	Exon 4 and part of 3'UTR	GATCACAATCCCAAAATGTATGTC	TCTTTATGGAACTCCCCTGTG	455	60
DKK1 x4B	Part of 3'UTR	ACAGGTAAGTGCCACACTGAG	AACGATGCAGGTTTAACAGTAAC	541	60
-294 Ins C	-294 Ins C polymorphism	FAM-TGCTATAACGCTCGCTGGTA	TTGGGAGGGAGACAACAAAG	180	60

Table 4.4. Details of *DKK1* PCR assays, including PCR primers, annealing temperatures and size of amplimers. FAM=fluorescent label

SNP No.	SNP Name	dbSNP Identity	Location	SNP Flanking Sequence	Fragment	Extension Primer (5'→3')	Expected Allele Peaks
1	-621 C>G	rs1528878	501bp upstream exon 1	AGGCGTCTTG**S**TAGAGCCATT	DKK1 PROM	GGTCTGTAATTCAATGGCTCTA	C (Black) & G (Blue)
2	-446 G>C	rs1528879	326bp upstream exon 1	TGCCAGGCAA**S**GGCACCCAAG	DKK1 PROM	CAACCCTTACTGCCAGGCAA	C (Black) & G (Blue)
3	-294 Ins C		174bp upstream exon 1	AAGGCCCCCCC**T**TCATGTACA	DKK1 PROM	Typed by PCR sizing	N/A
4	463 C>T		23bp upstream exon 2	GTGCCTCACC**Y**TCTCCCCGAA	DKK1 x2	CGTCTGGGTGCCTCACC	C (Black) & T (Red)
5	560 G>A	rs2241529	Exon 2 (Ala→Ala)	GAGGGGACGC**R**GGCGTGCAAA	DKK1 x2	ACCCGCGGAGGGGACGC	A (Green) & G (Blue)
6	2074 A>G	rs1569198	43bp upstream exon 4	TGCAGGTTTA**R**CAGTAACTAT	DKK1 x3	GTCTTTTGAATTATTTTAGTGAA ACGATGCAGGTTTA	A (Green) & G (Blue)

Table 4.5. List of polymorphisms identified in the *DKK1* gene, including the location of the polymorphism relative to the coding sequence, flanking sequence of the polymorphism, the extension primer used for SNaPshot (if applicable) and the expected allele peaks in the primer extension assay.

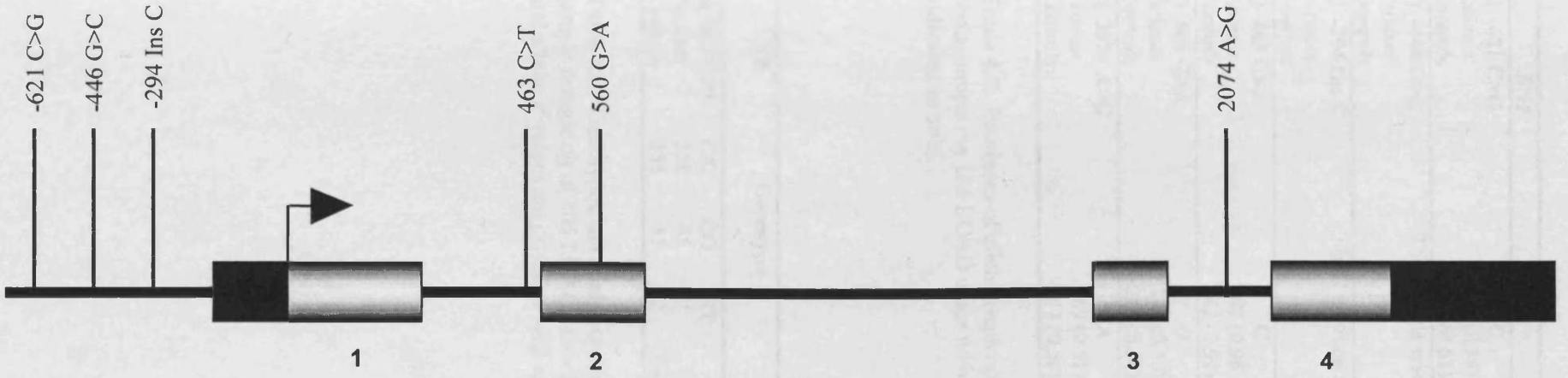

Figure 4.3. Diagram of the *DKK1* gene (not to scale), indicating the positions of identified polymorphisms. For numbering of polymorphisms, +1 indicates 'A' of ATG translation start codon. Grey blocks indicate coding sequence, black blocks indicate untranslated regions.

SNP	RFLP Sense Primer (5'→3')	RFLP Antisense Primer (5'→3')	Size (bp)	Annealing Temperature (°C)	Restriction Enzyme	Restriction Fragments (bp)
4) 463 C>T	TTCAGGACTCACCATTTTTGC	GACGTCTGGGTGCCTCAgC	217	60	*Alu* I	C=217 T=199, 18

Table 4.6. Assay details of genotyping assay of *DKK1* SNP, 463 C>T, including RFLP primers, amplimer size, PCR annealing temperature, restriction enzyme and expected RFLP fragment sizes. A lower case letter in the RFLP primer indicates the 'mismatched base' introduced to the RFLP amplimer to generate an artificial restriction site (see Chapter 2).

SNP	Allele		*P*
1) -621 C>G	**C**	**G**	
Patients	328 (0.88)	44 (0.12)	
Controls	327 (0.88)	45 (0.12)	0.9100
2) -446 G>C	The C allele was too rare to be detected in pools.		
Patients			
Controls			
3) -294 Ins C	The C insertion allele was too rare to be detected		
Patients	in pools.		
Controls			
4) 463 C>T	**C**	**T**	
Patients	357 (0.96)	15 (0.04)	
Controls	342 (0.92)	30 (0.08)	**0.0210**
5) 560 G>A	**G**	**A**	
Patients	185 (0.50)	187 (0.50)	
Controls	201 (0.54)	171 (0.46)	0.2403
6) 2074 A>G	**A**	**G**	
Patients	189 (0.51)	183 (0.49)	
Controls	187 (0.50)	185 (0.50)	0.8834

Table 4.7. Estimates of allele frequencies and counts of *DKK1* polymorphisms in DNA pools comparing 186 LOAD cases with 186 age- and sex-matched controls. *P* values<0.1 are indicated in bold.

SNP	Genotype			*P*	Allele		Odds Ratio (95% C.I.)	*P*
4) 463 C>T	**C/C**	**C/T**	**T/T**		**C**	**T**		
Patients	358	45	1		761 (0.94)	47 (0.06)	0.7834	
Controls	335	53	2	0.4715	723 (0.93)	57 (0.07)	(0.5255-1.1679)	0.2299

Table 4.8. Genotypes and allele counts for *DKK1* SNP, 463 C>T, in a subset of the MRC sample consisting of 405 LOAD cases and 405 age- and sex-matched controls. Genotypic and allelic *P* values are given, as well as odds ratios and 95% confidence intervals (C.I.).

4.3.3 UBE2D1

Determination of the exons and intron/exon boundaries was based on alignment of the cDNA sequence NM_003338.2 against genomic sequence available from the UCSC Genome Bioinformatics Site (http://genome.ucsc.edu). PCR primers and assay details can be found in Table 4.9 (p.133). Extension primers are listed in Table 4.10 (p.135). Eight SNPs were identified in the *UBE2D1* gene: one coding synonymous SNP P118P (32771 C>G) and seven intronic SNPs (144 G>T, 169 G>C, 182 C>T, 305 G>A, 26120 T>C, 28525 A>G, 32771 C>G and 33403 T>C). These SNPs are shown in Table 4.10 (p.135) and Figure 4.4 (p.136). Only four SNPs were successfully genotyped in the MRC pools. The estimated allele frequencies and counts calculated for each successfully typed SNP are shown in Table 4.11 (p.136). There were no significant differences observed in the allele frequencies of any of the SNPs between cases and controls.

Fragment name	Spanning	Sense Primer Sequence (5'→3')	Antisense Primer Sequence (5'→3')	Size (bp)	Annealing Temperature (°C)
UBE2D1 PROM	5' Flanking region	GTAGTTCCAGCCCTGTCCTC	TGCATAGGAATTGGAGAGTGG	580	63
UBE2D1 x1B	Part of 5'UTR	GAGGACAGGGCTGGAACTAC	TCACTTTCTGAATCCTCTTCAGC	346	66
UBE2D1 x1	Part of 5'UTR and exon 1	GCCTGGGACCTGACCCTGCT	ACGACCCACGCCCCTGAG	309	67
UBE2D1 Pr	Part of exon 1	TCGCTACAGCTATGTGACCTG	ATGGCGCTGAAGAGGATTC	657	62
UBE2D1 x2-3	Exons 2 & 3	ATGGCTGAGGGGGTTAATTT	CCCTTGTTTCATTGGGAAAA	288	59
UBE2D1 x4	Exon 4	TGCTAACCTCCCCACAGTCT	TCAAATGCTGATGCAAATCTT	228	59
UBE2D1 x5	Exon 5	TCTGCTGTATTTTTCCTGTCTCA	GGTGATTGTCATATTTTGTTGTTTT	205	63
UBE2D1 x6	Exon 6	TCTCAAAGAAAGGTTTACTCCATTG	GGGTTATTGTCTAATGTGATGTTCTC	285	59
UBE2D1 x7	Exon 7 and part of 3'UTR	AATGAAACAGTAAACAGTGCTCAA	TGCATGAACCTAAGTCACATTG	292	59
UBE2D1 x7B	Part of 3'UTR	AACTGTGTCTCCCTTGTCTTAGG	CCCAAATTACTCTAAATTCTCCTCTAC	533	59
UBE2D1 x7C	Part of 3'UTR	TCCTAAGACAAGGGAGACACAG	CATGCAAGAGAATGGACTCAG	589	60

Table 4.9. Details of *UBE2D1* PCR assays, including PCR primers, annealing temperatures and size of amplimers.

SNP No.	SNP Name	dbSNP Identity	Location	SNP Flanking Sequence	Fragment	Extension Primer (5'→3')	Expected Allele Peaks
1	144 G>T		120bp downstream exon 1	GCCGGGGTGC**K**GGCAGGGAGC	UBE2D1 x1	GCCTTCAGCTCCCTGCC	A (Green) & C (Black)
2	169 G>C		145bp downstream exon 1	GGCTCGGGCC**S**GGCCAGCGGG	UBE2D1 x1	AGCTGAAGGCTCGGGCC	C (Black) & G (Blue)
3	182 C>T	rs1905456	158bp downstream exon 1	CCAGCGGGCA**Y**CGGACAGGTG	UBE2D1 x1	TCCCACCTCACCTGTCCG	A (Green) & G (Blue)
4	305 G>A		281bp downstream exon 1	CCTCTTGCGC**R**TCCAGACCGT	UBE2D1 Pr	GGGTAGAGAGCCTCTTGCGC	A (Green) & G (Blue)
5	26120 T>C		17bp upstream exon 2	ACCTTACATA**Y**TTTTGATTTC	UBE2D1 x2-3	CACTCAATTCCTGAAGGAAA TCAAAA	A (Green) & G (Blue)
6	28525 A>G		40bp downstream exon 4	CCCATGTAAG**R**GATTTTATTC	UBE2D1 x4	GATTGATGTGACTCCCATGT AAG	A (Green) & G (Blue)
7	32771 C>G		Exon 6 (Pro→Pro)	CAGATGACCC**S**TTAGTACCAG	UBE2D1 x6	GATTTGTGCAATATCTGGTA CTAA	C (Black) & G (Blue)
8	33403 T>C	rs3802699	116bp upstream exon 7	GTAATTGATA**Y**ATGTGTGATT	UBE2D1 x7	CTTCTTATACTTAATTGCAA TAATCACACAT	A (Green) & G (Blue)

Table 4.10. List of polymorphisms identified in the *UBE2D1* gene, including the location of the polymorphism relative to the coding sequence, flanking sequence of the polymorphism, the extension primer used for SNaPshot and the expected allele peaks in the primer extension assay.

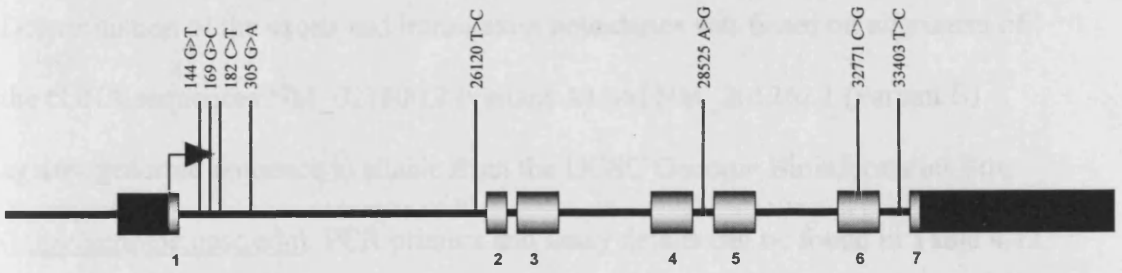

Figure 4.4. Diagram of the *UBE2D1* gene (not to scale), indicating the positions of identified polymorphisms. For numbering of polymorphisms, +1 indicates 'A' of ATG translation start codon. Grey blocks indicate coding sequence, black blocks indicate untranslated regions.

SNP	Allele		*P*
1) 144G>T			
Patients	The primer extension reaction could not be		
Controls	optimised.		
2) 169 G>C			
Patients	The primer extension reaction could not be		
Controls	optimised.		
3) 182 C>T			
Patients	The primer extension reaction could not be		
Controls	optimised.		
4) 305 G>A	**G**	**A**	
Patients	331 (0.89)	41 (0.11)	
Controls	335 (0.90)	37 (0.10)	0.6321
5) 26120 T>C			
Patients	The primer extension reaction could not be		
Controls	optimised.		
6) 28525 A>G	**A**	**G**	
Patients	356 (0.96)	16 (0.04)	
Controls	354 (0.95)	18 (0.05)	0.7255
7) 32771 C>G	**C**	**G**	
Patients	362 (0.97)	10 (0.03)	
Controls	362 (0.97)	10 (0.03)	1.0000
8) 33403 T>C	**T**	**C**	
Patients	350 (0.94)	22 (0.06)	
Controls	357 (0.96)	15 (0.04)	0.2377

Table 4.11. Estimates of allele frequencies and counts of *UBE2D1* polymorphisms in DNA pools comparing 186 LOAD cases with 186 age- and sex-matched controls.

4.3.4 DNAJC12

Determination of the exons and intron/exon boundaries was based on alignment of the cDNA sequences NM_021800.2 (variant A) and NM_201262.1 (variant B) against genomic sequence available from the UCSC Genome Bioinformatics Site (http://genome.ucsc.edu). PCR primers and assay details can be found in Table 4.12 (p.139). Extension primers are listed in Table 4.13 (p.141). Two SNPs were identified in the *DNAJC12* gene: one coding synonymous SNP S81S (26434 C>T) and one 5'UTR SNP (-17 C>T). These SNPs are shown in Figure 4.5 and Table 4.13 (p.141). Both SNPs were successfully genotyped in the MRC pools. The estimated allele frequencies and counts calculated for each SNP are shown in Table 4.14 (p.142). There were no significant differences observed in the allele frequencies of either SNP between cases and controls.

Fragment name	Spanning	Sense Primer Sequence (5'→3')	Antisense Primer Sequence (5'→3')	Size (bp)	Annealing Temperature (°C)
DNAJC12 PROM	5' Flanking region of both splice variants	CAAAACCCCCTCCTCTTAAA	GGCCACAGTCAATACACCAG	564	61
DNAJC12 x1	5'UTR and exon 1 of both splice variants	CAAGGTTAGGTTTGTAGGCAATG	CAAATGGTTCACATGCATCTCT	487	56
DNAJC12 x2	Exon 2 of both splice variants	TTACTATTCACTGGCTTTTGGTTC	CTGGTCTTATTCCTGGTGATCC	264	56
DNAJC12 x3	Exon 3 of both splice variants	GCATCCTGAGCTTCACAAATTC	TGGCAGTCATGGTTTTAGTAAGAG	283	56
DNAJC12 ISOB	Part of exon 3 and 3'UTR of splice variant B	CTAAGCCTTGAAAAGAGAGCAAG	AGTGAAGACGGTGGGTTTCTC	405	60
DNAJC12 x4	Exon 4 of splice variant A	CAGATTGAAAAAGTTAAGAATAAATGC	TCTTGTTAATAGTCAAGTCTAACATGC	434	56
DNAJC12 x5A	Part of 3'UTR of splice variant A	GAGCACAGGAGTTTGAGGTTGTATT	ATTCCTCCATCCTTGAATCAGTTCT	423	62
DNAJC12 x5B	Exon 5 and part of 3'UTR of splice variant A	GGGGTTCAGACAAGTAATTTCAC	CAAGATCGACTTTTCCTACTTCTG	564	60

Table 4.12. Details of *DNAJC12* PCR assays, including PCR primers, annealing temperatures and size of amplimers.

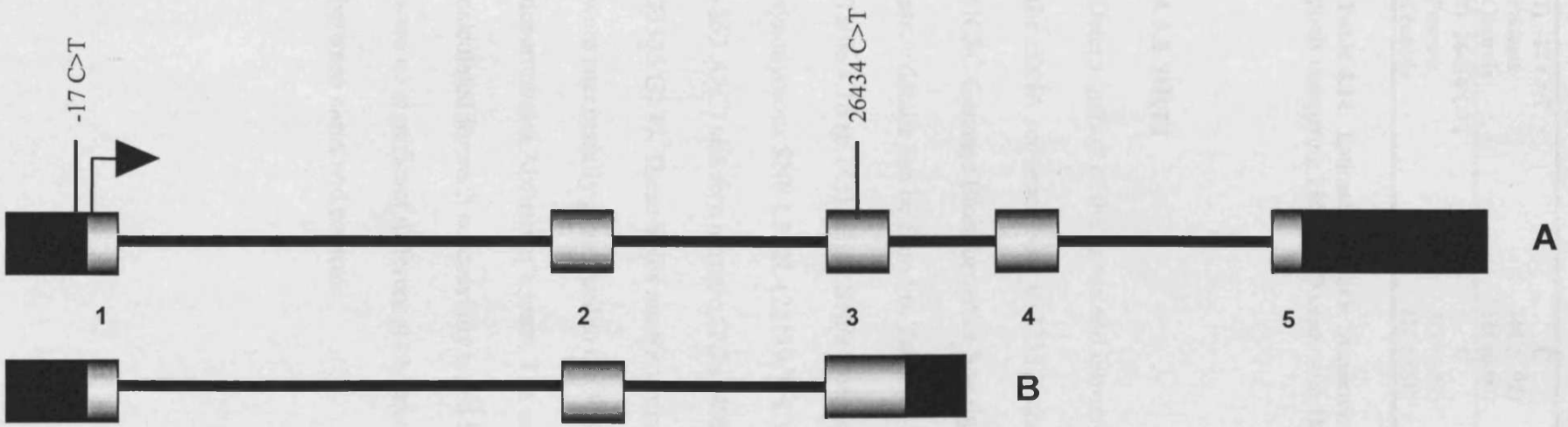

Figure 4.5. Diagram of the *DNAJC12* gene (not to scale), indicating the positions of identified polymorphisms. For numbering of polymorphisms, +1 indicates 'A' of ATG translation start codon. Grey blocks indicate coding sequence, black blocks indicate untranslated regions.

SNP No.	SNP Name	dbSNP Identity	Location	SNP Flanking Sequence	Fragment	Extension Primer (5'→3')	Expected Allele Peaks
1	-17 C>T	rs2273771	5'UTR	GGAAGAAGGA**Y**TGATTAAGTC	DNAJC12 x1	TGTTTCCGAGGGAAGAAGGA	C (Black) & T (Red)
2	26434 C>T	rs3740049	Exon 3 (Ser→Ser)	GGCGAAGGAG**Y**CAGATGTCGA	DNAJC12 x3	TATGACCACTGGCGAAGGAG	C (Black) & T (Red)

Table 4.13. List of polymorphisms identified in the *DNAJC12* gene, including the location of the polymorphism relative to the coding sequence, flanking sequence of the polymorphism, the extension primer used for SNaPshot and the expected allele peaks in the primer extension assay.

SNP	Allele		*P*
1) -17 C>T	**C**	**T**	
Patients	344 (0.92)	28 (0.08)	
Controls	336 (0.90)	36 (0.10)	0.2955
2) 26434 C>T	**C**	**T**	
Patients	327 (0.88)	45 (0.12)	
Controls	328 (0.88)	44 (0.12)	0.9100

Table 4.14. Estimates of allele frequencies and counts of *DNAJC12* polymorphisms in DNA pools comparing 186 LOAD cases with 186 age- and sex-matched controls.

4.3.5 SIRT1

Determination of the exons and intron/exon boundaries was based on alignment of the cDNA sequence NM_012238.3 against genomic sequence available from the UCSC Genome Bioinformatics Site (http://genome.ucsc.edu). PCR primers and assay details can be found in Table 4.15 (p.143). Extension primers are listed in Table 4.16 (p.145). Eight SNPs were identified in the *SIRT1* gene: one coding synonymous SNP L332L (22119 T>C), two 5'flanking region SNPs (-521 A>G and -263 A>C) and five intronic SNPs (4090 T>A, 6490 G>A, 6646 A>G, 6840 T>C and 23535 G>T). These SNPs are shown in Figure 4.6 and Table 4.16 (p.145). Six SNPs were successfully genotyped in the MRC pools by Luke Jehu, a member of the departmental Alzheimer's team. The estimated allele frequencies and counts calculated for each successfully typed SNP are shown in Table 4.17 (p.147). There were no significant differences observed in the allele frequencies of any of the SNPs between cases and controls.

Fragment name	Spanning	Sense Primer Sequence (5'→3')	Antisense Primer Sequence (5'→3')	Size (bp)	Annealing Temperature (°C)
SIRT1 PROM	5' Flank	GAACGGTGTGAGGAGAGTGG	AGACCACAACACTACGGGTCAC	413	60
SIRT1 x1A	5'UTR	GGAGCGGTAGACGCAACAG	GGCCCATTGTCTCCTTCC	533	GC54
SIRT1 x1B	Exon 1	GAGAGGCAGTTGGAAGATGG	AGCCGCCCTCAACCTCAG	529	GC56
SIRT1 x2	Exon 2	AATGAACAGTGCAAGCTGACC	AATTAACAGCTCTGAGCCATACC	293	60
SIRT1 x3	Exon 3	CCCTCACAGAATGCTAACTCA	GCAGTTCCCAAACATCCATT	457	58
SIRT1 x4	Exon 4	TGCATTTGCTTTAATTTGTTGG	GAGAAGGCCAAAGAAACAACC	479	60
SIRT1 x5	Exon 5	TGTAGGTGTGTGTCGCATCC	CGATGGCAGTCAGCTTTATAGG	386	60
SIRT1 x6	Exon 6	ACGTTTGTGGTGTGTTCAAG	AAGGTATTGAAAGGTTCTCGTG	320	60
SIRT1 x7	Exon 7	TTGGGCTTACTCTTTGCTTCTC	ATACAGACCCACAACCCATGAC	302	60
SIRT1 x8A	Part of exon 8	TAACTGCCCATCTGCTTGCT	AGAGGTGTGGGTGGCAACT	419	58
SIRT1 x8B	Part of exon 8	TGCCAAACTTTGCTGTAACC	TCAACTACATAAAGCTACCCTATCG	532	58
SIRT1 x9A	Exon 9	GCTGGAACCCACACTTCATT	CACCTTTCTGGTTTCCTTGC	523	58
SIRT1 x9B	Part of 3'UTR	GAATTGTTCCACCAGCATTAGG	TCCCCACATATTGTTGACTTCC	576	60
SIRT1 x9C	Part of 3'UTR	TCCAAAACTGTGGCAGCTAAC	TTAACACCAAATCCTCCCAATG	574	60
SIRT1 x9D	Part of 3'UTR	AGGCCCCTGATTATACAGTTCC	AGCCAAATAAATTCAGATTGAGAC	508	60
SIRT1 x9E	Part of 3'UTR	GCTAGGACCATTACTGCCAGAG	ATCACCTGCTACGATCAGCAC	545	60

Table 4.15. Details of *SIRT1* PCR assays, including PCR primers, annealing temperatures and size of amplimers. Annealing temperatures preceded by 'GC' indicate that amplimers are GC-rich and require the use of Q-solution for amplification (see Chapter 2).

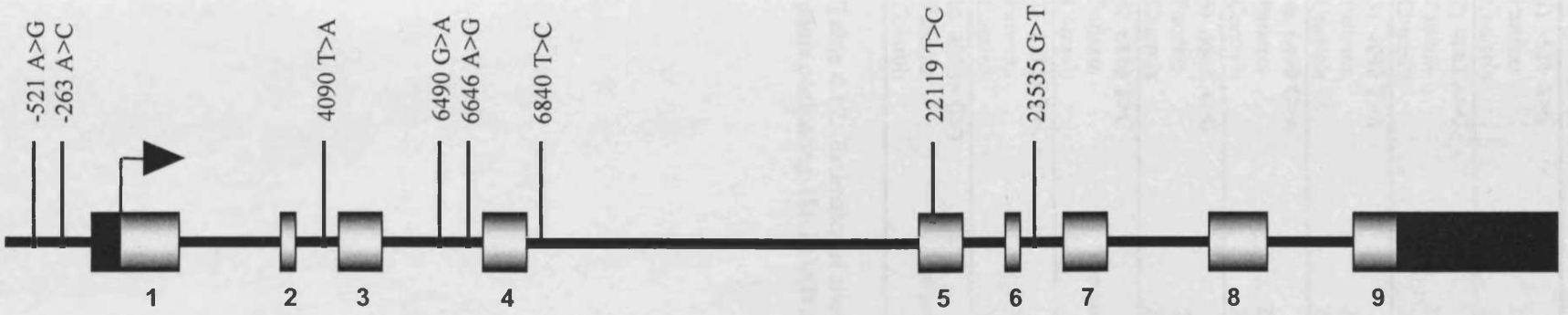

Figure 4.6. Diagram of the *SIRT1* gene (not to scale), indicating the positions of identified polymorphisms. For numbering of polymorphisms, +1 indicates 'A' of ATG translation start codon. Grey blocks indicate coding sequence, black blocks indicate untranslated regions.

SNP No.	SNP Name	dbSNP Identity	Location	SNP Flanking Sequence	Fragment	Extension Primer (5'→3')	Expected Allele Peaks
1	-521 A>G	rs3740051	468bp upstream exon 1	CTTCCTACTT**R**TTAACAAAAC	SIRT1 PROM	TTTTGCCTCTCTTCCTACTT	A (Green) & G (Blue)
2	-263 A>C	rs932658	210bp upstream exon 1	CACAAAGAGG**M**AGGGCCGCCG	SIRT1 PROM	ACACGCTCGCCACAAAGAGG	A (Green) & C (Black)
3	4090 T>A	rs2236318	71bp upstream exon 3	GCTAACTCAT**W**ACTTCAGAAA	SIRT1 x3	CTCACAGAATGCTAACTCAT	A (Green) & T (Red)
4	6490 G>A		191bp upstream exon 4	TATGAGGTAT**R**TTTAATTTTA	SIRT1 x4	AAAGATGGAATATGAGGTAT	A (Green) & G (Blue)
5	6646 A>G		35bp upstream exon 4	AAGGTAGAAG**R**TTTAATTTTA	SIRT1 x4	AGTTCCTATAAAGGTAGAAG	A (Green) & G (Blue)
6	6840 T>C		7bp downstream exon 4	AAAGGTACTA**Y**GAACTCTTCT	SIRT1 x4	TCAAGTTTGCAAAGGTACTA	C (Black) & T (Red)
7	22119 T>C	rs2273773	Exon 5 (Leu→Leu)	ATTCATAGCC**Y**TGTCAGATAA	SIRT1 x5	TCTGTCACAAATTCATAGCC	C (Black) & T (Red)
8	23535 G>T		132bp downstream exon 6	GTTAGCATTT**K**GGAATTTTGG	SIRT1 x6	GTGTATTTTACCAAAATTCC	A (Green) & C (Black)

Table 4.16. List of polymorphisms identified in the *SIRT1* gene, including the location of the polymorphism relative to the coding sequence, flanking sequence of the polymorphism, the extension primer used for SNaPshot and the expected allele peaks in the primer extension assay.

SNP	Allele		*P*
1) -521 A>G	**A**	**G**	
Patients	342 (0.92)	30 (0.08)	
Controls	331 (0.89)	41 (0.11)	0.1698
2) -263 A>C	**A**	**C**	
Patients	240 (0.65)	132 (0.35)	
Controls	233 (0.63)	139 (0.37)	0.5938
3) 4090 T>A	**T**	**A**	
Patients	204 (0.55)	168 (0.45)	
Controls	202 (0.54)	170 (0.46)	0.8829
4) 6490 G>A	**G**	**A**	
Patients	250 (0.67)	122 (0.33)	
Controls	242 (0.65)	130 (0.35)	0.5354
5) 6646 A>G	**A**	**G**	
Patients	236 (063)	136 (0.37)	
Controls	233 (0.63)	139 (0.37)	0.8197
6) 6840 T>C			
Patients	The primer extension reaction could not be optimised.		
Controls			
7) 22119 T>C	**T**	**C**	
Patients	335 (0.90)	37 (0.10)	
Controls	328 (0.88)	44 (0.12)	0.4099
8) 23535 G>T			
Patients	The primer extension reaction could not be optimised.		
Controls			

Table 4.17. Estimates of allele frequencies and counts of *SIRT1* polymorphisms in DNA pools comparing 186 LOAD cases with 186 age- and sex-matched controls.

4.3.6 SGPL1

Determination of the exons and intron/exon boundaries was based on alignment of the cDNA sequence NM_003901.1 against genomic sequence available from the UCSC Genome Bioinformatics Site (http://genome.ucsc.edu). PCR primers and assay details can be found in Table 4.18 (p.149). Extension primers are listed in Table 4.19 (p.150). RFLP primers and assay details are listed in Table 4.20 (p.151). Fourteen polymorphisms were identified in the *SGPL1* gene: one coding non-synonymous SNP V21L (27654 G>T), two coding synonymous SNPs K107K and V314V (37915 A>G and 55017 C>T respectively), one 3'UTR SNP (60567 T>A), two 5'flanking SNPs (-1068 G>A and –111 C>G), five intronic SNPs (37812 T>C, 40647 A>T, 51445 G>A, 53074 G>A and 55211 C>T) and two intronic 2bp deletions (55267-55268delCT and 58540-58541delTT). These polymorphisms are shown in Table 4.19 (p.150) and Figure 4.7 (p.151). Eleven polymorphisms were successfully genotyped in the MRC pools comprised of 186 cases and 186 age- and sex-matched controls. Of the three that failed, one (55267-55268delCT) had a successfully designed assay but the minor allele frequency was too low to be reliably estimated from pools. The estimated allele frequencies and counts calculated for each successfully typed polymorphism are shown in Table 4.21 (p.152). For the intronic SNP 53074 G>A, the A allele was significantly more frequent in cases than controls (P=0.0206). Therefore this SNP was genotyped individually in 405 cases and 405 age- and sex-matched controls (see Table 4.22, p.152). Although the association was again observed in the cases and controls that made up the pools (see Appendix A), in the enlarged sample the frequency of the A allele was similar in cases and controls (both 4 %; P=0.6555).

Fragment name	Spanning	Sense Primer Sequence (5'→3')	Antisense Primer Sequence (5'→3')	Size (bp)	Annealing Temperature (°C)
SGPL1 PROM	5'Flanking region	CTCCTGCGTCTCCCTCAG	AGGCGACCTTTGTGATCC	681	GC56
SGPL1 x1	Exon 1 (Part of 5'UTR)	CTCCGTCCCGACCCTCAC	CTGCCGGGCCTCCAATCT	202	GC60
SGPL1 x2	Part of 5'UTR & exon 2	AGCAAGCATCAGAGGTGAAATC	GAACCATAACTTGGCTGCTCTG	260	60
SGPL1 x3	Exon 3	TTGAGGCTAGTGACACACCAC	GCTGAAGAAGGGCAAGATCC	342	60
SGPL1 x4	Exon 4	AAGTGTCCCCTGGAGGTAAGAG	AATGGTTGCTATATGCCAGGTC	263	60
SGPL1 x5	Exon 5	AACCTGTGAAACAGAGAGTAGGC	GTGCCTAGCATTGAGCAGTTG	384	60
SGPL1 x6	Exon 6	TGTAAACTGGCACAGACCTCAC	ATAAGAATGCTGTTGGGTTTCC	264	60
SGPL1 x7	Exon 7	CTATTGGATGCCCCTTGC	TTTGATTTCACATCTGCTTGC	190	56
SGPL1 x8	Exon 8	GAAGAGAAGCAGCAGGAAAATG	GTCAAGATCAGGGCATGAAGAG	262	60
SGPL1 x9	Exon 9	ACTGGAAACGGCTAGTCAACAG	TCCTCTTCCTATTGCCAGAATG	419	60
SGPL1 x10	Exon 10	GTACTGCCCCATTAGGCTTTG	TCTTGGCAGCAGAAGAGAAGAG	238	60
SGPL1 x11	Exon 11	TATACCCCATCACCTGAACCAG	CATCTTTCCACCCATGTCTTG	405	60
SGPL1 x12	Exon 12	GCAGGTGCCTTGAGCCTAC	AGTTCTGGGACAAGGTCTGC	376	60
SGPL1 x13	Exon 13	CTGTACCACCCAAGTTCTTCC	TGACCAGGGGATTGTATGTG	277	60
SGPL1 x14	Exon 14	TTCAAACTCTCCACCAACACC	TATTGTGAAAGGGCAACCAG	287	60
SGPL1 x15	Exon 15	AAGAATCAGGACAGGTCAGAGC	AGCTAGGACTCGGGGAGAAG	571	60
55267-55268delCT	55267-55268delCT polymorphism	FAM-CTGCTTGTCACCTCTACCACT	GGTGAGCTAAGGAGGAGATCA	195	60
58540-58541delTT	58540-58541delTT polymorphism	FAM-GGATCCCAGAGCAATGACTG	TTTGAATGATTAAAGAGATAGT	152	60

Table 4.18. Details of *SGPL1* PCR assays, including PCR primers, annealing temperatures and size of amplimers. Annealing temperatures preceded by 'GC' indicate that amplimers are GC-rich and require the use of Q-solution for amplification (see Chapter 2). FAM=fluorescent label

Variant No.	Variant Name	dbSNP Identity	Location	Variant Flanking Sequence	Fragment	Extension Primer (5'→3')	Expected Allele Peaks
1	-1068 G>A		246bp upstream exon 1	GCCCCAGGACRGCCTGGTTGA	SGPL1 PROM	CAGACCCTCCAGTGAATGTC TCAACCAGGC	C (Black) & T (Red)
2	-111 C>G		68bp upstream exon 2	GCTGCTCTGGSGAATCTAGGC	SGPL1 x2	GCCAGCCCGCCTAGATTC	C (Black) & G (Blue)
3	27654 G>T		Exon 3 Val→Leu	GATTTTGGAAKTATACTCCAC	SGPL1 x3	CTTGGCTTTTGTGGAGTATA	A (Green) & C (Black)
4	37812 T>C	rs2171157	44bp upstream exon 5	CTGTCTCTACYGTACTCTTGC	SGPL1 x5	TTATCCAGATGCAAGAGTAC	A (Green) & G (Blue)
5	37915 A>G		Exon 5 Lys→Lys	CATTCCTGAARGTGGACAAAG	SGPL1 x5	TTCACATACTCTTTGTCCAC	C (Black) & T (Red)
6	40647 A>T	rs2297842	115bp upstream exon 6	TTGGGTTTCCWCTCAACATTT	SGPL1 x6	TCTGGATACAAAAGAAAAAA ATGTTGAG	A (Green) & T (Red)
7	51445 G>A		48bp upstream exon 8	ATGAAGAGCCRGGGCATTCCT	SGPL1 x8	GGGAGTCAGGAATGCCC	C (Black) & T (Red)
8	53074 G>A		29bp downstream exon 9	CCCACTGTCTRTGCTGGGCCC	SGPL1 x9	TGGAGGGCCCACTGTCT	A (Green) & G (Blue)
9	55017 C>T	rs865832	Exon 11 Val→Val	CCCTTCATGTYGACGCTTGTC	SGPL1 x11	GACGATGAGGAAGCCTCCCA GACAAGCGTC	A (Green) & G (Blue)
10	55211 C>T		77bp downstream exon 11	GTAGCTTCCCYGCAAAGTATA	SGPL1 x11	TAGTTAATTTTATACTTTGC	A (Green) & G (Blue)
11	55267-55268delCT		133/134bp downstream exon 11	TAAACTCTCTCTTTGCCGTCAC	SGPL1 x11	Typed by PCR sizing	N/A
12	58540-58541delTT	rs5786012	9/10bp upstream exon 13	ATTTATTTTTTTGTTTTAAGAC	SGPL1 x13	Typed by PCR sizing	N/A
13	59841 G>T	rs923177	32bp downstream exon 14	TTTCTTCTCTKGGAAATTTAG	SGPL1 x14	TAGGGACACTTGGAGTTTTT TTTCTTCTCT	G (Blue) & T (Red)
14	60567 T>A		3'UTR	AACTTTGACAWCTGGTCTTGC	SGPL1 x15	GCCGTGCACAACTTTGACA	A (Green) & T (Red)

Table 4.19. List of polymorphisms identified in the *SGPL1* gene, including the location of the polymorphism relative to the coding sequence, flanking sequence of the polymorphism, the extension primer used for SNaPshot (if applicable) and the expected allele peaks in the primer extension assay.

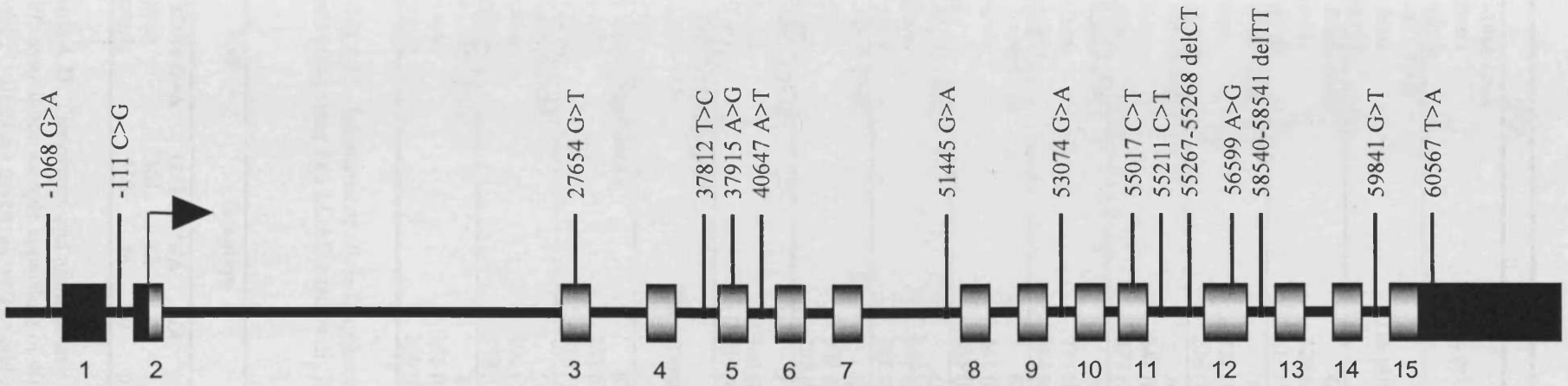

Figure 4.7. Diagram of the *SGPL1* gene (not to scale), indicating the positions of identified polymorphisms. For numbering of polymorphisms, +1 indicates 'A' of ATG translation start codon. Grey blocks indicate coding sequence, black blocks indicate untranslated regions.

SNP	RFLP Sense Primer (5'→3')	RFLP Antisense Primer (5'→3')	Size (bp)	Annealing Temperature (°C)	Restriction Enzyme	Restriction Fragments (bp)
8) 53074 G>A	GACTAGATCACCTCCCTTTCAGA	CTCTGGAGGGCCCACTGTgT	197	62	*Dra* III	**A**=197 **G**=179, 18

Table 4.20. Assay details of genotyping assay of *SGPL1* SNP, 53074 G>A, including RFLP primers, amplimer size, PCR annealing temperature, restriction enzyme and expected RFLP fragment sizes. A lower case letter in the RFLP primer indicates the 'mismatched base' introduced to the RFLP amplimer to generate an artificial restriction site (see Chapter 2).

SNP	Allele		*P*
1) -1068 G>A			
Patients	The primer extension reaction could not be		
Controls	optimised.		
2) -111 C>G			
Patients	The primer extension reaction could not be		
Controls	optimised.		
3) 27654 G>T	**G**	**T**	
Patients	320 (0.86)	52 (0.14)	
Controls	316 (0.85)	56 (0.15)	0.6771
4) 37812 T>C	**T**	**C**	
Patients	233 (0.63)	139 (0.37)	
Controls	236 (0.63)	136 (0.37)	0.8197
5) 37915 A>G	**A**	**G**	
Patients	344 (0.92)	28 (0.08)	
Controls	337 (0.91)	35 (0.09)	0.3566
6) 40647 A>T	**A**	**T**	
Patients	235 (0.63)	137 (0.37)	
Controls	234 (0.63)	138 (0.37)	0.9394
7) 51445 G>A	**G**	**A**	
Patients	341 (0.92)	31 (0.08)	
Controls	333 (0.90)	39 (0.10)	0.3150
8) 53074 G>A	**G**	**A**	
Patients	349 (0.94)	23 (0.06)	
Controls	362 (0.97)	10 (0.03)	**0.0206**
9) 55017 C>T	**C**	**T**	
Patients	303 (0.81)	69 (0.19)	
Controls	297 (0.80)	75 (0.20)	0.5776
10) 55211 C>T	**C**	**T**	
Patients	348 (0.94)	24 (0.06)	
Controls	339 (0.91)	33 (0.09)	0.2147
11) 55267-55268delCT			
Patients	The CT deletion allele was too rare to be detected		
Controls	in pools.		
12) 58540-58541delTT	**TT**	**delTT**	
Patients	253 (0.68)	119 (0.32)	
Controls	256 (0.69)	116 (0.31)	0.8129
13) 59841 G>T	**G**	**T**	
Patients	290 (0.78)	82 (0.22)	
Controls	279 (0.75)	93 (0.25)	0.3416
14) 60567 T>A	**T**	**A**	
Patients	355 (0.95)	17 (0.05)	
Controls	360 (0.97)	12 (0.03)	0.3435

Table 4.21. Estimates of allele frequencies and counts of *SGPL1* polymorphisms in DNA pools comparing 186 LOAD cases with 186 controls. *P* values<0.1 are indicated in bold.

SNP	Genotype			*P*	Allele		Odds Ratio (95% C.I.)	*P*
8) 53074 G>A	**G/G**	**G/A**	**A/A**		**G**	**A**		
Patients	364	32	0		760 (0.96)	32 (0.04)	1.1248	
Controls	360	28	0	0.6490	748 (0.96)	28 (0.04)	(0.6706-1.8866)	0.6555

Table 4.22. Genotypes and allele counts for *SGPL1* SNP, 53074 G>A, in a subset of the MRC association sample consisting of 405 LOAD cases and 405 controls. Genotypic and allelic *P* values are given, as well as odds ratios and 95% confidence intervals (C.I.).

4.3.7 SEC24C

Determination of the exons and intron/exon boundaries was based on alignment of the cDNA sequence NM_004922.1 against genomic sequence available from the UCSC Genome Bioinformatics Site (http://genome.ucsc.edu). PCR primers and assay details can be found in Table 4.23 (p.155). Extension primers are listed in Table 4.24 (p.156). Five SNPs were identified in the *SEC24C* gene: two coding synonymous SNPs Y28Y and T708T (84 T>C and 21118 A>G respectively), one 3'UTR SNP (24372 C>T) and two intronic SNPs (19409 G>A and 23423 C>T). These SNPs are shown in Figure 4.8 and Table 4.24 (p.156). Four SNPs were successfully genotyped in the MRC pools by Dragana Turic, a member of the departmental Alzheimer's team. The estimated allele frequencies and counts calculated for each successfully typed polymorphism are shown in Table 4.25 (p.157). There were no significant differences observed in the allele frequencies of any of the SNPs between cases and controls.

Fragment name	Spanning	Sense Primer Sequence (5'→3')	Antisense Primer Sequence (5'→3')	Size (bp)	Annealing Temperature (°C)
SEC24C PROM1	5'Flanking region	GTGGATCACGAGGTCAGGAGAT	CAGCAAACATCGAGTACCCTCTA	464	62
SEC24C PROM2	5'Flanking region	TGTCATTTCTGTAACTCAGCCTAAA	CCCAGCCAGCATTCAGATTA	386	62
SEC24C X1-2	5'UTR & exon 2	GTGACAAAGGGTGGATGGTC	CAACCCAACCTGAAGACTCTG	486	60
SEC24C X3	Exon 3	GCACTCAGCCTCATCAGACC	ATCCTTGCTTTGCATTCCTG	260	60
SEC24C X4	Exon 4	TCTGTAGACTTCAAAGGGTGTCC	CTCTGAACAGGGGACAGTAACA	280	60
SEC24C X5	Exon 5	CAAGGAGGCAGAATGACTGG	TGAAGCTACCCATCTAATTCACC	545	60
SEC24C X6	Exon 6	TTAGGAGTCTAGTCATTTTCCTGAG	GCAGACACAAACCCTTCCTC	265	60
SEC24C X7	Exon 7	TTTCACTCTTGGCACTCTGG	CCTGGGGGAGGAGCTAATTC	214	60
SEC24C X8	Exon 8	GAGAGCTGGTGTCTGGAAGG	TGGAATCACATCCAGGAAGAC	270	60
SEC24C X9	Exon 9	TCCTTTATGTCTGATCCCTTCC	GGAAGATACAATCAAGACCTTCC	225	60
SEC24C X10	Exon 10	GCTCAGCTAGGGCCAGAATAC	TCCTCCACTCACTGCTCCTC	225	60
SEC24C X11	Exon 11	AACTGGCCTGCTTACCATTC	TCTTCAGTCAACCCAGACACC	240	60
SEC24C X12	Exon 12	GGTGGCAAGTCTAGGTAACAATG	CCTCTGTTCAACTCCATGACC	305	60
SEC24C X13	Exon 13	CAGGGAATCGAGAACTGAGG	CCAGGGGATAAGATGGTCAG	231	60
SEC24C X14	Exon 14	TGACAAGGGAAGAGATGGATG	TGGAGTGTCTGGTCCTAGCC	271	63
SEC24C X15	Exon 15	TCTTCTCCCCATTTTCTTTCC	CAGATATTCCCAGCCCTGCT	249	62
SEC24C X16	Exon 16	AGATTGTCTGCACGATGAGC	TGCCTCCCTTCCATATTTAGC	211	60
SEC24C X17	Exon 17	ATATGGAAGGGAGGCATGTG	AAGCGAATGAAACACTTCCTG	257	62
SEC24C X18	Exon 18	GGGAGTGGCTCATTTCTCTC	CTCACCATCCTGGACCTCTC	288	62
SEC24C X19	Exon 19	AGTTGTGATGGTGGGAATGC	TGAGAAATCCCTCCCAAATG	256	62
SEC24C X20	Exon 20	TGCATTTGGGAGGGATTTC	ACTAGCCTATCCTTTCCTCCTC	310	60
SEC24C X21	Exon 21	CAGAAGGGGTGGTGTCTGAG	TCCACACCCATATTCTCCTTG	338	62
SEC24C X22	Exon 22	TTGCCTGTTTCAGATGATGC	TTACTCATTCCCCACCCAAC	263	62
SEC24C X23A	Exon 23 & Part of 3'UTR	TTTGGCCTTGCCTTATGAAC	CAAACCCCCAATACCGAATC	470	60
SEC24C X23B	Part of 3'UTR	CCCTCTTTTTCCTGCTAATCC	TCCCTACAGAACCATCCAGTG	491	60
SEC24C X23C	Part of 3'UTR	AGAGGTGACCGGAGAACTGAG	TGAGCTTTCGGGAGTAAAGATG	498	60

Table 4.23. Details of *SEC24C* PCR assays, including PCR primers, annealing temperatures and size of amplimers. Annealing temperatures preceded by 'GC' indicate that amplimers are GC-rich and require the use of Q-solution for amplification (see Chapter 2).

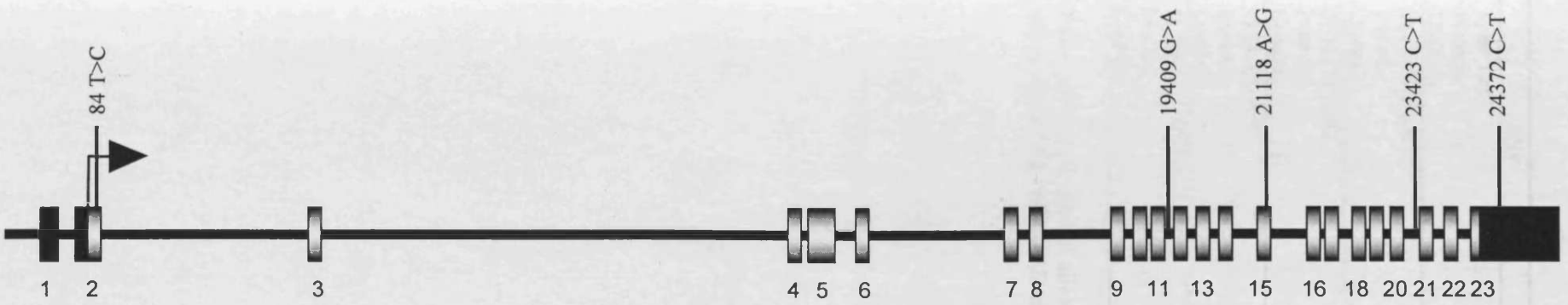

Figure 4.8. Diagram of the *SEC24C* gene (not to scale), indicating the positions of identified polymorphisms. For numbering of polymorphisms, +1 indicates 'A' of ATG translation start codon. Grey blocks indicate coding sequence, black blocks indicate untranslated regions.

Variant No.	Variant Name	dbSNP Identity	Location	Variant Flanking Sequence	Fragment	Extension Primer (5'→3')	Expected Allele Peaks
1	84 T>C	rs2306325	Exon 2 Tyr→Tyr	AGTCCAGCTA**Y**GGTGGGCAAT	SEC24C X1-2	GGGTATCATCAGTCCAGCTA	C (Black) & T (Red)
2	19409 G>A	rs3849969	31bp downstream exon 11	GTGTTTCCTG**R**GGTTAATGAT	SEC24C X11	CAGAACTGAGGTGTTTCCTG	A (Green) & G (Blue)
3	21118 A>G	rs4746147	Exon 15 Thr→Thr	ATGTGGCCAC**R**CTCTCTGTTG	SEC24C X15	CAGTATGTGGATGTGGCCAC	A (Green) & G (Blue)
4	23423 C>T	rs3088070	25bp upstream exon 21	CCTTGGTAAC**Y**TTTTGCTCCC	SEC24C X21	GTCTTATGGTCCTTGGTAAC	C (Black) & T (Red)
5	24372 C>T		3'UTR	CTCAGTCTCT**Y**TGGGGGGAGG	SEC24C X23A	GTAAGCTGACCTCAGTCTCT	C (Black) & T (Red)

Table 4.24. List of polymorphisms identified in the *SEC24C* gene, including the location of the polymorphism relative to the coding sequence, flanking sequence of the polymorphism, the extension primer used for SNaPshot and the expected allele peaks in the primer extension assay.

SNP	Allele		*P*
1) 84 T>C	**T**	**C**	
Patients	245 (0.66)	127 (0.34)	
Controls	231 (0.62)	141 (0.38)	0.2849
2) 19409 G>A	**G**	**A**	
Patients	309 (0.83)	63 (0.17)	
Controls	317 (0.85)	55 (0.15)	0.4220
3) 21118 A>G	**A**	**G**	
Patients	312 (0.84)	60 (0.16)	
Controls	324 (0.87)	48 (0.13)	0.2117
4) 23423 C>T			
Patients	The primer extension reaction could not be optimised.		
Controls			
5) 24372 C>T	**C**	**T**	
Patients	320 (0.86)	52 (0.14)	
Controls	324 (0.87)	48 (0.13)	0.6672

Table 4.25. Estimates of allele frequencies and counts of *SEC24C* polymorphisms in DNA pools comparing 186 LOAD cases with 186 age- and sex-matched controls.

4.4 Discussion

Seven genes in a region of linkage on chromosome 10 have been examined as putative susceptibility loci for LOAD risk. The strategy of testing candidates within a region of significant linkage is advantageous, as the *a priori* likelihood of detecting a risk variant must be increased, especially if the candidate gene is also of functional relevance to the disease. A two-stage approach was taken here. Sequence variants identified by DHPLC were initially genotyped in DNA pools of 186 LOAD cases and 186 age- and sex-matched controls. Pooled analysis is an extremely cost-effective method of genotyping and has been shown to be highly accurate[192]. Indeed, the MRC pools employed in this study have been validated and a pooling error of just 0.785% has been calculated (see Section 2.1.5.1). This pooled genotyping stage was intended as an exploratory step to detect possible signals in the region, and as the pooling methodology can only generate an estimate of allele frequencies, a relaxed significance level of α=0.1 was chosen to avoid type II errors. This sample has 76% power to detect a marker allele generating an odds ratio of 1.5, present at a frequency of 0.2 in the population. Polymorphisms showing association with LOAD with a P<0.1 were carried forward to stage two, where they were individually genotyped in a sample of 405 LOAD cases and 405 age- and sex-matched controls.

Fifty-two polymorphisms were detected by DHPLC. Of these fifty-two variants, thirty-seven were successfully genotyped in pools, the minor allele of five were too rare to attain a reliable estimate of allele frequency in pools and the primer extension reaction could not be optimised for the remaining ten. Primer extension reactions usually cannot be optimised if extraneous peaks are generated in the reaction. Assuming the reaction has been properly purified (*i.e.* complete removal of dNTPs

and ddNTPs at the appropriate stages) then extraneous peaks are most likely a result of primer hairpin or primer-dimer extension. While primer analysis software can help to identify potential problems, primer extension methods do not permit any flexibility with respect to the location of the 3′ end of the primer (other than either side of the SNP). Therefore if the sequence flanking the SNP is difficult to assay, then the SNP cannot be typed by this method.

Of the thirty-seven polymorphisms successfully genotyped in the MRC pools, two showed significant differences between case and control pools, with $P<0.05$ in each case: *DKK1* 463 C>T and *SGPL1* 53074 G>A. Both SNPs are intronic. Dkk1 negatively modulates the Wnt signalling pathway, thus activating the putative τ-phosphorylating enzyme glycogen synthase kinase-3β (GSK3β). Caricasole and colleagues[349] have recently shown that Aβ induces expression of *DKK1* and that inhibition of this expression slightly reduces neuronal death induced by Aβ. Moreover, these researchers have demonstrated that *DKK1* is upregulated in the AD brain. SGPL1 catalyses the last step in sphingolipid breakdown. Sphingolipids are an integral part of lipid rafts, which have been proposed to regulate APP processing by favouring the clustering of APP and BACE1[75]. In addition, the glycosphingolipid GM1 has been found to bind Aβ and this GM1-bound form of Aβ has been suggested to be involved in the initiation of amyloid fibril formation *in vivo* by acting as a seed[340]. A plausible case therefore can be made for both *DKK1* and *SGPL1* in the pathogenesis of LOAD.

On individual genotyping of the samples that made up the MRC pools, a significant difference was again observed between cases and controls, thus further validating the

pooling method (see Appendix A). However, in the larger sample of 405 cases and 405 controls (which includes the pool samples) no significant difference was observed in allele frequencies of either SNP between cases and controls (see Tables 4.8, p.131 and 4.22, p.152). This is perhaps not overly surprising as with the relaxed significance level of 0.1 employed, 3.7 positive findings would be expected to occur by chance for the thirty-seven polymorphisms successfully genotyped.

I therefore conclude that there is no evidence for association of any of the successfully typed polymorphisms in the seven candidate genes examined in this study with LOAD. Such a statement however should not imply that any of these genes can be excluded as LOAD candidate loci. To exclude a locus would at least require typing all non-redundant variation in a sufficiently powerful sample (although this is a simplistic view, there are many other prerequisites, *e.g.* there must be confidence that the sample is truly representative of both the disease and 'healthy' population). As most of the polymorphisms detected in this study were not genotyped in individual samples, the linkage disequilibrium (LD) structure across any particular gene could not be assessed. It is unlikely however that all non-redundant variation has been examined considering: i) introns were not routinely screened for variants; ii) SNPs not amenable to primer extension genotyping were not typed by any other method; iii) rare SNPs could not be typed in pools. Furthermore, the sample employed here may not have been sufficiently powerful to detect association with rare variants and/or susceptibility loci of small effect. Rectifying such problems comes at the cost of considerably more time and money. There are unfortunately no easy answers and until the cost of genotyping is reduced,

researchers must tolerate a certain degree of uncertainty in their conclusions of association studies.

4.5 Examples of Experimental Data

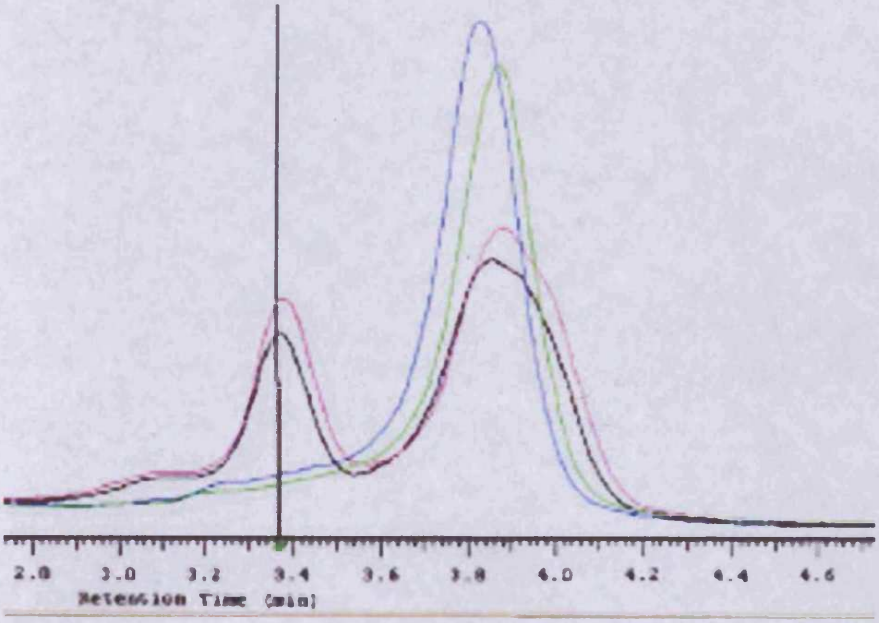

Figure 4.9. DHPLC traces from four individuals amplified for the DKK1 x3 fragment. The green and blue traces indicate homozygous individuals. The pink and black traces represent individuals heterozygous for the *DKK1* SNP 2074 A>G.

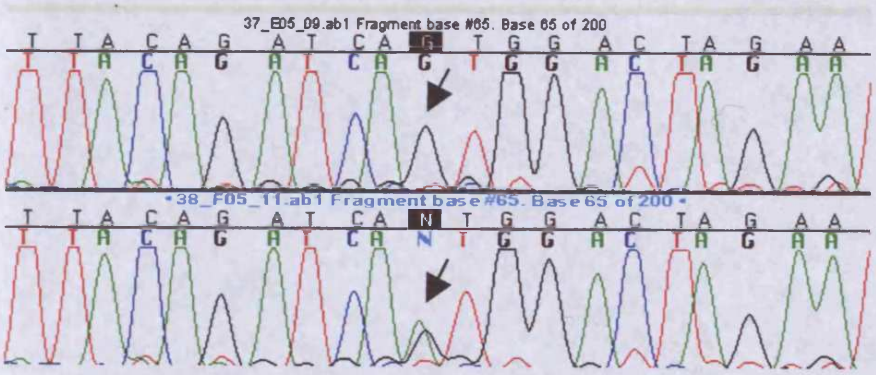

Figure 4.10. Sequence chromatograms for the *ALOX5* SNP -1700 G>A showing a G/G homozygote in the upper panel and an A/G heterozygote in the lower panel.

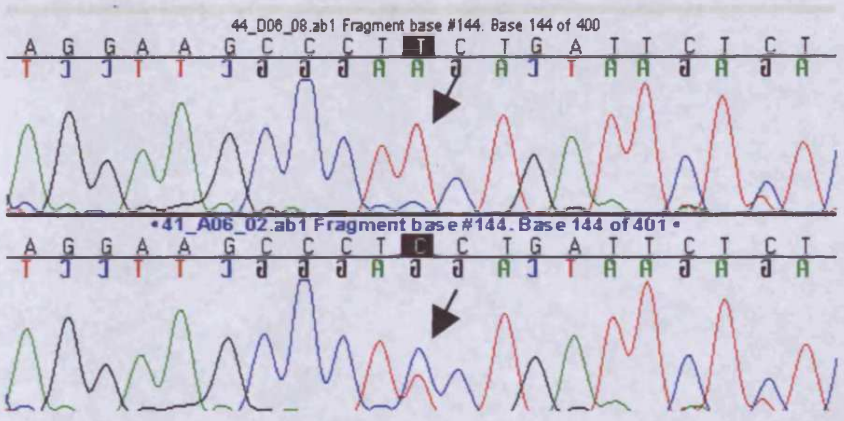

Figure 4.11. Sequence chromatograms for the *ALOX5* SNP -557 T>C showing a T/T homozygote in the upper panel and a C/T heterozygote in the lower panel.

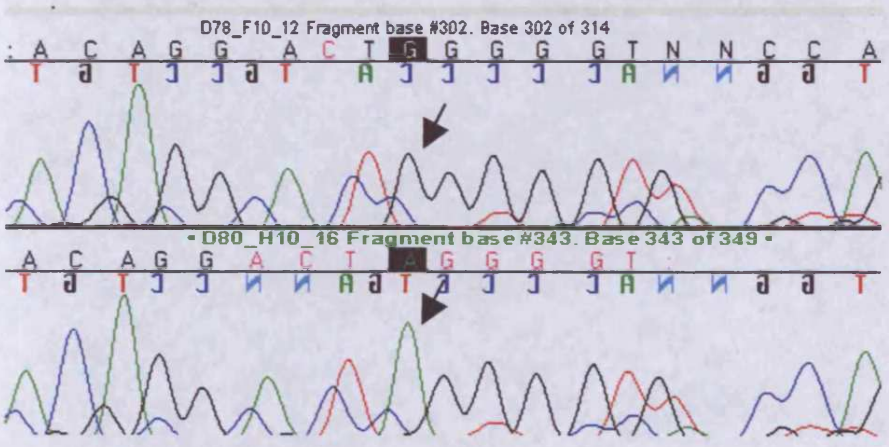

Figure 4.12. Sequence chromatograms for the *ALOX5* SNP 268 G>A showing a G/G homozygote in the upper panel and an A/A homozygote in the lower panel.

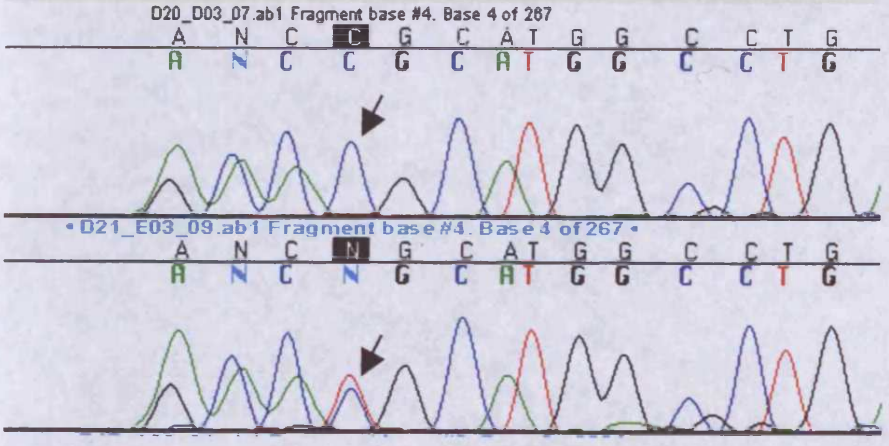

Figure 4.13. Sequence chromatograms for the *ALOX5* SNP 8172 C>T showing a C/C homozygote in the upper panel and a C/T heterozygote in the lower panel.

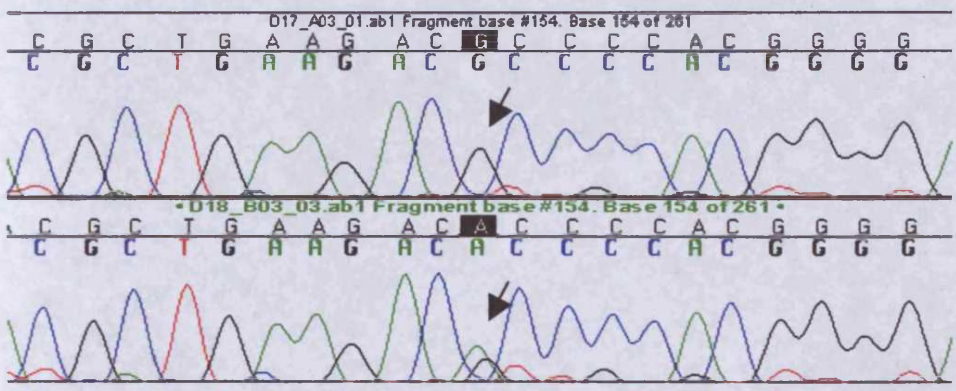

Figure 4.14. Sequence chromatograms for the *ALOX5* SNP 8323 G>A showing a G/G homozygote in the upper panel and an A/G heterozygote in the lower panel.

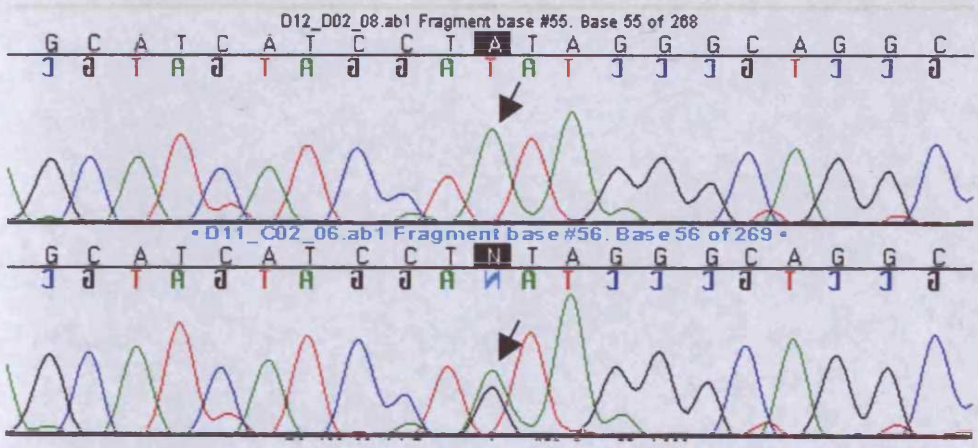

Figure 4.15. Sequence chromatograms for the *ALOX5* SNP 66971 A>G showing an A/A homozygote in the upper panel and an A/G heterozygote in the lower panel.

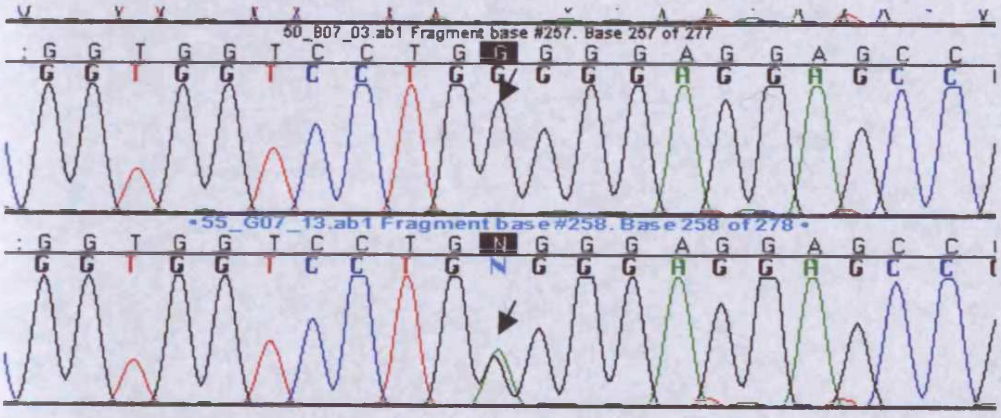

Figure 4.16. Sequence chromatograms for the *ALOX5* SNP 68965 G>A showing a G/G homozygote in the upper panel and an A/G heterozygote in the lower panel.

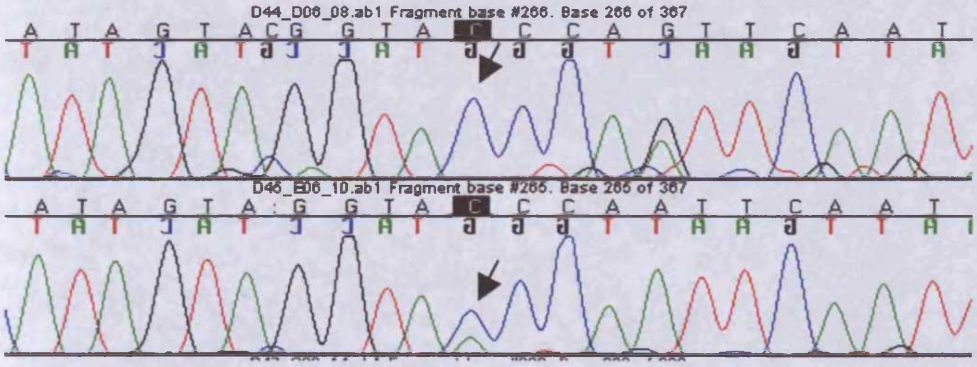

Figure 4.17. Sequence chromatograms for the *ALOX5* SNP 71772 C>A showing a C/C homozygote in the upper panel and an A/C heterozygote in the lower panel.

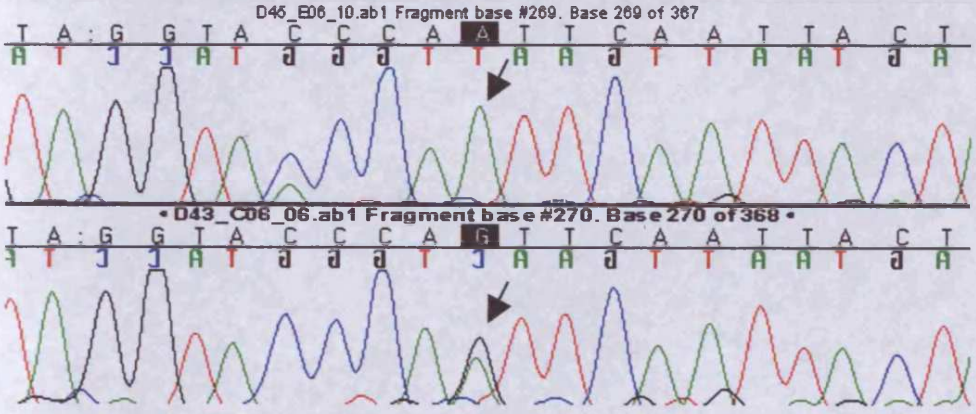

Figure 4.18. Sequence chromatograms for the *ALOX5* SNP 71776 A>G showing an A/A homozygote in the upper panel and an A/G heterozygote in the lower panel.

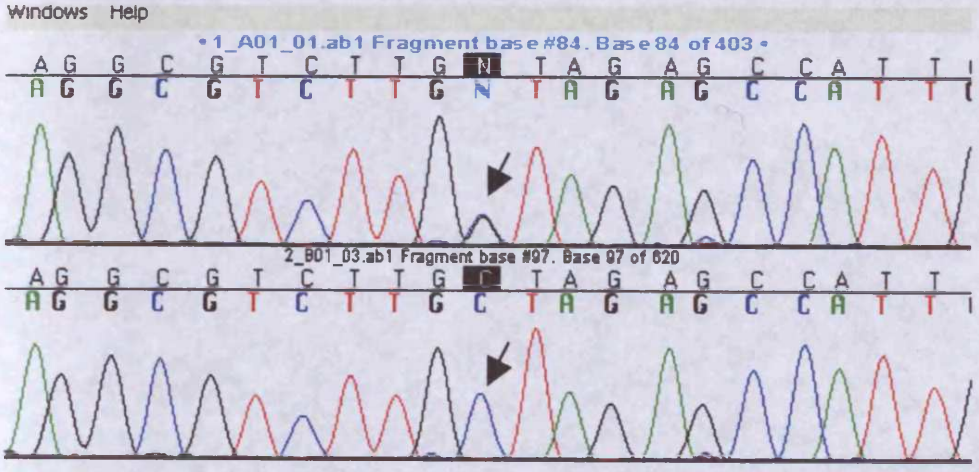

Figure 4.19. Sequence chromatograms for the *DKK1* SNP -621 C>G (rs1528878) showing a C/G heterozygote in the upper panel and a C/C homozygote in the lower panel.

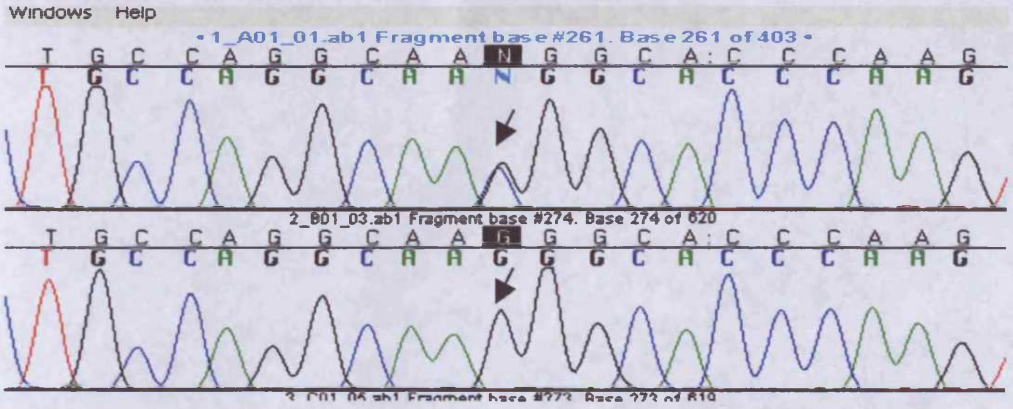

Figure 4.20. Sequence chromatograms for the *DKK1* SNP -446 G>C (rs1528879) showing a C/G heterozygote in the upper panel and a G/G homozygote in the lower panel.

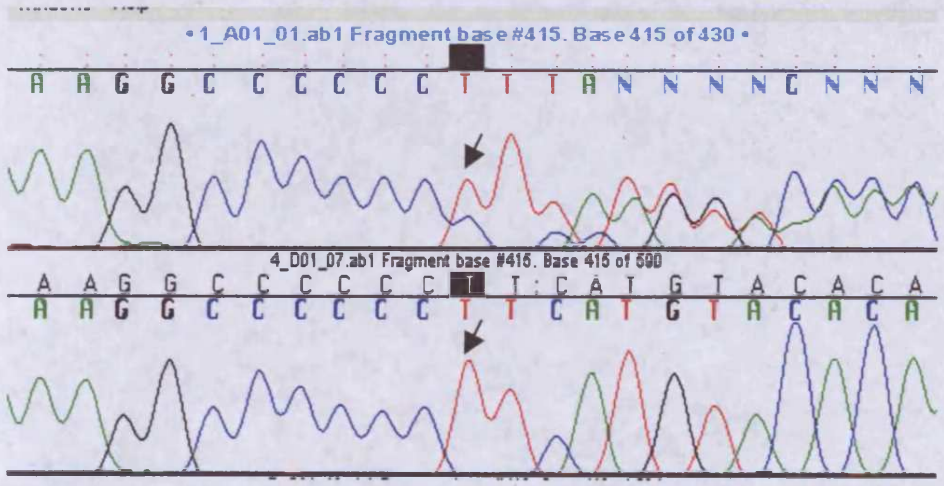

Figure 4.21. Sequence chromatograms for the *DKK1* variant -294 Ins C showing a C insertion heterozygote in the upper panel and a non-insertion homozygote in the lower panel.

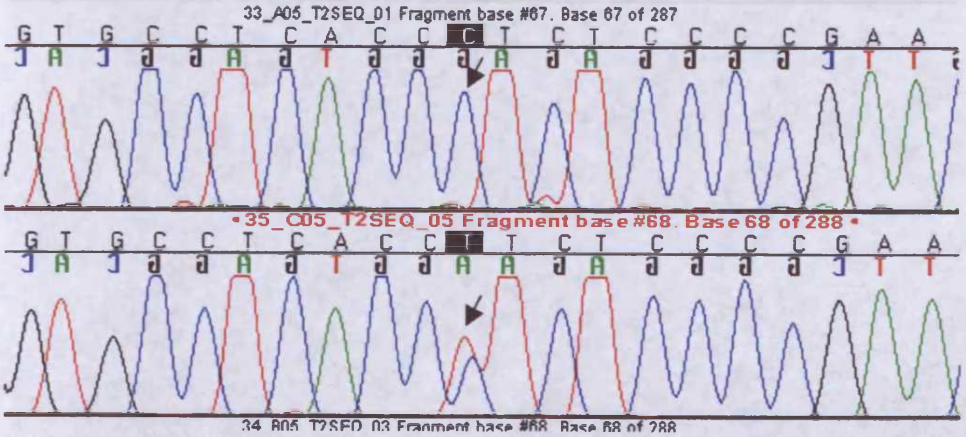

Figure 4.22. Sequence chromatograms for the *DKK1* SNP 463 C>T showing a C/C homozygote in the upper panel and a C/T heterozygote in the lower panel.

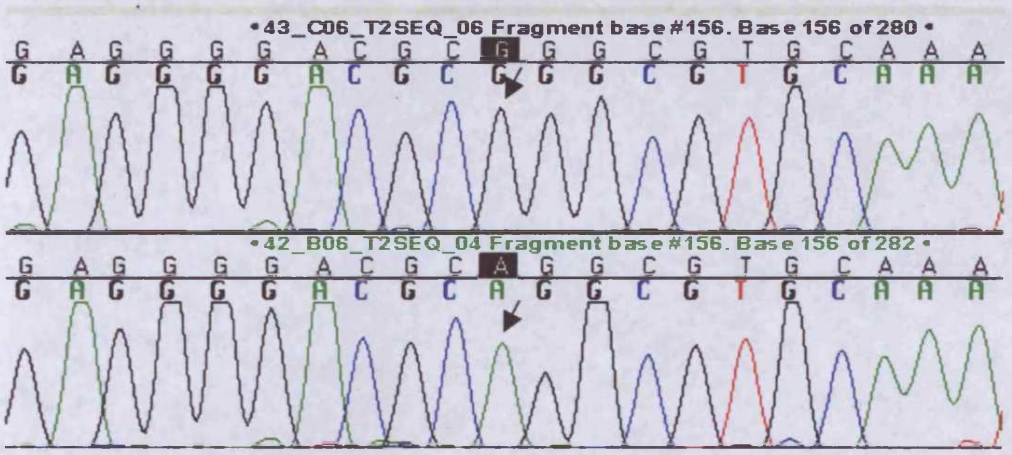

Figure 4.23. Sequence chromatograms for the *DKK1* SNP 560 G>A (rs2241529) showing a G/G homozygote in the upper panel and an A/A homozygote in the lower panel.

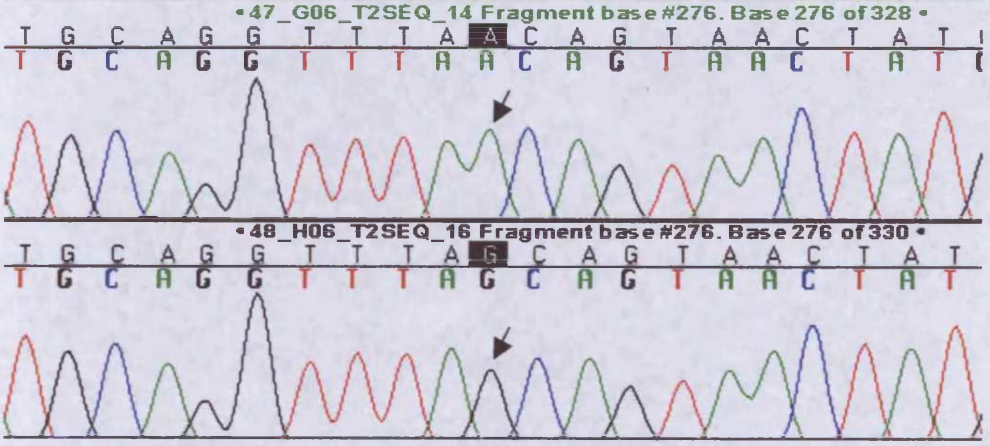

Figure 4.24. Sequence chromatograms for the *DKK1* SNP 2074 A>G (rs1569198) showing an A/A homozygote in the upper panel and a G/G homozygote in the lower panel.

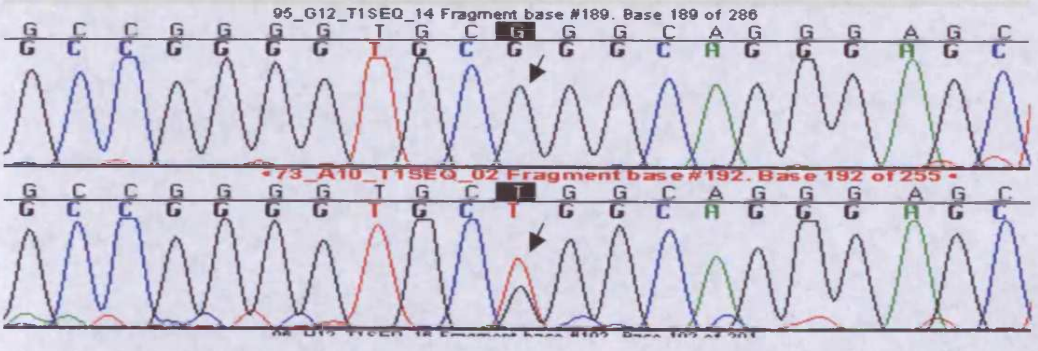

Figure 4.25. Sequence chromatograms for the *UBE2D1* SNP 144 G>T showing a G/G homozygote in the upper panel and a G/T heterozygote in the lower panel.

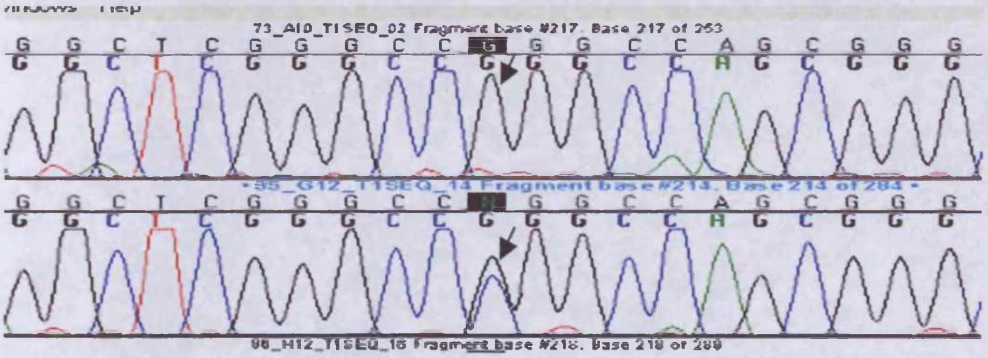

Figure 4.26. Sequence chromatograms for the *UBE2D1* SNP 169 G>C showing a G/G homozygote in the upper panel and a C/G heterozygote in the lower panel.

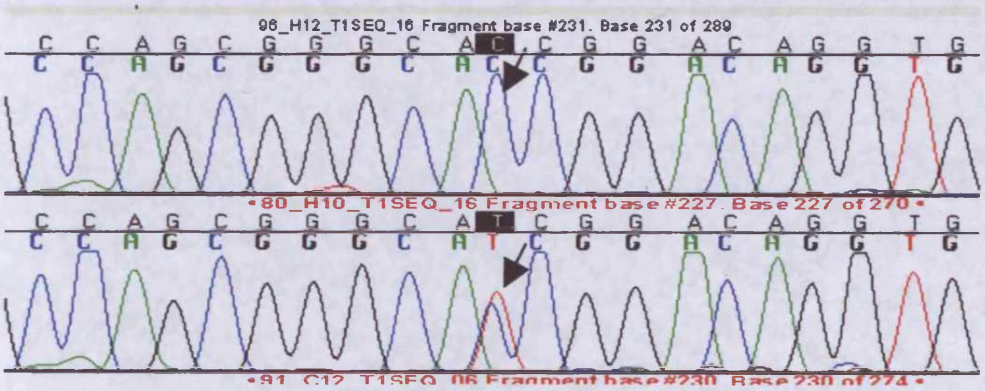

Figure 4.27. Sequence chromatograms for the *UBE2D1* SNP 182 C>T (rs1905456) showing a C/C homozygote in the upper panel and a C/T heterozygote in the lower panel.

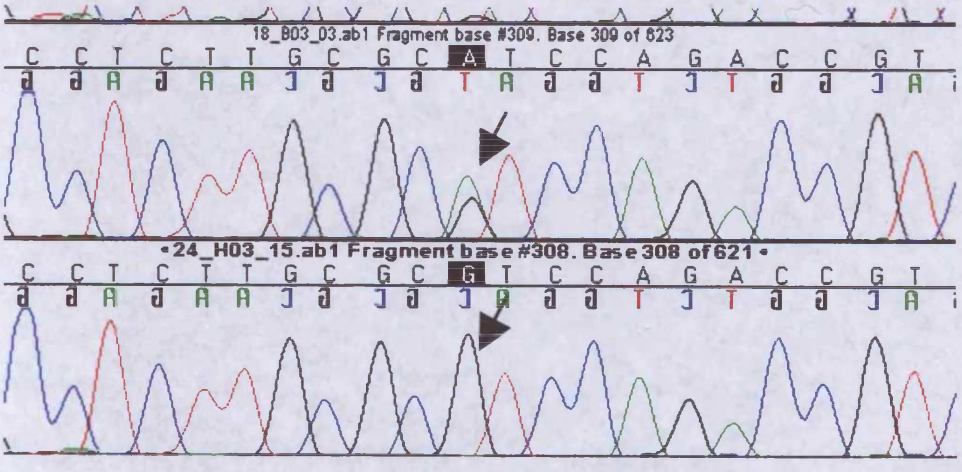

Figure 4.28. Sequence chromatograms for the *UBE2D1* SNP 305 G>A showing an A/G heterozygote in the upper panel and a G/G homozygote in the lower panel.

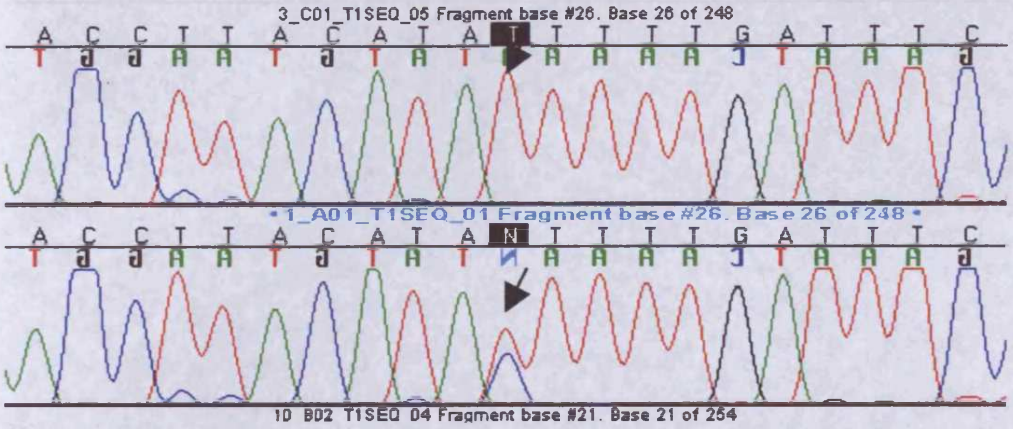

Figure 4.29. Sequence chromatograms for the *UBE2D1* SNP 26120 T>C showing a T/T homozygote in the upper panel and a C/T heterozygote in the lower panel.

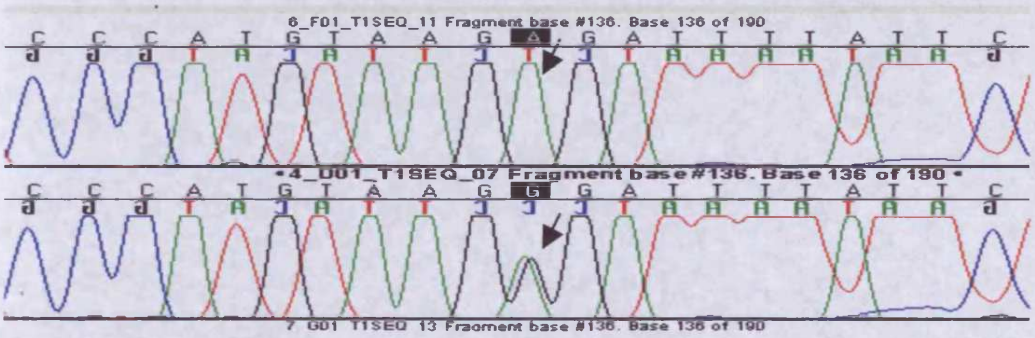

Figure 4.30. Sequence chromatograms for the *UBE2D1* SNP 28525 A>G showing an A/A homozygote in the upper panel and an A/G heterozygote in the lower panel.

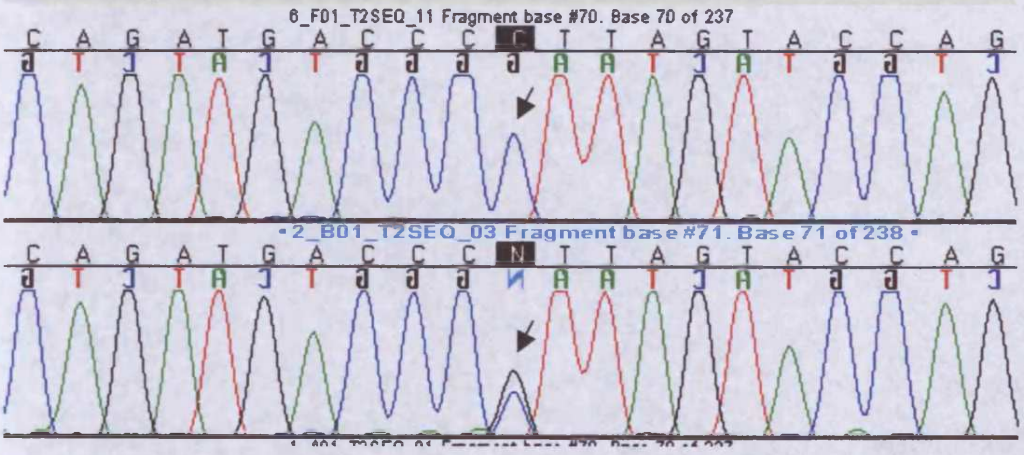

Figure 4.31. Sequence chromatograms for the *UBE2D1* SNP 32771 C>G showing a C/C homozygote in the upper panel and a C/G heterozygote in the lower panel.

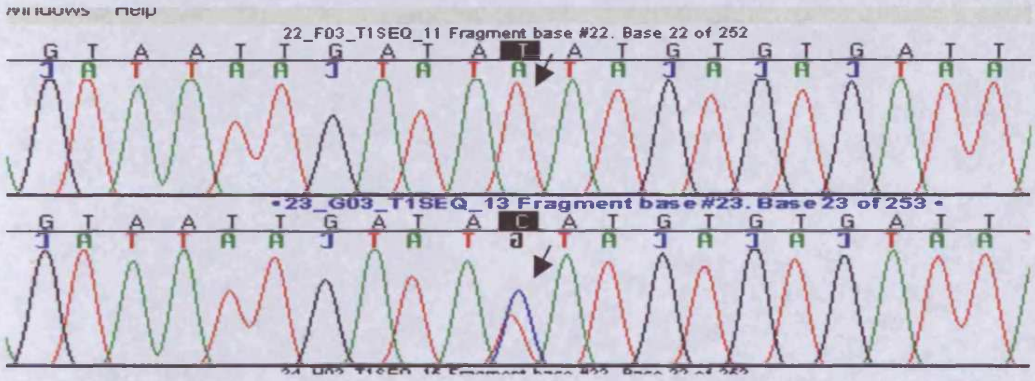

Figure 4.32. Sequence chromatograms for the *UBE2D1* SNP 33403 T>C (rs3802699) showing a T/T homozygote in the upper panel and a C/T heterozygote in the lower panel.

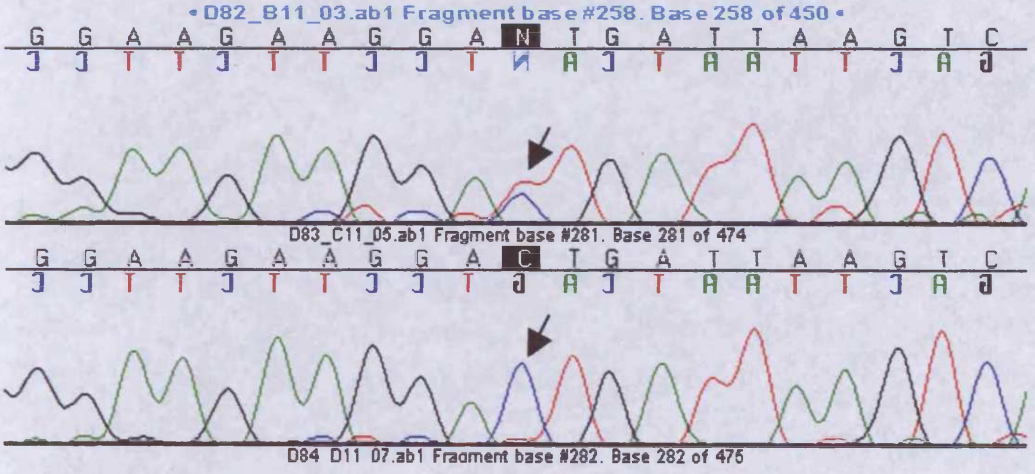

Figure 4.33. Sequence chromatograms for the *DNAJC12* SNP -17 C>T (rs2273771) showing a C/T heterozygote in the upper panel and a C/C homozygote in the lower panel.

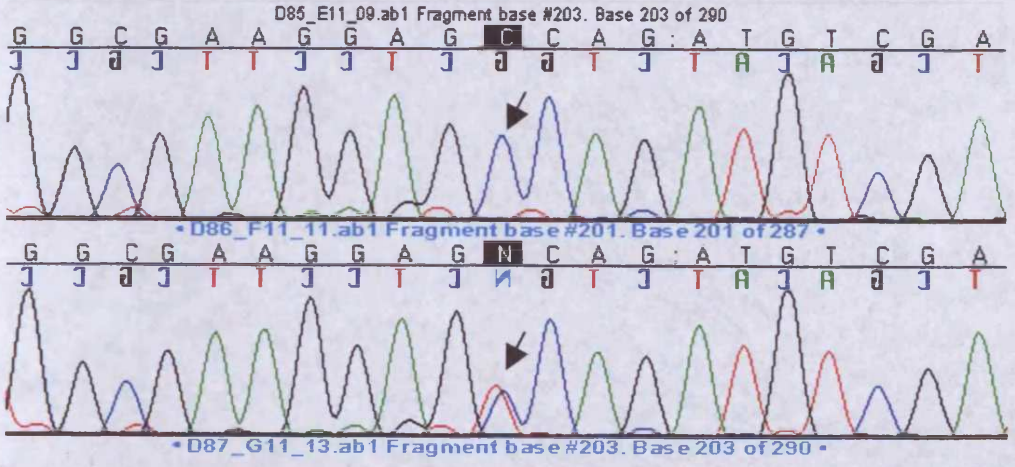

Figure 4.34. Sequence chromatograms for the *DNAJC12* SNP 26434 C>T (rs3740049) showing a C/C homozygote in the upper panel and a C/T heterozygote in the lower panel.

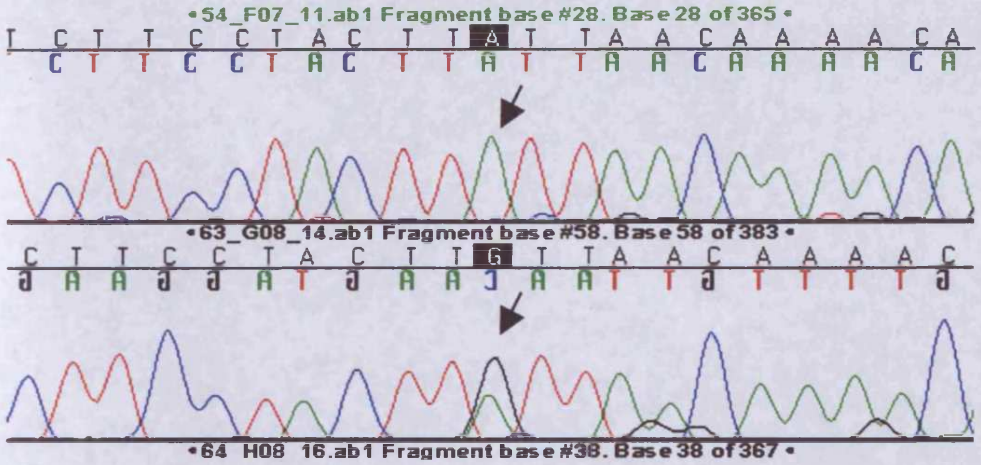

Figure 4.35. Sequence chromatograms for the *SIRT1* SNP -521 A>G (rs3740051) showing an A/A homozygote in the upper panel and an A/G heterozygote in the lower panel.

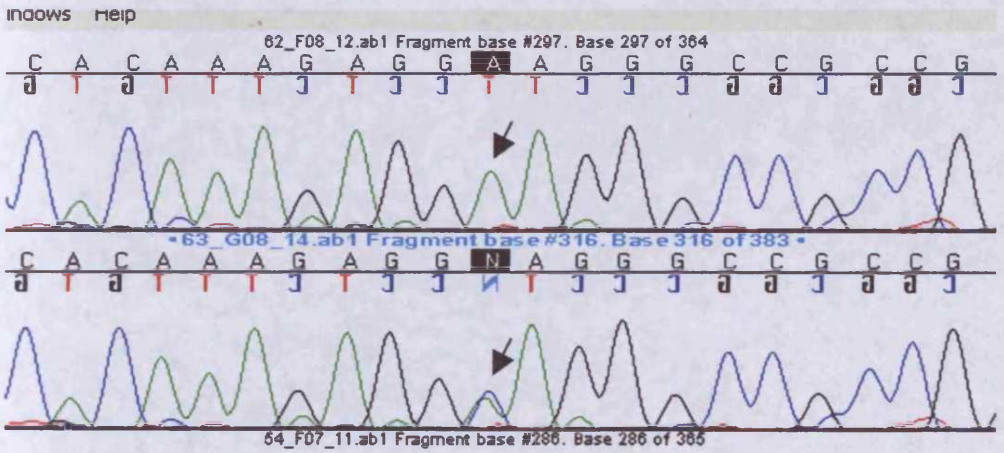

Figure 4.36. Sequence chromatograms for the *SIRT1* SNP -263 A>C (rs932658) showing an A/A homozygote in the upper panel and an A/C heterozygote in the lower panel.

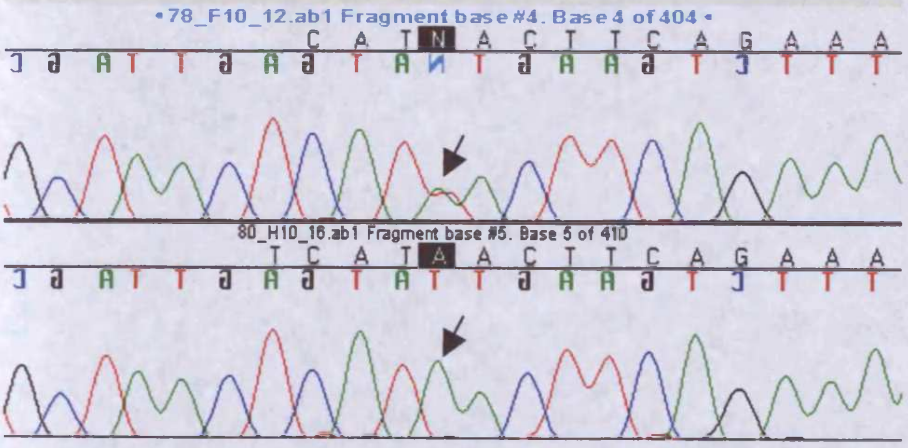

Figure 4.37. Sequence chromatograms for the *SIRT1* SNP 4090 T>A (rs2236318) showing an A/T heterozygote in the upper panel and an A/A homozygote in the lower panel.

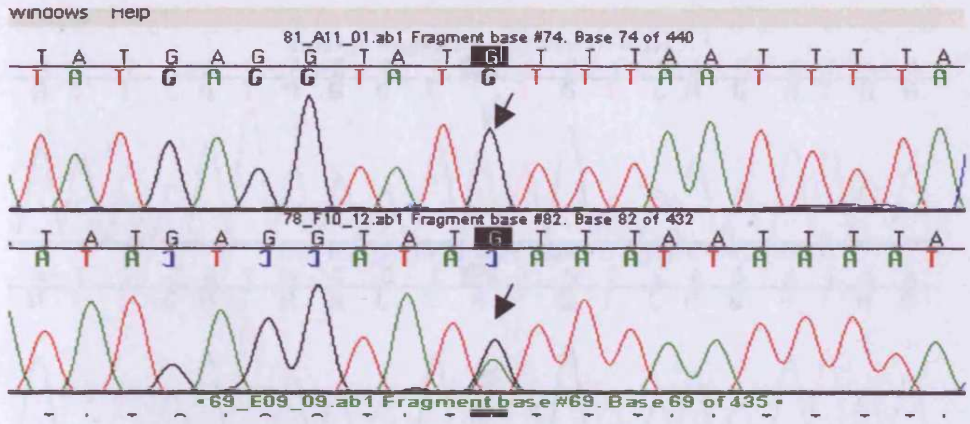

Figure 4.38. Sequence chromatograms for the *SIRT1* SNP 6490 G>A showing a G/G homozygote in the upper panel and an A/G heterozygote in the lower panel.

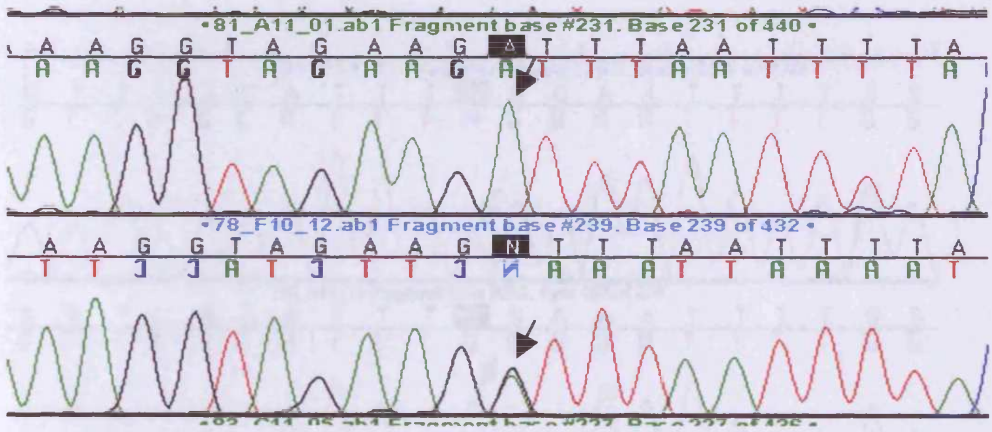

Figure 4.39. Sequence chromatograms for the *SIRT1* SNP 6646 A>G showing an A/A homozygote in the upper panel and an A/G heterozygote in the lower panel.

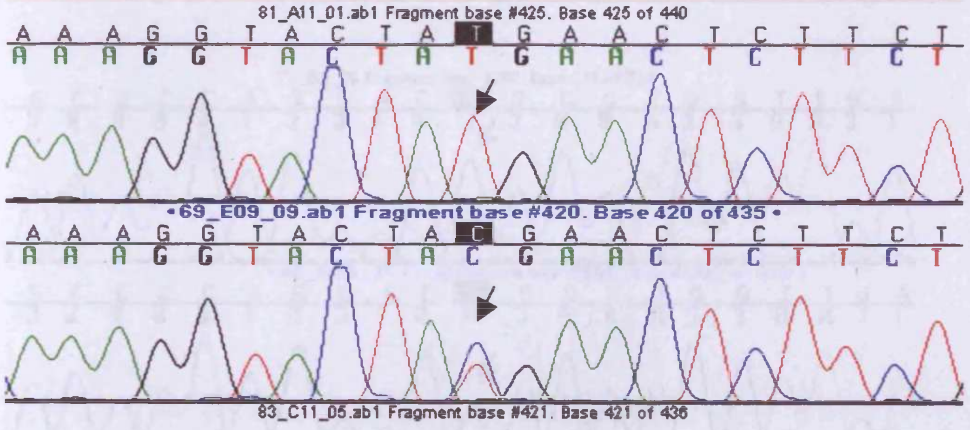

Figure 4.40. Sequence chromatograms for the *SIRT1* SNP 6840 T>C showing a T/T homozygote in the upper panel and a C/T heterozygote in the lower panel.

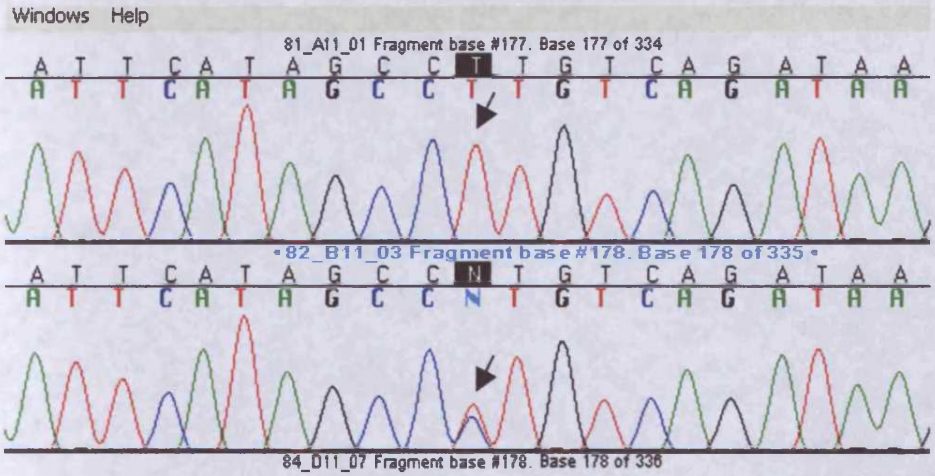

Figure 4.41. Sequence chromatograms for the *SIRT1* SNP 22119 T>C (rs2273773) showing a T/T homozygote in the upper panel and a C/T heterozygote in the lower panel.

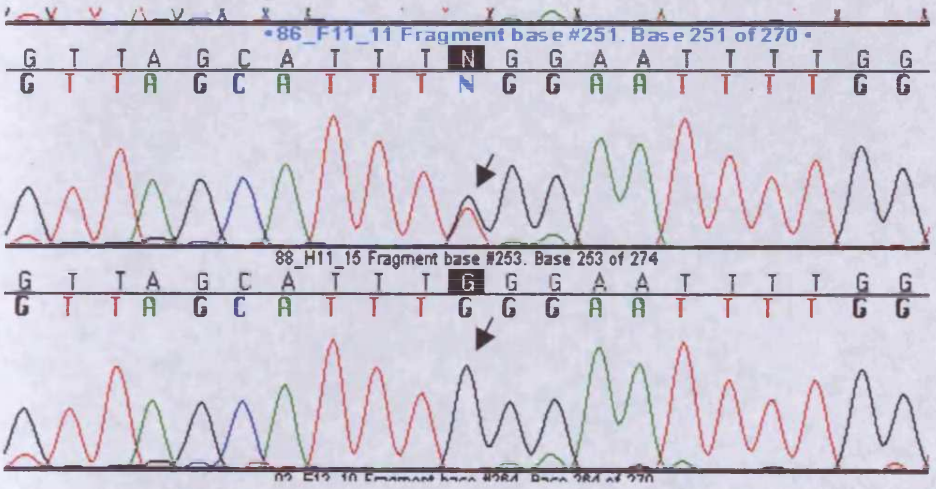

Figure 4.42. Sequence chromatograms for the *SIRT1* SNP 23535 G>T showing a G/T heterozygote in the upper panel and a G/G homozygote in the lower panel.

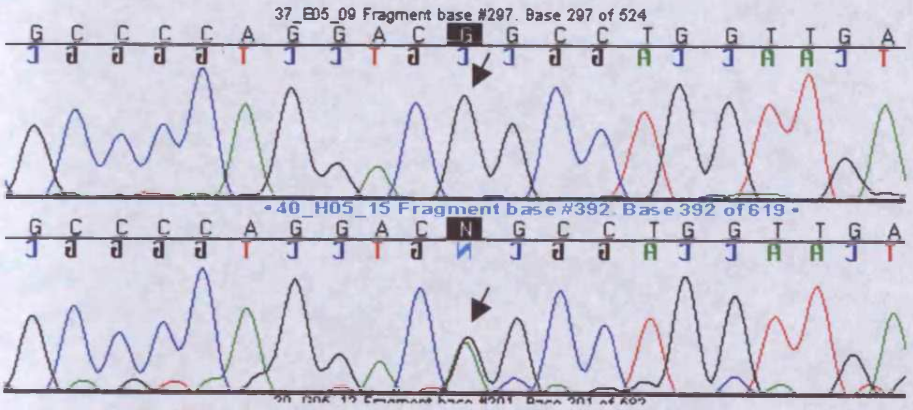

Figure 4.43. Sequence chromatograms for the *SGPL1* SNP -1068 G>A showing a G/G homozygote in the upper panel and an A/G heterozygote in the lower panel.

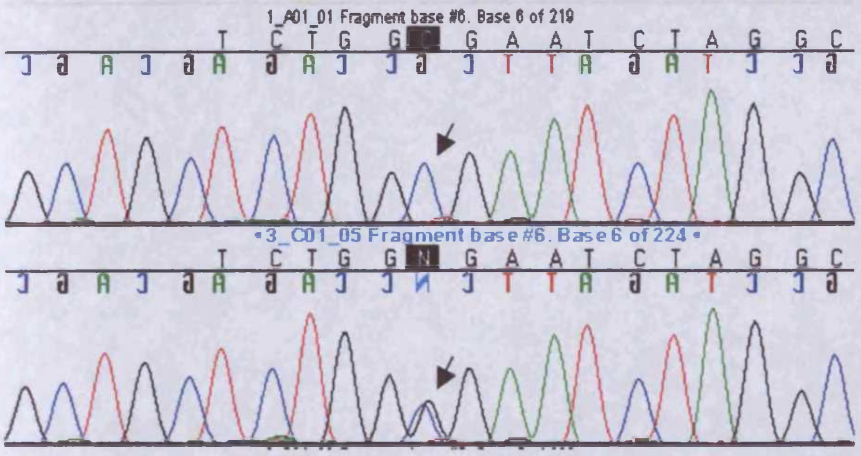

Figure 4.44. Sequence chromatograms for the *SGPL1* SNP -111 C>G showing a C/C homozygote in the upper panel and a C/G heterozygote in the lower panel.

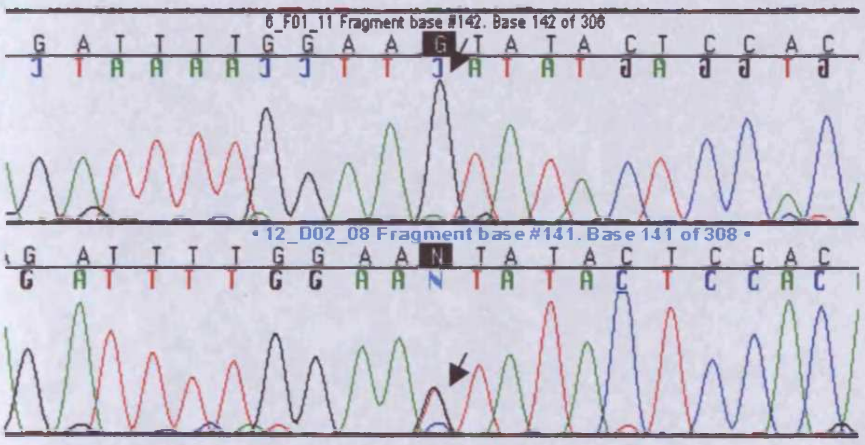

Figure 4.45. Sequence chromatograms for the *SGPL1* SNP 27654 G>T showing a G/G homozygote in the upper panel and a G/T heterozygote in the lower panel.

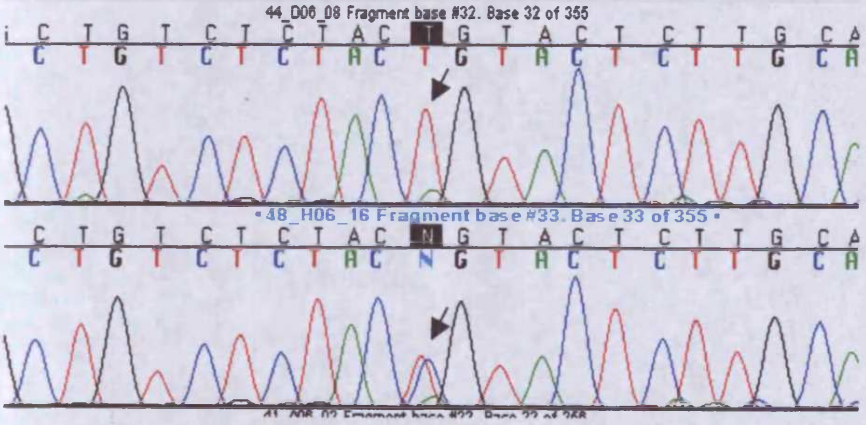

Figure 4.46. Sequence chromatograms for the *SGPL1* SNP 37812 T>C (rs2171157) showing a T/T homozygote in the upper panel and a C/T heterozygote in the lower panel.

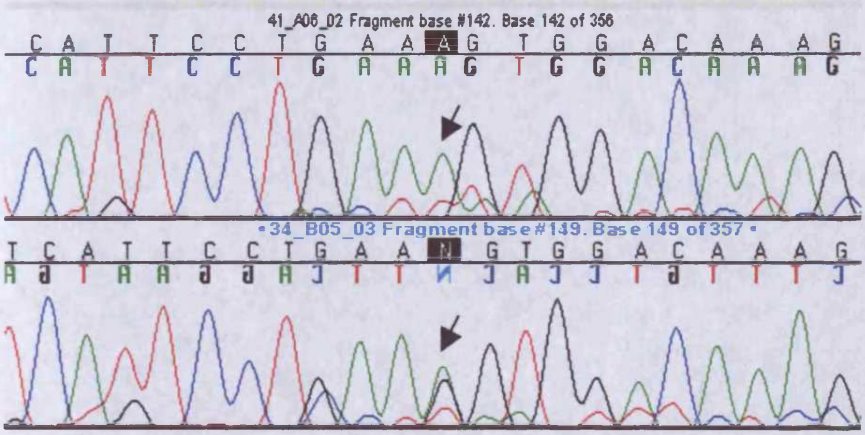

Figure 4.47. Sequence chromatograms for the *SGPL1* SNP 37915 A>G showing an A/A homozygote in the upper panel and an A/G heterozygote in the lower panel.

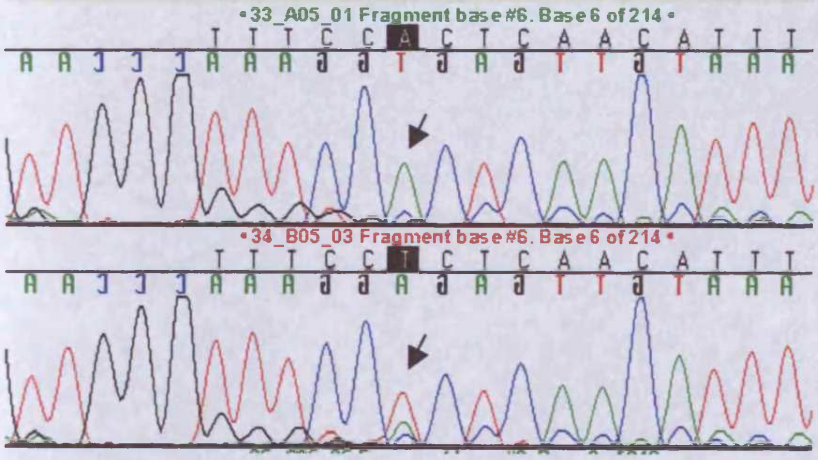

Figure 4.48. Sequence chromatograms for the *SGPL1* SNP 40647 A>T (rs2297842) showing an A/A homozygote in the upper panel and an A/T heterozygote in the lower panel.

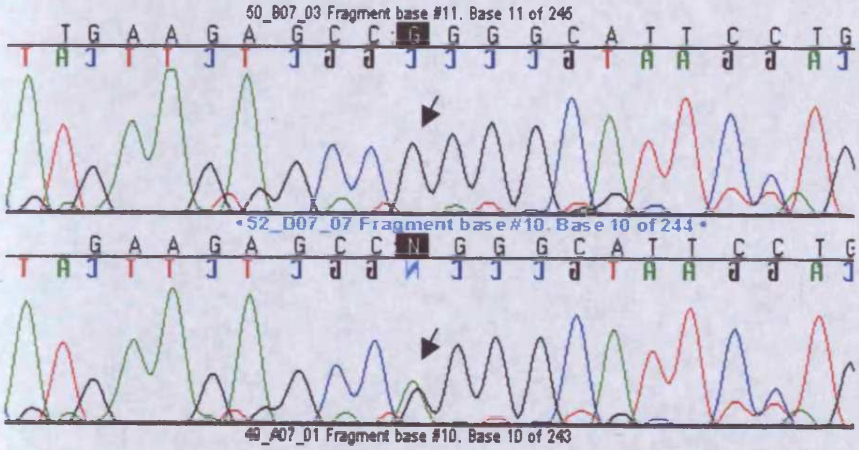

Figure 4.49. Sequence chromatograms for the *SGPL1* SNP 51445 G>A showing a G/G homozygote in the upper panel and an A/G heterozygote in the lower panel.

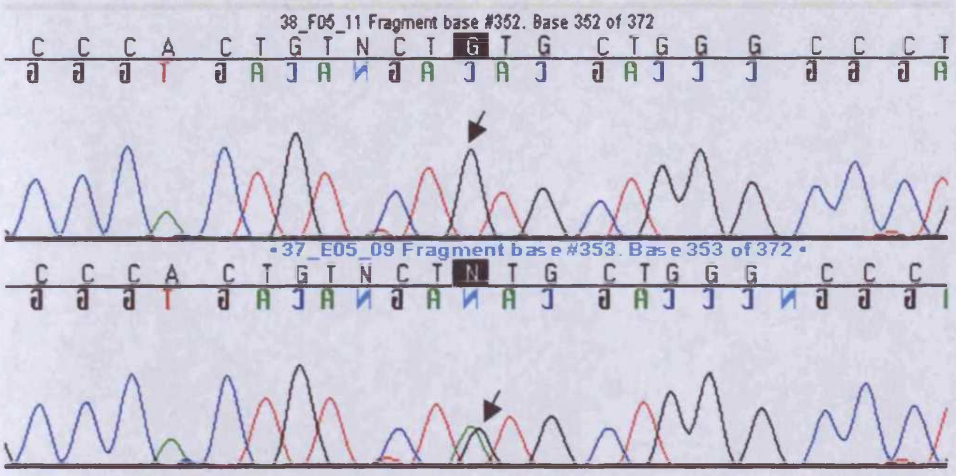

Figure 4.50. Sequence chromatograms for the *SGPL1* SNP 53074 G>A showing a G/G homozygote in the upper panel and an A/G heterozygote in the lower panel.

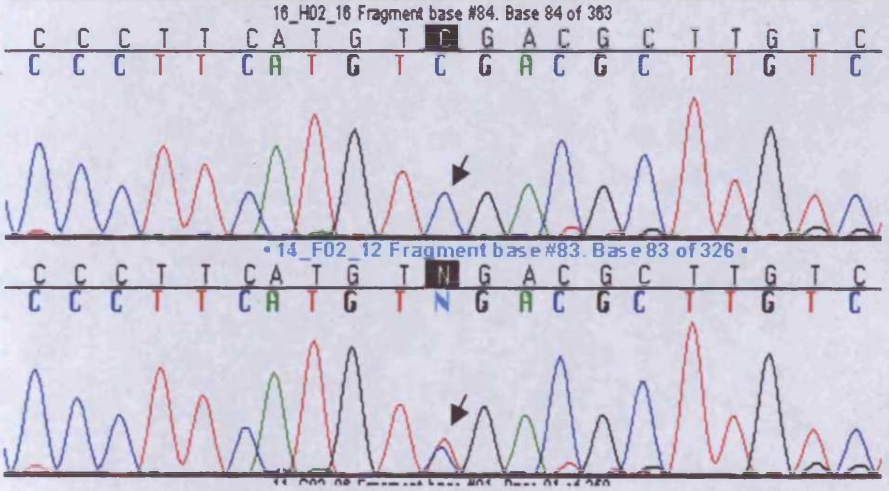

Figure 4.51. Sequence chromatograms for the *SGPL1* SNP 55017 C>T (rs865832) showing a C/C homozygote in the upper panel and a C/T heterozygote in the lower panel.

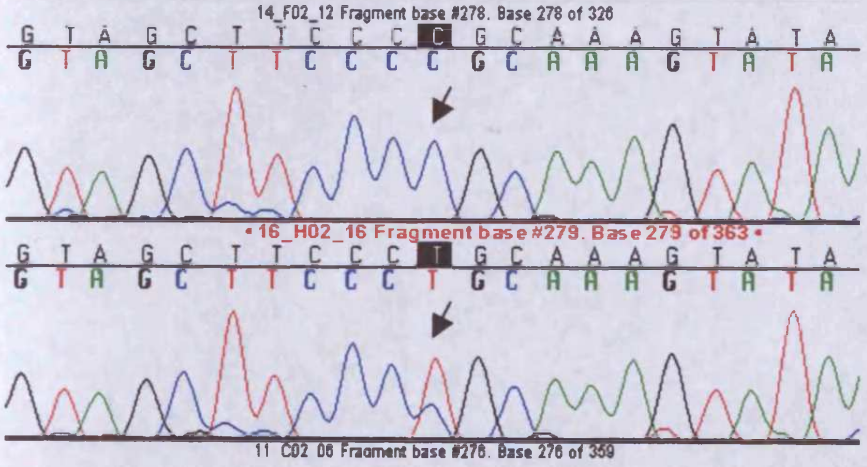

Figure 4.52. Sequence chromatograms for the *SGPL1* SNP 55211 C>T showing a C/C homozygote in the upper panel and a C/T heterozygote in the lower panel.

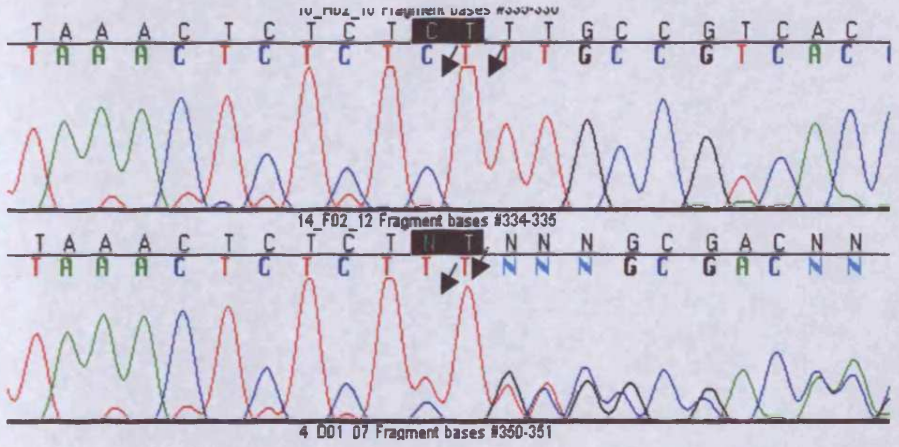

Figure 4.53. Sequence chromatograms for the *SGPL1* indel 55267-55268delCT showing a non-deletion homozygote in the upper panel and a CT deletion heterozygote in the lower panel.

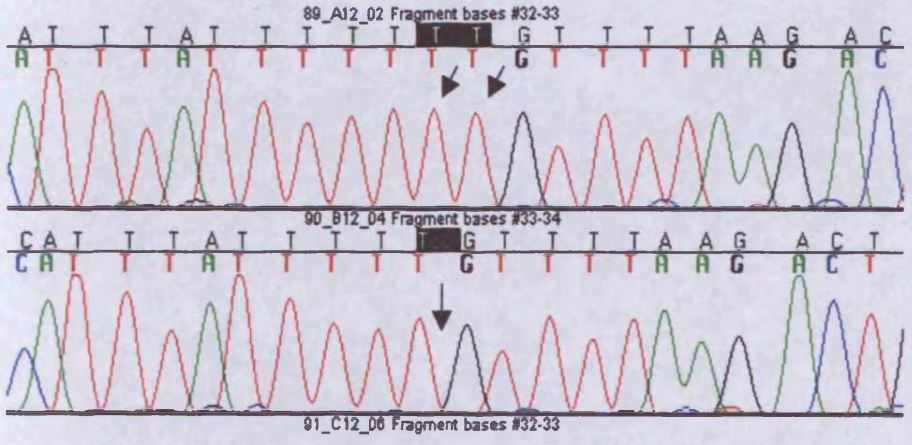

Figure 4.54. Sequence chromatograms for the *SGPL1* indel 58540-58541delTT (rs5786012) showing a non-deletion homozygote in the upper panel and a TT deletion homozygote in the lower panel.

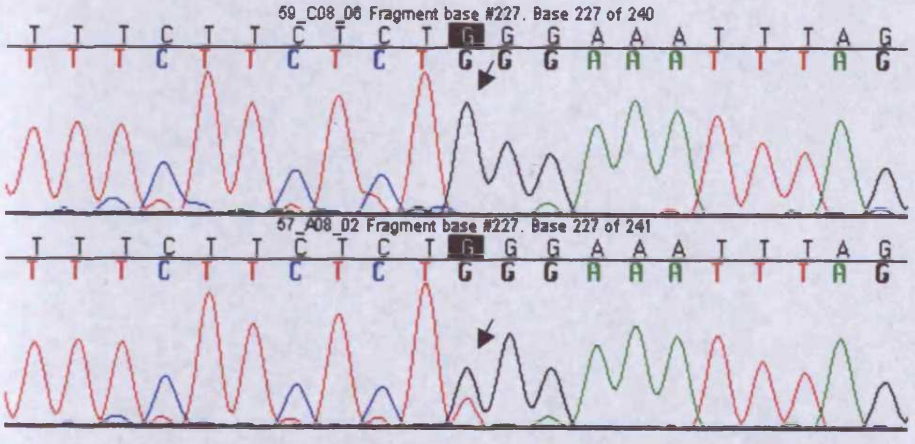

Figure 4.55. Sequence chromatograms for the *SGPL1* SNP 59841 G>T (rs923177) showing a G/G homozygote in the upper panel and a G/T heterozygote in the lower panel.

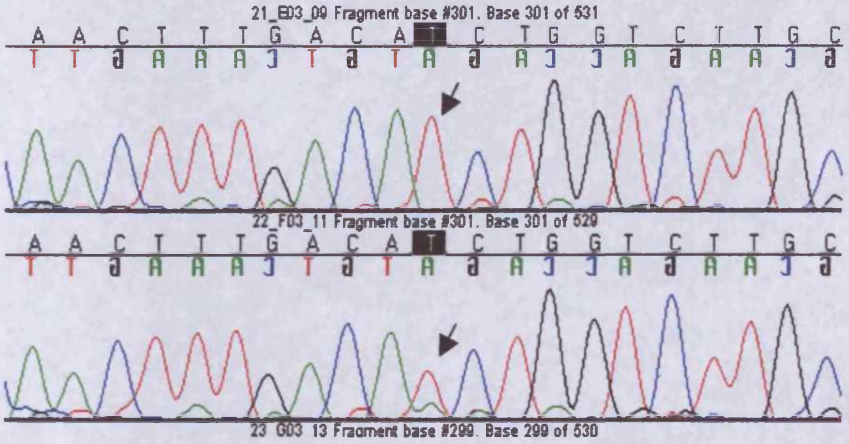

Figure 4.56. Sequence chromatograms for the *SGPL1* SNP 60567 T>A showing a T/T homozygote in the upper panel and an A/T heterozygote in the lower panel.

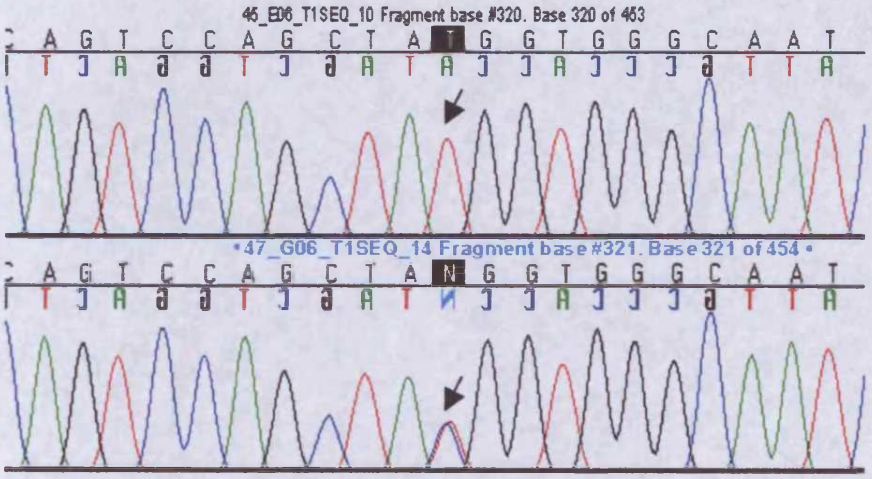

Figure 4.57. Sequence chromatograms for the *SEC24C* SNP 84 T>C (rs2306325) showing a T/T homozygote in the upper panel and a C/T heterozygote in the lower panel.

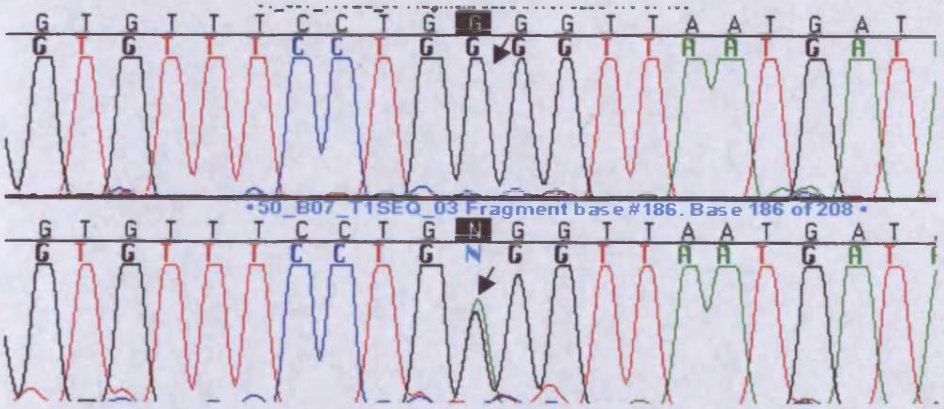

Figure 4.58. Sequence chromatograms for the *SEC24C* SNP 19409 G>A (rs3849969) showing a G/G homozygote in the upper panel and an A/G heterozygote in the lower panel.

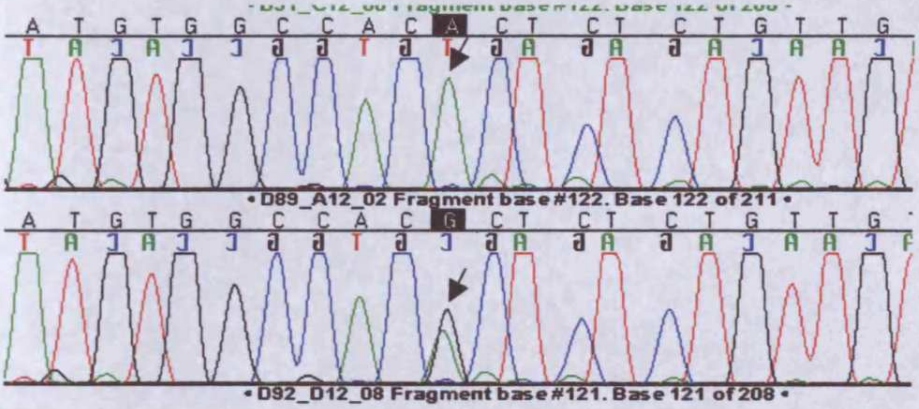

Figure 4.59. Sequence chromatograms for the *SEC24C* SNP 21118 A>G (rs4746147) showing an A/A homozygote in the upper panel and an A/G heterozygote in the lower panel.

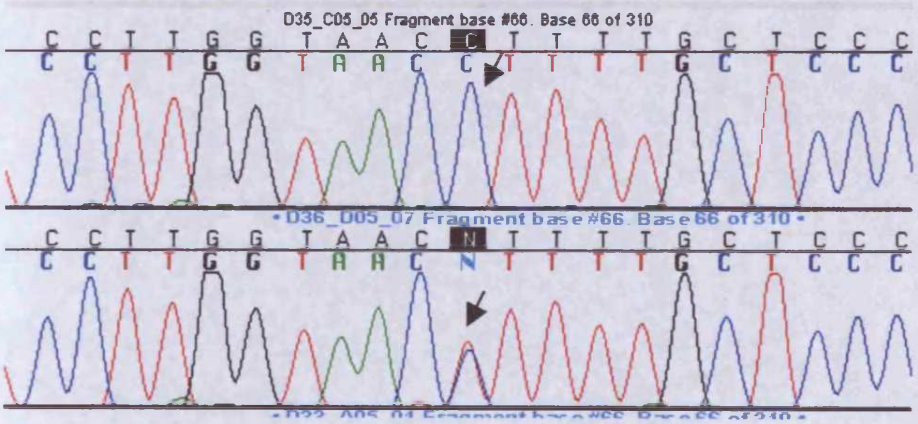

Figure 4.60. Sequence chromatograms for the *SEC24C* SNP 23423 C>T (rs3088070) showing a C/C homozygote in the upper panel and a C/T heterozygote in the lower panel.

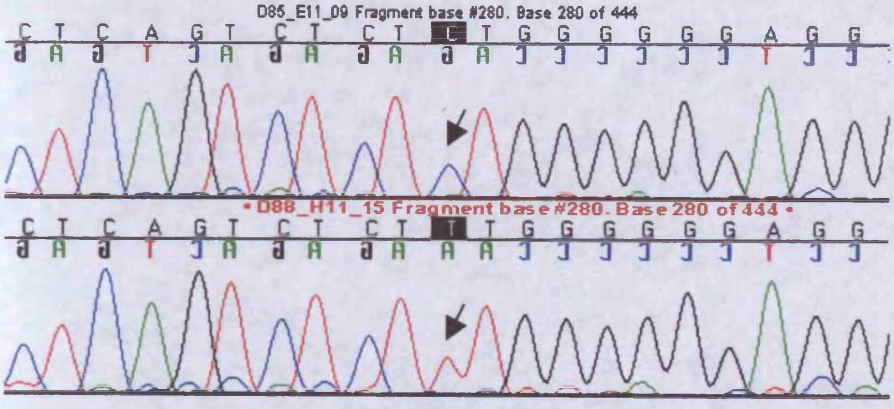

Figure 4.61. Sequence chromatograms for the *SEC24C* SNP 24372 C>T showing a C/C homozygote in the upper panel and a T/T homozygote in the lower panel.

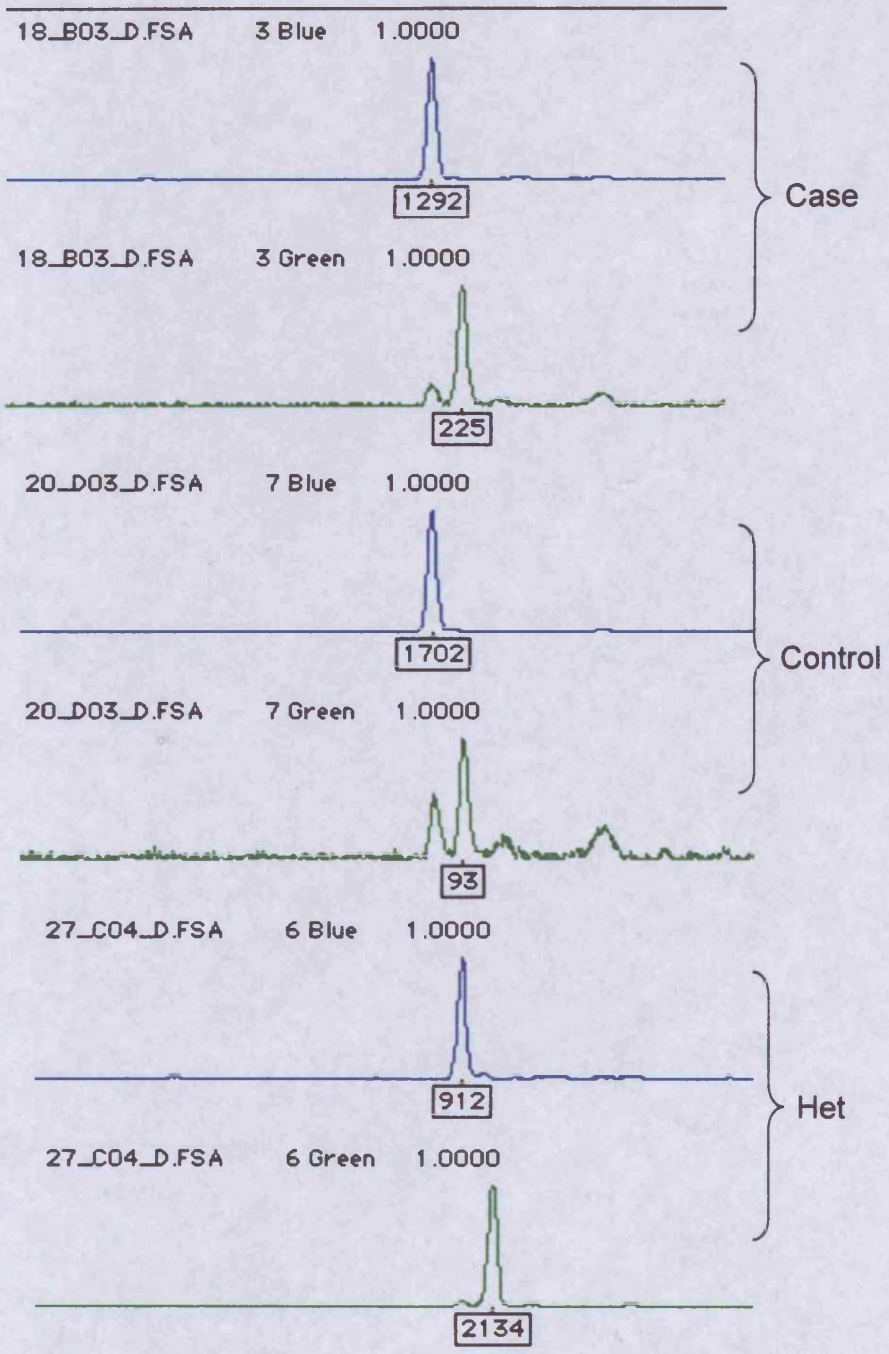

Figure 4.62. Traces generated from pooled genotyping of the *SGPL1* 53074 G>A SNP. The blue peak represents the G allele and the green peak represents the A allele. Data from individual case and control pools are shown, together with a heterozygote (het). Note the unequal peak heights in the heterozygote.

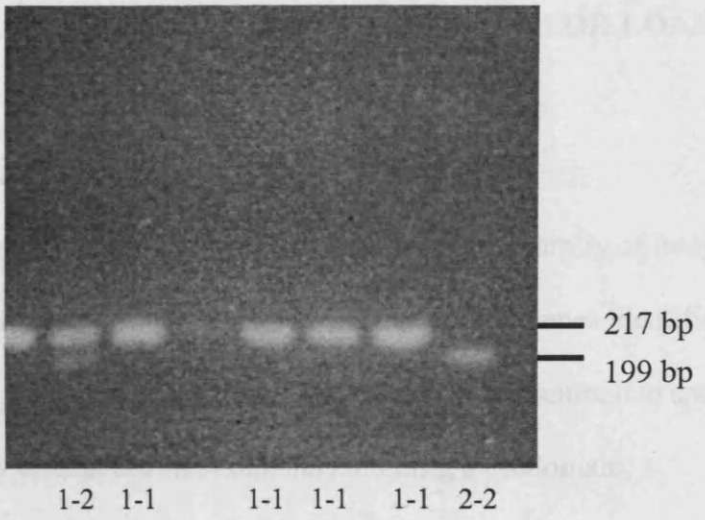

Figure 4.63. RFLP fragments generated by the *DKK1* 463 C>T *Alu* I assay. Individuals homozygous for the C allele (1-1) were defined by the presence of one band of size 217bp. Individuals homozygous for the T allele (2-2) were defined by the presence of two bands of size 199bp and 18bp. C/T heterozygotes (1-2) displayed three bands of size 217bp, 199bp, and 18bp. Note that the 18bp band ran off the gel due to the small size.

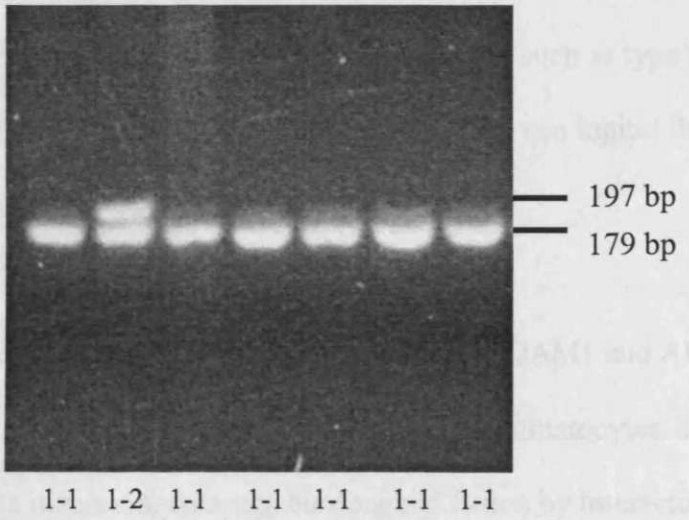

Figure 4.64. RFLP fragments generated by the *SGPL1* 53074 G>A *Dra* III assay. Individuals homozygous for the G allele (1-1) were defined by the presence of two bands of size 179bp and 18bp. A/G heterozygotes (1-2) displayed three bands of size 197bp, 179bp, and 18bp. No A/A homozygotes were observed. Note that the 18bp band ran off the gel due to the small size.

5. ADAM12: A FUNCTIONAL CANDIDATE FOR LOAD

5.1 The ADAMs Family

The ADAMs (for "a disintegrin and metalloprotease") are a family of integral membrane or secreted glycoproteins, encoded by at least 30 genes identified in *Caenorhabditis elegans, Drosophila, Xenopus* and various mammalian species. These proteins have several distinct domains including a prodomain, a metalloprotease domain, a disintegrin-like domain, a cysteine-rich region, an epidermal growth factor-like region and, in the case of membrane-anchored ADAMs, a transmembrane and cytoplasmic domain. The closest homologues of ADAMs are the highly toxic snake venom metalloproteases (SVMPs). Both SVMPs and ADAMs are members of the reprolysin/adamalysin subfamily of zinc dependent metalloproteases[350-352]. The SVMPs are processed to generate a metalloprotease, which is able to degrade proteins of the basement membrane such as type IV collagen and laminin[353] and a disintegrin-like domain, which can inhibit the function of platelets by interacting with platelet integrin GPIIb-IIIa[354].

The first described ADAMs were fertilin α and fertilin β (ADAM1 and ADAM2), which are expressed on the posterior head of mammalian spermatocytes. These proteins are thought to mediate sperm–egg binding and fusion by interacting with integrin α6β1 on the egg surface[355-358]. Since then, a number of ADAMs family members have been reported in the literature and have been implicated in many vital functions during development[359-362] and in the pathogenesis of cancer[363-365], rheumatoid arthritis[366], Alzheimer's disease[64-69] and inflammatory responses[364].

5.1.1 ADAM12

ADAM12 was first described by Yagami-Hiromasa and colleagues[367], who identified a protein they called meltrin α when searching for homologues of ADAMs 1 and 2 in a mouse myogenic cell line. The human orthologue of meltrin α was discovered by Gilpin *et al.* in 1998[368]. The human *ADAM12* gene is located on chromosome 10q26.3 and encodes two splice variants: a membrane bound form designated ADAM12-L and a shorter form designated ADAM12-S that is secreted as a soluble protein.

5.1.2 Structural Organisation of ADAM12

ADAM12-L contains 881 aa and has a calculated *Mr* of 96,917 and ADAM12-S contains 718 amino acids with an *Mr* of 77,775[368]. The structural organization of the transcripts is shown in Figure 5.1 (p.185). The two isoforms share a common region consisting of the prodomain (residues 29–206), the metalloprotease domain (residues 207–417), the disintegrin-like domain (residues 417–512), and the cysteine-rich region (residues 529–614). ADAM12-L has a 21-aa transmembrane domain and a 179-aa cytoplasmic domain. ADAM12-S has instead a shorter 34-aa carboxyl terminus with no apparent transmembrane domain.

Sequence comparison of ADAM12 with other reprolysins reveals that the metalloprotease domain contains the zinc binding sequence that characterises the active site of these proteases. The highly conserved HE*XX*H*XX*G*XX*H motif is present, including the glutamate residue that is required for the catalytic mechanism[369]. The disintegrin-like domain contains a putative integrin-binding loop, although it does not have an RGD sequence typical of "true" disintegrins[355]. The

cysteine-rich region contains a putative fusion peptide similar to the fusion peptides of fertilin[370] and some viruses[371] and an epidermal growth factor-like repeat[368]. The disintegrin-like and cysteine-rich domains of ADAM12 have been shown to support cell adhesion by binding to integrin α9β1 and syndecan-4, respectively[372-375]. ADAM12-L contains a 21-aa, highly hydrophobic transmembrane domain which is consistent with the consensus sequence motif for type I membrane proteins[376]. The flanking amino acid sequence is consistent with the amino terminus being exposed to the cell exterior[368]. The cytoplasmic tail of ADAM12-L is relatively long compared to other members of the ADAMs family and has four class I (R/K)*XX*P*XX*P and three class II P*XX*P*X*(R/K) SH3 domain-binding motifs grouped into four proline-rich regions, implying this region interacts with SH3 domain-containing signalling molecules[377].

Comparison of the human ADAM12-L sequence with mouse ADAM12 reveals an overall amino acid identity of 81%. The divergent carboxyl terminus of ADAM12-S does not show similarity to any other proteins in the databases[368].

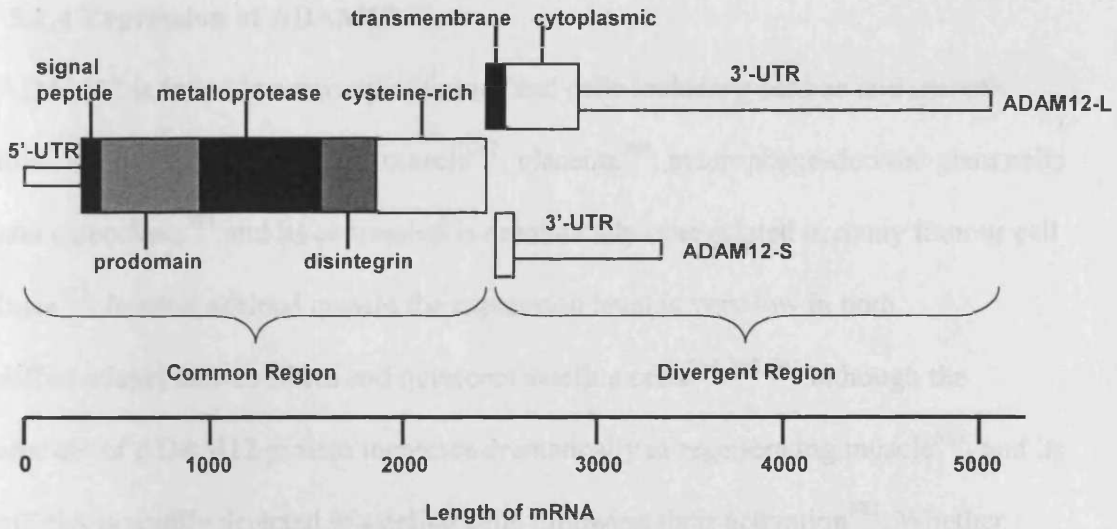

Figure 5.1. Schematic diagram of both isoforms of ADAM12, showing the location of the different domains.

5.1.3 Processing of ADAM12

Although mature ADAM12 is a catalytically active protease, it is synthesised as a zymogen, with the prodomain maintaining the metalloprotease in a latent state. This latency is achieved by means of a "cysteine switch", whereby an unpaired cysteine residue in the prodomain (Cys179) directly coordinates the zinc ion at the catalytic site[378, 379].

After glycosylation and proper folding in the endoplasmic reticulum, the zymogen proceeds through the Golgi apparatus. ADAM12 contains the sequence RHKR at the boundary between the prodomain and the metalloprotease, which corresponds to the consensus cleavage site of furin[380]. In the *trans*-Golgi network, furin or a related endopeptidase cleaves the protein at the junction between the prodomain and the catalytic domain, resulting in the dissociation of the cysteine residue from the active site. Activated ADAM12 is then either secreted from the cell (ADAM12-S) or targeted to the plasma membrane (ADAM12-L).

5.1.4 Expression of ADAM12

ADAM12 is found in a variety of tissues and cells including cardiac and smooth muscle[368], developing skeletal muscle[367], placenta[368], macrophage-derived giant cells and osteoclasts[381] and its expression is dramatically upregulated in many tumour cell lines[375]. In adult skeletal muscle the expression level is very low in both differentiated muscle fibres and quiescent satellite cells[367, 368, 382] although the amount of ADAM12 protein increases dramatically in regenerating muscle[383], and its mRNA is readily detected in satellite cells following their activation[382]. Whether ADAM12 is expressed in human brain is unclear. Gilpin *et al.* (1998)[368] failed to detect any transcripts in human brain by Northern blot examination, but Karkkainen *et al.* (2000)[384] revealed an 8.1-kb band of ADAM12 mRNA in rat CNS, but it only "could be detected after very long exposure times and the band was too faint for quantitation".

5.1.5 The Role of ADAM12 in Cell Differentiation

Several studies have pointed to an important role for ADAM12 in mesenchymal cell differentiation[367, 368]. Abe *et al.* (1999)[381] found that expression of meltrin-α (mouse ADAM12) is induced under conditions that promote giant cell formation and osteoclastogenesis *in vitro* and that interference with the expression of this transcript by antisense oligonucleotides results in inhibition of multinucleation, an essential step for the formation of either cell type.

Similarly, evidence for a role for ADAM12 in muscle differentiation was presented by Yagami-Hiromasa *et al.*[367] when they showed that transfection of C2C12 cells with antisense mRNA encoding ADAM12 inhibited cell fusion. The same study

showed that overexpression of full length ADAM12 also inhibited myoblast fusion. In agreement with the work of Yagami-Hiromasa and colleagues, Cao *et al.* (2003)[385] found that C2C12 cells in which the expression of ADAM12 has been attenuated by small interfering RNA (siRNA) have a decreased potential both to differentiate and to form quiescent reserve cells whereas enhanced expression of full length ADAM12 induced a quiescent cell-like phenotype and did not stimulate differentiation. Therefore ADAM12 appears to be involved in the mutually exclusive actions of promoting differentiation and maintaining quiescence, probably in response to the cellular environment. Additional evidence for involvement of ADAM12 in myogenesis has been provided by the generation of dystrophin-deficient *mdx* mice in which ADAM12 is overexpressed. These mice show significantly less muscle fibre necrosis and inflammation compared with *mdx* mice[386].

Notably, transgenic mice overexpressing ADAM12 show increased adipogenesis[387], whereas ADAM12-deficient mice showed decreased interscapular brown adipose tissue. Adipocytes also arise from the mesodermal stem cells that can also differentiate into muscle cells and osteoblasts[388, 389]. Once committed to an adipocyte lineage, preadipocytes can either remain quiescent or proliferate and undergo differentiation into fully mature lipid-laden adipocytes. In parallel to the situation with myoblasts, ADAM12 mRNA has been detected throughout most stages of adipogenesis but with maximal levels in preadipocytes just before the onset of differentiation[390].

5.1.6 The Role of ADAM12 in Proteolysis

As mentioned previously, ADAM12 has a catalytically active metalloprotease domain and a number of physiological substrates have now been identified. A well-studied mechanism by which the ADAM12 protease acts is in the ectodomain shedding of heparin-binding epidermal growth factor-like growth factor (HB-EGF)[391]. Like other members of the EGF family, HB-EGF is synthesised as a membrane-anchored form (proHBEGF), which is then proteolytically processed to become a bioactive soluble form. HB-EGF binds directly to the EGF receptor (EGFR) and thereby enhances its phosphorylation, resulting in cell growth and differentiation[392].

ADAM12 also seems to play an important role in pregnancy. It is well known that human placenta and maternal serum contain several aminopeptidases that regulate the activity of peptide hormones such as oxytocin, vasopressin, and angiotensins. Placental leucine aminopeptidase (P-LAP)/oxytocinase is one of these enzymes and is known to increase in maternal serum during pregnancy[393]. P-LAP is a type-II integral membrane protein[394, 395] and exists as a soluble form in maternal serum and a membrane-bound form in placenta. Soluble P-LAP is thought to be derived from the native membrane-bound form by ectodomain shedding. Ito *et al.* (2004)[396] have determined that ADAM proteases, including ADAM12, are involved in P-LAP shedding in human placenta.

ADAM 12-S has been shown to degrade insulin-like growth factor binding protein 3 (IGFBP-3) and to a lesser extent IGFBP-5[397]. There are six members of the IGFBP family, which are ubiquitously expressed in serum, other biological fluids and in

several tissues where they bind insulin-like growth factor (IGF) I and II and modulate their bioavailability[398-400]. During the course of pregnancy, much of the IGFBP-3 in maternal serum is degraded, presumably resulting in increased bioavailability of IGF. Laigaard *et al.* (2003)[401] have demonstrated that the concentration of ADAM12-S in maternal serum increases 60-fold during gestation and interestingly, is markedly decreased in the first trimester in pregnancies with foetal Down syndrome.

Three members of the ADAM family are candidate α-secretases, ADAM9, ADAM10 and ADAM17. It has been suggested that endogenous α-secretase is composed of several ADAM enzymes[402]. ADAM12 has demonstrated metalloprotease activity and so it is possible it also could have α-secretase activity, although this has not been tested. I have therefore examined the *ADAM12* gene as a functional candidate for involvement in LOAD.

5.2 Materials and Methods

Described here are the specific methods used to study *ADAM12*. More detailed descriptions of subject groups and methods are described in Chapter 2.

5.2.1 Subjects

The mutation screening sample consisted of 14 UK Caucasian patients, with age at onset >65 years. All SNPs identified were tested for association with LOAD in the MRC pools comprised of 186 UK Caucasian AD patients (age at onset 74.34 ± 6.461 years) and 186 age- and sex-matched controls (age at collection 75.42 ± 6.535 years). Some SNPs were additionally tested in the WashU pools comprised of 270 Caucasian AD patients (age at onset 75.83 ± 6.863) and 270 age- and sex-matched controls (age at last assessment 79.37 ± 7.012), recruited from the Greater St. Louis metropolitan area in the USA. Non-redundant SNPs that showed significant (P<0.1) differences between case and control pools were individually genotyped in the MRC sample comprising 546 UK Caucasian AD patients (age at onset 75.45 ± 6.485 years) and 546 age- and sex-matched controls (age at collection 76.30 ± 6.257 years). All patients were diagnosed according to NINCDS-ADRDA criteria[17]. Cognitive function of controls was assessed using the mini mental-state exam (MMSE)[18]. Only those with a score of at least 28 were included in the study.

5.2.2 Collection of Gene Sequences

ADAM12 encodes two splice variants; ADAM12-S, a shorter secreted form and ADAM12-L, a longer membrane-bound form that diverge at their 3' ends (Figure 5.1, p.185). The cDNA sequence for each splice variant was obtained from the GenBank database at NCBI (http://www.ncbi.nlm.nih.gov). Determination of coding

sequences, untranslated regions (UTRs) and intronic regions was based on alignment of the cDNA sequences with genomic clone sequences, using BLAST sequence homology searches. Specifically, NM_003474.2 encoding ADAM12-L and NM_021641.1 encoding ADAM12-S were aligned against genomic sequence available from the UCSC Genome Bioinformatics Site (http://genome.ucsc.edu).

5.2.3 Polymerase Chain Reaction (PCR)

PCR fragments spanning exons, UTRs and limited 5' flanking regions were designed using Primer 3.0 (http://www-genome.wi.mit.edu/cgi-bin/primer/primer3_www.cgi). Primers capable of specifically detecting a particular splice variant using cDNA derived from human brain as a template were also designed. These primer sequences are listed directly below in Table 5.1. Primers used to generate amplimers for the purpose of DHPLC are listed in Table 5.2 (p.197). PCR amplification was performed under standard conditions of 1X PCR buffer (Qiagen), 1.5 mM $MgCl_2$, 250 μM dNTPs, 0.5 μM of each primer, 0.6 units Hot Star Taq (Qiagen) and 48 ng genomic DNA in a 24 μl reaction. Cycling was conducted in a MJ Tetrad (MJ Research) with an initial denaturation of 94°C for 15min, followed by 35 cycles of 94°C for 30s, optimal annealing temperature for 30s and 72°C for 45s with a final extension step of 72°C for 10 min. Synthesis of appropriately sized PCR products was confirmed by electrophoresis on 2% agarose gels.

Splice Variant	Primer Sequence (5'→3')	Expected Size for Template Used (bp)	Annealing Temperature (°C)
ADAM12-L	Sense: TGCCGGATTTGTGGTTTATC Antisense: TCGGTGGGTAGGAATCTGG	Genomic DNA: 1135 cDNA: 191	62
ADAM12-S	Sense: GCTTTGGAGGAAGCACAGAC Antisense: CAGCACTGGTCACGGTCTC	Genomic DNA: 985 cDNA: 181	62

Table 5.1. Details of PCR assays designed to detect specific ADAM12 transcripts in human brain, including PCR primers, annealing temperatures and expected size of amplimers.

5.2.4 Denaturing High Performance Liquid Chromatography (DHPLC)

The search for polymorphisms was performed by DHPLC scanning on the Wave™ DNA Fragment Analysis System (Transgenomic). The 14 screening samples were amplified as described above, except the final extension in the PCR protocol was followed by denaturation at 94°C for 5min and then cooling to 54°C over 40min, to allow heteroduplex formation. Column temperature and acetonitrile gradient were determined with the DHPLC Melt program (http://insertion.stanford.edu/melt1.html). To ensure maximum sensitivity, in addition to the (highest) temperature suggested by the software (n°C), each fragment was also run at n+2°C. The resultant chromatograms were compared, with a shift in trace pattern indicative of a heteroduplex. An example of a DHPLC trace is displayed at the end of this chapter (Figure 5.6).

5.2.5 DNA Sequencing

For fragments that displayed a heteroduplex peak, the PCR products of one heterozygous and one homozygous sample were incubated at 37°C with 1 unit each of shrimp alkaline phosphatase and exonuclease I to remove unincorporated primers and dNTPs. Purified products were then bidirectionally sequenced on an ABI 3100 Genetic Analyser (Applied Biosystems) using the Big Dye Terminator (v2.0) Cycle Sequencing kit (Applied Biosystems). Sequence traces were subsequently exported to the Sequencher™ program in order to characterise polymorphisms. Sequence chromatograms for all SNPs identified are displayed at the end of this chapter (Figures 5.7 to 5.25).

5.2.6 Genotyping

5.2.6.1 Pooled Genotyping

Each SNP was typed in pools by primer extension, using the ABI SNaPshot™ Multiplex kit. Extension primers were designed to be 15-30 nucleotides long and directly adjacent to the polymorphism. PCR primers are listed in Table 5.3 (p.198-199) and extension primers are listed in Table 5.4 (p.200-201). For a particular SNP, each pool was PCR amplified in duplicate. Where available, an individual DNA sample heterozygous for each SNP was also amplified. Samples were then purified by incubation with 1 unit each of exonuclease I and shrimp alkaline phosphatase at 37°C for 1 hour. Primer extension was then performed according to SNaPshot™ kit instructions and products electrophoresed on the ABI 3100 Genetic Analyser. The resultant data was analysed using Genotyper® 2.5 and the calculated peak height ratios from each replicate were averaged. An example of the traces generated in pooled genotyping by the primer extension method is displayed at the end of this chapter (Figure 5.26).

5.2.6.2 Individual Genotyping

Any SNP showing an association in pools at the α=0.1 level was typed individually either in a small sample of 90 individuals to assess linkage disequilibrium, or in the full MRC association sample of 546 LOAD cases and 546 age- and sex-matched controls. Where a natural restriction site existed that could distinguish between the two alleles of a SNP, a restriction fragment length polymorphism (RFLP) assay was designed, using the original PCR primers. Where no natural site existed, an artificial restriction site was created by primer-generated mutagenesis. RFLP primers and enzymes are listed in Table 5.5 (p.202). For each RFLP assay, the required sample

was PCR amplified, then digested with 5 units of the appropriate restriction enzyme. Digested products were electrophoresed on 2.5-3% agarose gels. Examples of the expected profile for each genotype of an individually typed SNP are shown at the end of this chapter (Figures 5.27 to 5.51).

5.2.7 Statistical Analyses

$\chi 2$ and Fisher's exact test were used to analyse SNP associations using the Simple Interactive Statistical Analysis pages (http://home.clara.net/sisa); Fisher's exact test was used for analyses where one or more cell had a count of <5. All polymorphisms typed individually were tested for deviation from Hardy-Weinberg equilibrium using an updated version of the HW program written by Peter McGuffin and Peter Holmans (update by Marian Hamshere). Haplotypic association was tested using EHPLUS with PMPLUS implemented to obtain empirical significance levels[197]. The EHPLUS software was modified by Marian Hamshere and Valentina Moskvina. The square of the correlation coefficient (r^2) was used to determine the levels of linkage disequilibrium between polymorphisms. This was also performed using the modified EHPLUS program.

5.2.8 Allele Specific Expression

To investigate potential *cis*-acting influences on gene expression, differential allelic expression was assayed using DNA samples derived from human brain tissue and the synonymous coding SNP25, 323237 C>T, as a marker polymorphism. 60 samples were available with which to investigate allelic expression. *Post-mortem* brain tissue derived from frontal, parietal, or temporal cortex of these 60 unrelated, anonymous human adults was obtained from three sources (The MRC London

Neurodegenerative Diseases Brain Bank, United Kingdom; The Stanley Medical Research Institute Brain Bank, Bethesda; The Karolinska Institute, Stockholm). Subjects were drawn principally from psychiatric control groups. The DNA samples derived from these individuals were amplified by the use of primers that were based on single exonic sequence, capable of amplifying either cDNA or genomic DNA. PCR primers are listed in Table 5.3 (p.199); the extension primer was the same as that employed for genotyping SNP25 in pools and can be found in Table 5.4 (p.201). Genomic DNA from all subjects was initially genotyped to identify heterozygotes for the marker polymorphism. The corresponding cDNA samples were assayed twice as two separate reverse transcription (RT) reactions alongside the corresponding genomic DNA samples. The same analytic conditions were used for genomic DNA and cDNA to enable use of the average of the ratios observed from genomic DNA to correct allelic ratios obtained from cDNA analyses for any inequalities in allelic representation specific to each assay[195]. When a difference in allelic expression was observed, this entire process was repeated to confirm the initial observation. Peak heights of allele-specific extended primers were determined by the use of Genotyper version 2.5 (Applied Biosystems). The ratio of cDNA peak heights, corrected by use of the average genomic ratio from all heterozygous samples, was used to calculate relative expression of the two alleles in each individual sample.

Fragment name	Spanning	Sense Primer Sequence (5'→3')	Antisense Primer Sequence (5'→3')	Size (bp)	Annealing Temperature (°C)
ADAM12 PROM1	5'Flanking region S & L	GGGCTGGCAATGTCTTTAAC	CGTTGATAGATTGGCTCACG	427	GC56
ADAM12 PROM2	5'Flanking region S & L	ATGGAAACGTGAGCCAATCT	CGCGGAACAAATTATTGTCT	499	GC56
ADAM12 x1	5'UTR & exon 1 S & L	CCAAGGAATTGGCACCTG	CGCGGTAATAAGAACGGTGA	642	GC56
ADAM12 x2	Exon 2 S & L	GCTGATGCCAAACTCTTCCT	CTTCGGCAGTCTCAAAGCTG	198	62
ADAM12 x3	Exon 3 S & L	TCATTTGACTACGCCTGTGG	GGTGTCTTAACTTTCTCCTATCATGC	209	60
ADAM12 x4	Exon 4 S & L	TTGCTCCGAATAAAATGGCTAC	CTAAACTGGGAAGGCCCTAATG	318	60
ADAM12 x5	Exon 5 S & L	TCAGATATTCCCGACATAGACC	GAGCAGGAAAAGACAGAGGTTG	332	60
ADAM12 x6	Exon 6 S & L	GCCATAAACAAGAAGCTGTCC	CAAAATCAGGTATCCCCCTTAC	268	60
ADAM12 x7	Exon 7 S & L	CAATGGGTTGTTTCCATTGC	TGCCAGAGAGGCATTAAGAGA	248	60
ADAM12 x8	Exon 8 S & L	GGCAGAACCTCATCTCCTTG	CATTTCCAGAAGCCAGGAAG	248	62
ADAM12 x9	Exon 9 S & L	TGTGCAGGTGAAACGAAGG	AACTCCAATGCCAGTTTTGC	276	62
ADAM12 x10	Exon 10 S & L	TTATCAAGGGGAACCAGCTC	ACAGAACCATGACGCAACTG	314	62
ADAM12 x11	Exon 11 S & L	AAAGCAGATGGAAGCAATGG	GGGAAATAAGGCCAAGGAGA	234	62
ADAM12 x12	Exon 12 S & L	TGCCTAGCCGAGGATACAAG	CCATGCCCTGTGACTTACTG	274	62
ADAM12 x13	Exon 13 S & L	GAACCACCTGAACCTGTTGG	GCCCTCTTGGTCTTTCTTGC	255	62
ADAM12 x14	Exon 14 S & L	GTCTGCCAGTGCCTCTCC	GGGTGCATGTGTCATAAATGG	277	62
ADAM12 x15	Exon 15 S & L	TCCCAAGGAGAAACCATTTG	TGCAGGAGATGAAAATGCAG	232	57
ADAM12 x16	Exon 16 S & L	AACCTTGTAACCCAGTTCTTGC	GTTCCAAATGGTTTCTCCTTGG	331	60
ADAM12 x17	Exon 17 S & L	GCTGTAAAAGGGCAGCTCAG	AGGTTGGGTCTTCTCCAAGC	225	62
ADAM12 x18	Exon 18 S & L	GGTTTCTTGTTGGCTCTACCTG	ATATGCCCTAACCCCACGTC	251	60
ADAM12 x21	Exon 19 S & part of 3'UTR S	CTTGCTTCTCCCCCACTG	CAGGGGCAAGTCTAAATGATG	508	60
ADAM12 x20	Part of 3'UTR S	TGTTTAATGAGCCCCTGAGC	GCAGCAAGGAGGAAGAGGAC	599	62
ADAM12 x19	Exon 19 L	GCTGGGATTACAGGCTTGAG	AACTGCCTCCTTCTGTGAGC	257	62
ADAM12 x22	Exon 20 L	AACCTCATGTCTGCATGTGTG	CAGTGAGAAGGGGAAACACG	212	62
ADAM12 x23	Exon 21 L	TACAGAGGCACCGAGAAGTTAAG	CTGATATTTTTGAAACCCGCTAT	336	60
ADAM12 x24	Exon 22 L	GGTAAGTGACCCTGCCTAACC	GTCCTGGCTTGGATTAGTCG	245	62
ADAM12 x25	Exon 23 L & part of 3'UTR L	TACATCTCCAACCCCAGACC	CCTGAAAGCCAAACACAGC	666	60
ADAM12 x26	Part of 3'UTR L	CTGGATTCCCCATCTCAGG	ACCCATGAACATCACATTCC	647	60
ADAM12 x27	Part of 3'UTR L	AACAATTAGGCAGACTCTTTATGC	TTTGTGTGTGTTTGTGTCACG	678	60
ADAM12 x28	Part of 3'UTR L	AGAATCTTGGTTTGCCTTCC	GGCTCTCTGAAATAGAAGCATAGG	476	62

Table 5.2. Details of *ADAM12* PCR assays for the purpose of DHPLC, including PCR primers, annealing temperatures and size of amplimers. Annealing temperatures preceded by 'GC' indicate that amplimers are GC-rich and require the use of Q-solution for amplification (see Chapter 2). S: short splice variant; L: long splice variant.

SNP No.	SNP Name	dbSNP Identity	Sense Primer Sequence (5'→3')	Antisense Primer Sequence (5'→3')	Size (bp)	Annealing Temperature (°C)
1	17864 A>G	rs2366705	GCAGGACTCAACCTAATAACTGC	TGAAACCAGTGAAAGAAGCTGA	225	60
2	57690 C>G	rs3740199	GCTGATGCCAAACTCTTCCT	CTTCGGCAGTCTCAAAGCTG	198	62
3	73566 C>T	rs873957	AGGCCCTGAATATCATGCTG	GGAGCACCCTCCACTCATAA	241	60
4	96112 C>T	rs728104	CAGTCAGAGCTGGAGATTTGG	CTATCACTTCACCAGGCTTGC	249	60
5	109183 G>A		TCATTTGACTACGCCTGTGG	GGTGTCTTAACTTTCTCCTATCATGC	209	60
6	134449 C>G	rs2279755	GCTTAGGGCTCACCTCACTC	AGCTCCTGGACTCACTTTGC	220	60
7	159219 A>T	rs1011835	TTCCATTAGCGTGGTCATCTC	TGTAAATCCAGTGATTAAATGCAG	207	60
8	179169 A>G	rs1106955	TCATTGCTCTCTTGCTGGTC	TTACCACCCACATCTTTCTGG	200	60
9	201199 C>G	rs2126744	GCAGAGAGGAGCTGCAAGAC	GGATGGACAGCGAACAACAC	230	60
10	232559 C>A	rs1676724	TCCAGTTGGTGGAGACTGTG	CTCGGAACAATAGCCCACAC	202	60
11	232794 A>G	rs1466361	TTGCTCCGAATAAAATGGCTAC	CTAAACTGGGAAGGCCCTAATG	318	60
12	232959 C>T	rs1466360	TTGCTCCGAATAAAATGGCTAC	CTAAACTGGGAAGGCCCTAATG	318	60
13	259753 A>G	rs1278319	CACCTGAGCAGCCAACTAAG	AAGGTGAGGTGCCAATTCAG	212	60
14	265290 A>G	rs1278305	ACATCTGGCCTTTGGATGAC	GGGAAAGTGGAAATGAATACC	267	60
15	271466 G>C	rs1278390	AAACTGCTCTTATCGGAACCAG	CATGTCAAGGTGAGCCACAG	219	60
16	277611 G>T	rs1037804	CTGCTGCCTGAATCATCTCC	GGAAACTGTCAGACTAATGAACAGAG	212	60
17	287117 T>C	rs2290845	TACCTCGCAAATCCCATGAC	CAGGGTGTTCAGAGGGAGAC	245	60
18	289573 A>G	rs2290844	TTATCAAGGGGAACCAGCTC	ACAGAACCATGACGCAACTG	314	62
19	289746 C>T	rs2290842	TTATCAAGGGGAACCAGCTC	ACAGAACCATGACGCAACTG	314	62
20	291831 G>A	rs3758419	CAAGGAAGCAGAGATCCTCA	TTACCATGCTCTGGCACAAA	360	60
21	296783 G>A	rs3781030	ATGATCCCACATTCCTGTCC	TCCATTCTCCCACTCTCTCG	235	60
22	306526 A>T	rs1278341	GCTCGTTTAGCCTCCACTTC	TGACATTCTGCTTCCCACTG	244	60
23	316406 A>G	rs2290841	TGGAACTGAATGTGCCTCAC	TGGTCTCCAAGTCCTTCCTG	235	60

Table 5.3. Details of *ADAM12* PCR assays for the purpose of genotyping pools, including PCR primers, annealing temperatures and size of amplimers.

SNP No.	SNP Name	dbSNP Identity	Sense Primer Sequence (5'→3')	Antisense Primer Sequence (5'→3')	Size (bp)	Annealing Temperature (°C)
24	321073 A>G	rs1278281	ATGAGATCCGCCTGGACAC	GCCTGTTTCCGTCTGTTAGG	200	60
25	323237 C>T	rs1278279	GTCTGCCAGTGCCTCTCC	GGGTGCATGTGTCATAAATGG	277	62
25	323237 C>T	rs1278279	AACAGCGTGCAGGGACTC*	CACTGCTGCTCGTGAGTCTG*	162	62
26	323327 G>A	rs2279091	GTCTGCCAGTGCCTCTCC	GGGTGCATGTGTCATAAATGG	277	62
27	323354 A>G	rs2279090	GTCTGCCAGTGCCTCTCC	GGGTGCATGTGTCATAAATGG	277	62
28	323362 G>A		GTCTGCCAGTGCCTCTCC	GGGTGCATGTGTCATAAATGG	277	62
29	323441 C>T	rs1278278	CTCACGAGCAGCAGTGTGTC	CTCCAGGCAGTGTCCATTTC	247	60
30	327363 G>T	rs1278273	TGTGTAGAGCTTGGGCTGTG	CTCCCAGGACTGCATTTGTC	250	60
31	329734 T>A	rs1278265	CTCCCAAGGTCAGCACTCAG	AGCAGCCTGGGTAAATGAAC	225	60
32	338785 C>T	rs2292692	AACCTTGTAACCCAGTTCTTGC	GTTCCAAATGGTTTCTCCTTGG	331	60
33	341999 T>C		GCTGTAAAAGGGCAGCTCAG	AGGTTGGGTCTTCTCCAAGC	225	62
34	345179 C>T		GGTTTCTTGTTGGCTCTACCTG	ATATGCCCTAACCCCACGTC	251	60
35	345180 A>G		GGTTTCTTGTTGGCTCTACCTG	ATATGCCCTAACCCCACGTC	251	60
36	345518 T>G	rs1278260	AGTTCCTTAGCCTGCGACAC	GCAATGACTCCCACTGCTG	219	60
37	345987 G>A		CTTGCTTCTCCCCCACTG	CAGGGGCAAGTCTAAATGATG	508	60
38	346355 C>T	rs6693	TGTTTAATGAGCCCCTGAGC	GCAGCAAGGAGGAAGAGGAC	599	62
39	346571 T>A	rs4732	TGTTTAATGAGCCCCTGAGC	GCAGCAAGGAGGAAGAGGAC	599	62
40	348325 T>C	rs3781002	TGTCCAGCAAGAAAGCAATTC	GTGACAACGGCACAGTGG	215	60
41	366613 A>G	rs872328	CTGCTCCACCAGTGAGGATAC	CAGGTGTGTGGAAGATAAGCTG	238	60
42	370687 G>A	rs3781001	GTTGACTTGTGGGTGGGAAG	GATCTGGGCACTTGGTGTG	221	60
43	371311 C>T		TACATCTCCAACCCCAGACC	CCTGAAAGCCAAACACAGC	666	60
44	371348 G>A		TACATCTCCAACCCCAGACC	CCTGAAAGCCAAACACAGC	666	60
45	371435 G>C		CTGGATTCCCCATCTCAGG	ACCCATGAACATCACATTCC	647	60

Table 5.3 continued. Details of *ADAM12* PCR assays for the purpose of genotyping pools (*or for allele specific expression), including PCR primers, annealing temperatures and size of amplimers.

SNP No.	SNP Name	dbSNP Identity	SNP Flanking Sequence	Extension Primer (5'→3')	Expected Allele Peaks
1	17864 A>G	rs2366705	ACAAATTGCCRCAACTTAGTG	ATTTATTGCTGTATGACAAATTGCC	A (Green) & G (Blue)
2	57690 C>G	rs3740199	TGCCTCTGTTSGGAGTGGGGA	AAGTTGTCAGTGCCTCTGTT	C (Black) & G (Blue)
3	73566 C>T	rs873957	GACAAATCTTYTTTTCCTGAA	ACGACATGGACATTTTCAGGAAAA	A (Green) & G (Blue)
4	96112 C>T	rs728104	TTCATAAGTAYGTCTGGGCTT	TAGAGGACCAAGTTTTTCATAAGTA	C (Black) & T (Red)
5	109183 G>A		CTGAATATTCRACTACAACGG	TCCAGAAGTGCTGAATATTC	A (Green) & G (Blue)
6	134449 C>G	rs2279755	GCCCTCCCCCSACCCAACCCA	CAGATCTTTGTGGGTTGGGT	C (Black) & G (Blue)
7	159219 A>T	rs1011835	GCCAGTAAGAWTTTTTTTTAA	CTGTACACACTGCCAGTAAGA	A (Green) & T (Red)
8	179169 A>G	rs1106955	GTCATTTGACRATTCTCAGAG	AGAGATGTCTTGTCATTTGAC	A (Green) & G (Blue)
9	201199 C>G	rs2126744	CATATTTGCTSATGATGACTC	ATGGGGAATCTGAGTCATCAT	C (Black) & G (Blue)
10	232559 C>A	rs1676724	CCAGTGTGCGMATGAAGGAAT	CTCCCACCTCATTCCTTCAT	G (Blue) & T (Red)
11	232794 A>G	rs1466361	CAATGTATCARTGCAATTCTG	AAGATGAGTGCAGAATTGCA	C (Black) & T (Red)
12	232959 C>T	rs1466360	TCTTACACCAYTGGATCTGTG	ATCACCATAATCTTACACCA	C (Black) & T (Red)
13	259753 A>G	rs1278319	ACTAAGGCATRGCATCCTCAG	CAGGCCCCTGAGGATGC	C (Black) & T (Red)
14	265290 A>G	rs1278305	AAATGTTGCARTACAAAATGA	ATGGCAGTAACATTTCATTTTGTA	C (Black) & T (Red)
15	271466 G>C	rs1278390	GTTTCTAAGASTTTCTATGGC	GTGAGCACCTGCCATAGAAA	C (Black) & G (Blue)
16	277611 G>T	rs1037804	TGCAGTCTTAKTTTTTTCTTA	ACGGAAAGAAACAGAGTTAAGAAAAAA	A (Green) & C (Black)
17	287117 T>C	rs2290845	AAAGGAGTGCYCTCGGCGAAG	TGCTTAAAAAAAAAAGGAGTGC	C (Black) & T (Red)
18	289573 A>G	rs2290844	GGAATATCCARCAGAATTTTT	TTTTATTGCAGGAATATCCA	A (Green) & G (Blue)
19	289746 C>T	rs2290842	CCAAGGGCATYGGGAGCTGGT	TCATGGTAAGCCAAGGGCAT	C (Black) & T (Red)
20	291831 G>A	rs3758419	TCATTGATGCRTGAAAGAATG	ACATTCTGTTTATAATCATTGATGC	A (Green) & G (Blue)
21	296783 G>A	rs3781030	GGCTCAGTCARCCCTCAGTCA	GGTGATGGATGACTGAGGG	C (Black) & T (Red)
22	306526 A>T	rs1278341	CTGCTCAGACWTAGGCTTCGG	GAACTCAAGTCCGAAGCCTA	A (Green) & T (Red)
23	316406 A>G	rs2290841	AGATGTGGCCRGTGGGTGCCT	CCACAAGAAGGCACCCAC	C (Black) & T (Red)

Table 5.4. List of polymorphisms identified in the *ADAM12* gene (either by DHPLC of from dbSNP), including the location of the polymorphism relative to the coding sequence, flanking sequence of the polymorphism, the extension primer used for SNaPshot and the expected allele peaks in the primer extension assay.

SNP No.	SNP Name	dbSNP Identity	SNP Flanking Sequence	Extension Primer (5'→3')	Expected Allele Peaks
24	321073 A>G	rs1278281	TGATGTCCCC**R**GCCGGCCAGC	GACTAGAGTGATGTCCCC	A (Green) & G (Blue)
25	323237 C>T	rs1278279	GCCCAGCCAA**Y**GTGTACCTGC	TGCCCATCGTGCAGGTACAC	A (Green) & G (Blue)
26	323327 G>A	rs2279091	AGTGTGTCAC**R**CTCTGGGGAC	CGAGCAGCAGTGTGTCAC	A (Green) & G (Blue)
27	323354 A>G	rs2279090	CGTGGCCGCC**R**CAAGCTCRGC	GGACCAGGTACGTGGCCGCC	A (Green) & G (Blue)
28	323362 G>A		CCRCAAGCTC**R**GCATCAGGAG	CAGTGCCTCTCCTGATGC	C (Black) & T (Red)
29	323441 C>T	rs1278278	CCACTCCTGG**Y**GGGCGCTGTC	TTAGCCCCCACTCCTGG	C (Black) & T (Red)
30	327363 G>T	rs1278273	TGGAGGGGAG**K**GCGGATGTGA	CTGGATCTGGAGGGGAG	G (Blue) & T (Red)
31	329734 T>A	rs1278265	AAATCCAGAG**W**CATAGAAAAG	GTCTGCTGGTTTATCTTTTCTATG	A (Green) & T (Red)
32	338785 C>T	rs2292692	CAAACATCCC**Y**CTGCAGCAAG	TCCATAGAAACAAACATCCC	C (Black) & T (Red)
33	341999 T>C		TTGCTGTGTT**Y**TCCTCCTCCT	GCAGATCTGTAGGAGGAGGA	A (Green) & G (Blue)
34	345179 C>T		CAGCTGTCAG**Y**RTGGGTGCAG	GTGGGCTCGCCAGCTGTCAG	C (Black) & T (Red)
35	345180 A>G		AGCTGTCAG**Y**RTGGGTGCAGG	GTTGGCTCTACCTGCACCCA	C (Black) & T (Red)
36	345518 T>G	rs1278260	CACCTCTTAG**K**AAAGGTGACA	AAGACACCCACCTCTTAG	G (Blue) & T (Red)
37	345987 G>A		AGGAGCATGC**R**TCTACTGCCT	GTGGGATCGCAGGAGCATGC	A (Green) & G (Blue)
38	346355 C>T	rs6693	TCACTGAGCC**Y**CCACAGCAGT	GTCTGGCCTTTCACTGAGCC	C (Black) & T (Red)
39	346571 T>A	rs4732	CTGAATGGCA**W**TGAAACAAAC	GTCTGGCCTTTCACTGAGCC	A (Green) & T (Red)
40	348325 T>C	rs3781002	GGCAAATCTG**Y**GCTGGGGACT	AAATGTTTCCAGTCCCCAGC	A (Green) & G (Blue)
41	366613 A>G	rs872328	TTGTTCAGGG**R**CTTTTTCCTA	GACACATTGGGCTAGGAAAAAG	C (Black) & T (Red)
42	370687 G>A	rs3781001	GAGGGGCAGT**R**GTATCTGACA	CCGTTATGAGGGGCAGT	A (Green) & G (Blue)
43	371311 C>T		CCAAGTAGAA**Y**CTCAGTTGAT	TCAAGAGATCCCAAGTAGAA	C (Black) & T (Red)
44	371348 G>A		CTCAGGCCAG**R**GCCAAGGGGC	GATTCCCCATCTCAGGCCAG	A (Green) & G (Blue)
45	371435 G>C		CCCAGGGACA**S**CTGGGAGAAA	GAAGCCAGATTTCTCCCAG	C (Black) & G (Blue)

Table 5.4 continued. List of polymorphisms identified in the *ADAM12* gene (either by DHPLC of from dbSNP), including flanking sequence of the polymorphism, the extension primer used for SNaPshot and the expected allele peaks in the primer extension assay.

SNP No.	SNP Name	RFLP Sense Primer (5'→3')	RFLP Antisense Primer (5'→3')	Size (bp)	Anneal Temp (°C)	RFLP Enzyme	Restriction Fragments (bp)
2	57690 C>G	TGATGCCAAACTCTTCCTGAC	CAACCCTTGAATGAGAGAATACC	243	60	*Hpy*188 I	C=130, 113 G=243
5	109183 G>A	TCATTTGACTACGCCTGTGG	GGTGTCTTAACTTTCTCCTATCATGC	209	60	*Taq* I	G=112, 97 A=209
13	259753 A>G	CACCTGAGCAGCCAACTAAG	AAGGTGAGGTGCCAATTCAG	212	60	*Xcm* I	A=212 G=193, 19
15	271466 G>C	CCCTCATACCTGTGGATAGATGTCTG	AGGTTGTGAGCACCTGCCATAGAgA*	180	60	*Bsm*A I	G=160, 20 C=180
17	287117 T>C	CACTGAACATTCGGATCGTG	AGAAAGGTGGCAGCTCCTG	256	60	*Bsi*HKA I	T=232 C=209, 23
18	289573 A>G	GCGTATTTTATTGCAGGAATATgCA*	GCCCTTGGCTTACCATGAC	196	60	*Fnu*4H I	A=196 G=172, 24
19	289746 C>T	GTCATGGTAAGCCAAGGGCgT*	TTACATGCCCACCTTTCCTG	219	60	*Bsa*H I	C=201, 18 T=219
20	291831 G>A	CAAGGAAGCAGAGATCCTCA	TTACCATGCTCTGGCACAAA	360	60	*Nsi* I	G=360 A=245, 115
21	296783 G>A	ATGATCCCACATTCCTGTCC	TCCATTCTCCCACTCTCTCG	235	60	*Hinc* II	G= 235 A=125, 110
22	306526 A>T	GAAGTACAGATAGGCTGCcCAGA**	CAACCTCATATCGTCCACAGC	240	62	*Dde* I	A=240 T=216, 24
23	316406 A>G	TGGAACTGAATGTGCCTCAC	TGGTCTCCAAGTCCTTCCTG	235	60	*Msp* I	A=235 G=140, 95
24	321073 A>G	ATGAGATCCGCCTGGACAC	GCCTGTTTCCGTCTGTTAGG	200	60	*Nci* I	A=200 G=137, 63
25	323237 C>T	GTCTGCCAGTGCCTCTCC	GGGTGCATGTGTCATAAATGG	277	60	*Hpy*CH4 IV	C=129, 107, 41 T=236, 41
29	323441 C>T	AGGAGAGGCACTGGCAGAC	TGCAGCTCCCGTATCTCC	302	60	*Cac*8 I	C=227, 75 T=302
30	327363 G>T	TGTGTAGAGCTTGGGCTGTG	GATATTGTGAAGGATTCACATCgGC*	208	60	*Hae* III	G=184, 24 T=208
31	329734 T>A	CTCCCAAGGTCAGCACTCAG	AGCAGCCTGGGTAAATGAAC	225	60	*Hinf* I	T=175, 50 A=225
32	338785 C>T	ATCCAGACATCCTGGCAAAG	AATCCGGCCTCCTTGCTGCcG*	214	60	*Nci* I	C=193, 21 T=214
33	341999 T>C	GGAGAAATACTAAGAGATTTGCTGTGcT*	CACATGAAAAGGTCAAAAGAAATG	287	58	*Bsi*HKA I	T=287 C=259, 28
36	345518 T>G	CTTACTGGAAAGACACCCACCTCcTAG*	GCGAGATCACATTAGGCAAATTAC	233	58	*Sty* I	T=182, 51 G=159,51,23
40	348325 T>C	TGTCCAGCAAGAAAGCAATTC	GTGACAACGGCACAGTGG	215	60	*Hha* I	T=215 C=110, 105
41	366613 A>G	TCTAAGTCTGTCCCTTGTTCAGG	TGAATTTCTCTCACAGTGCCTATC	233	60	*Bsm*F I	A=197, 36 G=233
42	370687 G>A	GTTGACTTGTGGGTGGGAAG	GATCTGGGCACTTGGTGTG	221	60	*Bts* I	G=153, 68 A=221
43	371311 C>T	GCAGCTCAAGAGATCCCAAGTAGtA*	CCAGTCTCTATCCTGGTGTGG	245	60	*Rsa* I	C=221, 24 T=245
44	371348 G>A	CTTGAAATATCCTGCTTGATGG	CCTGAAAGCCAAACACAGCC	215	60	*Bst*N I	G=172, 22, 21 A=194, 21
45	371435 G>C	CTGGATTCCCCATCTCAGG	CACCACCTTTCCCAAGCTAA	379	60	*Pvu* II	G=268, 111 C=379

Table 5.5. Assay details of *ADAM12* RFLP genotyping assays, including RFLP primers, amplimer size, PCR annealing temperature, restriction enzyme and expected RFLP fragment sizes. A lower case letter in the RFLP primer indicates the 'mismatched base' introduced to the RFLP amplimer to generate an artificial restriction site (see Chapter 2).

5.3 Results

5.3.1 ADAM12 Expression in Brain

In view of the uncertainty as to whether ADAM12 is expressed in human brain, an experiment was performed to address this issue. A pair of exonic PCR primers specific to each splice variant was designed to amplify across a neighbouring exon junction. When amplifying from a cDNA template, only exonic sequence is amplified; when amplifying from a genomic template, intronic sequence is also amplified, generating a larger product (see Figure 5.2 below). This experiment was performed using cDNA derived from either human frontal lobe or cerebellum.

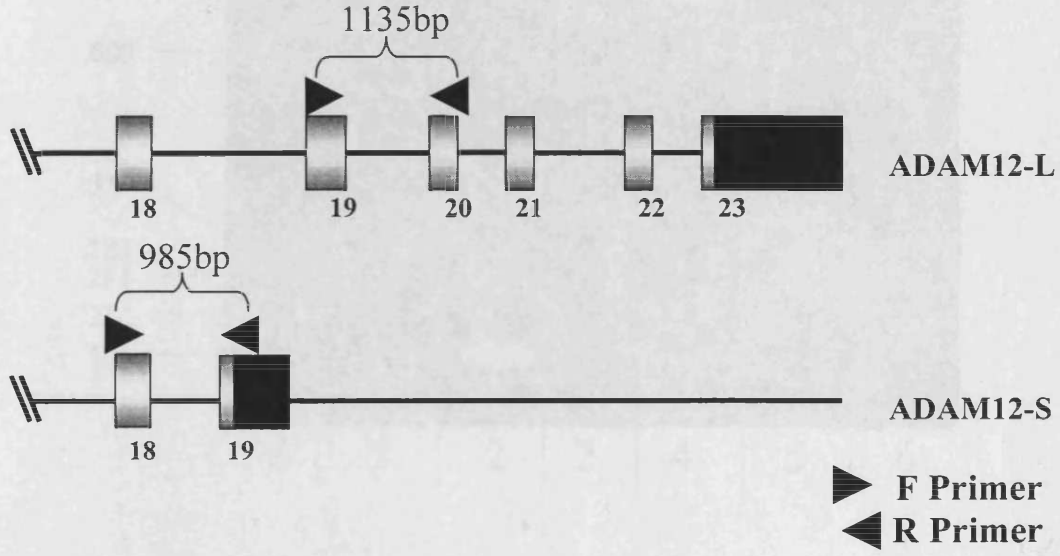

Figure 5.2. Schematic representation of the PCR assay designed to detect ADAM12 transcripts in human brain. Note that at least one of each pair of primers is specific to that splice variant

As indicated in Figure 5.3 overleaf, a fragment of appropriate size is generated with *ADAM12-L* specific primers when the DNA template is either genomic or brain (frontal lobe) derived cDNA. However, with *ADAM12-S* specific primers, no product

is generated from cDNA, although the PCR assay is successful when amplifying from genomic DNA. Similar results were obtained when this experiment was repeated with cDNA derived from another individual (cerebellum). This study therefore yielded evidence that the *ADAM12-L* transcript, but not the *ADAM12-S* transcript, is expressed in human frontal lobe and cerebellum.

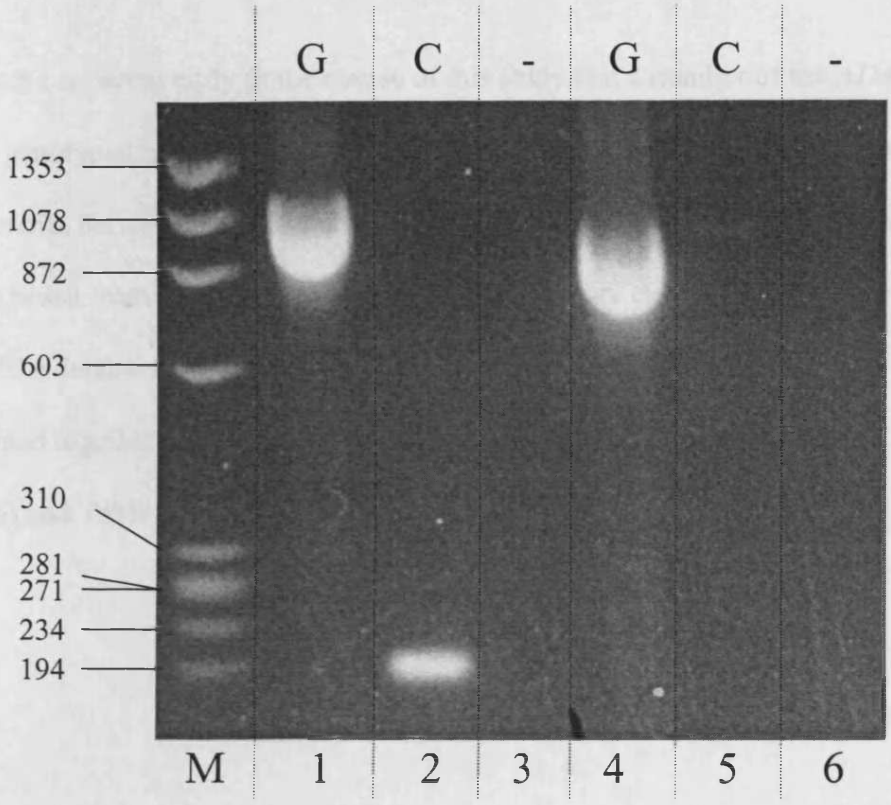

Figure 5.3. Detection of ADAM12 transcripts in brain. In lanes 1-3, PCR product generated from primers specific for the *ADAM12*-L variant are electrophoresed; in lanes 4-6, PCR products generated from primers specific for the ADAM12-S variant are electrophoresed. 'G' indicates genomic template was employed in the PCR assay; 'C' indicates cDNA template derived from human brain was used; '-' indicates water was used in place of DNA and therefore acts as a negative control. 'M' indicates the DNA size standard, ΦX174 DNA-Hae III digest and the sizes of each fragment are indicated on the side of the gel photo. Expected sizes of each PCR product are: 1=1135bp; 2=191bp; 4=985bp and 5=181bp.

5.3.2 Polymorphisms identified

A total of twenty SNPs in the *ADAM12* gene were identified by DHPLC (see Figure 5.4, p.206 and Table 5.6, p.207). Two were non-synonymous coding SNPs: a R48G

polymorphism in exon 2 (SNP2, 57690 C>G) and a R71Q polymorphism in exon 3 (SNP5, 109183 G>A). A further nine exonic SNPs were identified: four synonymous coding SNPs called N505N, T535T, P606P and A730A (SNPs 25, 26, 32 and 37 respectively) and five SNPs in 3' untranslated regions (SNPs 38, 39, 43, 44 and 45). The remaining nine SNPs were intronic.

It became apparent early in the course of this study that a number of the *ADAM12* SNPs genotyped in the MRC pools were exhibiting a significant difference in allele frequencies between cases and controls. Therefore an additional 25 validated SNPs were chosen from dbSNP in an attempt to attain a more even coverage of the gene. All of the database SNPs were intronic. Results for the total 45 SNPs will be presented together and details of each polymorphism can be found in Figure 5.4 (p.206) and Table 5.6 (p.207).

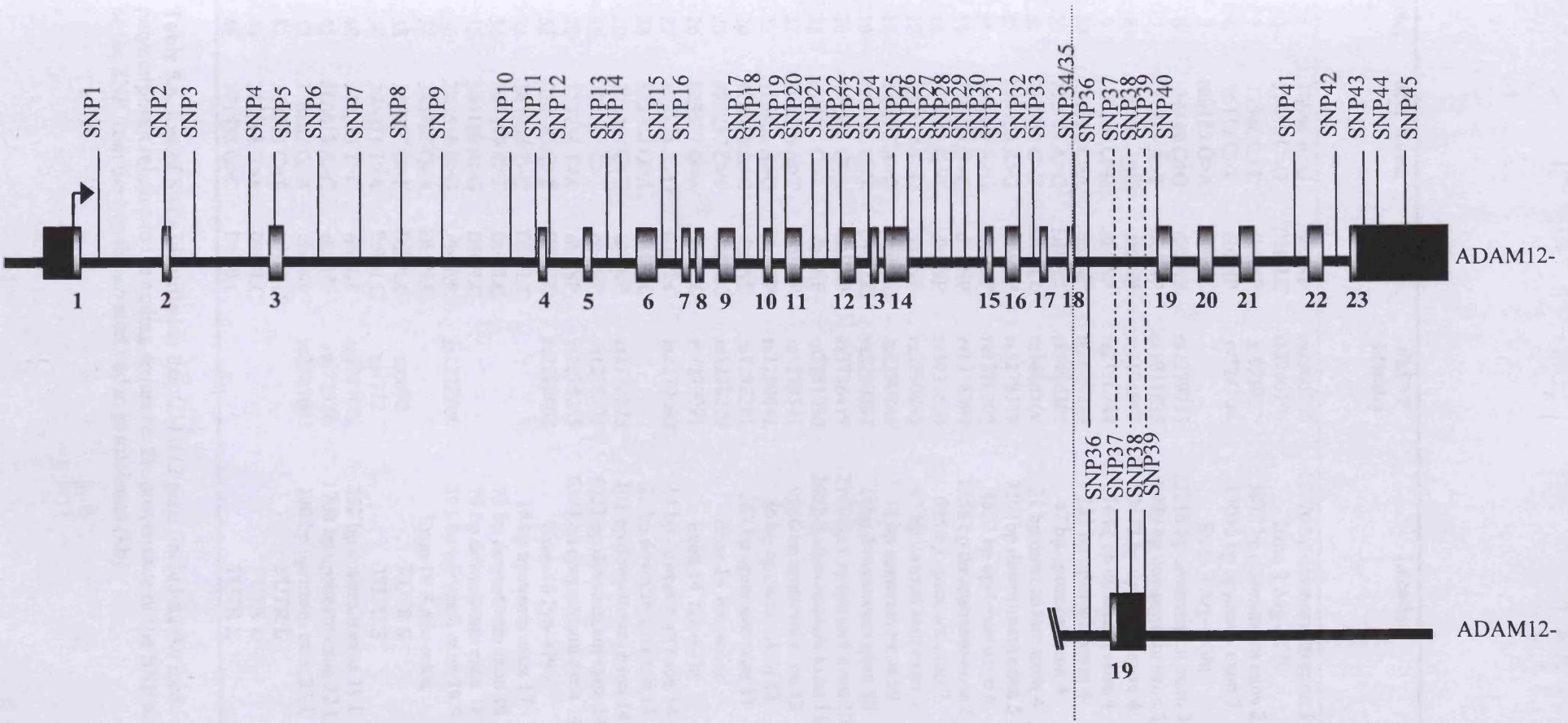

Figure 5.4. Diagram of the *ADAM12* gene (not to scale), indicating the positions of identified polymorphisms. Grey blocks indicate coding sequence, black blocks indicate untranslated regions.

No.	SNP Name	Source	dbSNP Identity	Location	Distance from ATG (kb)
1	17864 A>G	dbSNP	rs2366705	17776 bp downstream exon 1	18
2	57690 C>G	DHPLC	rs3740199	Exon 2 Arg→Gly	58
3	73566 C>T	dbSNP	rs873957	15832 bp downstream exon 2	74
4	96112 C>T	dbSNP	rs728104	13046 bp upstream exon 3	96
5	109183 G>A	DHPLC		Exon 3 Arg→Gln	109
6	134449 C>G	dbSNP	rs2279755	25218 bp downstream exon 3	134
7	159219 A>T	dbSNP	rs1011835	49989 bp downstream exon 3	159
8	179169 A>G	dbSNP	rs1106955	53673 bp upstream exon 4	179
9	201199 C>G	dbSNP	rs2126744	31642 bp upstream exon 4	201
10	232559 C>A	dbSNP	rs1676724	282 bp upstream exon 4	233
11	232794 A>G	DHPLC	rs1466361	47 bp upstream exon 4	233
12	232959 C>T	DHPLC	rs1466360	31 bp downstream exon 4	233
13	259753 A>G	dbSNP	rs1278319	7191bp downstream exon 5	260
14	265290 A>G	dbSNP	rs1278305	4632 bp upstream exon 6	265
15	271466 G>C	dbSNP	rs1278390	1358 bp downstream exon 6	271
16	277611 G>T	dbSNP	rs1037804	695 bp upstream exon 7	278
17	287117 T>C	dbSNP	rs2290845	43 bp downstream exon 9	287
18	289573 A>G	DHPLC	rs2290844	73 bp upstream exon 10	290
19	289746 C>T	DHPLC	rs2290842	16bp downstream exon 10	290
20	291831 G>A	dbSNP	rs3758419	2101 bp downstream exon 10	292
21	296783 G>A	dbSNP	rs3781030	2622 bp downstream exon 11	297
22	306526 A>T	dbSNP	rs1278341	9966 bp upstream exon 12	307
23	316406 A>G	dbSNP	rs2290841	86 bp upstream exon 12	316
24	321073 A>G	dbSNP	rs1278281	267 bp upstream exon 13	321
25	323237 C>T	DHPLC	rs1278279	Exon 14 Asn→Asn	323
26	323327 G>A	DHPLC	rs2279091	Exon 14 Thr→Thr	323
27	323354 A>G	DHPLC	rs2279090	14 bp downstream exon 14	323
28	323362 G>A	DHPLC		22 bp downstream exon 14	323
29	323441 C>T	dbSNP	rs1278278	101 bp downstream exon 14	323
30	327363 G>T	dbSNP	rs1278273	4023 bp downstream exon 14	327
31	329734 T>A	dbSNP	rs1278265	6394 bp downstream exon 14	330
32	338785 C>T	DHPLC	rs2292692	Exon 16 Pro→Pro	339
33	341999 T>C	DHPLC		15 bp upstream exon 17	342
34	345179 C>T	DHPLC		73 bp downstream exon 18	345
35	345180 A>G	DHPLC		74 bp downstream exon 18	345
36	345518 T>G	dbSNP	rs1278260	393 bp upstream exon 19 S	346
37	345987 G>A	DHPLC		Exon 19 S Ala→Ala	346
38	346355 C>T	DHPLC	rs6693	3'UTR S	346
39	346571 T>A	DHPLC	rs4732	3'UTR S	347
40	348325 T>C	dbSNP	rs3781002	392 bp upstream exon 19 L	348
41	366613 A>G	dbSNP	rs872328	1708 bp upstream exon 22 L	367
42	370687 G>A	dbSNP	rs3781001	120 bp upstream exon 23 L	371
43	371311 C>T	DHPLC		3'UTR L	371
44	371348 G>A	DHPLC		3'UTR L	371
45	371435 G>C	DHPLC		3'UTR L	371

Table 5.6. List of SNPs identified in the *ADAM12* gene, including the location of the polymorphism relative to the coding sequence, the provenance of the SNP and the distance of the SNP from the translation start codon in kilobases (kb).

5.3.3 Association Analysis

Of 45 SNPs examined, a total of 41 were successfully genotyped in the MRC pools comprised of 186 cases and 186 age- and sex-matched controls. Of the four that failed, two had successfully designed assays but the minor allele frequencies were too low to be reliably estimated from pools. The estimated allele frequencies and counts calculated for each successfully typed SNP are shown below in Table 5.7.

SNP	Allele		*P*
1) 17864 A>G*	**A**	**G**	
Patients	275 (0.74)	97 (0.26)	
Controls	258 (0.69)	114 (0.31)	0.1667
2) 57690 C>G	**C**	**G**	
Patients	199 (0.54)	173 (0.46)	
Controls	210 (0.56)	162 (0.44)	0.4176
3) 73566 C>T*	**C**	**T**	
Patients	192 (0.52)	180 (0.48)	
Controls	196 (0.53)	176 (0.47)	0.7690
4) 96112 C>T*	**C**	**T**	
Patients	327 (0.88)	45 (0.12)	
Controls	335 (0.90)	37 (0.10)	0.3489
5) 109183 G>A			
Patients	The A allele was too rare to be detected in pools.		
Controls			
6) 134449 C>G*	**C**	**G**	
Patients	281 (0.76)	91 (0.24)	
Controls	276 (0.74)	96 (0.26)	0.6726
7) 159219 A>T*	**A**	**T**	
Patients	353 (0.95)	19 (0.05)	
Controls	356 (0.96)	16 (0.04)	0.6034
8) 179169 A>G*	**A**	**G**	
Patients	301 (0.81)	71 (0.19)	
Controls	287 (0.77)	85 (0.23)	0.2073
9) 201199 C>G*	**C**	**G**	
Patients	349 (0.94)	23 (0.06)	
Controls	357 (0.96)	15 (0.04)	0.1827
10) 232559 C>A*	**C**	**A**	
Patients	271 (0.73)	101 (0.27)	
Controls	272 (0.73)	100 (0.27)	0.9341
11) 232794 A>G			
Patients	The primer extension reaction could not be optimised.		
Controls			

Table 5.7. Estimates of allele frequencies and counts of *ADAM12* SNPs in the MRC pools comparing 186 LOAD cases with 186 age- and sex-matched controls. *P* values<0.1 are indicated in bold. *The peaks generated by primer extension for these SNPs were not corrected for unequal allelic detection as no heterozygote was available and therefore these allele frequencies are unlikely to be correct unless the true heterozygote ratio is 1:1 (see Chapter 2). However, a difference in allele frequencies between cases and controls should still be detected.

SNP	Allele		*P*
12) 232959 C>T	**C**	**T**	
Patients	227 (0.61)	145 (0.39)	
Controls	233 (0.63)	139 (0.37)	0.6506
13) 259753 A>G*	**A**	**G**	
Patients	198 (0.53)	174 (0.47)	
Controls	175 (0.47)	197 (0.53)	**0.0917**
14) 265290 A>G*	**A**	**G**	
Patients	173 (0.47)	199 (0.53)	
Controls	194 (0.52)	178 (0.48)	0.1235
15) 271466 G>C*	**G**	**C**	
Patients	117 (0.31)	255 (0.69)	
Controls	93 (0.25)	279 (0.75)	**0.0505**
16) 277611 G>T*	**G**	**T**	
Patients	330 (0.89)	42 (0.11)	
Controls	330 (0.89)	42 (0.11)	1.000
17) 277611 T>C*	**T**	**C**	
Patients	346 (0.93)	26 (0.07)	
Controls	318 (0.85)	54 (0.15)	**0.0009**
18) 289573 A>G	**A**	**G**	
Patients	346 (0.93)	26 (0.07)	
Controls	320 (0.86)	52 (0.14)	**0.0018**
19) 289746 C>T	**C**	**T**	
Patients	270 (0.73)	102 (0.27)	
Controls	285 (0.77)	87 (0.23)	0.2064
20) 291831 G>A*	**G**	**A**	
Patients	262 (0.70)	110 (0.30)	
Controls	276 (0.74)	96 (0.26)	0.2513
21) 296783 G>A*	**G**	**A**	
Patients	289 (0.78)	83 (0.22)	
Controls	300 (0.81)	72 (0.19)	0.3207
22) 306526 A>T*	**A**	**T**	
Patients	241 (0.65)	131 (0.35)	
Controls	252 (0.68)	120 (0.32)	0.3936
23) 316406 A>G*	**A**	**G**	
Patients	279 (0.75)	93 (0.25)	
Controls	310 (0.83)	62 (0.17)	**0.0051**
24) 321073 A>G*	**A**	**G**	
Patients	300 (0.81)	72 (0.19)	
Controls	297 (0.80)	75 (0.20)	0.7823
25) 323237 C>T	**C**	**T**	
Patients	307 (0.82)	65 (0.18)	
Controls	284 (0.76)	88 (0.24)	**0.0369**
26) 323327 G>A	**G**	**A**	
Patients	327 (0.88)	45 (0.12)	
Controls	317 (0.85)	55 (0.15)	0.2824
27) 323354 A>G	**A**	**G**	
Patients	330 (0.89)	42 (0.11)	
Controls	331 (0.89)	41 (0.11)	0.9072

Table 5.7 continued. Estimates of allele frequencies and counts of *ADAM12* SNPs in the MRC pools comparing 186 LOAD cases with 186 age- and sex-matched controls. *P* values<0.1 are indicated in bold. *The peaks generated by primer extension for these SNPs were not corrected for unequal allelic detection as no heterozygote was available and therefore these allele frequencies are unlikely to be correct unless the true heterozygote ratio is 1:1 (see Chapter 2). However, a difference in allele frequencies between cases and controls should still be detected.

SNP	Allele		*P*
28) 323362 G>A			
Patients	The A allele was too rare to be detected in pools.		
Controls			
29) 323441 C>T*	**C**	**T**	
Patients	307 (0.83)	65 (0.17)	
Controls	288 (0.77)	84 (0.23)	**0.0817**
30) 327363 G>T*	**G**	**T**	
Patients	227 (0.61)	145 (0.39)	
Controls	224 (0.60)	148 (0.40)	0.8218
31) 329734 T>A*	**T**	**A**	
Patients	219 (0.59)	153 (0.41)	
Controls	204 (0.55)	168 (0.45)	0.2668
32) 338785 C>T	**C**	**T**	
Patients	331 (0.89)	41 (0.11)	
Controls	309 (0.83)	63 (0.17)	**0.0200**
33) 341999 T>C	**T**	**C**	
Patients	325 (0.87)	47 (0.13)	
Controls	304 (0.82)	68 (0.18)	**0.0331**
34) 345179 C>T	**C**	**T**	
Patients	284 (0.76)	88 (0.24)	
Controls	267 (0.72)	105 (0.28)	0.1550
35) 345180 A>G	**A**	**G**	
Patients	285 (0.77)	87 (0.23)	
Controls	270 (0.73)	102 (0.27)	0.2064
36) 345518 T>G*	**T**	**G**	
Patients	175 (0.47)	197 (0.53)	
Controls	204 (0.55)	168 (0.45)	**0.0334**
37) 345987 G>A	**G**	**A**	
Patients	353 (0.95)	19 (0.05)	
Controls	359 (0.96)	13 (0.04)	0.2782
38) 346355 C>T			
Patients	The primer extension reaction could not be		
Controls	optimised.		
39) 346571 T>A*	**T**	**A**	
Patients	348 (0.94)	24 (0.06)	
Controls	346 (0.93)	26 (0.07)	0.7696
40) 348325 T>C*	**T**	**C**	
Patients	275 (0.74)	97 (0.26)	
Controls	290 (0.78)	82 (0.22)	0.1982
41) 366613 A>G*	**A**	**G**	
Patients	205 (0.55)	167 (0.45)	
Controls	169 (0.45)	203 (0.55)	**0.0082**
42) 370687 G>A*	**G**	**A**	
Patients	276 (0.74)	96 (0.26)	
Controls	288 (0.78)	84 (0.66)	0.3042
43) 371311 C>T	**C**	**T**	
Patients	274 (0.74)	98 (0.26)	
Controls	240 (0.64)	132 (0.36)	**0.0069**

Table 5.7 continued. Estimates of allele frequencies and counts of *ADAM12* SNPs in the MRC pools comparing 186 LOAD cases with 186 age- and sex-matched controls. *P* values<0.1 are indicated in bold. *The peaks generated by primer extension for these SNPs were not corrected for unequal allelic detection as no heterozygote was available and therefore these allele frequencies are unlikely to be correct unless the true heterozygote ratio is 1:1 (see Chapter 2). However, a difference in allele frequencies between cases and controls should still be detected.

SNP	Allele		*P*
44) 371348 G>A	**G**	**A**	
Patients	270 (0.73)	102 (0.27)	
Controls	244 (0.65)	128 (0.35)	**0.0391**
45) 371435 G>C	**G**	**C**	
Patients	279 (0.75)	93 (0.25)	
Controls	256 (0.69)	116 (0.31)	**0.0606**

Table 5.7 continued. Estimates of allele frequencies and counts of *ADAM12* SNPs in the MRC pools comparing 186 LOAD cases with 186 age- and sex-matched controls. *P* values<0.1 are indicated in bold.

Fourteen SNPs were found to exhibit a difference in allele frequencies between cases and controls at the $P \leq 0.1$ significance level (SNPs 13, 15, 17, 18, 23, 25, 29, 32, 33, 36, 41, 43, 44 and 45). Rather than follow up all fourteen SNPs by individually genotyping the entire MRC sample, a subset of 90 individuals was typed for each of the significant SNPs to assess the degree of linkage disequilibrium between them. An additional nine polymorphisms in the vicinity of significant SNPs plus the two non-synonymous coding SNPs were also typed in this subset. Inter-marker r^2 values are shown overleaf in Table 5.8. Levels of linkage disequilibrium across the *ADAM12* gene are generally low but some SNPs are in high or complete LD with each other. Two of the significant SNPs, SNPs 13 and 15, are in high LD (r^2=0.889) and therefore only SNP15 was individually genotyped in the entire MRC sample. Similarly, SNPs 17 and 18 are in high LD (r^2=0.928), so only SNP18 was individually genotyped; SNPs 25 and 29 are in high LD (r^2=0.930), so only SNP25 was individually genotyped; SNPs 32 and 33 are in complete LD (r^2=1.000), so only SNP33 was individually genotyped; LD between SNPs 41, 43, 44 and 45 is high (r^2>0.948), so only SNP44 was individually genotyped. SNPs 23 and 36 are in moderate LD (r^2=0.404) and although not ideal, only SNP23 was individually genotyped due to time constraints. Therefore the number of SNPs requiring

individual genotyping in the full MRC sample was reduced from fourteen to six: SNPs 15, 18, 23, 25, 33 and 44.

SNP	5	13	15	17	18	19	20	21	22	23	24	25	29	30	31	32	33	36	40	41	42	43	44	45
2	0.002	0.009	0.001	0.028	0.032	0.007	0.007	0.006	0.017	0.036	0.012	0.002	0.000	0.008	0.004	0.001	0.001	0.000	0.000	0.039	0.005	0.039	0.039	0.040
5		0.017	0.011	0.004	0.004	0.027	0.024	0.024	0.026	0.010	0.006	0.003	0.002	0.002	0.005	0.019	0.020	0.001	0.002	0.010	0.003	0.010	0.010	0.007
13			0.889	0.118	0.127	0.014	0.017	0.014	0.008	0.002	0.028	0.029	0.018	0.052	0.077	0.000	0.000	0.002	0.015	0.003	0.014	0.003	0.003	0.009
15				0.109	0.118	0.019	0.023	0.018	0.009	0.001	0.033	0.026	0.015	0.062	0.094	0.000	0.000	0.004	0.016	0.015	0.004	0.015	0.015	0.024
17					0.928	0.032	0.033	0.033	0.042	0.002	0.016	0.184	0.169	0.016	0.026	0.003	0.004	0.007	0.049	0.065	0.000	0.065	0.065	0.044
18						0.035	0.036	0.036	0.045	0.001	0.019	0.210	0.194	0.021	0.031	0.014	0.014	0.001	0.053	0.048	0.000	0.048	0.048	0.031
19							0.972	0.972	0.591	0.086	0.312	0.010	0.010	0.036	0.001	0.052	0.044	0.020	0.032	0.014	0.007	0.014	0.014	0.017
20								0.946	0.555	0.089	0.289	0.022	0.027	0.045	0.003	0.073	0.063	0.012	0.040	0.020	0.008	0.020	0.020	0.015
21									0.601	0.089	0.330	0.015	0.015	0.045	0.002	0.051	0.043	0.023	0.023	0.016	0.002	0.016	0.016	0.019
22										0.112	0.685	0.045	0.043	0.110	0.000	0.111	0.103	0.039	0.006	0.057	0.054	0.057	0.057	0.052
23											0.093	0.031	0.024	0.109	0.249	0.030	0.029	0.404	0.102	0.029	0.022	0.029	0.029	0.023
24												0.063	0.046	0.089	0.036	0.183	0.184	0.080	0.004	0.030	0.021	0.030	0.030	0.025
25													0.930	0.184	0.007	0.588	0.588	0.001	0.056	0.168	0.057	0.168	0.168	0.120
29														0.197	0.008	0.546	0.547	0.000	0.064	0.168	0.039	0.168	0.168	0.118
30															0.545	0.112	0.108	0.213	0.050	0.067	0.156	0.067	0.067	0.050
31																0.087	0.088	0.263	0.161	0.000	0.187	0.000	0.000	0.000
32																	1.000	0.000	0.020	0.042	0.000	0.042	0.042	0.012
33																		0.000	0.020	0.040	0.000	0.040	0.040	0.011
36																			0.186	0.028	0.056	0.028	0.028	0.040
40																				0.255	0.254	0.255	0.255	0.242
41																					0.182	1.000	1.000	0.948
42																						0.182	0.182	0.171
43																							1.000	0.948
44																								0.948

Table 5.8. Intermarker LD values as measured by r^2.

Prior to individual genotyping, these six SNPs (SNPs 15, 18, 23, 25, 33 and 44) were typed in the WashU pools, comprised of 270 Caucasian LOAD cases and 270 Caucasian age- and sex-matched controls recruited from the USA. The estimated allele frequencies and counts calculated for each SNP are shown below in Table 5.9.

SNP	Allele		*P*
15) 271466 G>C	**G**	**C**	
Patients	292 (0.54)	248 (0.46)	
Controls	311 (0.58)	229 (0.42)	0.2443
18) 289573 A>G	**A**	**G**	
Patients	466 (0.86)	74 (0.14)	
Controls	482 (0.89)	58 (0.11)	0.1371
23) 316406 A>G	**A**	**G**	
Patients	442 (0.82)	98 (0.18)	
Controls	429 (0.79)	111 (0.21)	0.3166
25) 323237 C>T	**C**	**T**	
Patients	406 (0.75)	134 (0.25)	
Controls	407 (0.75)	133 (0.25)	0.9437
33) 341999 T>C	**T**	**C**	
Patients	455 (0.84)	85 (0.16)	
Controls	463 (0.86)	77 (0.14)	0.4953
44) 371348 G>A	**G**	**A**	
Patients	364 (0.67)	176 (0.33)	
Controls	370 (0.68)	170 (0.32)	0.6955

Table 5.9. Estimates of allele frequencies and counts of *ADAM12* SNPs in the WashU pools comparing 270 LOAD cases with 270 age- and sex-matched controls.

No significant difference was observed in allele frequencies between cases and controls. However as the WashU sample was derived from a different (and likely more heterogeneous) population to the one in which association was originally observed (*i.e.* UK), individual genotyping of the MRC sample was still performed. Genotype and allele counts in this sample of 546 cases and 546 controls are shown overleaf in Table 5.10.

SNP	Genotype			*P*	Allele		Odds Ratio (95% C.I.)	*P*
15) 271466 G>C	**G/G**	**G/C**	**C/C**		**G**	**C**		
Patients	193	268	78		654 (0.61)	424 (0.39)	0.8583	
Controls	165	275	91	0.1998	605 (0.57)	457 (0.43)	(0.7224- 1.0197)	0.0820
18) 289573 A>G	**A/A**	**A/G**	**G/G**		**A**	**G**		
Patients	468	65	5		1001 (0.93)	75 (0.07)	0.7900	
Controls	442	86	3	0.1275	970 (0.91)	92 (0.09)	(0.5751-1.0851)	0.1447
23) 316406 A>G	**A/A**	**A/G**	**G/G**		**A**	**G**		
Patients	313	198	27		824 (0.77)	252 (0.23)	1.3314	
Controls	347	168	15	**0.0226**	862 (0.81)	198 (0.19)	(1.0801-1.6412)	**0.0072**
25) 323237 C>T	**C/C**	**C/T**	**T/T**		**C**	**T**		
Patients	371	155	14		897 (0.83)	183 (0.17)	0.7982	
Controls	341	167	25	0.0921	849 (0.80)	217 (0.20)	(0.6419-0.9926)	**0.0424**
33) 341999 T>C	**T/T**	**T/C**	**C/C**		**T**	**C**		
Patients	429	105	5		963 (0.89)	115 (0.11)	0.7817	
Controls	404	115	13	0.0946	923 (0.87)	141 (0.13)	(0.6014-1.0162)	0.0652
44) 371348 G>A	**G/G**	**G/A**	**A/A**		**G**	**A**		
Patients*	260	243	36		763 (0.71)	315 (0.29)	0.9009	
Controls	247	237	49	0.3068	731 (0.69)	335 (0.31)	(0.7493-1.0831)	0.2666

Table 5.10. Genotypes and allele counts for *ADAM12* SNPs 15,18,23,25,33 and 44 in the MRC sample consisting of 546 LOAD cases and 546 age- and sex-matched controls. Genotypic and allelic *P* values are given, as well as odds ratios and 95% confidence intervals (C.I.). *P* values<0.05 are indicated in bold. *Genotypes deviate from Hardy-Weinberg equilibrium.

The original association of SNPs 15, 18, 33 and 44 with LOAD was again observed in the samples that made up the MRC pools (see Appendix A), but was not maintained in the larger sample (Table 5.10 above). SNPs 23 and 25 however were both significant at the $P \leq 0.05$ level. To determine whether variation at the *ADAM12* locus might interact with variation at the *APOE* locus to influence susceptibility to LOAD, the MRC sample data was reanalysed, comparing i) cases with at least one *APOE* ε4 allele (ε4-positive cases) against all controls and ii) cases with no *APOE* ε4 allele (ε4-negative cases) against all controls. There were 341 ε4-positive cases and 202 ε4-negative cases (*APOE* genotype data was unavailable for three cases). The stratified data are presented in Tables 5.11 and 5.12 (p.217).

SNP	Genotype			*P*	Allele		Odds Ratio (95% C.I.)	*P*
15) 271466 G>C	**G/G**	**G/C**	**C/C**		**G**	**C**		
Patients	120	170	47		410 (0.61)	264 (0.39)	0.8524	
Controls	165	275	91	0.2613	605 (0.57)	457 (0.43)	(0.7002-1.0377)	0.1114
18) 289573 A>G	**A/A**	**A/G**	**G/G**		**A**	**G**		
Patients*	294	38	4		626 (0.93)	46 (0.07)	0.7748	
Controls	442	86	3	0.0874	970 (0.91)	92 (0.09)	(0.5363-1.1193)	0.1730
23) 316406 A>G	**A/A**	**A/G**	**G/G**		**A**	**G**		
Patients	195	119	22		509 (0.76)	163 (0.24)	1.3942	
Controls	347	168	15	**0.0094**	862 (0.81)	198 (0.19)	(1.1028-1.7625)	**0.0053**
25) 323237 C>T	**C/C**	**C/T**	**T/T**		**C**	**T**		
Patients	230	98	9		558 (0.83)	116 (0.17)	0.8133	
Controls	341	167	25	0.2151	849 (0.80)	217 (0.20)	(0.6338-1.0438)	0.1041
33) 341999 T>C	**T/T**	**T/C**	**C/C**		**T**	**C**		
Patients	262	71	3		595 (0.89)	77 (0.11)	0.8471	
Controls	404	115	13	0.2440	923 (0.87)	141 (0.13)	(0.6299-1.1392)	0.2720
44) 371348 G>A	**G/G**	**G/A**	**A/A**		**G**	**A**		
Patients	173	138	25		484 (0.72)	188 (0.28)	0.8476	
Controls	247	237	49	0.2977	731 (0.69)	335 (0.31)	(0.6854-1.0481)	0.1267

Table 5.11. Genotypes and allele counts for *ADAM12* SNPs 15,18,23,25,33 and 44 in the stratified MRC sample consisting of 341 ε4-positive LOAD cases and 546 controls. Genotypic and allelic *P* values are given, as well as odds ratios and 95% confidence intervals (C.I.). *P* values<0.05 are indicated in bold. *Genotypes deviate from Hardy-Weinberg equilibrium.

SNP	Genotype			*P*	Allele		Odds Ratio (95% C.I.)	*P*
15) 271466 G>C	**G/G**	**G/C**	**C/C**		**G**	**C**		
Patients	73	97	31		243 (0.60)	159 (0.40)	0.8662	
Controls	165	275	91	0.3968	605 (0.57)	457 (0.43)	(0.6855-1.0945)	0.2287
18) 289573 A>G	**A/A**	**A/G**	**G/G**		**A**	**G**		
Patients	173	27	1		373 (0.93)	29 (0.07)	0.8197	
Controls	442	86	3	0.6465	970 (0.91)	92 (0.09)	(0.5310-1.2654)	0.3688
23) 316406 A>G	**A/A**	**A/G**	**G/G**		**A**	**G**		
Patients	118	78	5		314 (0.78)	88 (0.22)	1.2201	
Controls	347	168	15	0.1921	862 (0.81)	198 (0.19)	(0.9199-1.6182)	0.1669
25) 323237 C>T	**C/C**	**C/T**	**T/T**		**C**	**T**		
Patients	140	57	5		337 (0.83)	67 (0.17)	0.7778	
Controls	341	167	25	0.2389	849 (0.80)	217 (0.20)	(0.5753-1.0517)	0.1019
33) 341999 T>C	**T/T**	**T/C**	**C/C**		**T**	**C**		
Patients	166	34	2		366 (0.91)	38 (0.09)	0.6796	
Controls	404	115	13	0.1423	923 (0.87)	141 (0.13)	(0.4656-0.992)	**0.0442**
44) 371348 G>A	**G/G**	**G/A**	**A/A**		**G**	**A**		
Patients*	87	104	11		278 (0.69)	126 (0.31)	0.9009	
Controls	247	237	49	0.1096	731 (0.69)	335 (0.31)	(0.7725-1.2662)	0.9301

Table 5.12. Genotypes and allele counts for *ADAM12* SNPs 15,18,23,25,33 and 44 in the stratified MRC sample consisting of 202 ε4-negative LOAD cases and 546 controls. Genotypic and allelic *P* values are given, as well as odds ratios and 95% confidence intervals (C.I.). *P* values<0.05 are indicated in bold. *Genotypes deviate from Hardy-Weinberg equilibrium.

SNP44 genotypes deviated from Hardy-Weinberg equilibrium in the entire MRC case population (more heterozygotes than expected, P=0.0369) and in the ε4-negative case population (again more heterozygotes than expected, P=0.0046). A random selection of samples (n=95) was genotyped again with exactly the same results, implying this is not due to genotyping error. Similarly, SNP18 genotypes deviated from Hardy-Weinberg equilibrium in the ε4-positive case population (more G/G homozygotes than expected, P=0.0380). Again, repeat genotyping results implied that this is not due to lab error. These findings may be a result of selection or may be just chance effects.

While SNP23 is slightly more significant when comparing ε4-positive cases against controls and SNP33 crosses the significance threshold when comparing ε4-negative cases with controls, the allele frequencies in each stratum vary only slightly. Therefore the slightly increased significance in these SNPs may not truly indicate an interaction with *APOE*. As such, haplotype analysis was restricted to the MRC sample as a whole in order to minimise the number of statistical tests performed. Haplotypes consisting of 2 to 6 markers were examined and the results are shown in Tables 5.13-5.17 (p.219-220). The most significant haplotype contains the two markers that give significant results when examined individually *i.e.* SNPs 23 and 35 (P=0.0051, Table 5.13, p.219). In fact all significant haplotypes involve SNP23.

Marker 1	Marker 2	*P*
SNP15	SNP18	0.3373
SNP15	SNP23	0.0624
SNP15	SNP25	0.0960
SNP15	SNP33	0.0976
SNP15	SNP44	0.0994
SNP18	SNP23	**0.0067**
SNP18	SNP25	0.1507
SNP18	SNP33	0.1517
SNP18	SNP44	0.2806
SNP23	SNP25	**0.0051**
SNP23	SNP33	**0.0289**
SNP23	SNP44	0.0579
SNP25	SNP33	0.1813
SNP25	SNP44	0.1057
SNP33	SNP44	0.1308

Table 5.13. *ADAM12* 2-marker haplotype association with LOAD in 546 cases and 546 age- and sex-matched controls. *P* values<0.05 are indicated in bold.

Marker 1	Marker 2	Marker 3	*P*
SNP15	SNP18	SNP23	**0.0323**
SNP15	SNP18	SNP25	0.2936
SNP15	SNP18	SNP33	0.0783
SNP15	SNP18	SNP44	0.1092
SNP15	SNP23	SNP25	**0.0149**
SNP15	SNP23	SNP33	**0.0398**
SNP15	SNP23	SNP44	0.0577
SNP15	SNP25	SNP33	0.3038
SNP15	SNP25	SNP44	0.0763
SNP15	SNP33	SNP44	0.1251
SNP18	SNP23	SNP25	**0.0265**
SNP18	SNP23	SNP33	**0.0287**
SNP18	SNP23	SNP44	0.0807
SNP18	SNP25	SNP33	0.3601
SNP18	SNP25	SNP44	0.3305
SNP18	SNP33	SNP44	0.3659
SNP23	SNP25	SNP33	**0.0387**
SNP23	SNP25	SNP44	**0.0403**
SNP23	SNP33	SNP44	0.0999
SNP25	SNP33	SNP44	0.3465

Table 5.14. *ADAM12* 3-marker haplotype association with LOAD in 546 cases and 546 age- and sex-matched controls. *P* values<0.05 are indicated in bold.

Marker 1	Marker 2	Marker 3	Marker 4	*P*
SNP15	SNP18	SNP23	SNP25	0.0972
SNP15	SNP18	SNP23	SNP33	**0.0290**
SNP15	SNP18	SNP23	SNP44	0.1006
SNP15	SNP18	SNP25	SNP33	0.3841
SNP15	SNP18	SNP25	SNP44	0.2748
SNP15	SNP18	SNP33	SNP44	0.2642
SNP15	SNP23	SNP25	SNP33	0.1087
SNP15	SNP23	SNP25	SNP44	**0.0353**
SNP15	SNP23	SNP33	SNP44	0.0859
SNP15	SNP25	SNP33	SNP44	0.3351
SNP18	SNP23	SNP25	SNP33	0.1137
SNP18	SNP23	SNP25	SNP44	0.1666
SNP18	SNP23	SNP33	SNP44	0.1397
SNP18	SNP25	SNP33	SNP44	0.4363
SNP23	SNP25	SNP33	SNP44	0.0927

Table 5.15. *ADAM12* 4-marker haplotype association with LOAD in 546 cases and 546 age- and sex-matched controls. *P* values<0.05 are indicated in bold.

Marker 1	Marker 2	Marker 3	Marker 4	Marker 5	*P*
SNP15	SNP18	SNP23	SNP25	SNP33	0.2375
SNP15	SNP18	SNP23	SNP25	SNP44	0.2280
SNP15	SNP18	SNP23	SNP33	SNP44	0.2289
SNP15	SNP18	SNP25	SNP33	SNP44	0.4897
SNP15	SNP23	SNP25	SNP33	SNP44	0.1262
SNP18	SNP23	SNP25	SNP33	SNP44	0.5543

Table 5.16. *ADAM12* 5-marker haplotype association with LOAD in 546 cases and 546 age- and sex-matched controls.

Marker 1	Marker 2	Marker 3	Marker 4	Marker 5	Marker 6	*P*
SNP15	SNP18	SNP23	SNP25	SNP33	SNP44	0.5106

Table 5.17. *ADAM12* 6-marker haplotype association with LOAD in 546 cases and 546 age- and sex-matched controls.

5.3.4 Allele Specific Expression

To investigate potential *cis*-acting influences on *ADAM12* gene expression, differential allelic expression was assessed using the synonymous coding SNP25 as a marker polymorphism. Of 60 individuals tested, nineteen were heterozygous for SNP25. Primer extension was performed on brain derived cDNA and genomic DNA from these individuals. The ratio of cDNA peak heights, corrected by use of the average genomic ratio from all heterozygous samples, was used to calculate relative expression of the two alleles in each individual sample. Six samples displayed a difference in the level of expression of the two alleles (see Table 5.18, p.222 and Figure 5.5, p.223). When the experiment was repeated with these samples, only four displayed a difference in allelic expression. In the case of the other two, both alleles appeared to be similarly expressed. The reason for the occurrence of these false positives in the original experiment is unclear, but as measurement error of the primer extension method has been estimated at approximately 1%[192], this is unlikely to be the cause. Neither is it due to the existence of polymorphisms at primer-annealing sites as the relative allelic representation in all genomic samples was equivalent. Possibly some variability was introduced at the PCR stage. Whatever the cause, such an occurrence highlights the need for repeat experiments. For the other four samples, the difference in allelic expression was similar in both experiments (see Table 5.18, p.222). Three samples displayed an increase in expression of the C allele relative to the T allele, whereas one sample displayed lower expression of the C allele relative to the T allele. Therefore there does appear to be evidence for polymorphic *cis*-acting effects on the *ADAM12* gene as indicated by the difference in the expression of chromosome specific transcripts in some individuals. These results however do

not imply a causative role for SNP25 in this differential expression, or even that the SNP is in LD with a causative variant. The different alleles of individuals heterozygous for this SNP were merely employed as copy-specific tags for each transcript.

Sample	Corrected Ratio of C:T Allele in Genomic Sample		Corrected Ratio of C:T Allele in cDNA Sample	
	Experiment 1	Experiment 2	Experiment 1	Experiment 2
1	1.06	0.99	0.79	1.03
2	0.93	0.96	1.28	1.21
3	0.99	1.00	1.38	1.35
4	1.02	1.04	0.78	0.78
5	0.97	1.00	1.61	1.57
6	1.07	1.01	1.91	1.08

Table 5.18. Comparison of corrected genomic ratios for the six samples assayed in both experiment 1 and experiment 2. Note that with the exception of the genomic data from experiment 1, all values are the average of two measurements for each individual sample.

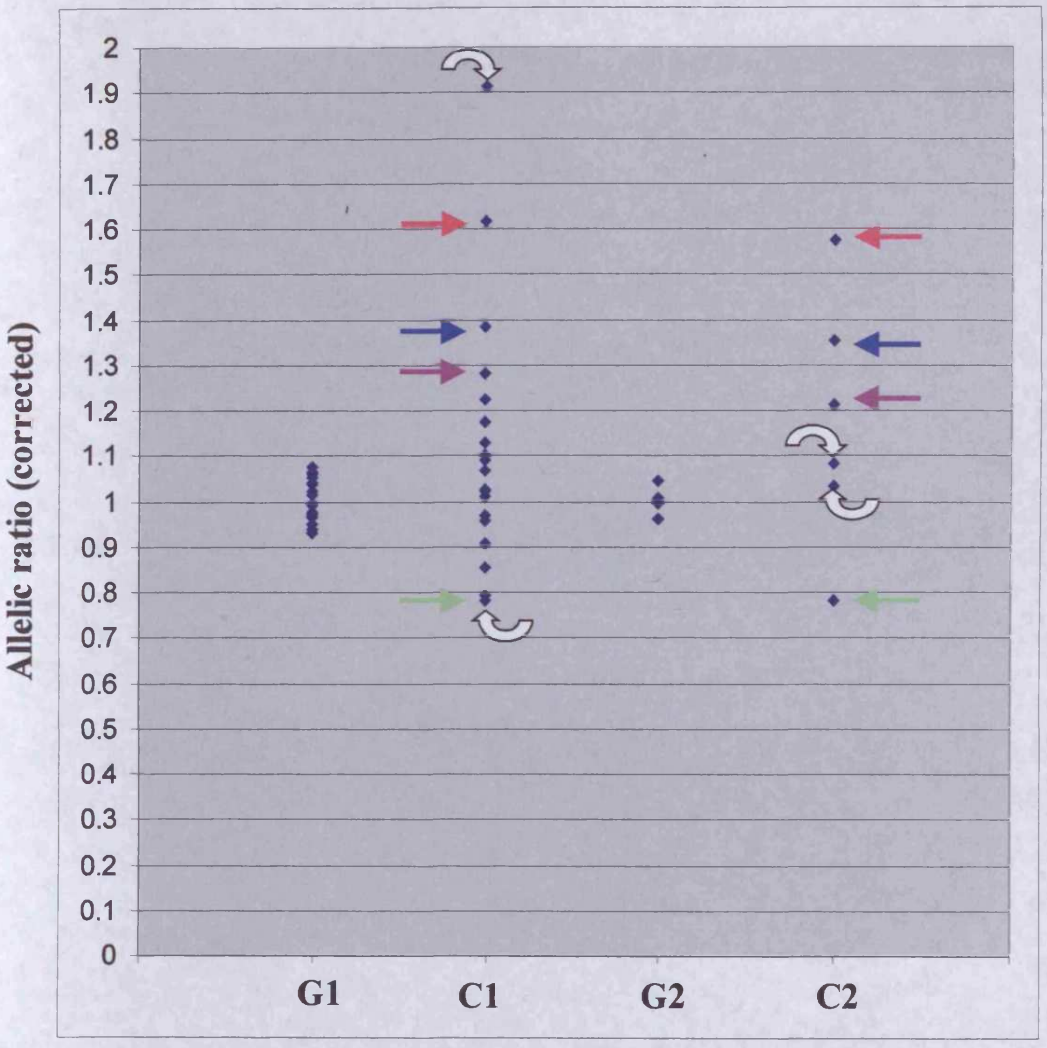

Figure 5.5. Comparison between genomic ratios and cDNA ratios assayed at SNP25, corrected with the average observed genomic ratio. Data are expressed as a ratio of C:T alleles. G indicates data for genomic DNA and C indicates data for cDNA; 1 indicates the initial experiment (19 samples) and 2 indicates the repeat experiment (6 samples). Coloured arrows indicate samples showing differential allelic expression in both experiments. White curved arrows indicate false positives.

5.4 Discussion

The *ADAM12* gene has been examined as a functional candidate for involvement in LOAD susceptibility. This gene encodes two splice variants and spans just over 373kb. The 45 polymorphic markers employed in this study were identified both experimentally by DHPLC, and from dbSNP. The average intermarker distance was approximately 8kb, with a range from 1bp to 40kb. As in the positional candidate study, all SNPs were genotyped in DNA pools of 186 LOAD cases and 186 age- and sex-matched controls using a relaxed significance threshold of 0.1. The minor alleles of two SNPs were too rare to be reliably estimated in pools and assays could not be optimised for another two SNPs. Of the other forty-one SNPs, fourteen displayed a significant difference in allele frequencies between cases and controls at the $P<0.1$ level. Rather than genotype all fourteen SNPs in the available sample of 546 LOAD cases and 546 controls, they were typed in a smaller sample of 90 individuals in order to assess the level of linkage disequilibrium between SNPs. This effort was well rewarded as the high LD between some SNPs reduced the number requiring genotyping in the entire sample from fourteen to six. This translates into genotyping 7,272 individual samples as opposed to 15,288 samples (and therefore 50% of the labour and cost).

The LD analysis revealed that the general levels of linkage disequilibrium across the *ADAM12* gene are quite low. Of the 300 possible intermarker r^2 values calculated, 230 had values less than 0.1. The longest stretch of sequence over which a moderate to high level of LD was maintained ($r^2>0.5$) was the 16,780bp between SNPs 19 and 22.

When the six selected SNPs were typed in the larger sample of 546 LOAD cases and 546 controls, a significant association with LOAD was detected with two SNPs: the intronic SNP23 and the synonymous coding SNP25. There was practically no LD between these SNPs (r^2=0.031), implying that these two signals are independent. Stratifying the cases based on the presence or absence of an *APOE* ε4 allele had no very striking effect on the data. Similarly, haplotype analysis did not provide much new information as all significant haplotypes involved SNP23 and the most significant haplotype was comprised of SNPs 23 and 25. In addition, the *P* values were not markedly lower than those obtained in single marker analysis.

A large number of statistical tests were performed in this study. Excluding the pooling analyses on the basis that they were an exploratory measure, eighteen independent tests were performed on the single marker association tests (on the assumption that tests for genotypic/allelic association are not independent). Applying the Bonferroni correction, a *P* value of less than 0.002778 (0.05/18) is required just to be significant at the 0.05 level (and this doesn't even account for all the haplotype association tests performed). According to these criteria, no significant association with LOAD is observed. The results of the WashU pooling analysis may seem to confirm this, as no association was observed in this sample at all. However, as described in Chapter 1, there are a number of reasons why a replication study may not detect a true association. In this case, the WashU sample is derived from a different, more heterogeneous population (US) than the one in which association was originally observed (UK). Although the US Caucasian population cannot be expected to differ hugely from the UK Caucasian population,

confounding factors may have combined to obscure association. Alternatively, the risk allele(s) involved may differ between the particular US and UK populations sampled here (*i.e.* allelic heterogeneity). Indeed, in the UK sample, two seemingly independent signals were observed. Therefore, it may have been necessary to genotype all SNPs in the US sample instead of the six chosen. Of course, should SNPs 23 and 25 truly represent susceptibility loci, the effect size in each case is small. The odds ratio associated with SNP23 is just 1.33 and the Washington sample comprised of 270 cases and 270 controls has just 51% power to detect such an association. Finally, it should be noted that the Washington pools were not validated, and as such may not be providing accurate estimates of allele frequencies.

Therefore although I cannot conclude that the *ADAM12* gene is associated with increased risk of LOAD, neither would I discount it and further investigation is definitely warranted. As the average intermarker distance was approximately 8kb, and there were gaps of up to 40kb, genotyping additional SNPs (especially in the region of SNPs 23 and 25) in the MRC sample would provide more information, particularly when used for haplotype analysis, as such analyses will have more power to detect unobserved risk loci (*i.e.* loci that haven't themselves been genotyped). In addition, replication of the SNP23 and SNP25 association in an independent sample would certainly generate more confidence in these findings. However such a sample must be of sufficient size *i.e.* 580 cases and 580 controls to have 80% power to detect the SNP23 association or 1022 cases and 1022 controls to detect the SNP25 association.

How might SNP23 or SNP25 affect the function of ADAM12 such that this change contributes to LOAD susceptibility? SNP23 is intronic, located 86bp upstream of exon 12 and SNP25 is a synonymous coding SNP located in exon 14 (Asn→Asn). A number of elements regulating gene expression have been found within intronic sequences[403] and SNP23 may affect such an element. Similarly, seemingly benign synonymous coding changes can affect mRNA stability and expression[404] suggesting a possible role for SNP25. Alternatively, these SNPs may be in LD with functional variants. The allele-specific expression experiment has provided evidence for the existence of *cis*-acting variation in the *ADAM12* gene affecting expression levels. Such variation may directly contribute to increased LOAD risk.

The *ADAM12-L* transcript at least, has been shown to be expressed in human brain. *ADAM12-S* may also be expressed in areas of the brain not examined in this study. Bernstein *et al.* (2004)[405] have recently shown that in human prefrontal cortex, *ADAM12* expression is almost exclusively localised to oligodendrocytes (although they did not distinguish between *ADAM12-L* and *ADAM12-S*). As such this lessens the plausibility of a putative role for ADAM12 in α-secretase activity (although still possible, as APP is expressed in these cells). The protein may however be involved in the regulation of survival of neurons, the promotion of neurogenesis and the induction of astrocyte and multipotent progenitor cells, via the ectodomain shedding of HB-EGF, which has been shown to be expressed both in neurons and in oligodendrocytes[406,407] and plays an important role in these functions[408-410]. ADAM12 may also be involved in the complex regulatory mechanism controlling myelination[405], an intriguing possibility as late-myelinating neocortical regions are

the most vulnerable to developing AD pathology[411]. However, such speculation is premature and involvement of ADAM12 in LOAD must first be either established or refuted at the genetic level.

5.5 Examples of Experimental Data

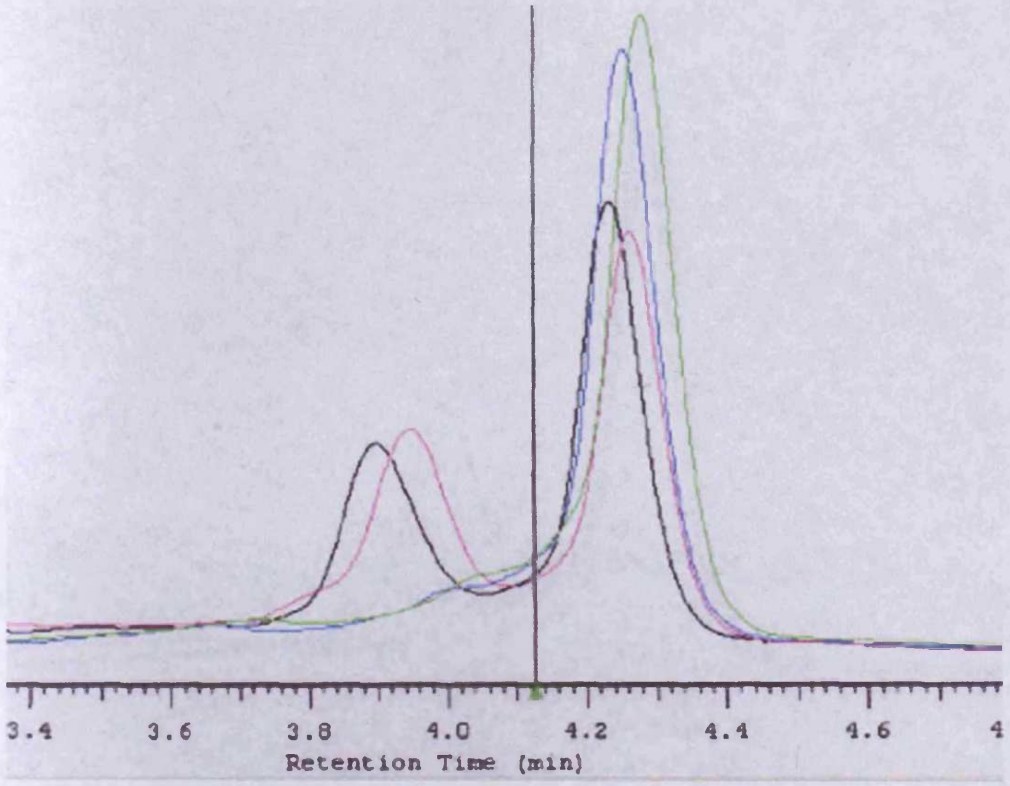

Figure 5.6. DHPLC traces from four individuals amplified for the ADAM12 x17 fragment. The green and blue traces indicate homozygous individuals. The pink and black traces represent individuals heterozygous for *ADAM12* SNP33.

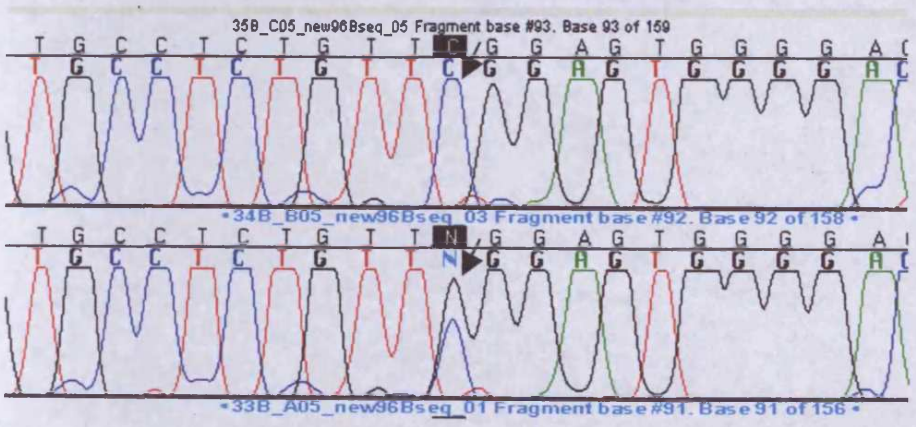

Figure 5.7. Sequence chromatograms for *ADAM12* SNP2 57690 C>G (rs3740199) showing a C/C homozygote in the upper panel and a C/G heterozygote in the lower panel.

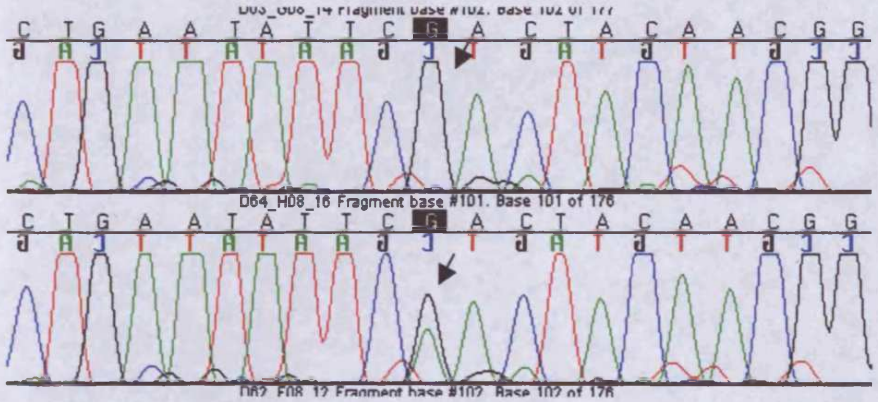

Figure 5.8. Sequence chromatograms for *ADAM12* SNP5 109183 G>A showing a G/G homozygote in the upper panel and an A/G heterozygote in the lower panel.

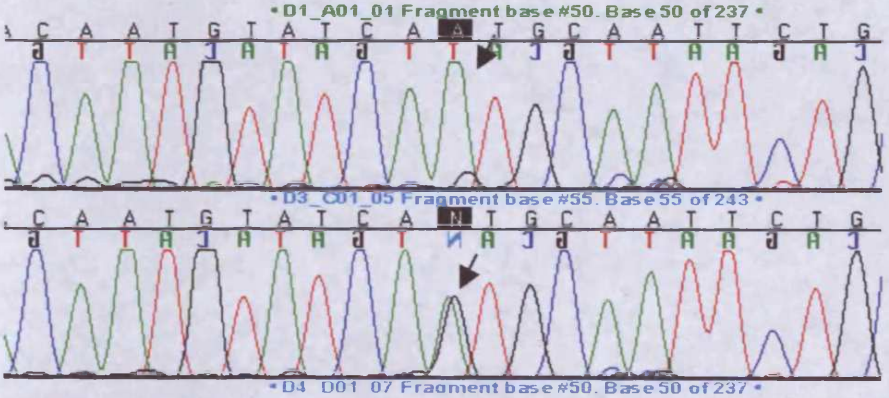

Figure 5.9. Sequence chromatograms for *ADAM12* SNP11 232794 A>G (rs1466361) showing an A/A homozygote in the upper panel and an A/G heterozygote in the lower panel.

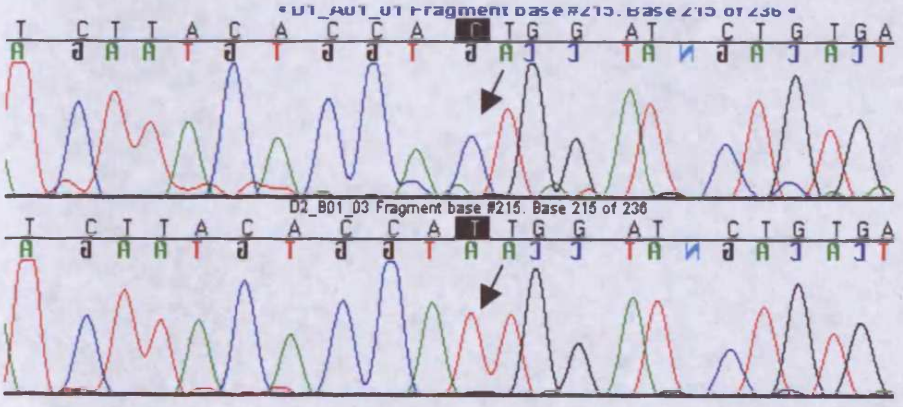

Figure 5.10. Sequence chromatograms for *ADAM12* SNP12 232959 C>T (rs1466360) showing a C/C homozygote in the upper panel and a T/T homozygote in the lower panel.

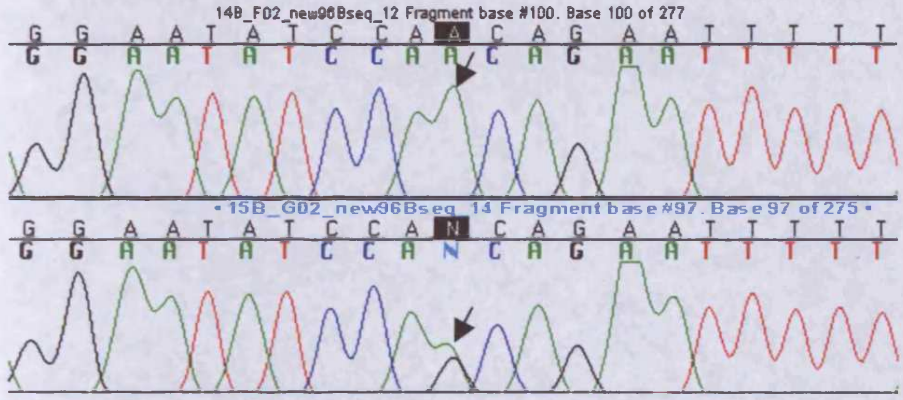

Figure 5.11. Sequence chromatograms for *ADAM12* SNP18 289573 A>G (rs2290844) showing an A/A homozygote in the upper panel and an A/G heterozygote in the lower panel.

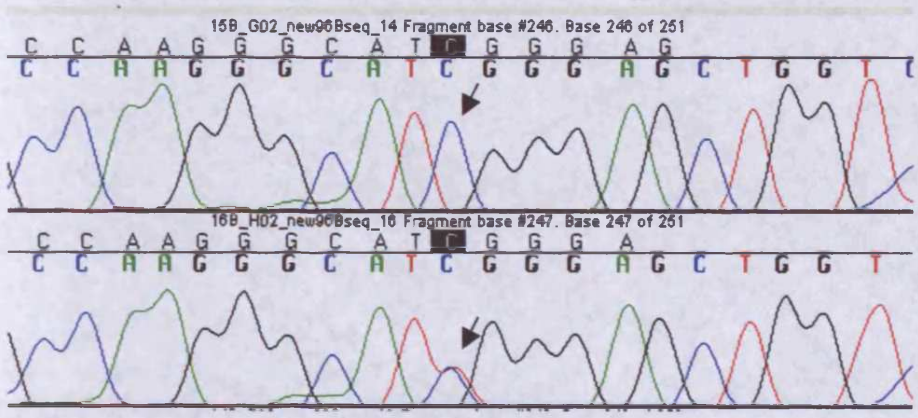

Figure 5.12. Sequence chromatograms for *ADAM12* SNP19 289746 C>T (rs2290842) showing a C/C homozygote in the upper panel and a C/T heterozygote in the lower panel.

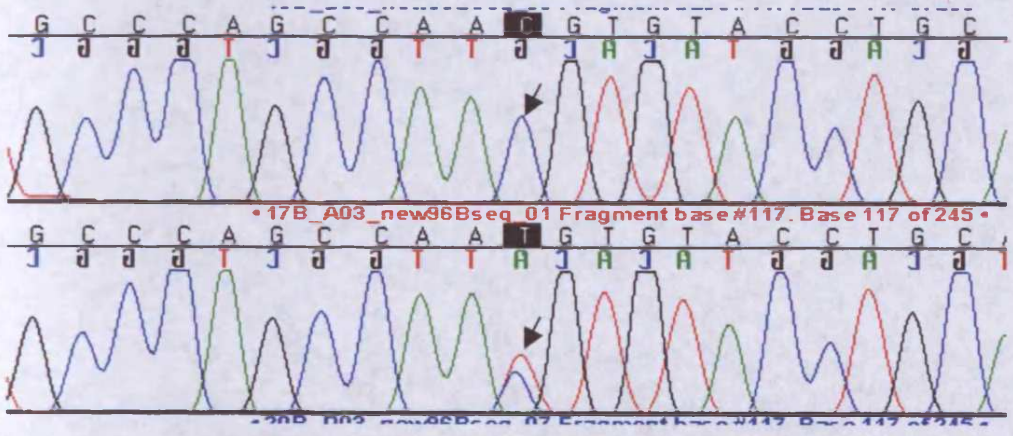

Figure 5.13. Sequence chromatograms for *ADAM12* SNP25 323237 C>T (rs1278279) showing a C/C homozygote in the upper panel and a C/T heterozygote in the lower panel.

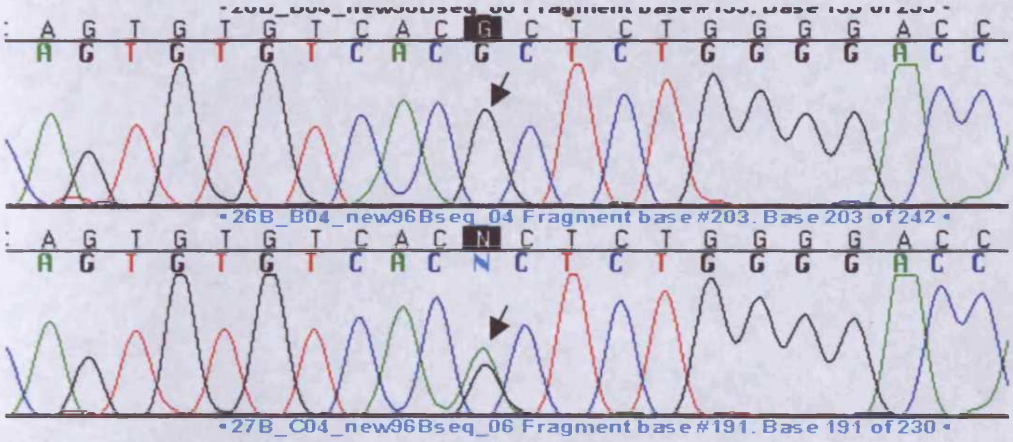

Figure 5.14. Sequence chromatograms for *ADAM12* SNP26 323327 G>A (rs2279091) showing a G/G homozygote in the upper panel and an A/G heterozygote in the lower panel.

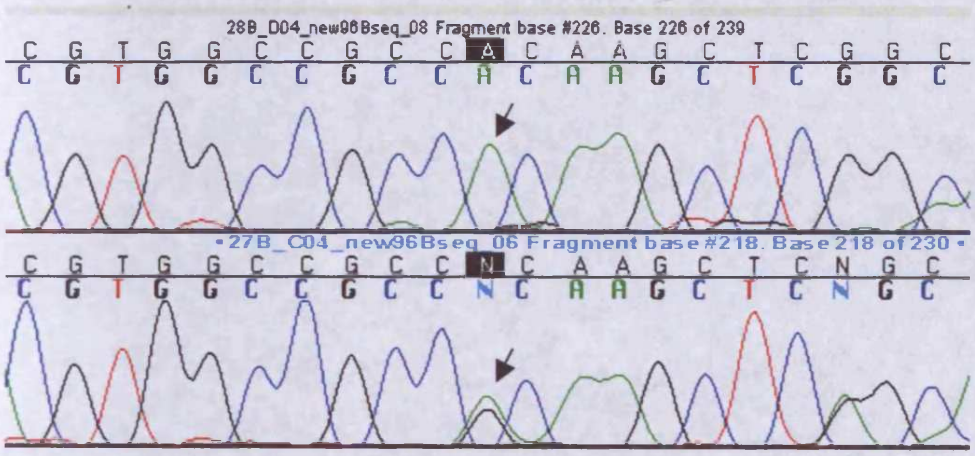

Figure 5.15. Sequence chromatograms for *ADAM12* SNP27 323354 A>G (rs2279090) showing an A/A homozygote in the upper panel and an A/G heterozygote in the lower panel.

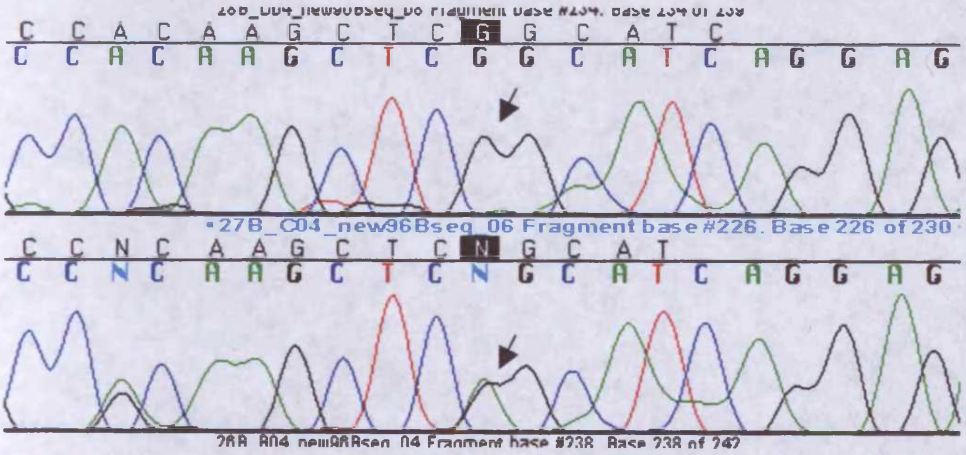

Figure 5.16. Sequence chromatograms for *ADAM12* SNP28 323362 G>A showing a G/G homozygote in the upper panel and an A/G heterozygote in the lower panel.

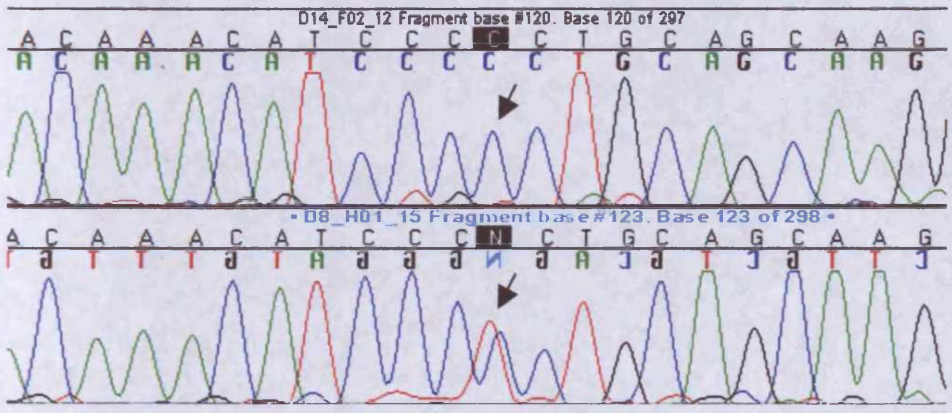

Figure 5.17. Sequence chromatograms for *ADAM12* SNP32 338785 C>T (rs2292692) showing a C/C homozygote in the upper panel and a C/T heterozygote in the lower panel.

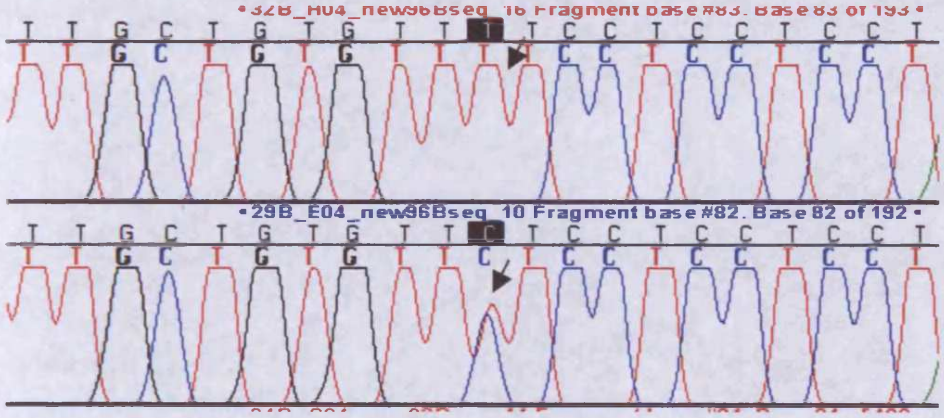

Figure 5.18. Sequence chromatograms for *ADAM12* SNP33 341999 T>C showing a T/T homozygote in the upper panel and a C/T heterozygote in the lower panel.

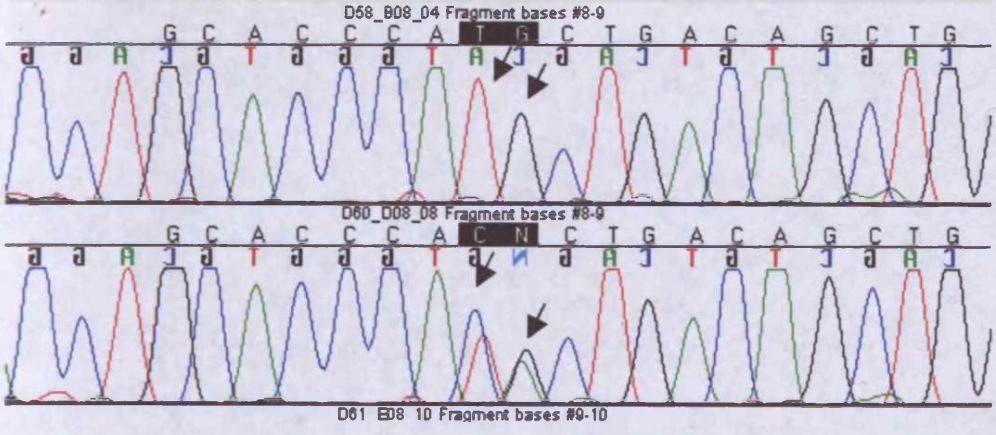

Figure 5.19. Sequence chromatograms for *ADAM12* SNP34 345179 C>T and *ADAM12* SNP35 345180 A>G showing respectively a T/T and G/G homozygote in the upper panel and a C/T and an A/G heterozygote in the lower panel.

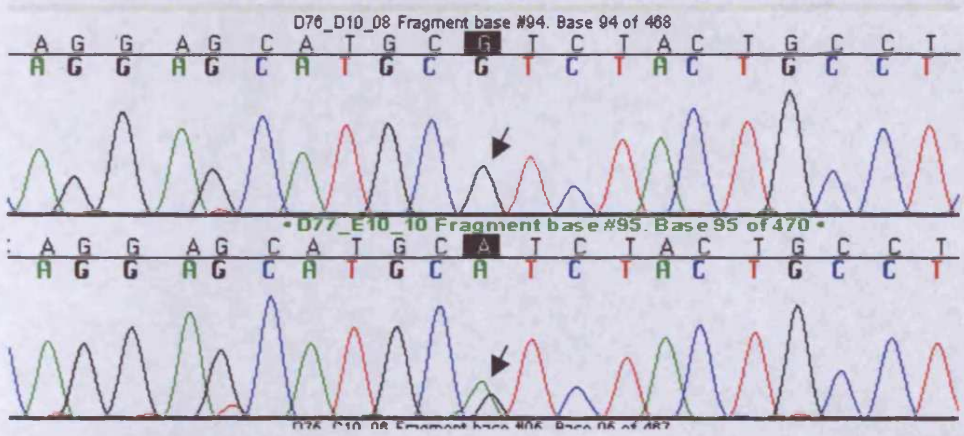

Figure 5.20. Sequence chromatograms for *ADAM12* SNP37 345987 G>A showing a G/G homozygote in the upper panel and an A/G heterozygote in the lower panel.

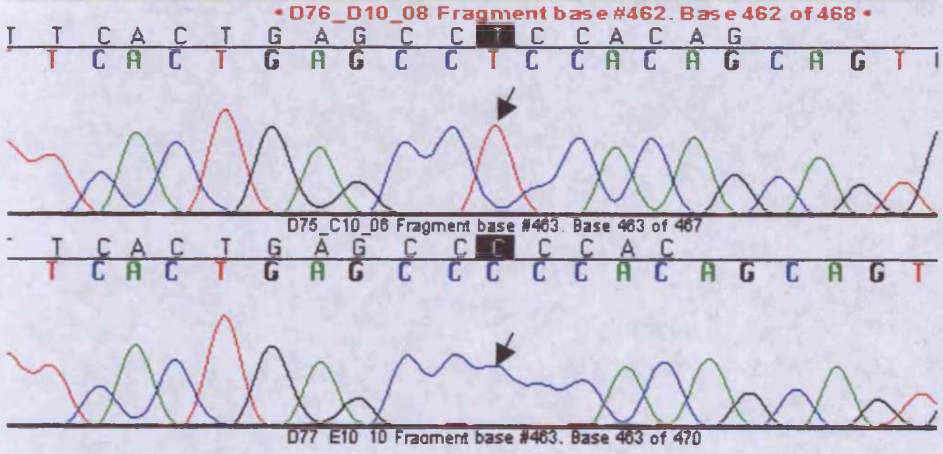

Figure 5.21. Sequence chromatograms for *ADAM12* SNP38 346355 C>T (rs6693) showing a T/T homozygote in the upper panel and a C/C homozygote in the lower panel.

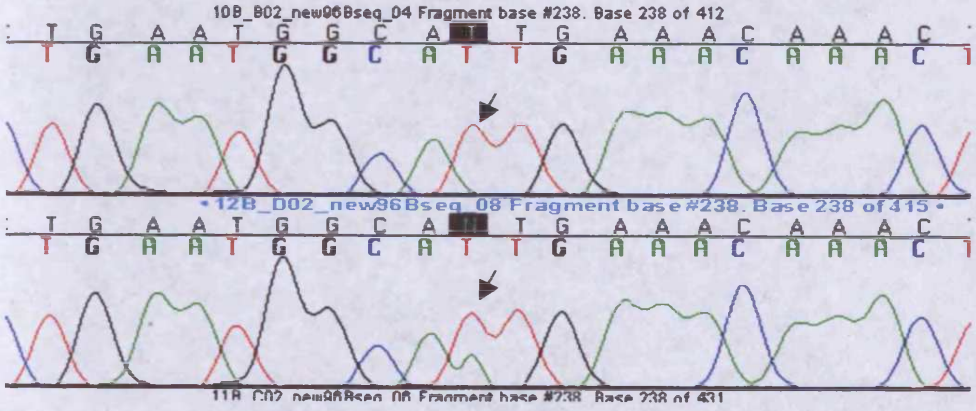

Figure 5.22. Sequence chromatograms for *ADAM12* SNP39 346571 T>A (rs4732) showing a T/T homozygote in the upper panel and an A/T heterozygote in the lower panel.

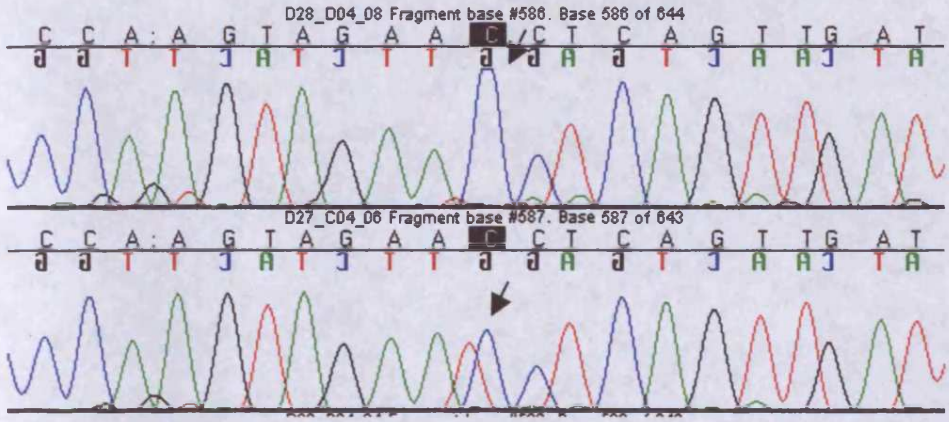

Figure 5.23. Sequence chromatograms for *ADAM12* SNP43 371311 C>T showing a C/C homozygote in the upper panel and a C/T heterozygote in the lower panel.

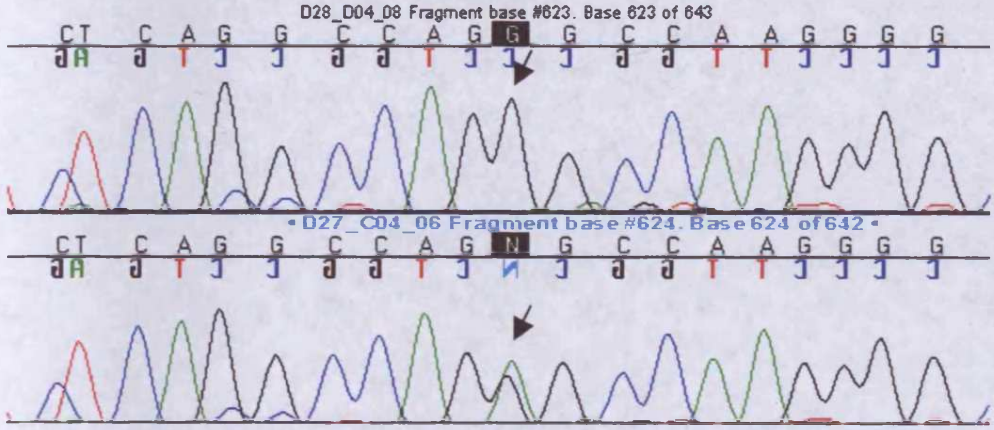

Figure 5.24. Sequence chromatograms for *ADAM12* SNP44 371348 G>A showing a G/G homozygote in the upper panel and an A/G heterozygote in the lower panel.

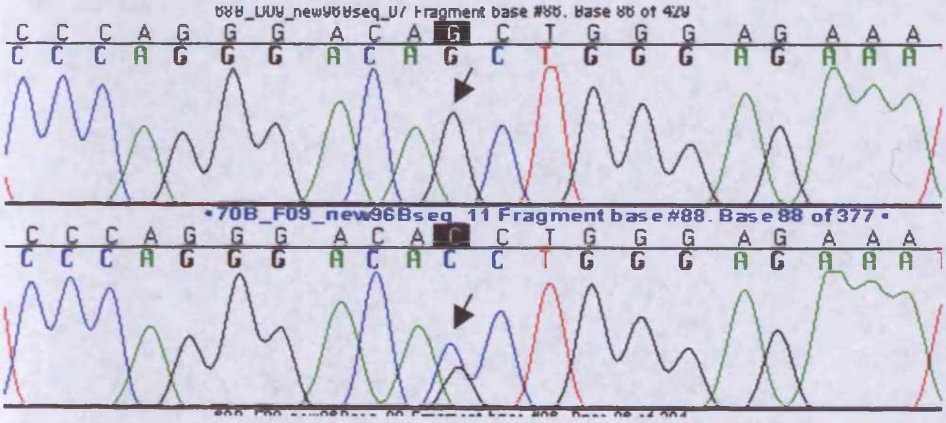

Figure 5.25. Sequence chromatograms for *ADAM12* SNP45 371435 G>C showing a G/G homozygote in the upper panel and a C/G heterozygote in the lower panel.

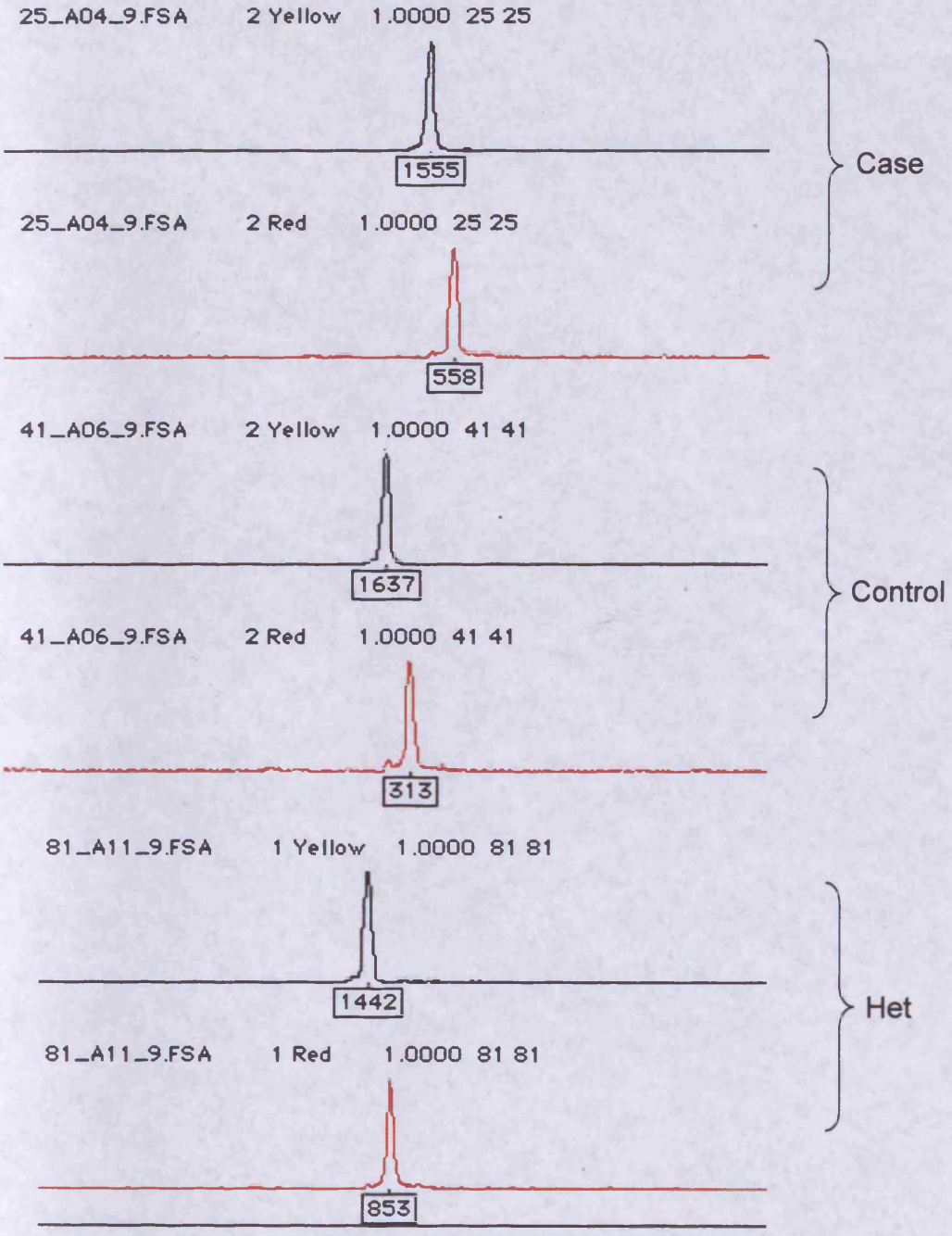

Figure 5.26. Traces generated from pooled genotyping of *ADAM12* SNP43 371311 C>T. The black peak represents the C allele and the red peak represents the T allele. Data from individual case and control pools are shown, together with a heterozygote (het). Note the unequal peak heights in the heterozygote.

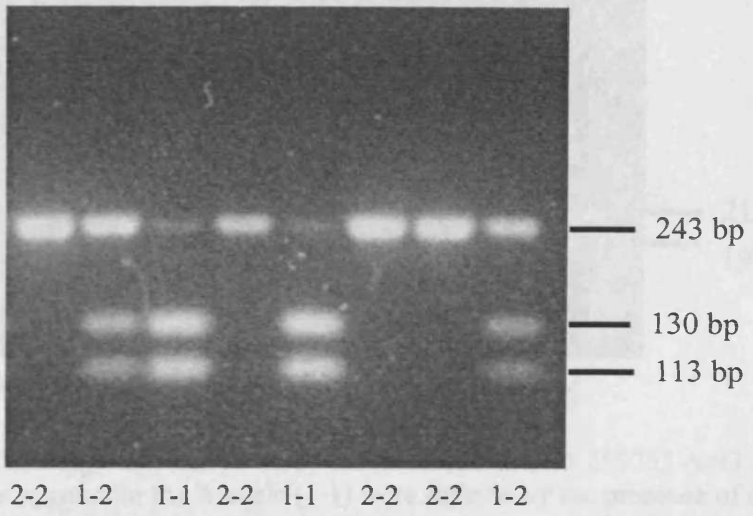

Figure 5.27. RFLP fragments generated by the *ADAM12* SNP2 57690 C>G *Hpy*188 I assay. Individuals homozygous for the C allele (1-1) were defined by the presence of two bands of size 130bp and 113bp. Individuals homozygous for the G allele (2-2) were defined by the presence of one band of size 243bp. C/G heterozygotes (1-2) displayed three bands of size 243bp, 130bp, and 113bp.

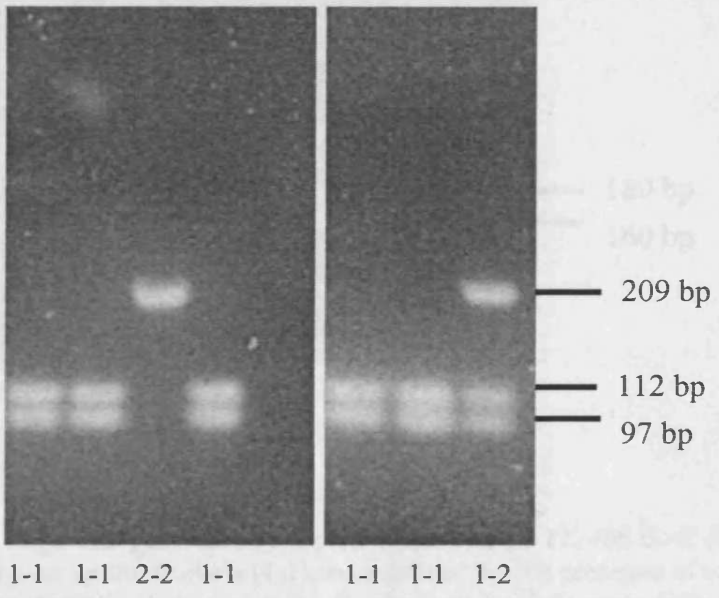

Figure 5.28. RFLP fragments generated by the *ADAM12* SNP5 109183 G>A *Taq* I assay. Individuals homozygous for the G allele (1-1) were defined by the presence of two bands of size 112bp and 97bp. Individuals homozygous for the A allele (2-2) were defined by the presence of one band of size 209bp. A/G heterozygotes (1-2) displayed three bands of size 209bp, 112bp, and 97bp.

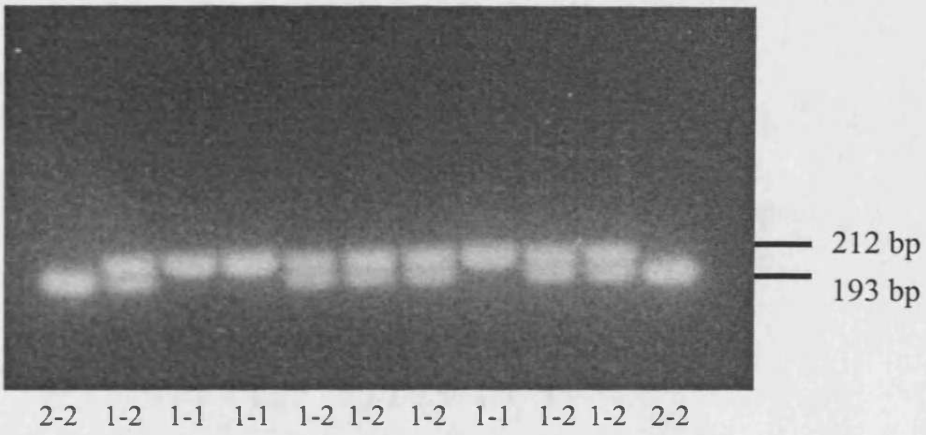

Figure 5.29. RFLP fragments generated by the *ADAM12* SNP13 259753 A>G *Xcm* I assay. Individuals homozygous for the A allele (1-1) were defined by the presence of one band of size 212bp. Individuals homozygous for the G allele (2-2) were defined by the presence of two bands of size 193bp and 19bp. A/G heterozygotes (1-2) displayed three bands of size 212bp, 193bp, and 19bp. Note that the 19bp band ran off the gel due to the small size.

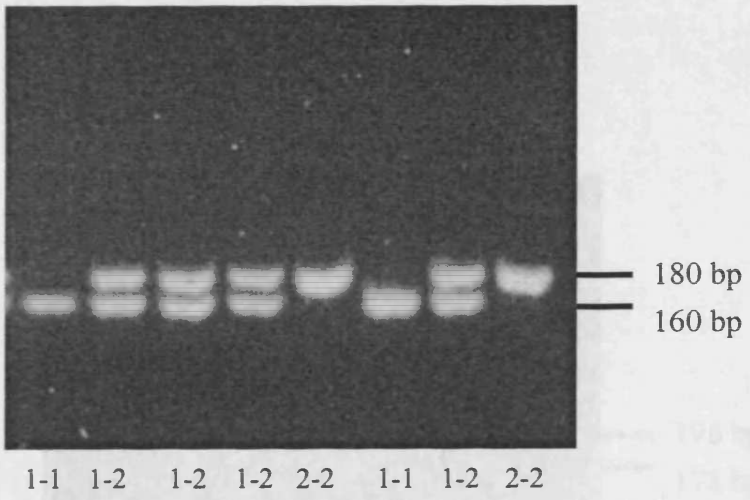

Figure 5.30. RFLP fragments generated by the *ADAM12* SNP15 271466 G>C *Bsm*A I assay. Individuals homozygous for the G allele (1-1) were defined by the presence of two bands of size 160bp and 20bp. Individuals homozygous for the C allele (2-2) were defined by the presence of one band of size 180bp. C/G heterozygotes (1-2) displayed three bands of size 180bp, 160bp, and 20bp. Note that the 20bp band ran off the gel due to the small size.

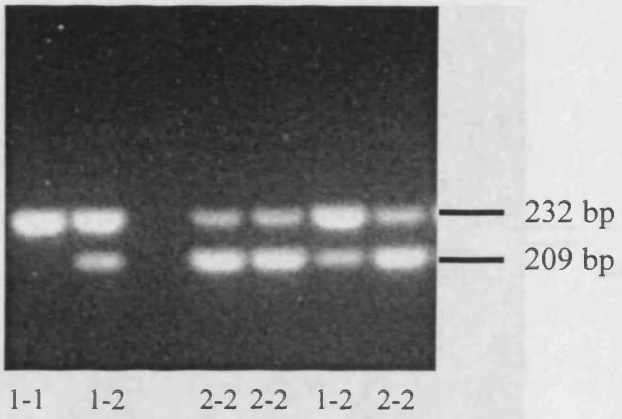

Figure 5.31. RFLP fragments generated by the *ADAM12* SNP17 287117 T>C *Bsi*HKA I assay. Individuals homozygous for the T allele (1-1) were defined by the presence of one band of size 232bp. Individuals homozygous for the C allele (2-2) were defined by the presence of two bands of size 209bp and 23bp. C/T heterozygotes (1-2) displayed three bands of size 232bp, 209bp, and 23bp. Note that the 19bp band ran off the gel due to the small size. Although this fragment only partially digests, C/T heterozygotes and C/C homozygotes can still be distinguished by the brightness of the 232bp and 209bp bands respectively.

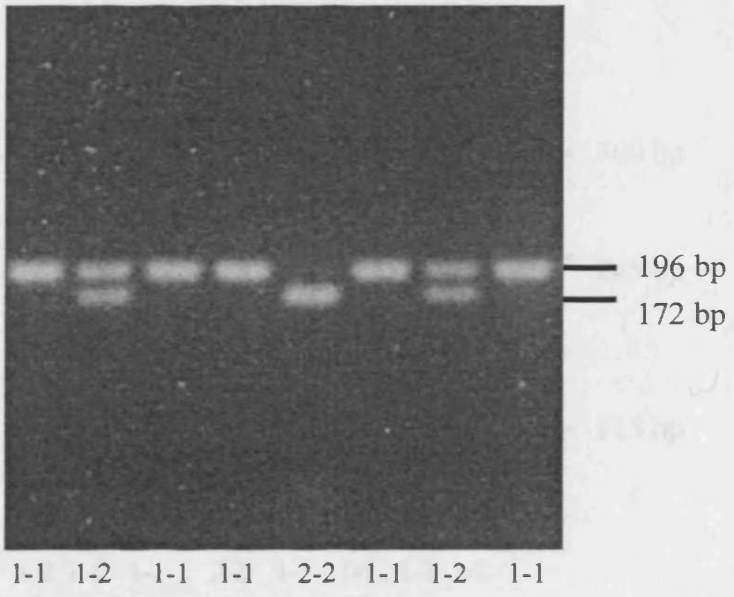

Figure 5.32. RFLP fragments generated by the *ADAM12* SNP18 289573 A>G *Fnu*4H I assay. Individuals homozygous for the A allele (1-1) were defined by the presence of one band of size 196bp. Individuals homozygous for the G allele (2-2) were defined by the presence of two bands of size 172bp and 24bp. A/G heterozygotes (1-2) displayed three bands of size 196bp, 172bp, and 24bp. Note that the 24bp band ran off the gel due to the small size.

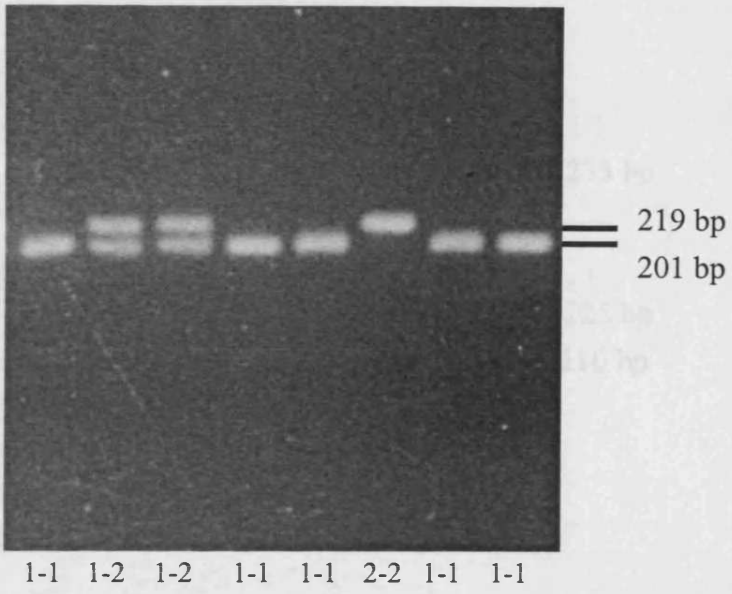

Figure 5.33. RFLP fragments generated by the *ADAM12* SNP19 289746 C>T *Bsa*H I assay. Individuals homozygous for the C allele (1-1) were defined by the presence of two bands of size 201bp and 18bp. Individuals homozygous for the T allele (2-2) were defined by the presence of one band of size 219bp. C/T heterozygotes (1-2) displayed three bands of size 219bp, 201bp, and 18bp. Note that the 18bp band ran off the gel due to the small size.

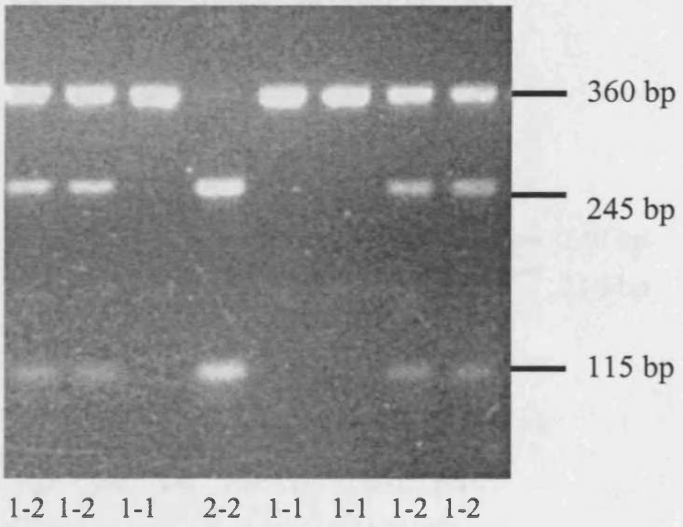

Figure 5.34. RFLP fragments generated by the *ADAM12* SNP20 291831 G>A *Nsi* I assay. Individuals homozygous for the G allele (1-1) were defined by the presence of one band of size 360bp. Individuals homozygous for the A allele (2-2) were defined by the presence of two bands of size 245bp and 115bp. A/G heterozygotes (1-2) displayed three bands of size 360bp, 245bp, and 115bp.

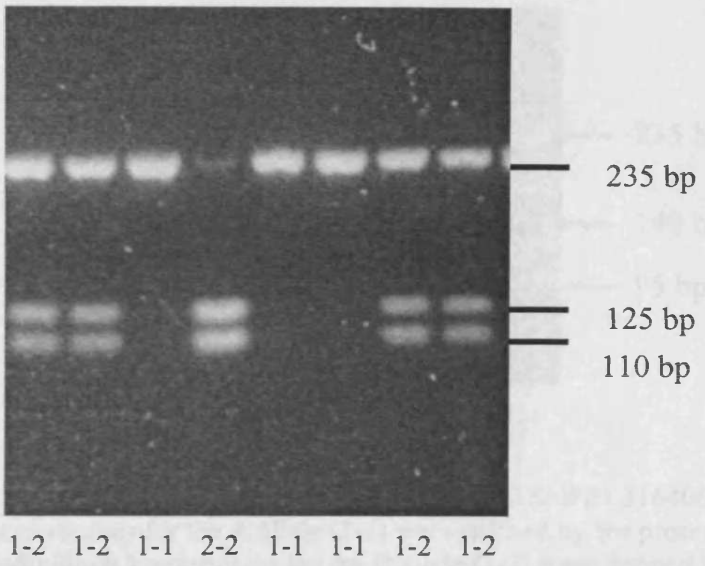

Figure 5.35. RFLP fragments generated by the *ADAM12* SNP21 296783 G>A *Hinc* II assay. Individuals homozygous for the G allele (1-1) were defined by the presence of one band of size 235bp. Individuals homozygous for the A allele (2-2) were defined by the presence of two bands of size 125bp and 110bp. A/G heterozygotes (1-2) displayed three bands of size 235bp, 125bp, and 110bp.

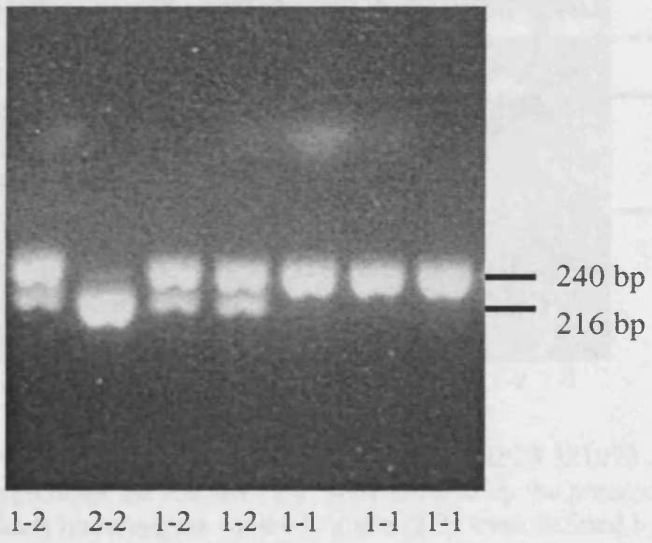

Figure 5.36. RFLP fragments generated by the *ADAM12* SNP22 306526 A>T *Dde* I assay. Individuals homozygous for the A allele (1-1) were defined by the presence of one band of size 240bp. Individuals homozygous for the T allele (2-2) were defined by the presence of two bands of size 216bp and 24bp. A/T heterozygotes (1-2) displayed three bands of size 240bp, 216bp, and 24bp. Note that the 24bp band ran off the gel due to the small size.

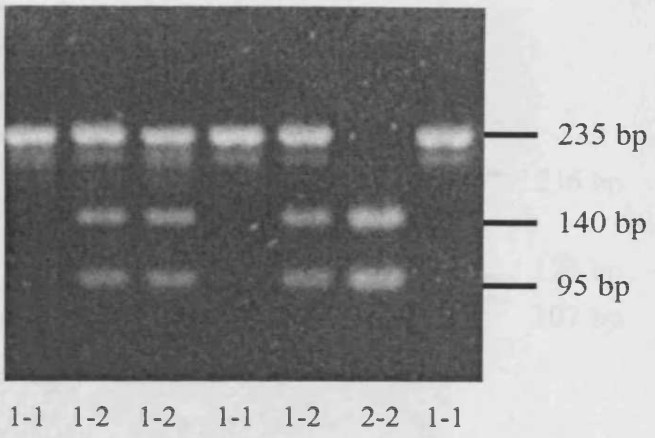

Figure 5.37. RFLP fragments generated by the *ADAM12* SNP23 316406 A>G *Msp* I assay. Individuals homozygous for the A allele (1-1) were defined by the presence of one band of size 235bp. Individuals homozygous for the G allele (2-2) were defined by the presence of two bands of size 140bp and 95bp. A/G heterozygotes (1-2) displayed three bands of size 235bp, 140bp, and 95bp.

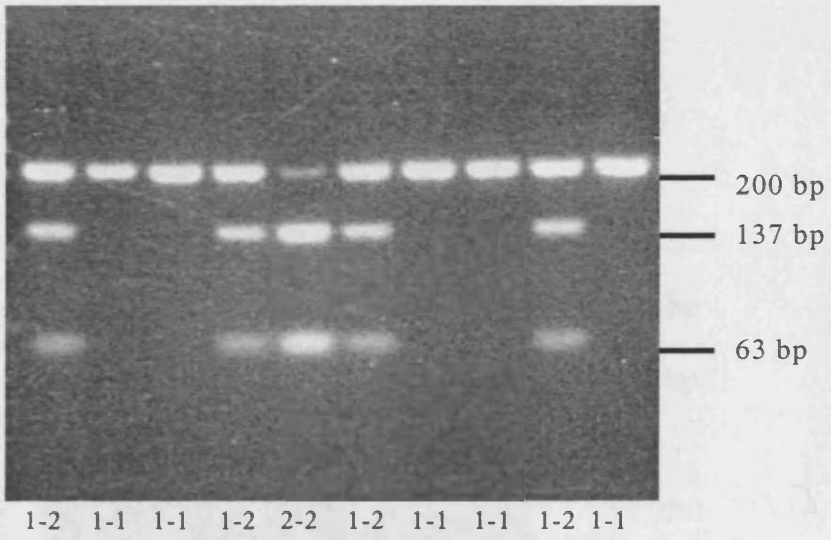

Figure 5.38. RFLP fragments generated by the *ADAM12* SNP24 321073 A>G *Nci* I assay. Individuals homozygous for the A allele (1-1) were defined by the presence of one band of size 200bp. Individuals homozygous for the G allele (2-2) were defined by the presence of two bands of size 137bp and 63bp. A/G heterozygotes (1-2) displayed three bands of size 200bp, 137bp, and 63bp.

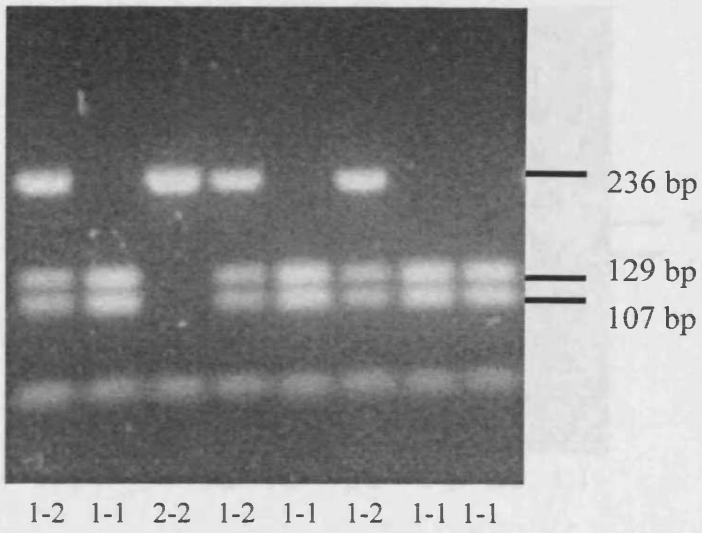

Figure 5.39. RFLP fragments generated by the *ADAM12* SNP25 323237 C>T *Hpy*CH4 IV assay. Individuals homozygous for the C allele (1-1) were defined by the presence of two bands of size 129bp and 107bp. Individuals homozygous for the T allele (2-2) were defined by the presence of one band of size 236bp. C/T heterozygotes (1-2) displayed three bands of size 236bp, 129bp, and 107bp.

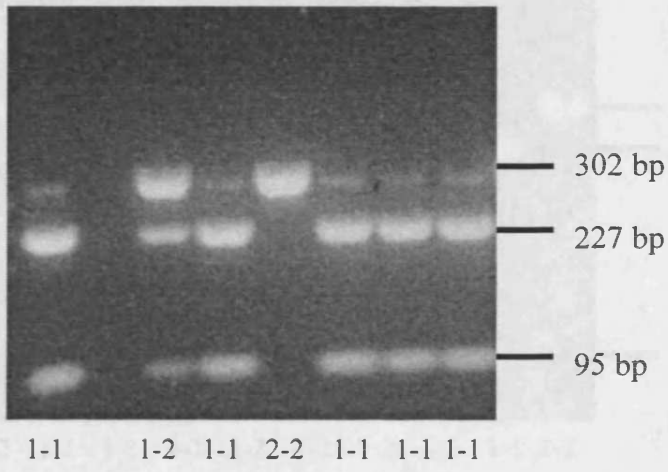

Figure 5.40. RFLP fragments generated by the *ADAM12* SNP29 323441 C>T *Cac*8 I assay. Individuals homozygous for the C allele (1-1) were defined by the presence of two bands of size 227bp and 95bp. Individuals homozygous for the T allele (2-2) were defined by the presence of one band of size 302bp. C/T heterozygotes (1-2) displayed three bands of size 302bp, 227bp, and 95bp.

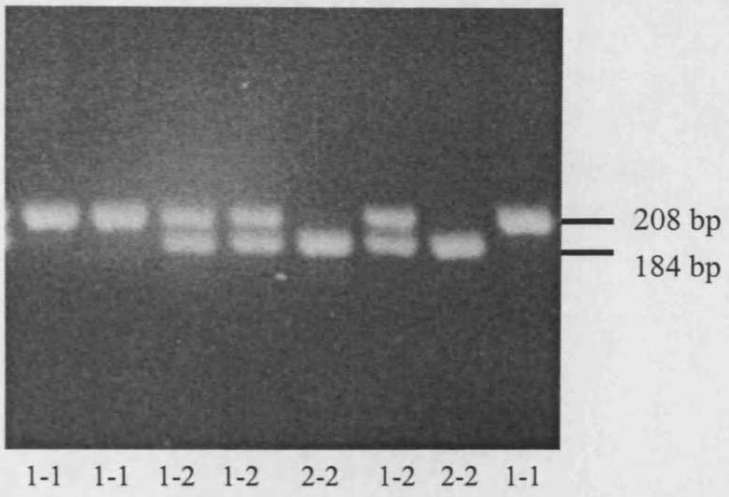

Figure 5.41. RFLP fragments generated by the *ADAM12* SNP30 327363 G>T *Hae* III assay. Individuals homozygous for the G allele (1-1) were defined by the presence of one band of size 208bp. Individuals homozygous for the T allele (2-2) were defined by the presence of two bands of size 184bp and 24bp. G/T heterozygotes (1-2) displayed three bands of size 208bp, 184bp, and 24bp. Note that the 24bp band ran off the gel due to the small size.

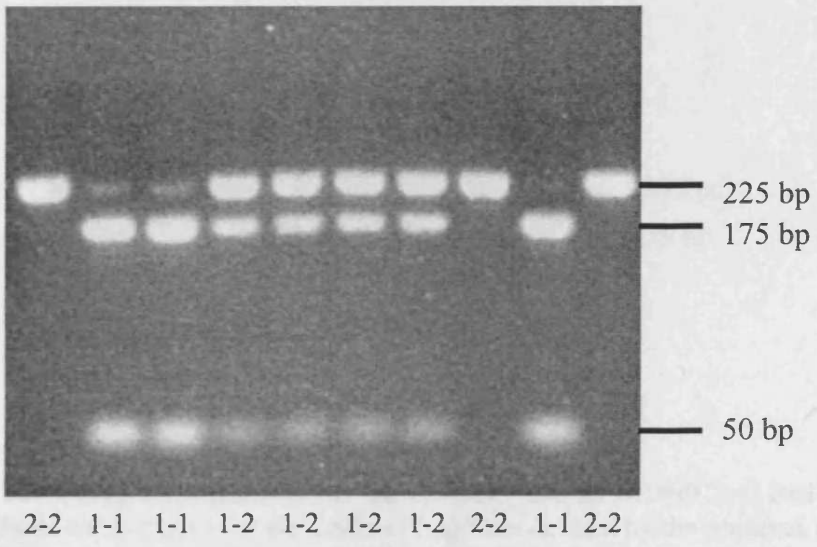

Figure 5.42. RFLP fragments generated by the *ADAM12* SNP31 329734 T>A *Hinf* I assay. Individuals homozygous for the T allele (1-1) were defined by the presence of two bands of size 175bp and 50bp. Individuals homozygous for the A allele (2-2) were defined by the presence of one band of size 225bp. A/T heterozygotes (1-2) displayed three bands of size 225bp, 175bp, and 50bp.

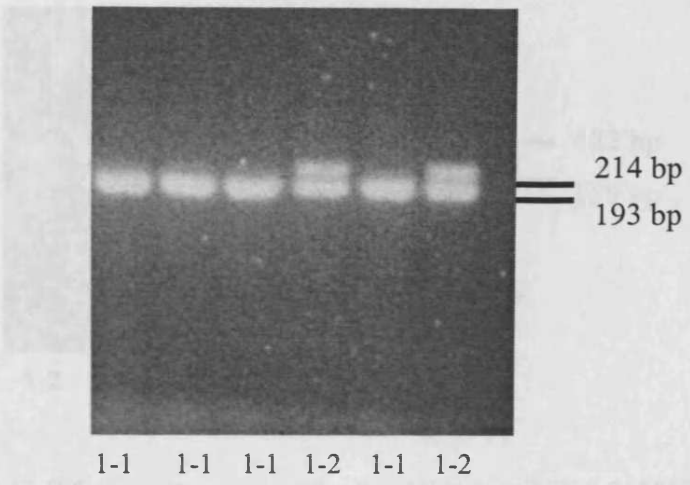

Figure 5.43. RFLP fragments generated by the *ADAM12* SNP32 338785 C>T *Nci* I assay. Individuals homozygous for the C allele (1-1) were defined by the presence of two bands of size 193bp and 21bp. C/T heterozygotes (1-2) displayed three bands of size 214bp, 193bp, and 21bp. No T/T homozygotes were observed. Note that the 21bp band ran off the gel due to the small size.

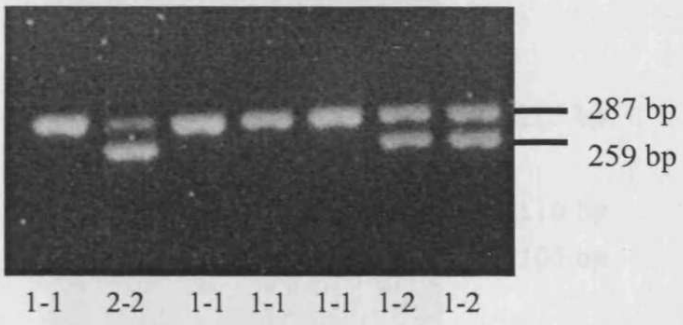

Figure 5.44. RFLP fragments generated by the *ADAM12* SNP33 341999 T>C *Bsi*HKA I assay. Individuals homozygous for the T allele (1-1) were defined by the presence of one band of size 287bp. Individuals homozygous for the C allele (2-2) were defined by the presence of two bands of size 259bp and 28bp. C/T heterozygotes (1-2) displayed three bands of size 287bp, 259bp, and 28bp. Note that the 28bp band ran off the gel due to the small size.

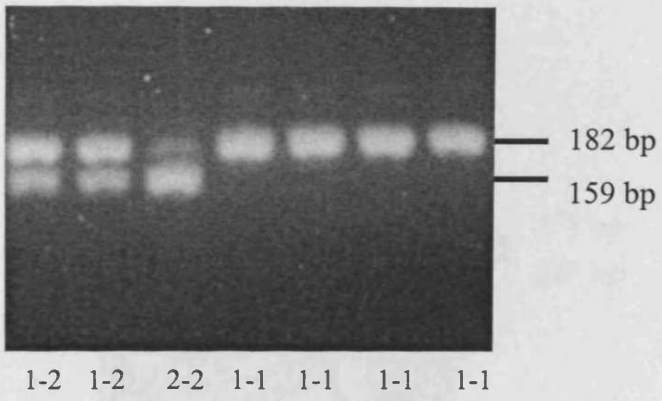

Figure 5.45. RFLP fragments generated by the *ADAM12* SNP36 345518 T>G *Sty* I assay. Individuals homozygous for the T allele (1-1) were defined by the presence of two bands of size 182bp and 51bp. Individuals homozygous for the G allele (2-2) were defined by the presence of three bands of size 159bp, 51bp and 23bp. G/T heterozygotes (1-2) displayed four bands of size 182bp, 159bp, 51bp and 23bp. Note that the 51bp and 23bp bands ran off the gel due to their small size.

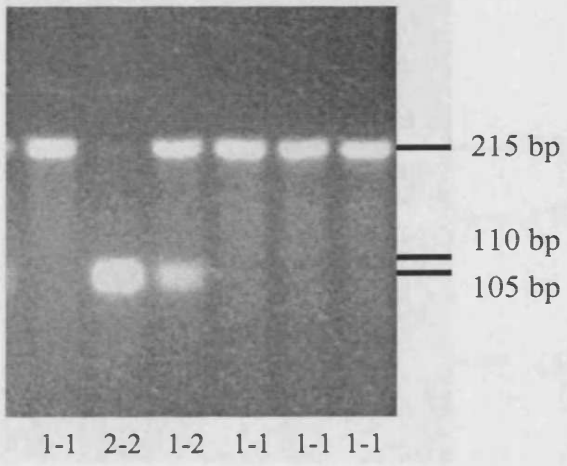

Figure 5.46. RFLP fragments generated by the *ADAM12* SNP40 348325 T>C *Hha* I assay. Individuals homozygous for the T allele (1-1) were defined by the presence of one band of size 215bp. Individuals homozygous for the C allele (2-2) were defined by the presence of two bands of size 110bp and 105bp. C/T heterozygotes (1-2) displayed three bands of size 215bp, 110bp, and 105bp.

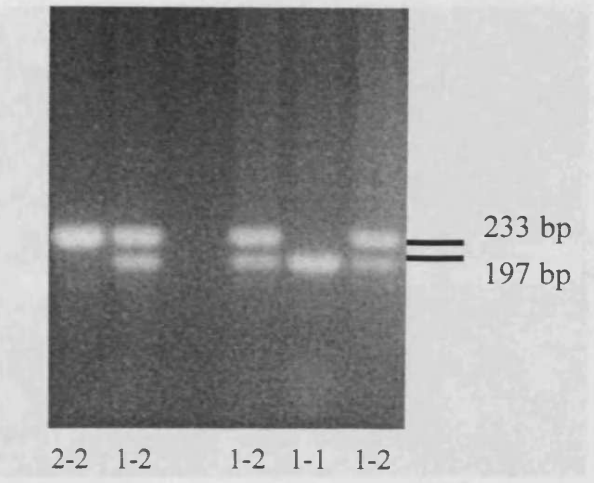

Figure 5.47. RFLP fragments generated by the *ADAM12* SNP41 366613 A>G *Bsm*F I assay. Individuals homozygous for the A allele (1-1) were defined by the presence of two bands of size 197bp and 36bp. Individuals homozygous for the G allele (2-2) were defined by the presence of one band of size 233bp. A/G heterozygotes (1-2) displayed three bands of size 233bp, 197bp, and 36bp. Note that the 36bp band ran off the gel due to the small size.

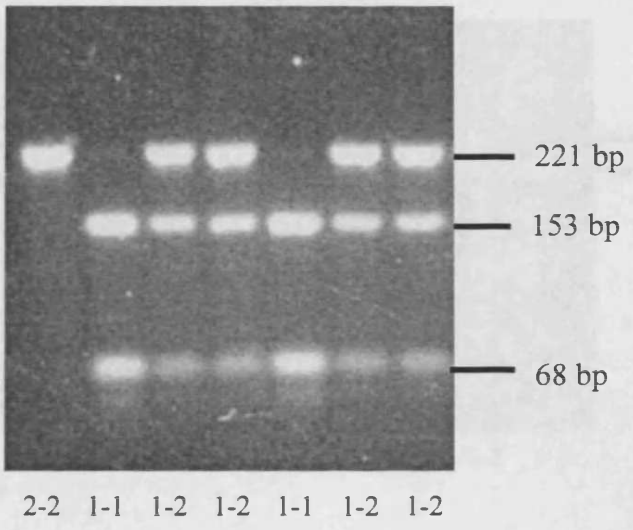

Figure 5.48. RFLP fragments generated by the *ADAM12* SNP42 370687 G>A *Bts* I assay. Individuals homozygous for the G allele (1-1) were defined by the presence of two bands of size 153bp and 68bp. Individuals homozygous for the A allele (2-2) were defined by the presence of one band of size 221bp. A/G heterozygotes (1-2) displayed three bands of size 221bp, 153bp, and 68bp.

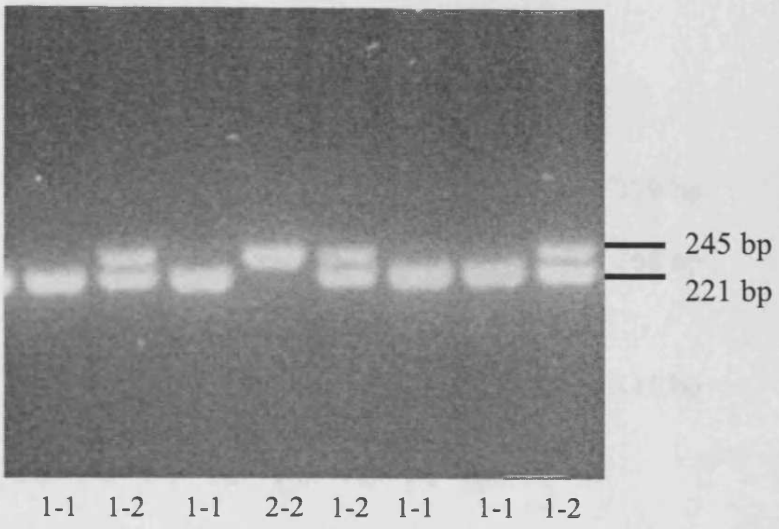

Figure 5.49. RFLP fragments generated by the *ADAM12* SNP43 371311 C>T *Rsa* I assay. Individuals homozygous for the C allele (1-1) were defined by the presence of two bands of size 221bp and 24bp. Individuals homozygous for the T allele (2-2) were defined by the presence of one band of size 245bp. C/T heterozygotes (1-2) displayed three bands of size 245bp, 221bp, and 24bp. Note that the 24bp band ran off the gel due to the small size.

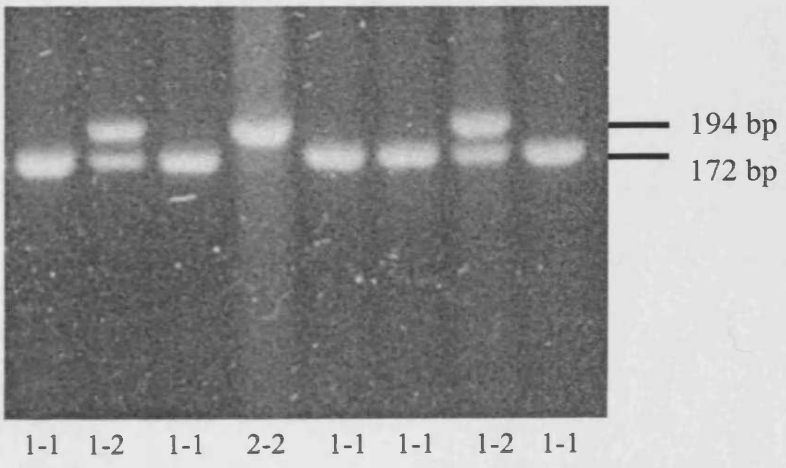

Figure 5.50. RFLP fragments generated by the *ADAM12* SNP44 371348 G>A *Bst*N I assay. Individuals homozygous for the G allele (1-1) were defined by the presence of three bands of size 172bp, 22bp and 21bp. Individuals homozygous for the A allele (2-2) were defined by the presence of two bands of size 194bp and 21bp. A/G heterozygotes (1-2) displayed four bands of size 194bp, 172bp, 22bp and 21bp. Note that the 22bp and 21bp bands ran off the gel due to their small size.

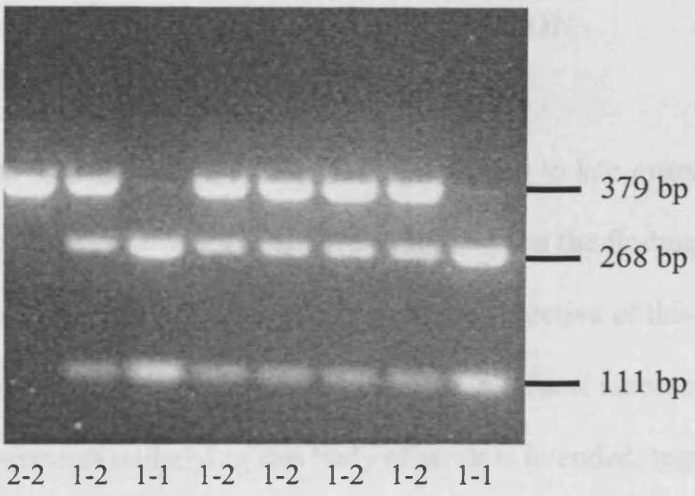

Figure 5.51. RFLP fragments generated by the *ADAM12* SNP45 371435 G>C *Pvu* II assay. Individuals homozygous for the G allele (1-1) were defined by the presence of two bands of size 268bp and 111bp. Individuals homozygous for the C allele (2-2) were defined by the presence of one band of size 379bp. C/G heterozygotes (1-2) displayed three bands of size 379bp, 268bp, and 111bp.

6. GENERAL DISCUSSION

In an attempt to uncover susceptibility loci contributing to late-onset Alzheimer's disease, a number of candidate genes have examined and the findings therein have been discussed in the relevant chapters. It is not the objective of this chapter to reiterate the conclusions drawn previously. Rather, a critical assessment of the methods and premises underlying this body of work is intended, together with what general observations may be made.

Ten genes have been assessed as candidates for involvement in LOAD and similar steps were involved in the investigation of each one. A prerequisite for a candidate gene study is the availability of polymorphic markers and single nucleotide polymorphisms (SNPs) are usually selected due to their abundance in the human genome. In the research presented here, polymorphisms were identified by denaturing high performance liquid chromatography, DHPLC (although additional SNPs were identified from a publicly available SNP database, dbSNP, for the ADAM12 study). In this strategy, exons, intron/exon boundaries and limited 5'flanking regions were screened for variants.

A total of 58,752bp were screened and eighty-nine polymorphisms were identified: eighty-five SNPs, three indels and one VNTR (see Appendix B). Polymorphisms were most commonly found in intronic regions (on average one every 475bp), with coding SNPs the least common subtype (one every 897bp). Non-synonymous coding SNPs were particularly rare; only six in the eighty-nine polymorphisms found. Four of these amino acid changes were conservative, one was moderately conservative

and one was moderately radical. 73% of SNPs were transitions (C⇔T and A⇔G), even though transitions represent only one third of the possible types of mutation. This is probably at least partly due to the methylation of cytosine bases in CpG dinucleotides, as 5-methylcytosines are susceptible to spontaneous deamination to give thymine.

Of the eighty-nine polymorphisms identified, forty-two (~50%) are currently described in dbSNP. This proportion probably does not accurately reflect the large numbers of markers present in this database. Idealistically, identification of all variation in the human genome is desirable. However, for researchers of limited resources, it may be more appropriate to select SNPs from databases rather than screening for them experimentally. Such a measure will save both time and money, which may be better spent examining more SNPs than might otherwise have been possible. Indeed, examining markers evenly spaced throughout a gene is more likely to detect association arising from non-coding functional variants than the approach taken here (*i.e.* assessing variation in coding sequence and limited 5'flanking regions).

With the exception of the cholinergic gene locus study, genotyping of all SNPs was attempted in DNA pools using a primer extension method; similarly, genotyping of indels was attempted in pools by PCR sizing. This extremely cost-effective approach allows a large number of polymorphisms to be assessed as risk loci in a relatively short time and a highly accurate manner (see Appendix A). Of course, such a method does not allow for haplotype construction or analysis of sub-phenotypes, but as an initial screen for association, it is certainly advantageous. Genotyping in pools was

attempted for seventy-two experimentally identified polymorphisms. Of these, seven (~10%) were too rare to be typed in pools and the primer extension method could not optimised for another twelve (~17%). As no attempt was made to genotype these variants by another method or to identify alternative, 'equivalent' markers, any association of these polymorphisms with LOAD will have gone undetected, unless picked up by another marker. Such a flaw in the study may have been at least partially avoided by selecting (additional) markers from a database, rather than being limited by variants identified by DHPLC. For example, twenty-five SNPs were chosen from dbSNP for the ADAM12 study in addition to those identified by DHPLC. Prior to their selection, the flanking sequence of each SNP was assessed for potential problems in extension primer design and only 'amenable' SNPs were chosen. Similarly, SNPs with a rare minor allele frequency (< 3%) were not selected. As a result, all twenty-five SNPs were successfully typed in pools. Of course the problem inherent in this approach is the bias against rare variants; the magnitude of this problem is dependent on how much truth there is in the common disease/common variant hypothesis. Should LOAD risk variants be present in the population at a similar frequency to that of the *APOE* ε4 allele (~14%; see Section 2.8.2.1), then this bias is irrelevant. If however the risk variant is rare and only common markers are tested, then the difference in allele frequencies at the risk and marker loci will considerably reduce the power to detect association, even if the two polymorphisms are in complete LD (as measured by D'; an r^2 value of 1 cannot be achieved unless the allele frequencies at the two loci are identical). In such a situation, the only hope of detecting association is if the effect size of the rare variant is large; even though the observed effect size at a marker locus will be diluted, a sufficiently powerful sample should still be able to detect it (assuming of course that

a marker in sufficient LD with the risk locus is tested). At α=0.1, the MRC DNA pool sample employed here (186 cases and 186 controls) has 76% power to detect a marker allele generating an odds ratio of 1.5, present at a frequency of 0.2 in the population. Should LD not be complete between the marker and risk loci and/or allele frequencies differ between and the two, then the odds ratio at the risk locus must be correspondingly higher to maintain this power.

Polymorphisms showing a significant association with LOAD in DNA pools were individually genotyped in a larger sample (which incorporates the samples in the pools). Similarly, variants at the cholinergic gene locus showing association in the Cardiff sample were genotyped in two additional case-control samples. Two SNPs in the *ADAM12* gene maintained association with LOAD in a larger sample, although these may be false positives, as neither was significant after correction for multiple testing. The occurrence of false positives may be a result of chance. Alternatively, it may reflect some kind of population stratification within the sample. While the samples employed here were carefully selected, as described in Chapter 2, it may have been prudent to perform a genomic control experiment, whereby a set of randomly selected, unlinked markers are genotyped in the sample. Such a method automatically accounts for non-independence in a case-control sample caused by population stratification and subsequent tests of association can be adjusted accordingly. However, given the large number of SNPs examined here showing no difference in allele frequencies between cases and controls (at least in pools), stratification is unlikely. Should the signals in the *ADAM12* gene represent true association with LOAD, then their detection may reflect the improved strategy employed in this study. In particular, the variant with the greatest odds ratio was

identified from dbSNP and the signal would not have been identified using only the experimentally identified SNPs.

A number of suggestions have been made as to how the approach employed here could have been improved. However, even with large samples and dense marker grids, there are no guarantees when it comes to mapping complex disease genes. Factors such as low LD, small effect size, heterogeneity and epistasis can all obscure association. Be that as it may, such obstacles should not be allowed to deter us. Strategies are continually being devised to circumvent these problems and with improved statistical methods, increased knowledge of the human genome and it's structure and through multidisciplinary collaborations, there is certainly hope for the future. And to quote Robert Browning, "a man's reach should exceed his grasp, or what's a heaven for?"

APPENDIX A

The accuracy of pooled analysis was assessed using the available genotype data from ten SNPs. Two of these SNPs (*CHAT* 1803 C>T and *CHAT* 1882 G>A) were genotyped in pools and the corresponding individual samples for the express purpose of assessing pooling accuracy (see Chapter 2). Data from the other eight SNPs was generated in the course of the research described in Chapters 4 and 5. Individual and pooled genotyping data are given in Table A.1 below. Estimation of differences between cases and control pools (Δ) was extremely accurate, with the mean error for Δ of 0.60% (maximum error: 1.47%).

SNP	% Major Allele in Cases		% Major Allele in Controls		% Difference between Cases and Controls (Δ)		Error (%)
	Pools	Real	Pools	Real	Pools	Real	
CHAT 1803 C>T	88.44	84.14	87.37	83.33	1.08	0.81	0.27
CHAT 1882 G>A	74.50	74.73	70.97	69.89	3.54	4.84	1.30
DKK1 463 C>T	96.04	96.31	91.90	92.47	4.14	3.84	0.30
SGPL1 53074 G>A	93.74	94.79	97.33	98.30	3.59	3.51	0.08
ADAM12 SNP15*	62.51	61.83	54.77	55.41	7.74	6.42	1.32
ADAM12 SNP18	92.98	94.62	86.04	88.17	6.94	6.45	0.49
ADAM12 SNP23*	72.02	74.19	81.04	83.15	9.02	8.96	0.06
ADAM12 SNP25	82.44	83.33	76.24	77.69	6.20	5.64	0.56
ADAM12 SNP33	87.24	89.79	81.70	84.41	5.54	5.38	0.16
ADAM12 SNP44	72.62	74.19	65.49	65.59	7.13	8.60	1.47
Average							**0.60**

Table A.1. Accuracy of estimating allele frequencies in DNA pools. The estimated allele frequencies in pools, together with the corresponding real allele frequency (as determined from individual genotyping) in 186 cases and 186 control samples are presented for each SNP. Δ: Difference in allele frequencies between cases and controls. Error: error of pooling defined as the discrepancy between the Δ obtained by pooled and individual genotyping. The estimate of error assumes that individual genotyping is 100% accurate. *Note that the pooled data for these SNPs differs from that presented in Chapter 5, which was uncorrected for unequal allelic detection. These SNPs were therefore genotyped again in pools with a heterozygote, so that this comparison could be performed.

APPENDIX B

Gene	Number of Base Pairs Screened						
	5'Flank	5'UTR	Coding	Intronic	3'UTR	3'Flank	Total
ALOX5	1082	44	2025	2106	426	57	5740
CHAT	2435	410	2287	5434	58	103	10727
SLC18A3	541	440	1599	0	380	0	2960
DKK1	618	120	798	439	576	38	2589
UBE2D1	684	194	444	1418	873	189	3802
DNAJC12	525	169	624	763	736	101	2918
SIRT1	524	53	2244	1766	1793	173	6553
SGPL1	572	210	1707	2490	247	88	5314
SEC24C	696	114	3377	2685	972	34	7878
ADAM12	954	310	2834	3317	2795	61	10271
Total	**8631**	**2064**	**17939**	**20418**	**8856**	**844**	**58752**

Table B.1. Number of basepairs screened by DHPLC in each gene.

Gene	Number of Polymorphisms Detected						
	5'Flank	5'UTR	Coding	Intronic	3'UTR	3'Flank	Total
ALOX5	2	0	1	4	2	0	9
CHAT	3	2	4	5	0	0	14
SLC18A3	1	1	0	0	1	0	3
DKK1	3	0	1	2	0	0	6
UBE2D1	0	0	1	7	0	0	8
DNAJC12	0	1	1	0	0	0	2
SIRT1	2	0	1	5	0	0	8
SGPL1	1	0	3	9	1	0	14
SEC24C	0	0	2	2	1	0	5
ADAM12	0	0	6	9	5	0	20
Total	**12**	**4**	**20**	**43**	**10**	**0**	**89**

Table B.2. Number of polymorphisms detected by DHPLC in each gene.

	Transitions		Transversions			
	A⇔G	C⇔T	A⇔C	A⇔T	G⇔C	G⇔T
Number of SNPs	33	29	3	4	9	7

Table B.3. Number of transitions/transversions detected.

Gene	SNP	Amino Acid Change	Physiochemical Distance	Type of Change	Frequency of Minor Allele
CHAT	1882 G>A	Asp→Asn	23	Conservative	0.25
CHAT	2384 G>A	Ala→Thr	58	Moderately Conservative	0.25
CHAT	7936 C>T	Leu→Phe	22	Conservative	0.07
SGPL1	27654 G>T	Val→Leu	32	Conservative	0.15
ADAM12	57690 C>G	Arg→Gly	125	Moderately Radical	0.44
ADAM12	109183 G>A	Arg→Gln	43	Conservative	0.04

Table B.4. Non-synonymous coding SNPs detected. The type of change is categorised based upon Grantham values[412], which are derived from physiochemical considerations. The range that was used for Grantham values corresponds to that of Li *et al.* (1984)[413] and is as follows: conservative is <50; moderately conservative is between 51 and 100; moderately radical is between 101 and 150; and radical is ≥151.

REFERENCES

1. Wilkins R.H. & Brody I.A. (1969) Alzheimer's disease. *Arch Neurol*, **21,** 109.
2. Blessed G., Tomlinson B.E. & Roth M. (1968) The association between quantitative measures of dementia and of senile change in the cerebral grey matter of elderly subjects. *Br J Psychiatry*, **114,** 797.
3. Mendez Ashla M.F. (2000) Cognitive function, mood, and behavior assessments. In: *Comprehensive geriatric assessment* (ed. D. Osterweil, K. Brummel-Smith & J. C. Beck), p. 67. McGraw-Hill, New York.
4. de Leon M.J., Convit A., DeSanti S., Bobinski M., George A.E., Wisniewski H.M., Rusinek H., Carroll R. & Saint Louis L.A. (1997) Contribution of structural neuroimaging to the early diagnosis of Alzheimer's disease. *Int Psychogeriatr*, **9 Suppl 1,** 183.
5. Bobinski M., de Leon M.J., Convit A., De Santi S., Wegiel J., Tarshish C.Y., Saint Louis L.A. & Wisniewski H.M. (1999) MRI of entorhinal cortex in mild Alzheimer's disease. *Lancet*, **353,** 38.
6. Petersen R.C., Smith G.E., Waring S.C., Ivnik R.J., Kokmen E. & Tangelos E.G. (1997) Aging, memory, and mild cognitive impairment. *Int Psychogeriatr*, **9 Suppl 1,** 65.
7. Mann U.M., Mohr E., Gearing M. & Chase T.N. (1992) Heterogeneity in Alzheimer's disease: progression rate segregated by distinct neuropsychological and cerebral metabolic profiles. *J Neurol Neurosurg Psychiatry*, **55,** 956.
8. Mendez M.F. & Cummings J.L. (2003) *Dementia: a clinical approach.*, 3rd edn. Butterworth Heinemann.

9. Jarrett J.T., Berger E.P. & Lansbury P.T., Jr. (1993) The carboxy terminus of the beta amyloid protein is critical for the seeding of amyloid formation: implications for the pathogenesis of Alzheimer's disease. *Biochemistry*, **32,** 4693.

10. Lemere C.A., Blusztajn J.K., Yamaguchi H., Wisniewski T., Saido T.C. & Selkoe D.J. (1996) Sequence of deposition of heterogeneous amyloid beta-peptides and APO E in Down syndrome: implications for initial events in amyloid plaque formation. *Neurobiol Dis*, **3,** 16.

11. Cummings J.L. & Cole G. (2002) Alzheimer disease. *JAMA*, **287,** 2335.

12. Clark C.M., Trojanowski J.Q. & Lee M.-Y.L. (1997) Neurofibrillary tangles in Alzheimer's disease: clinical and pathological implications. In: *Pharmacological Treatment of Alzheimer's Disease: Molecular and Neurobiological Foundations.* (ed. J. D. Brioni & M. W. Decker), p. 217. Wiley-Liss, New York.

13. Lee V.M., Balin B.J., Otvos L., Jr. & Trojanowski J.Q. (1991) A68: a major subunit of paired helical filaments and derivatized forms of normal Tau. *Science*, **251,** 675.

14. Cummings J.L. (2003) Alzheimer's disease: from molecular biology to neuropsychiatry. *Semin Clin Neuropsychiatry*, **8,** 31.

15. Suzuki N., Iwatsubo T., Odaka A., Ishibashi Y., Kitada C. & Ihara Y. (1994) High tissue content of soluble beta 1-40 is linked to cerebral amyloid angiopathy. *Am J Pathol*, **145,** 452.

16. Lantos P. & Cairns N. (2000) The neuropathology of Alzheimer's disease. In: *Dementia* (ed. J. O'Brien, D. Arnes & A. Burns), 2nd edn, p. 443. Arnold, London.

17. McKhann G., Drachman D., Folstein M., Katzman R., Price D. & Stadlan E.M. (1984) Clinical diagnosis of Alzheimer's disease: report of the NINCDS-ADRDA Work Group under the auspices of Department of Health and Human Services Task Force on Alzheimer's Disease. *Neurology*, **34,** 939.

18. Folstein M.F., Folstein S.E. & McHugh P.R. (1975) "Mini-mental state". A practical method for grading the cognitive state of patients for the clinician. *J Psychiatr Res*, **12,** 189.

19. Mayeux R., Saunders A.M., Shea S., Mirra S., Evans D., Roses A.D., Hyman B.T., Crain B., Tang M.X. & Phelps C.H. (1998) Utility of the apolipoprotein E genotype in the diagnosis of Alzheimer's disease. Alzheimer's Disease Centers Consortium on Apolipoprotein E and Alzheimer's Disease. *N Engl J Med*, **338,** 506.

20. Lobo A., Launer L.J., Fratiglioni L., Andersen K., Di Carlo A., Breteler M.M., Copeland J.R., Dartigues J.F., Jagger C., Martinez-Lage J., Soininen H. & Hofman A. (2000) Prevalence of dementia and major subtypes in Europe: A collaborative study of population-based cohorts. Neurologic Diseases in the Elderly Research Group. *Neurology*, **54,** S4.

21. Fratiglioni L., Viitanen M., von Strauss E., Tontodonati V., Herlitz A. & Winblad B. (1997) Very old women at highest risk of dementia and Alzheimer's disease: incidence data from the Kungsholmen Project, Stockholm. *Neurology*, **48,** 132.

22. Heyman A., Peterson B., Fillenbaum G. & Pieper C. (1996) The consortium to establish a registry for Alzheimer's disease (CERAD). Part XIV: Demographic and clinical predictors of survival in patients with Alzheimer's disease. *Neurology*, **46,** 656.

23. Mortimer J.A., van Duijn C.M., Chandra V., Fratiglioni L., Graves A.B., Heyman A., Jorm A.F., Kokmen E., Kondo K., Rocca W.A. & et al. (1991) Head trauma as a risk factor for Alzheimer's disease: a collaborative re-analysis of case-control studies. EURODEM Risk Factors Research Group. *Int J Epidemiol*, **20 Suppl 2,** S28.

24. Stern Y., Gurland B., Tatemichi T.K., Tang M.X., Wilder D. & Mayeux R. (1994) Influence of education and occupation on the incidence of Alzheimer's disease. *JAMA*, **271,** 1004.

25. Snowdon D.A., Greiner L.H., Mortimer J.A., Riley K.P., Greiner P.A. & Markesbery W.R. (1997) Brain infarction and the clinical expression of Alzheimer disease. The Nun Study. *JAMA*, **277,** 813.

26. Etminan M., Gill S. & Samii A. (2003) Effect of non-steroidal anti-inflammatory drugs on risk of Alzheimer's disease: systematic review and meta-analysis of observational studies. *BMJ*, **327,** 128.

27. Wolozin B., Kellman W., Ruosseau P., Celesia G.G. & Siegel G. (2000) Decreased prevalence of Alzheimer disease associated with 3-hydroxy-3-methyglutaryl coenzyme A reductase inhibitors. *Arch Neurol*, **57,** 1439.

28. Jick H., Zornberg G.L., Jick S.S., Seshadri S. & Drachman D.A. (2000) Statins and the risk of dementia. *Lancet*, **356,** 1627.

29. van Duijn C.M., Clayton D., Chandra V., Fratiglioni L., Graves A.B., Heyman A., Jorm A.F., Kokmen E., Kondo K., Mortimer J.A. & et al. (1991) Familial aggregation of Alzheimer's disease and related disorders: a collaborative re-analysis of case-control studies. EURODEM Risk Factors Research Group. *Int J Epidemiol*, **20 Suppl 2,** S13.

30. Plassman B.L. & Breitner J.C. (1996) Recent advances in the genetics of Alzheimer's disease and vascular dementia with an emphasis on gene-environment interactions. *J Am Geriatr Soc*, **44**, 1242.

31. Campion D., Dumanchin C., Hannequin D., Dubois B., Belliard S., Puel M., Thomas-Anterion C., Michon A., Martin C., Charbonnier F., Raux G., Camuzat A., Penet C., Mesnage V., Martinez M., Clerget-Darpoux F., Brice A. & Frebourg T. (1999) Early-onset autosomal dominant Alzheimer disease: prevalence, genetic heterogeneity, and mutation spectrum. *Am J Hum Genet*, **65**, 664.

32. Shastry B.S. & Giblin F.J. (1999) Genes and susceptible loci of Alzheimer's disease. *Brain Res Bull*, **48**, 121.

33. Risch N. & Merikangas K. (1996) The future of genetic studies of complex human diseases. *Science*, **273**, 1516.

34. Lander E. & Kruglyak L. (1995) Genetic dissection of complex traits: guidelines for interpreting and reporting linkage results. *Nat Genet*, **11**, 241.

35. Mann D.M. (1988) Alzheimer's disease and Down's syndrome. *Histopathology*, **13**, 125.

36. Mann D.M. (1988) The pathological association between Down syndrome and Alzheimer disease. *Mech Ageing Dev*, **43**, 99.

37. St George-Hyslop P.H., Tanzi R.E., Polinsky R.J., Haines J.L., Nee L., Watkins P.C., Myers R.H., Feldman R.G., Pollen D., Drachman D. & et al. (1987) The genetic defect causing familial Alzheimer's disease maps on chromosome 21. *Science*, **235**, 885.

38. Goate A., Chartier-Harlin M.C., Mullan M., Brown J., Crawford F., Fidani L., Giuffra L., Haynes A., Irving N., James L. & et al. (1991) Segregation of

a missense mutation in the amyloid precursor protein gene with familial Alzheimer's disease. *Nature*, **349,** 704.

39. Sherrington R., Rogaev E.I., Liang Y., Rogaeva E.A., Levesque G., Ikeda M., Chi H., Lin C., Li G., Holman K. & et al. (1995) Cloning of a gene bearing missense mutations in early-onset familial Alzheimer's disease. *Nature*, **375,** 754.

40. Van Broeckhoven C., Backhovens H., Cruts M., De Winter G., Bruyland M., Cras P. & Martin J.J. (1992) Mapping of a gene predisposing to early-onset Alzheimer's disease to chromosome 14q24.3. *Nat Genet*, **2,** 335.

41. Levy-Lahad E., Wijsman E.M., Nemens E., Anderson L., Goddard K.A., Weber J.L., Bird T.D. & Schellenberg G.D. (1995) A familial Alzheimer's disease locus on chromosome 1. *Science*, **269,** 970.

42. Levy-Lahad E., Wasco W., Poorkaj P., Romano D.M., Oshima J., Pettingell W.H., Yu C.E., Jondro P.D., Schmidt S.D., Wang K. & et al. (1995) Candidate gene for the chromosome 1 familial Alzheimer's disease locus. *Science*, **269,** 973.

43. Rogaev E.I., Sherrington R., Rogaeva E.A., Levesque G., Ikeda M., Liang Y., Chi H., Lin C., Holman K., Tsuda T. & et al. (1995) Familial Alzheimer's disease in kindreds with missense mutations in a gene on chromosome 1 related to the Alzheimer's disease type 3 gene. *Nature*, **376,** 775.

44. Nussbaum R.L. & Ellis C.E. (2003) Alzheimer's disease and Parkinson's disease. *N Engl J Med*, **348,** 1356.

45. Pericak-Vance M.A., Bebout J.L., Gaskell P.C., Jr., Yamaoka L.H., Hung W.Y., Alberts M.J., Walker A.P., Bartlett R.J., Haynes C.A., Welsh K.A. &

et al. (1991) Linkage studies in familial Alzheimer disease: evidence for chromosome 19 linkage. *Am J Hum Genet*, **48,** 1034.

46. Corder E.H., Saunders A.M., Strittmatter W.J., Schmechel D.E., Gaskell P.C., Small G.W., Roses A.D., Haines J.L. & Pericak-Vance M.A. (1993) Gene dose of apolipoprotein E type 4 allele and the risk of Alzheimer's disease in late onset families. *Science*, **261,** 921.

47. Warwick Daw E., Payami H., Nemens E.J., Nochlin D., Bird T.D., Schellenberg G.D. & Wijsman E.M. (2000) The number of trait loci in late-onset Alzheimer disease. *Am J Hum Genet*, **66,** 196.

48. Sorbi S., Nacmias B., Forleo P., Piacentini S., Latorraca S. & Amaducci L. (1995) Epistatic effect of APP717 mutation and apolipoprotein E genotype in familial Alzheimer's disease. *Ann Neurol*, **38,** 124.

49. Pastor P., Roe C.M., Villegas A., Bedoya G., Chakraverty S., Garcia G., Tirado V., Norton J., Rios S., Martinez M., Kosik K.S., Lopera F. & Goate A.M. (2003) Apolipoprotein Eepsilon4 modifies Alzheimer's disease onset in an E280A PS1 kindred. *Ann Neurol*, **54,** 163.

50. Selkoe D.J. (2001) Alzheimer's disease: genes, proteins, and therapy. *Physiol Rev*, **81,** 741.

51. Bayer T.A., Cappai R., Masters C.L., Beyreuther K. & Multhaup G. (1999) It all sticks together--the APP-related family of proteins and Alzheimer's disease. *Mol Psychiatry*, **4,** 524.

52. Kang J., Lemaire H.G., Unterbeck A., Salbaum J.M., Masters C.L., Grzeschik K.H., Multhaup G., Beyreuther K. & Muller-Hill B. (1987) The precursor of Alzheimer's disease amyloid A4 protein resembles a cell-surface receptor. *Nature*, **325,** 733.

53. Russo C., Salis S., Dolcini V., Venezia V., Song X.H., Teller J.K. & Schettini G. (2001) Amino-terminal modification and tyrosine phosphorylation of [corrected] carboxy-terminal fragments of the amyloid precursor protein in Alzheimer's disease and Down's syndrome brain. *Neurobiol Dis*, **8,** 173.

54. Shioi J., Anderson J.P., Ripellino J.A. & Robakis N.K. (1992) Chondroitin sulfate proteoglycan form of the Alzheimer's beta-amyloid precursor. *J Biol Chem*, **267,** 13819.

55. Shioi J., Refolo L.M., Efthimiopoulos S. & Robakis N.K. (1993) Chondroitin sulfate proteoglycan form of cellular and cell-surface Alzheimer amyloid precursor. *Neurosci Lett*, **154,** 121.

56. Suzuki T., Oishi M., Marshak D.R., Czernik A.J., Nairn A.C. & Greengard P. (1994) Cell cycle-dependent regulation of the phosphorylation and metabolism of the Alzheimer amyloid precursor protein. *Embo J*, **13,** 1114.

57. Thinakaran G., Slunt H.H. & Sisodia S.S. (1995) Novel regulation of chondroitin sulfate glycosaminoglycan modification of amyloid precursor protein and its homologue, APLP2. *J Biol Chem*, **270,** 16522.

58. Chapman P.F., Falinska A.M., Knevett S.G. & Ramsay M.F. (2001) Genes, models and Alzheimer's disease. *Trends Genet*, **17,** 254.

59. Nitsch R.M., Slack B.E., Wurtman R.J. & Growdon J.H. (1992) Release of Alzheimer amyloid precursor derivatives stimulated by activation of muscarinic acetylcholine receptors. *Science*, **258,** 304.

60. Nunan J. & Small D.H. (2000) Regulation of APP cleavage by alpha-, beta- and gamma-secretases. *FEBS Lett*, **483,** 6.

61. Parvathy S., Hussain I., Karran E.H., Turner A.J. & Hooper N.M. (1998) Alzheimer's amyloid precursor protein alpha-secretase is inhibited by hydroxamic acid-based zinc metalloprotease inhibitors: similarities to the angiotensin converting enzyme secretase. *Biochemistry*, **37,** 1680.

62. Parvathy S., Hussain I., Karran E.H., Turner A.J. & Hooper N.M. (1999) Cleavage of Alzheimer's amyloid precursor protein by alpha-secretase occurs at the surface of neuronal cells. *Biochemistry*, **38,** 9728.

63. Hooper N.M., Karran E.H. & Turner A.J. (1997) Membrane protein secretases. *Biochem J*, **321 (Pt 2),** 265.

64. Buxbaum J.D., Liu K.N., Luo Y., Slack J.L., Stocking K.L., Peschon J.J., Johnson R.S., Castner B.J., Cerretti D.P. & Black R.A. (1998) Evidence that tumor necrosis factor alpha converting enzyme is involved in regulated alpha-secretase cleavage of the Alzheimer amyloid protein precursor. *J Biol Chem*, **273,** 27765.

65. Koike H., Tomioka S., Sorimachi H., Saido T.C., Maruyama K., Okuyama A., Fujisawa-Sehara A., Ohno S., Suzuki K. & Ishiura S. (1999) Membrane-anchored metalloprotease MDC9 has an alpha-secretase activity responsible for processing the amyloid precursor protein. *Biochem J*, **343 Pt 2,** 371.

66. Lammich S., Kojro E., Postina R., Gilbert S., Pfeiffer R., Jasionowski M., Haass C. & Fahrenholz F. (1999) Constitutive and regulated alpha-secretase cleavage of Alzheimer's amyloid precursor protein by a disintegrin metalloprotease. *Proc Natl Acad Sci U S A*, **96,** 3922.

67. Skovronsky D.M., Moore D.B., Milla M.E., Doms R.W. & Lee V.M. (2000) Protein kinase C-dependent alpha-secretase competes with beta-secretase for

cleavage of amyloid-beta precursor protein in the trans-golgi network. *J Biol Chem*, **275,** 2568.

68. Colciaghi F., Borroni B., Pastorino L., Marcello E., Zimmermann M., Cattabeni F., Padovani A. & Di Luca M. (2002) [alpha]-Secretase ADAM10 as well as [alpha]APPs is reduced in platelets and CSF of Alzheimer disease patients. *Mol Med*, **8,** 67.

69. Postina R., Schroeder A., Dewachter I., Bohl J., Schmitt U., Kojro E., Prinzen C., Endres K., Hiemke C., Blessing M., Flamez P., Dequenne A., Godaux E., van Leuven F. & Fahrenholz F. (2004) A disintegrin-metalloproteinase prevents amyloid plaque formation and hippocampal defects in an Alzheimer disease mouse model. *J Clin Invest*, **113,** 1456.

70. Hussain I., Powell D., Howlett D.R., Tew D.G., Meek T.D., Chapman C., Gloger I.S., Murphy K.E., Southan C.D., Ryan D.M., Smith T.S., Simmons D.L., Walsh F.S., Dingwall C. & Christie G. (1999) Identification of a novel aspartic protease (Asp 2) as beta-secretase. *Mol Cell Neurosci*, **14,** 419.

71. Lin X., Koelsch G., Wu S., Downs D., Dashti A. & Tang J. (2000) Human aspartic protease memapsin 2 cleaves the beta-secretase site of beta-amyloid precursor protein. *Proc Natl Acad Sci U S A*, **97,** 1456.

72. Sinha S., Anderson J.P., Barbour R., Basi G.S., Caccavello R., Davis D., Doan M., Dovey H.F., Frigon N., Hong J., Jacobson-Croak K., Jewett N., Keim P., Knops J., Lieberburg I., Power M., Tan H., Tatsuno G., Tung J., Schenk D., Seubert P., Suomensaari S.M., Wang S., Walker D., John V. & et al. (1999) Purification and cloning of amyloid precursor protein beta-secretase from human brain. *Nature*, **402,** 537.

73. Vassar R., Bennett B.D., Babu-Khan S., Kahn S., Mendiaz E.A., Denis P., Teplow D.B., Ross S., Amarante P., Loeloff R., Luo Y., Fisher S., Fuller J., Edenson S., Lile J., Jarosinski M.A., Biere A.L., Curran E., Burgess T., Louis J.C., Collins F., Treanor J., Rogers G. & Citron M. (1999) Beta-secretase cleavage of Alzheimer's amyloid precursor protein by the transmembrane aspartic protease BACE. *Science*, **286,** 735.

74. Yan R., Bienkowski M.J., Shuck M.E., Miao H., Tory M.C., Pauley A.M., Brashier J.R., Stratman N.C., Mathews W.R., Buhl A.E., Carter D.B., Tomasselli A.G., Parodi L.A., Heinrikson R.L. & Gurney M.E. (1999) Membrane-anchored aspartyl protease with Alzheimer's disease beta-secretase activity. *Nature*, **402,** 533.

75. Ehehalt R., Keller P., Haass C., Thiele C. & Simons K. (2003) Amyloidogenic processing of the Alzheimer beta-amyloid precursor protein depends on lipid rafts. *J Cell Biol*, **160,** 113.

76. Vassar R. (2001) The beta-secretase, BACE: a prime drug target for Alzheimer's disease. *J Mol Neurosci*, **17,** 157.

77. Cai H., Wang Y., McCarthy D., Wen H., Borchelt D.R., Price D.L. & Wong P.C. (2001) BACE1 is the major beta-secretase for generation of Abeta peptides by neurons. *Nat Neurosci*, **4,** 233.

78. Luo Y., Bolon B., Kahn S., Bennett B.D., Babu-Khan S., Denis P., Fan W., Kha H., Zhang J., Gong Y., Martin L., Louis J.C., Yan Q., Richards W.G., Citron M. & Vassar R. (2001) Mice deficient in BACE1, the Alzheimer's beta-secretase, have normal phenotype and abolished beta-amyloid generation. *Nat Neurosci*, **4,** 231.

79. Gouras G.K., Xu H., Jovanovic J.N., Buxbaum J.D., Wang R., Greengard P., Relkin N.R. & Gandy S. (1998) Generation and regulation of beta-amyloid peptide variants by neurons. *J Neurochem*, **71,** 1920.

80. Bennett B.D., Denis P., Haniu M., Teplow D.B., Kahn S., Louis J.C., Citron M. & Vassar R. (2000) A furin-like convertase mediates propeptide cleavage of BACE, the Alzheimer's beta -secretase. *J Biol Chem*, **275,** 37712.

81. Farzan M., Schnitzler C.E., Vasilieva N., Leung D. & Choe H. (2000) BACE2, a beta -secretase homolog, cleaves at the beta site and within the amyloid-beta region of the amyloid-beta precursor protein. *Proc Natl Acad Sci U S A*, **97,** 9712.

82. Hussain I., Powell D.J., Howlett D.R., Chapman G.A., Gilmour L., Murdock P.R., Tew D.G., Meek T.D., Chapman C., Schneider K., Ratcliffe S.J., Tattersall D., Testa T.T., Southan C., Ryan D.M., Simmons D.L., Walsh F.S., Dingwall C. & Christie G. (2000) ASP1 (BACE2) cleaves the amyloid precursor protein at the beta-secretase site. *Mol Cell Neurosci*, **16,** 609.

83. Sisodia S.S. & St George-Hyslop P.H. (2002) gamma-Secretase, Notch, Abeta and Alzheimer's disease: where do the presenilins fit in? *Nat Rev Neurosci*, **3,** 281.

84. Weihofen A. & Martoglio B. (2003) Intramembrane-cleaving proteases: controlled liberation of proteins and bioactive peptides. *Trends Cell Biol*, **13,** 71.

85. De Strooper B., Annaert W., Cupers P., Saftig P., Craessaerts K., Mumm J.S., Schroeter E.H., Schrijvers V., Wolfe M.S., Ray W.J., Goate A. & Kopan R. (1999) A presenilin-1-dependent gamma-secretase-like protease mediates release of Notch intracellular domain. *Nature*, **398,** 518.

86. Schroeter E.H., Kisslinger J.A. & Kopan R. (1998) Notch-1 signalling requires ligand-induced proteolytic release of intracellular domain. *Nature*, **393,** 382.

87. Huse J.T. & Doms R.W. (2000) Closing in on the amyloid cascade: recent insights into the cell biology of Alzheimer's disease. *Mol Neurobiol*, **22,** 81.

88. Mushegian A. (2002) Refining structural and functional predictions for secretasome components by comparative sequence analysis. *Proteins*, **47,** 69.

89. Thinakaran G., Borchelt D.R., Lee M.K., Slunt H.H., Spitzer L., Kim G., Ratovitsky T., Davenport F., Nordstedt C., Seeger M., Hardy J., Levey A.I., Gandy S.E., Jenkins N.A., Copeland N.G., Price D.L. & Sisodia S.S. (1996) Endoproteolysis of presenilin 1 and accumulation of processed derivatives in vivo. *Neuron*, **17,** 181.

90. Capell A., Grunberg J., Pesold B., Diehlmann A., Citron M., Nixon R., Beyreuther K., Selkoe D.J. & Haass C. (1998) The proteolytic fragments of the Alzheimer's disease-associated presenilin-1 form heterodimers and occur as a 100-150-kDa molecular mass complex. *J Biol Chem*, **273,** 3205.

91. Haass C. & Steiner H. (2002) Alzheimer disease gamma-secretase: a complex story of GxGD-type presenilin proteases. *Trends Cell Biol*, **12,** 556.

92. De Strooper B., Saftig P., Craessaerts K., Vanderstichele H., Guhde G., Annaert W., Von Figura K. & Van Leuven F. (1998) Deficiency of presenilin-1 inhibits the normal cleavage of amyloid precursor protein. *Nature*, **391,** 387.

93. Herreman A., Serneels L., Annaert W., Collen D., Schoonjans L. & De Strooper B. (2000) Total inactivation of gamma-secretase activity in presenilin-deficient embryonic stem cells. *Nat Cell Biol*, **2,** 461.

94. Zhang Z., Nadeau P., Song W., Donoviel D., Yuan M., Bernstein A. & Yankner B.A. (2000) Presenilins are required for gamma-secretase cleavage of beta-APP and transmembrane cleavage of Notch-1. *Nat Cell Biol*, **2,** 463.

95. Esler W.P., Kimberly W.T., Ostaszewski B.L., Diehl T.S., Moore C.L., Tsai J.Y., Rahmati T., Xia W., Selkoe D.J. & Wolfe M.S. (2000) Transition-state analogue inhibitors of gamma-secretase bind directly to presenilin-1. *Nat Cell Biol*, **2,** 428.

96. Li Y.M., Xu M., Lai M.T., Huang Q., Castro J.L., DiMuzio-Mower J., Harrison T., Lellis C., Nadin A., Neduvelil J.G., Register R.B., Sardana M.K., Shearman M.S., Smith A.L., Shi X.P., Yin K.C., Shafer J.A. & Gardell S.J. (2000) Photoactivated gamma-secretase inhibitors directed to the active site covalently label presenilin 1. *Nature*, **405,** 689.

97. Kimberly W.T., LaVoie M.J., Ostaszewski B.L., Ye W., Wolfe M.S. & Selkoe D.J. (2002) Complex N-linked glycosylated nicastrin associates with active gamma-secretase and undergoes tight cellular regulation. *J Biol Chem*, **277,** 35113.

98. Wolfe M.S., Xia W., Ostaszewski B.L., Diehl T.S., Kimberly W.T. & Selkoe D.J. (1999) Two transmembrane aspartates in presenilin-1 required for presenilin endoproteolysis and gamma-secretase activity. *Nature*, **398,** 513.

99. De Strooper B. (2003) Aph-1, Pen-2, and Nicastrin with Presenilin generate an active gamma-Secretase complex. *Neuron*, **38,** 9.

100. Yu G., Nishimura M., Arawaka S., Levitan D., Zhang L., Tandon A., Song Y.Q., Rogaeva E., Chen F., Kawarai T., Supala A., Levesque L., Yu H., Yang D.S., Holmes E., Milman P., Liang Y., Zhang D.M., Xu D.H., Sato C., Rogaev E., Smith M., Janus C., Zhang Y., Aebersold R., Farrer L.S., Sorbi S.,

Bruni A., Fraser P. & St George-Hyslop P. (2000) Nicastrin modulates presenilin-mediated notch/glp-1 signal transduction and betaAPP processing. *Nature*, **407,** 48.

101. Francis R., McGrath G., Zhang J., Ruddy D.A., Sym M., Apfeld J., Nicoll M., Maxwell M., Hai B., Ellis M.C., Parks A.L., Xu W., Li J., Gurney M., Myers R.L., Himes C.S., Hiebsch R., Ruble C., Nye J.S. & Curtis D. (2002) aph-1 and pen-2 are required for Notch pathway signaling, gamma-secretase cleavage of betaAPP, and presenilin protein accumulation. *Dev Cell*, **3,** 85.

102. Edbauer D., Winkler E., Regula J.T., Pesold B., Steiner H. & Haass C. (2003) Reconstitution of gamma-secretase activity. *Nat Cell Biol*, **5,** 486.

103. Weidemann A., Eggert S., Reinhard F.B., Vogel M., Paliga K., Baier G., Masters C.L., Beyreuther K. & Evin G. (2002) A novel epsilon-cleavage within the transmembrane domain of the Alzheimer amyloid precursor protein demonstrates homology with Notch processing. *Biochemistry*, **41,** 2825.

104. Cao X. & Sudhof T.C. (2001) A transcriptionally [correction of transcriptively] active complex of APP with Fe65 and histone acetyltransferase Tip60. *Science*, **293,** 115.

105. Bergman A., Religa D., Karlstrom H., Laudon H., Winblad B., Lannfelt L., Lundkvist J. & Naslund J. (2003) APP intracellular domain formation and unaltered signaling in the presence of familial Alzheimer's disease mutations. *Exp Cell Res*, **287,** 1.

106. Aguzzi A. & Haass C. (2003) Games played by rogue proteins in prion disorders and Alzheimer's disease. *Science*, **302,** 814.

107. Hardy J. & Selkoe D.J. (2002) The amyloid hypothesis of Alzheimer's disease: progress and problems on the road to therapeutics. *Science*, **297,** 353.

108. Citron M., Oltersdorf T., Haass C., McConlogue L., Hung A.Y., Seubert P., Vigo-Pelfrey C., Lieberburg I. & Selkoe D.J. (1992) Mutation of the beta-amyloid precursor protein in familial Alzheimer's disease increases beta-protein production. *Nature*, **360,** 672.

109. Suzuki N., Cheung T.T., Cai X.D., Odaka A., Otvos L., Jr., Eckman C., Golde T.E. & Younkin S.G. (1994) An increased percentage of long amyloid beta protein secreted by familial amyloid beta protein precursor (beta APP717) mutants. *Science*, **264,** 1336.

110. Borchelt D.R., Thinakaran G., Eckman C.B., Lee M.K., Davenport F., Ratovitsky T., Prada C.M., Kim G., Seekins S., Yager D., Slunt H.H., Wang R., Seeger M., Levey A.I., Gandy S.E., Copeland N.G., Jenkins N.A., Price D.L., Younkin S.G. & Sisodia S.S. (1996) Familial Alzheimer's disease-linked presenilin 1 variants elevate Abeta1-42/1-40 ratio in vitro and in vivo. *Neuron*, **17,** 1005.

111. Cummings J.L. (2004) Alzheimer's disease. *N Engl J Med*, **351,** 56.

112. Walsh D.M., Klyubin I., Fadeeva J.V., Rowan M.J. & Selkoe D.J. (2002) Amyloid-beta oligomers: their production, toxicity and therapeutic inhibition. *Biochem Soc Trans*, **30,** 552.

113. Pappolla M.A., Chyan Y.J., Omar R.A., Hsiao K., Perry G., Smith M.A. & Bozner P. (1998) Evidence of oxidative stress and in vivo neurotoxicity of beta-amyloid in a transgenic mouse model of Alzheimer's disease: a chronic oxidative paradigm for testing antioxidant therapies in vivo. *Am J Pathol*, **152,** 871.

114. Quon D., Wang Y., Catalano R., Scardina J.M., Murakami K. & Cordell B. (1991) Formation of beta-amyloid protein deposits in brains of transgenic mice. *Nature*, **352,** 239.

115. Games D., Adams D., Alessandrini R., Barbour R., Berthelette P., Blackwell C., Carr T., Clemens J., Donaldson T., Gillespie F. & et al. (1995) Alzheimer-type neuropathology in transgenic mice overexpressing V717F beta-amyloid precursor protein. *Nature*, **373,** 523.

116. Hsiao K., Chapman P., Nilsen S., Eckman C., Harigaya Y., Younkin S., Yang F. & Cole G. (1996) Correlative memory deficits, Abeta elevation, and amyloid plaques in transgenic mice. *Science*, **274,** 99.

117. Sturchler-Pierrat C., Abramowski D., Duke M., Wiederhold K.H., Mistl C., Rothacher S., Ledermann B., Burki K., Frey P., Paganetti P.A., Waridel C., Calhoun M.E., Jucker M., Probst A., Staufenbiel M. & Sommer B. (1997) Two amyloid precursor protein transgenic mouse models with Alzheimer disease-like pathology. *Proc Natl Acad Sci U S A*, **94,** 13287.

118. Holcomb L., Gordon M.N., McGowan E., Yu X., Benkovic S., Jantzen P., Wright K., Saad I., Mueller R., Morgan D., Sanders S., Zehr C., O'Campo K., Hardy J., Prada C.M., Eckman C., Younkin S., Hsiao K. & Duff K. (1998) Accelerated Alzheimer-type phenotype in transgenic mice carrying both mutant amyloid precursor protein and presenilin 1 transgenes. *Nat Med*, **4,** 97.

119. Chishti M.A., Yang D.S., Janus C., Phinney A.L., Horne P., Pearson J., Strome R., Zuker N., Loukides J., French J., Turner S., Lozza G., Grilli M., Kunicki S., Morissette C., Paquette J., Gervais F., Bergeron C., Fraser P.E., Carlson G.A., George-Hyslop P.S. & Westaway D. (2001) Early-onset amyloid deposition and cognitive deficits in transgenic mice expressing a

double mutant form of amyloid precursor protein 695. *J Biol Chem*, **276,** 21562.

120. Lewis J., McGowan E., Rockwood J., Melrose H., Nacharaju P., Van Slegtenhorst M., Gwinn-Hardy K., Paul Murphy M., Baker M., Yu X., Duff K., Hardy J., Corral A., Lin W.L., Yen S.H., Dickson D.W., Davies P. & Hutton M. (2000) Neurofibrillary tangles, amyotrophy and progressive motor disturbance in mice expressing mutant (P301L) tau protein. *Nat Genet*, **25,** 402.

121. Lewis J., Dickson D.W., Lin W.L., Chisholm L., Corral A., Jones G., Yen S.H., Sahara N., Skipper L., Yager D., Eckman C., Hardy J., Hutton M. & McGowan E. (2001) Enhanced neurofibrillary degeneration in transgenic mice expressing mutant tau and APP. *Science*, **293,** 1487.

122. Calhoun M.E., Wiederhold K.H., Abramowski D., Phinney A.L., Probst A., Sturchler-Pierrat C., Staufenbiel M., Sommer B. & Jucker M. (1998) Neuron loss in APP transgenic mice. *Nature*, **395,** 755.

123. Takeuchi A., Irizarry M.C., Duff K., Saido T.C., Hsiao Ashe K., Hasegawa M., Mann D.M., Hyman B.T. & Iwatsubo T. (2000) Age-related amyloid beta deposition in transgenic mice overexpressing both Alzheimer mutant presenilin 1 and amyloid beta precursor protein Swedish mutant is not associated with global neuronal loss. *Am J Pathol*, **157,** 331.

124. Higgins G.A. & Jacobsen H. (2003) Transgenic mouse models of Alzheimer's disease: phenotype and application. *Behav Pharmacol*, **14,** 419.

125. Avila J., Lucas J.J., Perez M. & Hernandez F. (2004) Role of tau protein in both physiological and pathological conditions. *Physiol Rev*, **84,** 361.

126. Terry R.D. (1998) The cytoskeleton in Alzheimer disease. *J Neural Transm Suppl*, **53,** 141.

127. Hsia A.Y., Masliah E., McConlogue L., Yu G.Q., Tatsuno G., Hu K., Kholodenko D., Malenka R.C., Nicoll R.A. & Mucke L. (1999) Plaque-independent disruption of neural circuits in Alzheimer's disease mouse models. *Proc Natl Acad Sci U S A*, **96,** 3228.

128. Mucke L., Masliah E., Yu G.Q., Mallory M., Rockenstein E.M., Tatsuno G., Hu K., Kholodenko D., Johnson-Wood K. & McConlogue L. (2000) High-level neuronal expression of abeta 1-42 in wild-type human amyloid protein precursor transgenic mice: synaptotoxicity without plaque formation. *J Neurosci*, **20,** 4050.

129. Johnson-Wood K., Lee M., Motter R., Hu K., Gordon G., Barbour R., Khan K., Gordon M., Tan H., Games D., Lieberburg I., Schenk D., Seubert P. & McConlogue L. (1997) Amyloid precursor protein processing and A beta42 deposition in a transgenic mouse model of Alzheimer disease. *Proc Natl Acad Sci U S A*, **94,** 1550.

130. Spillantini M.G., Goedert M., Crowther R.A., Murrell J.R., Farlow M.R. & Ghetti B. (1997) Familial multiple system tauopathy with presenile dementia: a disease with abundant neuronal and glial tau filaments. *Proc Natl Acad Sci U S A*, **94,** 4113.

131. Pericak-Vance M.A. & Haines J.L. (1995) Genetic susceptibility to Alzheimer disease. *Trends Genet*, **11,** 504.

132. Schmechel D.E., Saunders A.M., Strittmatter W.J., Crain B.J., Hulette C.M., Joo S.H., Pericak-Vance M.A., Goldgaber D. & Roses A.D. (1993) Increased amyloid beta-peptide deposition in cerebral cortex as a consequence of apolipoprotein E genotype in late-onset Alzheimer disease. *Proc Natl Acad Sci U S A*, **90,** 9649.

133. Zubenko G.S., Stiffler S., Stabler S., Kopp U., Hughes H.B., Cohen B.M. & Moossy J. (1994) Association of the apolipoprotein E epsilon 4 allele with clinical subtypes of autopsy-confirmed Alzheimer's disease. *Am J Med Genet*, **54,** 199.

134. Gearing M., Schneider J.A., Robbins R.S., Hollister R.D., Mori H., Games D., Hyman B.T. & Mirra S.S. (1995) Regional variation in the distribution of apolipoprotein E and A beta in Alzheimer's disease. *J Neuropathol Exp Neurol*, **54,** 833.

135. Hyman B.T., West H.L., Rebeck G.W., Buldyrev S.V., Mantegna R.N., Ukleja M., Havlin S. & Stanley H.E. (1995) Quantitative analysis of senile plaques in Alzheimer disease: observation of log-normal size distribution and molecular epidemiology of differences associated with apolipoprotein E genotype and trisomy 21 (Down syndrome). *Proc Natl Acad Sci U S A*, **92,** 3586.

136. Nagy Z., Esiri M.M., Jobst K.A., Johnston C., Litchfield S., Sim E. & Smith A.D. (1995) Influence of the apolipoprotein E genotype on amyloid deposition and neurofibrillary tangle formation in Alzheimer's disease. *Neuroscience*, **69,** 757.

137. Polvikoski T., Sulkava R., Haltia M., Kainulainen K., Vuorio A., Verkkoniemi A., Niinisto L., Halonen P. & Kontula K. (1995) Apolipoprotein E, dementia, and cortical deposition of beta-amyloid protein. *N Engl J Med*, **333,** 1242.

138. Gomez-Isla T., West H.L., Rebeck G.W., Harr S.D., Growdon J.H., Locascio J.J., Perls T.T., Lipsitz L.A. & Hyman B.T. (1996) Clinical and pathological

correlates of apolipoprotein E epsilon 4 in Alzheimer's disease. *Ann Neurol*, **39,** 62.

139. Olichney J.M., Hansen L.A., Galasko D., Saitoh T., Hofstetter C.R., Katzman R. & Thal L.J. (1996) The apolipoprotein E epsilon 4 allele is associated with increased neuritic plaques and cerebral amyloid angiopathy in Alzheimer's disease and Lewy body variant. *Neurology*, **47,** 190.

140. Bales K.R., Verina T., Dodel R.C., Du Y., Altstiel L., Bender M., Hyslop P., Johnstone E.M., Little S.P., Cummins D.J., Piccardo P., Ghetti B. & Paul S.M. (1997) Lack of apolipoprotein E dramatically reduces amyloid beta-peptide deposition. *Nat Genet*, **17,** 263.

141. Bales K.R., Verina T., Cummins D.J., Du Y., Dodel R.C., Saura J., Fishman C.E., DeLong C.A., Piccardo P., Petegnief V., Ghetti B. & Paul S.M. (1999) Apolipoprotein E is essential for amyloid deposition in the APP(V717F) transgenic mouse model of Alzheimer's disease. *Proc Natl Acad Sci U S A*, **96,** 15233.

142. Farrer L.A., Cupples L.A., Haines J.L., Hyman B., Kukull W.A., Mayeux R., Myers R.H., Pericak-Vance M.A., Risch N. & van Duijn C.M. (1997) Effects of age, sex, and ethnicity on the association between apolipoprotein E genotype and Alzheimer disease. A meta-analysis. APOE and Alzheimer Disease Meta Analysis Consortium. *JAMA*, **278,** 1349.

143. Kehoe P., Wavrant-De Vrieze F., Crook R., Wu W.S., Holmans P., Fenton I., Spurlock G., Norton N., Williams H., Williams N., Lovestone S., Perez-Tur J., Hutton M., Chartier-Harlin M.C., Shears S., Roehl K., Booth J., Van Voorst W., Ramic D., Williams J., Goate A., Hardy J. & Owen M.J. (1999) A full genome scan for late onset Alzheimer's disease. *Hum Mol Genet*, **8,** 237.

144. Myers A., Holmans P., Marshall H., Kwon J., Meyer D., Ramic D., Shears S., Booth J., DeVrieze F.W., Crook R., Hamshere M., Abraham R., Tunstall N., Rice F., Carty S., Lillystone S., Kehoe P., Rudrasingham V., Jones L., Lovestone S., Perez-Tur J., Williams J., Owen M.J., Hardy J. & Goate A.M. (2000) Susceptibility locus for Alzheimer's disease on chromosome 10. *Science*, **290,** 2304.

145. Myers A., Wavrant De-Vrieze F., Holmans P., Hamshere M., Crook R., Compton D., Marshall H., Meyer D., Shears S., Booth J., Ramic D., Knowles H., Morris J.C., Williams N., Norton N., Abraham R., Kehoe P., Williams H., Rudrasingham V., Rice F., Giles P., Tunstall N., Jones L., Lovestone S., Williams J., Owen M.J., Hardy J. & Goate A. (2002) Full genome screen for Alzheimer disease: stage II analysis. *Am J Med Genet*, **114,** 235.

146. Ertekin-Taner N., Graff-Radford N., Younkin L.H., Eckman C., Baker M., Adamson J., Ronald J., Blangero J., Hutton M. & Younkin S.G. (2000) Linkage of plasma Abeta42 to a quantitative locus on chromosome 10 in late-onset Alzheimer's disease pedigrees. *Science*, **290,** 2303.

147. Wijsman E.M., Daw E.W., Yu C.E., Payami H., Steinbart E.J., Nochlin D., Conlon E.M., Bird T.D. & Schellenberg G.D. (2004) Evidence for a novel late-onset Alzheimer disease locus on chromosome 19p13.2. *Am J Hum Genet*, **75,** 398.

148. Meyer J.M. & Breitner J.C. (1998) Multiple threshold model for the onset of Alzheimer's disease in the NAS-NRC twin panel. *Am J Med Genet*, **81,** 92.

149. Pedersen N.L., Posner S.F. & Gatz M. (2001) Multiple-threshold models for genetic influences on age of onset for Alzheimer disease: findings in Swedish twins. *Am J Med Genet*, **105,** 724.

150. Bertram L., Blacker D., Mullin K., Keeney D., Jones J., Basu S., Yhu S., McInnis M.G., Go R.C., Vekrellis K., Selkoe D.J., Saunders A.J. & Tanzi R.E. (2000) Evidence for genetic linkage of Alzheimer's disease to chromosome 10q. *Science*, **290,** 2302.

151. Li Y.J., Scott W.K., Hedges D.J., Zhang F., Gaskell P.C., Nance M.A., Watts R.L., Hubble J.P., Koller W.C., Pahwa R., Stern M.B., Hiner B.C., Jankovic J., Allen F.A., Jr., Goetz C.G., Mastaglia F., Stajich J.M., Gibson R.A., Middleton L.T., Saunders A.M., Scott B.L., Small G.W., Nicodemus K.K., Reed A.D., Schmechel D.E., Welsh-Bohmer K.A., Conneally P.M., Roses A.D., Gilbert J.R., Vance J.M., Haines J.L. & Pericak-Vance M.A. (2002) Age at onset in two common neurodegenerative diseases is genetically controlled. *Am J Hum Genet*, **70,** 985.

152. Pericak-Vance M.A., Bass M.P., Yamaoka L.H., Gaskell P.C., Scott W.K., Terwedow H.A., Menold M.M., Conneally P.M., Small G.W., Vance J.M., Saunders A.M., Roses A.D. & Haines J.L. (1997) Complete genomic screen in late-onset familial Alzheimer disease. Evidence for a new locus on chromosome 12. *JAMA*, **278,** 1237.

153. Scott W.K., Grubber J.M., Conneally P.M., Small G.W., Hulette C.M., Rosenberg C.K., Saunders A.M., Roses A.D., Haines J.L. & Pericak-Vance M.A. (2000) Fine mapping of the chromosome 12 late-onset Alzheimer disease locus: potential genetic and phenotypic heterogeneity. *Am J Hum Genet*, **66,** 922.

154. Rogaeva E., Premkumar S., Song Y., Sorbi S., Brindle N., Paterson A., Duara R., Levesque G., Yu G., Nishimura M., Ikeda M., O'Toole C., Kawarai T., Jorge R., Vilarino D., Bruni A.C., Farrer L.A. & St George-Hyslop P.H.

(1998) Evidence for an Alzheimer disease susceptibility locus on chromosome 12 and for further locus heterogeneity. *JAMA*, **280,** 614.

155. Wu W.S., Holmans P., Wavrant-DeVrieze F., Shears S., Kehoe P., Crook R., Booth J., Williams N., Perez-Tur J., Roehl K., Fenton I., Chartier-Harlin M.C., Lovestone S., Williams J., Hutton M., Hardy J., Owen M.J. & Goate A. (1998) Genetic studies on chromosome 12 in late-onset Alzheimer disease. *JAMA*, **280,** 619.

156. Myers A.J. & Goate A.M. (2001) The genetics of late-onset Alzheimer's disease. *Curr Opin Neurol*, **14,** 433.

157. Pericak-Vance M.A., Grubber J., Bailey L.R., Hedges D., West S., Santoro L., Kemmerer B., Hall J.L., Saunders A.M., Roses A.D., Small G.W., Scott W.K., Conneally P.M., Vance J.M. & Haines J.L. (2000) Identification of novel genes in late-onset Alzheimer's disease. *Exp Gerontol*, **35,** 1343.

158. Scott W.K., Hauser E.R., Schmechel D.E., Welsh-Bohmer K.A., Small G.W., Roses A.D., Saunders A.M., Gilbert J.R., Vance J.M., Haines J.L. & Pericak-Vance M.A. (2003) Ordered-subsets linkage analysis detects novel Alzheimer disease Loci on chromosomes 2q34 and 15q22. *Am J Hum Genet*, **73,** 1041.

159. Olson J.M., Goddard K.A. & Dudek D.M. (2001) The amyloid precursor protein locus and very-late-onset Alzheimer disease. *Am J Hum Genet*, **69,** 895.

160. Olson J.M., Goddard K.A. & Dudek D.M. (2002) A second locus for very-late-onset Alzheimer disease: a genome scan reveals linkage to 20p and epistasis between 20p and the amyloid precursor protein region. *Am J Hum Genet*, **71,** 154.

161. Blacker D., Bertram L., Saunders A.J., Moscarillo T.J., Albert M.S., Wiener H., Perry R.T., Collins J.S., Harrell L.E., Go R.C., Mahoney A., Beaty T., Fallin M.D., Avramopoulos D., Chase G.A., Folstein M.F., McInnis M.G., Bassett S.S., Doheny K.J., Pugh E.W. & Tanzi R.E. (2003) Results of a high-resolution genome screen of 437 Alzheimer's disease families. *Hum Mol Genet*, **12,** 23.

162. Qiu W.Q., Walsh D.M., Ye Z., Vekrellis K., Zhang J., Podlisny M.B., Rosner M.R., Safavi A., Hersh L.B. & Selkoe D.J. (1998) Insulin-degrading enzyme regulates extracellular levels of amyloid beta-protein by degradation. *J Biol Chem*, **273,** 32730.

163. Edland S.D., Wavrant-De Vriese F., Compton D., Smith G.E., Ivnik R., Boeve B.F., Tangalos E.G. & Petersen R.C. (2003) Insulin degrading enzyme (IDE) genetic variants and risk of Alzheimer's disease: evidence of effect modification by apolipoprotein E (APOE). *Neurosci Lett*, **345,** 21.

164. Prince J.A., Feuk L., Gu H.F., Johansson B., Gatz M., Blennow K. & Brookes A.J. (2003) Genetic variation in a haplotype block spanning IDE influences Alzheimer disease. *Hum Mutat*, **22,** 363.

165. Ertekin-Taner N., Allen M., Fadale D., Scanlin L., Younkin L., Petersen R.C., Graff-Radford N. & Younkin S.G. (2004) Genetic variants in a haplotype block spanning IDE are significantly associated with plasma Abeta42 levels and risk for Alzheimer disease. *Hum Mutat*, **23,** 334.

166. Abraham R., Myers A., Wavrant-DeVrieze F., Hamshere M.L., Thomas H.V., Marshall H., Compton D., Spurlock G., Turic D., Hoogendoorn B., Kwon J.M., Petersen R.C., Tangalos E., Norton J., Morris J.C., Bullock R., Liolitsa D., Lovestone S., Hardy J., Goate A., O'Donovan M., Williams J.,

Owen M.J. & Jones L. (2001) Substantial linkage disequilibrium across the insulin-degrading enzyme locus but no association with late-onset Alzheimer's disease. *Hum Genet*, **109,** 646.

167. Boussaha M., Hannequin D., Verpillat P., Brice A., Frebourg T. & Campion D. (2002) Polymorphisms of insulin degrading enzyme gene are not associated with Alzheimer's disease. *Neurosci Lett*, **329,** 121.

168. Qiu Z., Strickland D.K., Hyman B.T. & Rebeck G.W. (1999) Alpha2-macroglobulin enhances the clearance of endogenous soluble beta-amyloid peptide via low-density lipoprotein receptor-related protein in cortical neurons. *J Neurochem*, **73,** 1393.

169. Blacker D., Wilcox M.A., Laird N.M., Rodes L., Horvath S.M., Go R.C., Perry R., Watson B., Jr., Bassett S.S., McInnis M.G., Albert M.S., Hyman B.T. & Tanzi R.E. (1998) Alpha-2 macroglobulin is genetically associated with Alzheimer disease. *Nat Genet*, **19,** 357.

170. Liao A., Nitsch R.M., Greenberg S.M., Finckh U., Blacker D., Albert M., Rebeck G.W., Gomez-Isla T., Clatworthy A., Binetti G., Hock C., Mueller-Thomsen T., Mann U., Zuchowski K., Beisiegel U., Staehelin H., Growdon J.H., Tanzi R.E. & Hyman B.T. (1998) Genetic association of an alpha2-macroglobulin (Val1000Ile) polymorphism and Alzheimer's disease. *Hum Mol Genet*, **7,** 1953.

171. Dow D.J., Lindsey N., Cairns N.J., Brayne C., Robinson D., Huppert F.A., Paykel E.S., Xuereb J., Wilcock G., Whittaker J.L. & Rubinsztein D.C. (1999) Alpha-2 macroglobulin polymorphism and Alzheimer disease risk in the UK. *Nat Genet*, **22,** 16.

172. Gibson A.M., Singleton A.B., Smith G., Woodward R., McKeith I.G., Perry R.H., Ince P.G., Ballard C.G., Edwardson J.A. & Morris C.M. (2000) Lack of association of the alpha2-macroglobulin locus on chromosome 12 in AD. *Neurology*, **54,** 433.

173. Koster M.N., Dermaut B., Cruts M., Houwing-Duistermaat J.J., Roks G., Tol J., Ott A., Hofman A., Munteanu G., Breteler M.M., van Duijn C.M. & Van Broeckhoven C. (2000) The alpha2-macroglobulin gene in AD: a population-based study and meta-analysis. *Neurology*, **55,** 678.

174. Poduslo S.E., Shook B., Drigalenko E. & Yin X. (2002) Lack of association of the two polymorphisms in alpha-2 macroglobulin with Alzheimer disease. *Am J Med Genet*, **110,** 30.

175. Rogaeva E.A., Premkumar S., Grubber J., Serneels L., Scott W.K., Kawarai T., Song Y., Hill D.L., Abou-Donia S.M., Martin E.R., Vance J.J., Yu G., Orlacchio A., Pei Y., Nishimura M., Supala A., Roberge B., Saunders A.M., Roses A.D., Schmechel D., Crane-Gatherum A., Sorbi S., Bruni A., Small G.W., Pericak-Vance M.A. & et al. (1999) An alpha-2-macroglobulin insertion-deletion polymorphism in Alzheimer disease. *Nat Genet*, **22,** 19.

176. Rudrasingham V., Wavrant-De Vrieze F., Lambert J.C., Chakraverty S., Kehoe P., Crook R., Amouyel P., Wu W., Rice F., Perez-Tur J., Frigard B., Morris J.C., Carty S., Petersen R., Cottel D., Tunstall N., Holmans P., Lovestone S., Chartier-Harlin M.C., Goate A., Hardy J., Owen M.J. & Williams J. (1999) Alpha-2 macroglobulin gene and Alzheimer disease. *Nat Genet*, **22,** 17.

177. Sodeyama N., Yamada M., Itoh Y., Suematsu N., Matsushita M., Otomo E. & Mizusawa H. (2000) Alpha2-macroglobulin polymorphism is not associated with AD or AD-type neuropathology in the Japanese. *Neurology*, **54,** 443.

178. Wavrant-DeVrieze F., Rudrasingham V., Lambert J.C., Chakraverty S., Kehoe P., Crook R., Amouyel P., Wu W., Holmans P., Rice F., Perez-Tur J., Frigard B., Morris J.C., Carty S., Cottel D., Tunstall N., Lovestone S., Petersen R.C., Chartier-Harlin M.C., Goate A., Owen M.J., Williams J. & Hardy J. (1999) No association between the alpha-2 macroglobulin I1000V polymorphism and Alzheimer's disease. *Neurosci Lett*, **262,** 137.

179. Morton N.E. & Collins A. (1998) Tests and estimates of allelic association in complex inheritance. *Proc Natl Acad Sci U S A*, **95,** 11389.

180. Pritchard J.K. & Przeworski M. (2001) Linkage disequilibrium in humans: models and data. *Am J Hum Genet*, **69,** 1.

181. Kruglyak L. (1999) Prospects for whole-genome linkage disequilibrium mapping of common disease genes. *Nat Genet*, **22,** 139.

182. Mirra S.S., Heyman A., McKeel D., Sumi S.M., Crain B.J., Brownlee L.M., Vogel F.S., Hughes J.P., van Belle G. & Berg L. (1991) The Consortium to Establish a Registry for Alzheimer's Disease (CERAD). Part II. Standardization of the neuropathologic assessment of Alzheimer's disease. *Neurology*, **41,** 479.

183. Holmes C., Cairns N., Lantos P. & Mann A. (1999) Validity of current clinical criteria for Alzheimer's disease, vascular dementia and dementia with Lewy bodies. *Br J Psychiatry*, **174,** 45.

184. Roth M., Tym E., Mountjoy C.Q., Huppert F.A., Hendrie H., Verma S. & Goddard R. (1986) CAMDEX. A standardised instrument for the diagnosis of mental disorder in the elderly with special reference to the early detection of dementia. *Br J Psychiatry*, **149,** 698.

185. Bucks R.S., Ashworth D.L., Wilcock G.K. & Siegfried K. (1996) Assessment of activities of daily living in dementia: development of the Bristol Activities of Daily Living Scale. *Age Ageing*, **25,** 113.

186. Reisberg B., Borenstein J., Salob S.P., Ferris S.H., Franssen E. & Georgotas A. (1987) Behavioral symptoms in Alzheimer's disease: phenomenology and treatment. *J Clin Psychiatry*, **48 Suppl,** 9.

187. Webster D.D. (1968) Critical analysis of the disability in Parkinson's disease. *Mod Treat*, **5,** 257.

188. Alexopoulos G.S., Abrams R.C., Young R.C. & Shamoian C.A. (1988) Cornell Scale for Depression in Dementia. *Biol Psychiatry*, **23,** 271.

189. Cummings J.L. (1997) The Neuropsychiatric Inventory: assessing psychopathology in dementia patients. *Neurology*, **48,** S10.

190. Sheikh J.I. & Yesavage J.A. (1986) Geriatric Depression Scale (GDS): Recent evidence and development of a shorter version. In: *Clinical Gerontology: A Guide to Assessment and Intervention* (ed. T. L. Brink), p. 165. Haworth Press.

191. Sanger F., Nicklen S. & Coulson A.R. (1977) DNA sequencing with chain-terminating inhibitors. *Proc Natl Acad Sci U S A*, **74,** 5463.

192. Norton N., Williams N.M., Williams H.J., Spurlock G., Kirov G., Morris D.W., Hoogendoorn B., Owen M.J. & O'Donovan M.C. (2002) Universal,

robust, highly quantitative SNP allele frequency measurement in DNA pools. *Hum Genet*, **110**, 471.

193. Liu Q., Thorland E.C. & Sommer S.S. (1997) Inhibition of PCR amplification by a point mutation downstream of a primer. *Biotechniques*, **22**, 292.

194. Haff L.A. & Smirnov I.P. (1997) Single-nucleotide polymorphism identification assays using a thermostable DNA polymerase and delayed extraction MALDI-TOF mass spectrometry. *Genome Res*, **7**, 378.

195. Hoogendoorn B., Norton N., Kirov G., Williams N., Hamshere M.L., Spurlock G., Austin J., Stephens M.K., Buckland P.R., Owen M.J. & O'Donovan M.C. (2000) Cheap, accurate and rapid allele frequency estimation of single nucleotide polymorphisms by primer extension and DHPLC in DNA pools. *Hum Genet*, **107**, 488.

196. Bray N.J., Buckland P.R., Owen M.J. & O'Donovan M.C. (2003) Cis-acting variation in the expression of a high proportion of genes in human brain. *Hum Genet*, **113**, 149.

197. Zhao J.H., Curtis D. & Sham P.C. (2000) Model-free analysis and permutation tests for allelic associations. *Hum Hered*, **50**, 133.

198. Berrard S., Varoqui H., Cervini R., Israel M., Mallet J. & Diebler M.F. (1995) Coregulation of two embedded gene products, choline acetyltransferase and the vesicular acetylcholine transporter. *J Neurochem*, **65**, 939.

199. Berse B. & Blusztajn J.K. (1995) Coordinated up-regulation of choline acetyltransferase and vesicular acetylcholine transporter gene expression by the retinoic acid receptor alpha, cAMP, and leukemia inhibitory factor/ciliary

neurotrophic factor signaling pathways in a murine septal cell line. *J Biol Chem*, **270,** 22101.

200. Berse B. & Blusztajn J.K. (1997) Modulation of cholinergic locus expression by glucocorticoids and retinoic acid is cell-type specific. *FEBS Lett*, **410,** 175.

201. Misawa H., Takahashi R. & Deguchi T. (1995) Coordinate expression of vesicular acetylcholine transporter and choline acetyltransferase in sympathetic superior cervical neurones. *Neuroreport*, **6,** 965.

202. Tian X., Sun X. & Suszkiw J.B. (1996) Developmental age-dependent upregulation of choline acetyltransferase and vesicular acetylcholine transporter mRNA expression in neonatal rat septum by nerve growth factor. *Neurosci Lett*, **209,** 134.

203. Shimojo M., Wu D. & Hersh L.B. (1998) The cholinergic gene locus is coordinately regulated by protein kinase A II in PC12 cells. *J Neurochem*, **71,** 1118.

204. Oosawa H., Fujii T. & Kawashima K. (1999) Nerve growth factor increases the synthesis and release of acetylcholine and the expression of vesicular acetylcholine transporter in primary cultured rat embryonic septal cells. *J Neurosci Res*, **57,** 381.

205. Misawa H., Matsuura J., Oda Y., Takahashi R. & Deguchi T. (1997) Human choline acetyltransferase mRNAs with different 5'-region produce a 69-kDa major translation product. *Brain Res Mol Brain Res*, **44,** 323.

206. Ohno K., Tsujino A., Brengman J.M., Harper C.M., Bajzer Z., Udd B., Beyring R., Robb S., Kirkham F.J. & Engel A.G. (2001) Choline acetyltransferase mutations cause myasthenic syndrome associated with episodic apnea in humans. *Proc Natl Acad Sci U S A*, **98,** 2017.

207. Pahud G., Salem N., van de Goor J., Medilanski J., Pellegrinelli N. & Eder-Colli L. (1998) Study of subcellular localization of membrane-bound choline acetyltransferase in Drosophila central nervous system and its association with membranes. *Eur J Neurosci*, **10,** 1644.

208. Resendes M.C., Dobransky T., Ferguson S.S. & Rylett R.J. (1999) Nuclear localization of the 82-kDa form of human choline acetyltransferase. *J Biol Chem*, **274,** 19417.

209. Gill S.K., Bhattacharya M., Ferguson S.S. & Rylett R.J. (2003) Identification of a novel nuclear localization signal common to 69- and 82-kDa human choline acetyltransferase. *J Biol Chem*, **278,** 20217.

210. Gilmor M.L., Nash N.R., Roghani A., Edwards R.H., Yi H., Hersch S.M. & Levey A.I. (1996) Expression of the putative vesicular acetylcholine transporter in rat brain and localization in cholinergic synaptic vesicles. *J Neurosci*, **16,** 2179.

211. Weihe E., Tao-Cheng J.H., Schafer M.K., Erickson J.D. & Eiden L.E. (1996) Visualization of the vesicular acetylcholine transporter in cholinergic nerve terminals and its targeting to a specific population of small synaptic vesicles. *Proc Natl Acad Sci U S A*, **93,** 3547.

212. Karczmar A.G. (1993) Brief presentation of the story and present status of studies of the vertebrate cholinergic system. *Neuropsychopharmacology*, **9,** 181.

213. Oda Y. (1999) Choline acetyltransferase: the structure, distribution and pathologic changes in the central nervous system. *Pathol Int*, **49,** 921.

214. Perry E., Walker M., Grace J. & Perry R. (1999) Acetylcholine in mind: a neurotransmitter correlate of consciousness? *Trends Neurosci*, **22,** 273.

215. Bartus R.T., Dean R.L., 3rd, Beer B. & Lippa A.S. (1982) The cholinergic hypothesis of geriatric memory dysfunction. *Science*, **217,** 408.

216. Drachman D.A. & Leavitt J. (1974) Human memory and the cholinergic system. A relationship to aging? *Arch Neurol*, **30,** 113.

217. Aigner T.G. & Mishkin M. (1986) The effects of physostigmine and scopolamine on recognition memory in monkeys. *Behav Neural Biol*, **45,** 81.

218. Aigner T.G., Mitchell S.J., Aggleton J.P., DeLong M.R., Struble R.G., Price D.L., Wenk G.L., Pettigrew K.D. & Mishkin M. (1991) Transient impairment of recognition memory following ibotenic-acid lesions of the basal forebrain in macaques. *Exp Brain Res*, **86,** 18.

219. Fibiger H.C., Damsma G. & Day J.C. (1991) Behavioral pharmacology and biochemistry of central cholinergic neurotransmission. *Adv Exp Med Biol*, **295,** 399.

220. Miller E.K. & Desimone R. (1993) Scopolamine affects short-term memory but not inferior temporal neurons. *Neuroreport*, **4,** 81.

221. Bowen D.M., Smith C.B., White P. & Davison A.N. (1976) Neurotransmitter-related enzymes and indices of hypoxia in senile dementia and other abiotrophies. *Brain*, **99,** 459.

222. Davies P. & Maloney A.J. (1976) Selective loss of central cholinergic neurons in Alzheimer's disease. *Lancet*, **2,** 1403.

223. Perry E.K., Perry R.H., Blessed G. & Tomlinson B.E. (1977) Necropsy evidence of central cholinergic deficits in senile dementia. *Lancet*, **1,** 189.

224. Henke H. & Lang W. (1983) Cholinergic enzymes in neocortex, hippocampus and basal forebrain of non-neurological and senile dementia of Alzheimer-type patients. *Brain Res*, **267,** 281.

225. Bird T.D., Stranahan S., Sumi S.M. & Raskind M. (1983) Alzheimer's disease: choline acetyltransferase activity in brain tissue from clinical and pathological subgroups. *Ann Neurol*, **14,** 284.

226. Etienne P., Robitaille Y., Wood P., Gauthier S., Nair N.P. & Quirion R. (1986) Nucleus basalis neuronal loss, neuritic plaques and choline acetyltransferase activity in advanced Alzheimer's disease. *Neuroscience*, **19,** 1279.

227. Cullen K.M. & Halliday G.M. (1998) Neurofibrillary degeneration and cell loss in the nucleus basalis in comparison to cortical Alzheimer pathology. *Neurobiol Aging*, **19,** 297.

228. Coyle J.T., Price D.L. & DeLong M.R. (1983) Alzheimer's disease: a disorder of cortical cholinergic innervation. *Science*, **219,** 1184.

229. Perry E.K., Tomlinson B.E., Blessed G., Bergmann K., Gibson P.H. & Perry R.H. (1978) Correlation of cholinergic abnormalities with senile plaques and mental test scores in senile dementia. *Br Med J*, **2,** 1457.

230. Jhamandas J.H., Cho C., Jassar B., Harris K., MacTavish D. & Easaw J. (2001) Cellular mechanisms for amyloid beta-protein activation of rat cholinergic basal forebrain neurons. *J Neurophysiol*, **86,** 1312.

231. Samuel W., Alford M., Hofstetter C.R. & Hansen L. (1997) Dementia with Lewy bodies versus pure Alzheimer disease: differences in cognition, neuropathology, cholinergic dysfunction, and synapse density. *J Neuropathol Exp Neurol*, **56,** 499.

232. Wilcock G.K., Esiri M.M., Bowen D.M. & Smith C.C. (1982) Alzheimer's disease. Correlation of cortical choline acetyltransferase activity with the severity of dementia and histological abnormalities. *J Neurol Sci*, **57,** 407.

233. Bierer L.M., Haroutunian V., Gabriel S., Knott P.J., Carlin L.S., Purohit D.P., Perl D.P., Schmeidler J., Kanof P. & Davis K.L. (1995) Neurochemical correlates of dementia severity in Alzheimer's disease: relative importance of the cholinergic deficits. *J Neurochem*, **64,** 749.

234. Gauthier S. (1999) Acetylcholinesterase inhibitors in the treatment of Alzheimer's disease. *Expert Opin Investig Drugs*, **8,** 1511.

235. Gauthier S. (2002) Advances in the pharmacotherapy of Alzheimer's disease. *Cmaj*, **166,** 616.

236. Davis K.L., Mohs R.C., Marin D., Purohit D.P., Perl D.P., Lantz M., Austin G. & Haroutunian V. (1999) Cholinergic markers in elderly patients with early signs of Alzheimer disease. *JAMA*, **281,** 1401.

237. DeKosky S.T., Ikonomovic M.D., Styren S.D., Beckett L., Wisniewski S., Bennett D.A., Cochran E.J., Kordower J.H. & Mufson E.J. (2002) Upregulation of choline acetyltransferase activity in hippocampus and frontal cortex of elderly subjects with mild cognitive impairment. *Ann Neurol*, **51,** 145.

238. Quirion R. (1993) Cholinergic markers in Alzheimer disease and the autoregulation of acetylcholine release. *J Psychiatry Neurosci*, **18,** 226.

239. Court J.A., Martin-Ruiz C., Graham A. & Perry E. (2000) Nicotinic receptors in human brain: topography and pathology. *J Chem Neuroanat*, **20,** 281.

240. Paterson D. & Nordberg A. (2000) Neuronal nicotinic receptors in the human brain. *Prog Neurobiol*, **61,** 75.

241. Nordberg A. (2001) Nicotinic receptor abnormalities of Alzheimer's disease: therapeutic implications. *Biol Psychiatry*, **49,** 200.

242. Alkondon M., Pereira E.F., Barbosa C.T. & Albuquerque E.X. (1997) Neuronal nicotinic acetylcholine receptor activation modulates gamma-aminobutyric acid release from CA1 neurons of rat hippocampal slices. *J Pharmacol Exp Ther*, **283,** 1396.

243. Mansvelder H.D. & McGehee D.S. (2000) Long-term potentiation of excitatory inputs to brain reward areas by nicotine. *Neuron*, **27,** 349.

244. Ji D., Lape R. & Dani J.A. (2001) Timing and location of nicotinic activity enhances or depresses hippocampal synaptic plasticity. *Neuron*, **31,** 131.

245. Levin E.D. & Simon B.B. (1998) Nicotinic acetylcholine involvement in cognitive function in animals. *Psychopharmacology (Berl)*, **138,** 217.

246. Jones S., Sudweeks S. & Yakel J.L. (1999) Nicotinic receptors in the brain: correlating physiology with function. *Trends Neurosci*, **22,** 555.

247. Wang H.Y., Lee D.H., Davis C.B. & Shank R.P. (2000) Amyloid peptide Abeta(1-42) binds selectively and with picomolar affinity to alpha7 nicotinic acetylcholine receptors. *J Neurochem*, **75,** 1155.

248. Liu Q., Kawai H. & Berg D.K. (2001) beta -Amyloid peptide blocks the response of alpha 7-containing nicotinic receptors on hippocampal neurons. *Proc Natl Acad Sci U S A*, **98,** 4734.

249. Nordberg A. (1992) Neuroreceptor changes in Alzheimer disease. *Cerebrovasc Brain Metab Rev*, **4,** 303.

250. Pavia J., de Ceballos M.L. & Sanchez de la Cuesta F. (1998) Alzheimer's disease: relationship between muscarinic cholinergic receptors, beta-amyloid and tau proteins. *Fundam Clin Pharmacol*, **12,** 473.

251. Warpman U., Alafuzoff I. & Nordberg A. (1993) Coupling of muscarinic receptors to GTP proteins in postmortem human brain--alterations in Alzheimer's disease. *Neurosci Lett*, **150,** 39.

252. Ladner C.J. & Lee J.M. (1998) Pharmacological drug treatment of Alzheimer disease: the cholinergic hypothesis revisited. *J Neuropathol Exp Neurol*, **57,** 719.

253. Beach T.G., Kuo Y.M., Spiegel K., Emmerling M.R., Sue L.I., Kokjohn K. & Roher A.E. (2000) The cholinergic deficit coincides with Abeta deposition at the earliest histopathologic stages of Alzheimer disease. *J Neuropathol Exp Neurol*, **59,** 308.

254. Fisher A., Brandeis R., Bar-Ner R.H., Kliger-Spatz M., Natan N., Sonego H., Marcovitch I. & Pittel Z. (2002) AF150(S) and AF267B: M1 muscarinic agonists as innovative therapies for Alzheimer's disease. *J Mol Neurosci*, **19,** 145.

255. Lin L., Georgievska B., Mattsson A. & Isacson O. (1999) Cognitive changes and modified processing of amyloid precursor protein in the cortical and hippocampal system after cholinergic synapse loss and muscarinic receptor activation. *Proc Natl Acad Sci U S A*, **96,** 12108.

256. Muller D.M., Mendla K., Farber S.A. & Nitsch R.M. (1997) Muscarinic M1 receptor agonists increase the secretion of the amyloid precursor protein ectodomain. *Life Sci*, **60,** 985.

257. Sadot E., Gurwitz D., Barg J., Behar L., Ginzburg I. & Fisher A. (1996) Activation of m1 muscarinic acetylcholine receptor regulates tau phosphorylation in transfected PC12 cells. *J Neurochem*, **66,** 877.

258. Genis I., Fisher A. & Michaelson D.M. (1999) Site-specific dephosphorylation of tau of apolipoprotein E-deficient and control mice by M1 muscarinic agonist treatment. *J Neurochem*, **72,** 206.

259. Kar S., Seto D., Gaudreau P. & Quirion R. (1996) Beta-amyloid-related peptides inhibit potassium-evoked acetylcholine release from rat hippocampal slices. *J Neurosci*, **16,** 1034.

260. Kar S., Issa A.M., Seto D., Auld D.S., Collier B. & Quirion R. (1998) Amyloid beta-peptide inhibits high-affinity choline uptake and acetylcholine release in rat hippocampal slices. *J Neurochem*, **70,** 2179.

261. Hoshi M., Takashima A., Murayama M., Yasutake K., Yoshida N., Ishiguro K., Hoshino T. & Imahori K. (1997) Nontoxic amyloid beta peptide 1-42 suppresses acetylcholine synthesis. Possible role in cholinergic dysfunction in Alzheimer's disease. *J Biol Chem*, **272,** 2038.

262. Wang H.Y., Wild K.D., Shank R.P. & Lee D.H. (1999) Galanin inhibits acetylcholine release from rat cerebral cortex via a pertussis toxin-sensitive G(i)protein. *Neuropeptides*, **33,** 197.

263. Kristofikova Z., Tejkalova H. & Klaschka J. (2001) Amyloid beta peptide 1-40 and the function of rat hippocampal hemicholinium-3 sensitive choline carriers: effects of a proteolytic degradation in vitro. *Neurochem Res*, **26,** 203.

264. Vaucher E., Aumont N., Pearson D., Rowe W., Poirier J. & Kar S. (2001) Amyloid beta peptide levels and its effects on hippocampal acetylcholine release in aged, cognitively-impaired and -unimpaired rats. *J Chem Neuroanat*, **21,** 323.

265. Korsching S., Auburger G., Heumann R., Scott J. & Thoenen H. (1985) Levels of nerve growth factor and its mRNA in the central nervous system of the rat correlate with cholinergic innervation. *Embo J*, **4,** 1389.

266. Whittemore S.R., Ebendal T., Larkfors L., Olson L., Seiger A., Stromberg I. & Persson H. (1986) Development and regional expression of beta nerve growth factor messenger RNA and protein in the rat central nervous system. *Proc Natl Acad Sci U S A*, **83,** 817.

267. Whittemore S.R., Friedman P.L., Larhammar D., Persson H., Gonzalez-Carvajal M. & Holets V.R. (1988) Rat beta-nerve growth factor sequence and site of synthesis in the adult hippocampus. *J Neurosci Res*, **20,** 403.

268. Conner J.M., Muir D., Varon S., Hagg T. & Manthorpe M. (1992) The localization of nerve growth factor-like immunoreactivity in the adult rat basal forebrain and hippocampal formation. *J Comp Neurol*, **319,** 454.

269. Capsoni S., Ugolini G., Comparini A., Ruberti F., Berardi N. & Cattaneo A. (2000) Alzheimer-like neurodegeneration in aged antinerve growth factor transgenic mice. *Proc Natl Acad Sci U S A*, **97,** 6826.

270. Mufson E.J., Kroin J.S., Liu Y.T., Sobreviela T., Penn R.D., Miller J.A. & Kordower J.H. (1996) Intrastriatal and intraventricular infusion of brain-derived neurotrophic factor in the cynomologous monkey: distribution, retrograde transport and co-localization with substantia nigra dopamine-containing neurons. *Neuroscience*, **71,** 179.

271. Mufson E.J., Lavine N., Jaffar S., Kordower J.H., Quirion R. & Saragovi H.U. (1997) Reduction in p140-TrkA receptor protein within the nucleus basalis and cortex in Alzheimer's disease. *Exp Neurol*, **146,** 91.

272. Salehi A., Verhaagen J. & Swaab D.F. (1998) Neurotrophin receptors in Alzheimer's disease. *Prog Brain Res*, **117,** 71.

273. Goedert M., Fine A., Hunt S.P. & Ullrich A. (1986) Nerve growth factor mRNA in peripheral and central rat tissues and in the human central nervous system: lesion effects in the rat brain and levels in Alzheimer's disease. *Brain Res*, **387,** 85.

274. Crutcher K.A., Scott S.A., Liang S., Everson W.V. & Weingartner J. (1993) Detection of NGF-like activity in human brain tissue: increased levels in Alzheimer's disease. *J Neurosci*, **13,** 2540.

275. Murase K., Nabeshima T., Robitaille Y., Quirion R., Ogawa M. & Hayashi K. (1993) NGF level of is not decreased in the serum, brain-spinal fluid, hippocampus, or parietal cortex of individuals with Alzheimer's disease. *Biochem Biophys Res Commun*, **193,** 198.

276. Scott S.A., Mufson E.J., Weingartner J.A., Skau K.A. & Crutcher K.A. (1995) Nerve growth factor in Alzheimer's disease: increased levels throughout the brain coupled with declines in nucleus basalis. *J Neurosci*, **15,** 6213.

277. Hellweg R., Gericke C.A., Jendroska K., Hartung H.D. & Cervos-Navarro J. (1998) NGF content in the cerebral cortex of non-demented patients with amyloid-plaques and in symptomatic Alzheimer's disease. *Int J Dev Neurosci*, **16,** 787.

278. Hock C., Heese K., Muller-Spahn F., Hulette C., Rosenberg C. & Otten U. (1998) Decreased trkA neurotrophin receptor expression in the parietal cortex of patients with Alzheimer's disease. *Neurosci Lett*, **241,** 151.

279. Mufson E.J., Conner J.M., Varon S. & Kordower J.H. (1994) Nerve growth factor-like immunoreactive profiles in the primate basal forebrain and hippocampal formation. *J Comp Neurol*, **341,** 507.

280. Mufson E.J., Conner J.M. & Kordower J.H. (1995) Nerve growth factor in Alzheimer's disease: defective retrograde transport to nucleus basalis. *Neuroreport*, **6,** 1063.

281. Sham P.C. & Curtis D. (1995) Monte Carlo tests for associations between disease and alleles at highly polymorphic loci. *Ann Hum Genet*, **59 (Pt 1),** 97.

282. Mubumbila V., Sutter A., Ptok U., Heun R. & Quirin-Stricker C. (2002) Identification of a single nucleotide polymorphism in the choline acetyltransferase gene associated with Alzheimer's disease. *Neurosci Lett*, **333,** 9.

283. Schwarz S., Eisele T., Diehl J., Muller U., Forstl H., Kurz A. & Riemenschneider M. (2003) Lack of association between a single nucleotide polymorphism within the choline acetyltransferase gene and patients with Alzheimer's disease. *Neurosci Lett*, **343,** 167.

284. Klegeris A. & McGeer P.L. (2002) Cyclooxygenase and 5-lipoxygenase inhibitors protect against mononuclear phagocyte neurotoxicity. *Neurobiol Aging*, **23,** 787.

285. Hoshiko S., Radmark O. & Samuelsson B. (1990) Characterization of the human 5-lipoxygenase gene promoter. *Proc Natl Acad Sci U S A*, **87,** 9073.

286. Lammers C.H., Schweitzer P., Facchinetti P., Arrang J.M., Madamba S.G., Siggins G.R. & Piomelli D. (1996) Arachidonate 5-lipoxygenase and its

activating protein: prominent hippocampal expression and role in somatostatin signaling. *J Neurochem*, **66,** 147.

287. Uz T., Pesold C., Longone P. & Manev H. (1998) Aging-associated up-regulation of neuronal 5-lipoxygenase expression: putative role in neuronal vulnerability. *Faseb J*, **12,** 439.

288. Manev H., Uz T. & Qu T. (1998) Early Upregulation of Hippocampal 5-lipoxygenase Following Systemic Administration of Kainate to Rats. *Restor Neurol Neurosci*, **12,** 81.

289. Lu M.C., Peters-Golden M., Hostetler D.E., Robinson N.E. & Derksen F.J. (1996) Age-related enhancement of 5-lipoxygenase metabolic capacity in cattle alveolar macrophages. *Am J Physiol*, **271,** L547.

290. Meydani S.N. & Hayek M.G. (1995) Vitamin E and aging immune response. *Clin Geriatr Med*, **11,** 567.

291. Breitner J.C. (1996) Inflammatory processes and antiinflammatory drugs in Alzheimer's disease: a current appraisal. *Neurobiol Aging*, **17,** 789.

292. McGeer P.L. & McGeer E.G. (1995) The inflammatory response system of brain: implications for therapy of Alzheimer and other neurodegenerative diseases. *Brain Res Brain Res Rev*, **21,** 195.

293. McGeer P.L., Schulzer M. & McGeer E.G. (1996) Arthritis and anti-inflammatory agents as possible protective factors for Alzheimer's disease: a review of 17 epidemiologic studies. *Neurology*, **47,** 425.

294. in t' Veld B.A., Ruitenberg A., Hofman A., Launer L.J., van Duijn C.M., Stijnen T., Breteler M.M. & Stricker B.H. (2001) Nonsteroidal antiinflammatory drugs and the risk of Alzheimer's disease. *N Engl J Med*, **345,** 1515.

295. Stewart W.F., Kawas C., Corrada M. & Metter E.J. (1997) Risk of Alzheimer's disease and duration of NSAID use. *Neurology*, **48,** 626.

296. Zandi P.P., Anthony J.C., Hayden K.M., Mehta K., Mayer L. & Breitner J.C. (2002) Reduced incidence of AD with NSAID but not H2 receptor antagonists: the Cache County Study. *Neurology*, **59,** 880.

297. Glinka A., Wu W., Delius H., Monaghan A.P., Blumenstock C. & Niehrs C. (1998) Dickkopf-1 is a member of a new family of secreted proteins and functions in head induction. *Nature*, **391,** 357.

298. Krupnik V.E., Sharp J.D., Jiang C., Robison K., Chickering T.W., Amaravadi L., Brown D.E., Guyot D., Mays G., Leiby K., Chang B., Duong T., Goodearl A.D., Gearing D.P., Sokol S.Y. & McCarthy S.A. (1999) Functional and structural diversity of the human Dickkopf gene family. *Gene*, **238,** 301.

299. Bhanot P., Brink M., Samos C.H., Hsieh J.C., Wang Y., Macke J.P., Andrew D., Nathans J. & Nusse R. (1996) A new member of the frizzled family from Drosophila functions as a Wingless receptor. *Nature*, **382,** 225.

300. Mao J., Wang J., Liu B., Pan W., Farr G.H., 3rd, Flynn C., Yuan H., Takada S., Kimelman D., Li L. & Wu D. (2001) Low-density lipoprotein receptor-related protein-5 binds to Axin and regulates the canonical Wnt signaling pathway. *Mol Cell*, **7,** 801.

301. Pinson K.I., Brennan J., Monkley S., Avery B.J. & Skarnes W.C. (2000) An LDL-receptor-related protein mediates Wnt signalling in mice. *Nature*, **407,** 535.

302. Semenov M.V., Tamai K., Brott B.K., Kuhl M., Sokol S. & He X. (2001) Head inducer Dickkopf-1 is a ligand for Wnt coreceptor LRP6. *Curr Biol*, **11,** 951.

303. Wehrli M., Dougan S.T., Caldwell K., O'Keefe L., Schwartz S., Vaizel-Ohayon D., Schejter E., Tomlinson A. & DiNardo S. (2000) arrow encodes an LDL-receptor-related protein essential for Wingless signalling. *Nature*, **407,** 527.

304. Huelsken J. & Birchmeier W. (2001) New aspects of Wnt signaling pathways in higher vertebrates. *Curr Opin Genet Dev*, **11,** 547.

305. Kikuchi A. (2000) Regulation of beta-catenin signaling in the Wnt pathway. *Biochem Biophys Res Commun*, **268,** 243.

306. Doble B.W. & Woodgett J.R. (2003) GSK-3: tricks of the trade for a multi-tasking kinase. *J Cell Sci*, **116,** 1175.

307. Mao B., Wu W., Li Y., Hoppe D., Stannek P., Glinka A. & Niehrs C. (2001) LDL-receptor-related protein 6 is a receptor for Dickkopf proteins. *Nature*, **411,** 321.

308. Nakamura T., Aoki S., Kitajima K., Takahashi T. & Matsumoto K. (2001) Molecular cloning and characterization of Kremen, a novel kringle-containing transmembrane protein. *Biochim Biophys Acta*, **1518,** 63.

309. Mao B., Wu W., Davidson G., Marhold J., Li M., Mechler B.M., Delius H., Hoppe D., Stannek P., Walter C., Glinka A. & Niehrs C. (2002) Kremen proteins are Dickkopf receptors that regulate Wnt/beta-catenin signalling. *Nature*, **417,** 664.

310. Takashima A., Honda T., Yasutake K., Michel G., Murayama O., Murayama M., Ishiguro K. & Yamaguchi H. (1998) Activation of tau protein kinase I/glycogen synthase kinase-3beta by amyloid beta peptide (25-35) enhances phosphorylation of tau in hippocampal neurons. *Neurosci Res*, **31,** 317.

311. De Strooper B. & Annaert W. (2001) Where Notch and Wnt signaling meet. The presenilin hub. *J Cell Biol*, **152,** F17.

312. Ciechanover A. (1998) The ubiquitin-proteasome pathway: on protein death and cell life. *Embo J*, **17,** 7151.

313. Mori H., Kondo J. & Ihara Y. (1987) Ubiquitin is a component of paired helical filaments in Alzheimer's disease. *Science*, **235,** 1641.

314. Kamura T., Sato S., Iwai K., Czyzyk-Krzeska M., Conaway R.C. & Conaway J.W. (2000) Activation of HIF1alpha ubiquitination by a reconstituted von Hippel-Lindau (VHL) tumor suppressor complex. *Proc Natl Acad Sci U S A*, **97,** 10430.

315. Gehrke S.G., Riedel H.D., Herrmann T., Hadaschik B., Bents K., Veltkamp C. & Stremmel W. (2003) UbcH5A, a member of human E2 ubiquitin-conjugating enzymes, is closely related to SFT, a stimulator of iron transport, and is up-regulated in hereditary hemochromatosis. *Blood*, **101,** 3288.

316. Bukau B. & Horwich A.L. (1998) The Hsp70 and Hsp60 chaperone machines. *Cell*, **92,** 351.

317. Hartl F.U. (1996) Molecular chaperones in cellular protein folding. *Nature*, **381,** 571.

318. Gething M.J. (1997) Protein folding. The difference with prokaryotes. *Nature*, **388,** 329.

319. Lee J., Hahn Y., Yun J.H., Mita K. & Chung J.H. (2000) Characterization of JDP genes, an evolutionarily conserved J domain-only protein family, from human and moths. *Biochim Biophys Acta*, **1491,** 355.

320. Ostrerova N., Petrucelli L., Farrer M., Mehta N., Choi P., Hardy J. & Wolozin B. (1999) alpha-Synuclein shares physical and functional homology with 14-3-3 proteins. *J Neurosci*, **19,** 5782.

321. Carmichael J., Chatellier J., Woolfson A., Milstein C., Fersht A.R. & Rubinsztein D.C. (2000) Bacterial and yeast chaperones reduce both aggregate formation and cell death in mammalian cell models of Huntington's disease. *Proc Natl Acad Sci U S A*, **97,** 9701.

322. Warrick J.M., Chan H.Y., Gray-Board G.L., Chai Y., Paulson H.L. & Bonini N.M. (1999) Suppression of polyglutamine-mediated neurodegeneration in Drosophila by the molecular chaperone HSP70. *Nat Genet*, **23,** 425.

323. Sittler A., Lurz R., Lueder G., Priller J., Lehrach H., Hayer-Hartl M.K., Hartl F.U. & Wanker E.E. (2001) Geldanamycin activates a heat shock response and inhibits huntingtin aggregation in a cell culture model of Huntington's disease. *Hum Mol Genet*, **10,** 1307.

324. Guarente L. (2000) Sir2 links chromatin silencing, metabolism, and aging. *Genes Dev*, **14,** 1021.

325. Gartenberg M.R. (2000) The Sir proteins of Saccharomyces cerevisiae: mediators of transcriptional silencing and much more. *Curr Opin Microbiol*, **3,** 132.

326. Gasser S.M. & Cockell M.M. (2001) The molecular biology of the SIR proteins. *Gene*, **279,** 1.

327. Kaeberlein M., McVey M. & Guarente L. (1999) The SIR2/3/4 complex and SIR2 alone promote longevity in Saccharomyces cerevisiae by two different mechanisms. *Genes Dev*, **13,** 2570.

328. Sinclair D.A. & Guarente L. (1997) Extrachromosomal rDNA circles--a cause of aging in yeast. *Cell*, **91,** 1033.

329. Tissenbaum H.A. & Guarente L. (2001) Increased dosage of a sir-2 gene extends lifespan in Caenorhabditis elegans. *Nature*, **410,** 227.

330. Vaziri H., Dessain S.K., Ng Eaton E., Imai S.I., Frye R.A., Pandita T.K., Guarente L. & Weinberg R.A. (2001) hSIR2(SIRT1) functions as an NAD-dependent p53 deacetylase. *Cell*, **107,** 149.

331. Luo J., Nikolaev A.Y., Imai S., Chen D., Su F., Shiloh A., Guarente L. & Gu W. (2001) Negative control of p53 by Sir2alpha promotes cell survival under stress. *Cell*, **107,** 137.

332. Bitterman K.J., Anderson R.M., Cohen H.Y., Latorre-Esteves M. & Sinclair D.A. (2002) Inhibition of silencing and accelerated aging by nicotinamide, a putative negative regulator of yeast sir2 and human SIRT1. *J Biol Chem*, **277,** 45099.

333. van Veldhoven P.P. & Mannaerts G.P. (1993) Sphingosine-phosphate lyase. *Adv Lipid Res*, **26,** 69.

334. Van Veldhoven P.P., Gijsbers S., Mannaerts G.P., Vermeesch J.R. & Brys V. (2000) Human sphingosine-1-phosphate lyase: cDNA cloning, functional expression studies and mapping to chromosome 10q22(1). *Biochim Biophys Acta*, **1487,** 128.

335. Brown D.A. & London E. (2000) Structure and function of sphingolipid- and cholesterol-rich membrane rafts. *J Biol Chem*, **275,** 17221.

336. Simons K. & Toomre D. (2000) Lipid rafts and signal transduction. *Nat Rev Mol Cell Biol*, **1,** 31.

337. Simons K. & Ehehalt R. (2002) Cholesterol, lipid rafts, and disease. *J Clin Invest*, **110,** 597.

338. Choo-Smith L.P. & Surewicz W.K. (1997) The interaction between Alzheimer amyloid beta(1-40) peptide and ganglioside GM1-containing membranes. *FEBS Lett*, **402,** 95.

339. Yanagisawa K., McLaurin J., Michikawa M., Chakrabartty A. & Ihara Y. (1997) Amyloid beta-protein (A beta) associated with lipid molecules: immunoreactivity distinct from that of soluble A beta. *FEBS Lett*, **420,** 43.

340. Yanagisawa K., Odaka A., Suzuki N. & Ihara Y. (1995) GM1 ganglioside-bound amyloid beta-protein (A beta): a possible form of preamyloid in Alzheimer's disease. *Nat Med*, **1,** 1062.

341. Kaiser C.A. & Schekman R. (1990) Distinct sets of SEC genes govern transport vesicle formation and fusion early in the secretory pathway. *Cell*, **61,** 723.

342. Pryer N.K., Salama N.R., Schekman R. & Kaiser C.A. (1993) Cytosolic Sec13p complex is required for vesicle formation from the endoplasmic reticulum in vitro. *J Cell Biol*, **120,** 865.

343. Salama N.R., Yeung T. & Schekman R.W. (1993) The Sec13p complex and reconstitution of vesicle budding from the ER with purified cytosolic proteins. *Embo J*, **12,** 4073.

344. Barlowe C., Orci L., Yeung T., Hosobuchi M., Hamamoto S., Salama N., Rexach M.F., Ravazzola M., Amherdt M. & Schekman R. (1994) COPII: a membrane coat formed by Sec proteins that drive vesicle budding from the endoplasmic reticulum. *Cell*, **77,** 895.

345. Barlowe C. (2000) Traffic COPs of the early secretory pathway. *Traffic*, **1,** 371.

346. Springer S. & Schekman R. (1998) Nucleation of COPII vesicular coat complex by endoplasmic reticulum to Golgi vesicle SNAREs. *Science*, **281,** 698.

347. Peng R., De Antoni A. & Gallwitz D. (2000) Evidence for overlapping and distinct functions in protein transport of coat protein Sec24p family members. *J Biol Chem*, **275,** 11521.

348. Kirchhausen T. (2000) Three ways to make a vesicle. *Nat Rev Mol Cell Biol*, **1,** 187.

349. Caricasole A., Copani A., Caraci F., Aronica E., Rozemuller A.J., Caruso A., Storto M., Gaviraghi G., Terstappen G.C. & Nicoletti F. (2004) Induction of Dickkopf-1, a negative modulator of the Wnt pathway, is associated with neuronal degeneration in Alzheimer's brain. *J Neurosci*, **24,** 6021.

350. Rawlings N.D. & Barrett A.J. (1995) Families of aspartic peptidases, and those of unknown catalytic mechanism. *Methods Enzymol*, **248,** 105.

351. Bjarnason J.B. & Fox J.W. (1995) Snake venom metalloendopeptidases: reprolysins. *Methods Enzymol*, **248,** 345.

352. Jia L.G., Shimokawa K., Bjarnason J.B. & Fox J.W. (1996) Snake venom metalloproteinases: structure, function and relationship to the ADAMs family of proteins. *Toxicon*, **34,** 1269.

353. Hite L.A., Jia L.G., Bjarnason J.B. & Fox J.W. (1994) cDNA sequences for four snake venom metalloproteinases: structure, classification, and their relationship to mammalian reproductive proteins. *Arch Biochem Biophys*, **308,** 182.

354. Paine M.J., Desmond H.P., Theakston R.D. & Crampton J.M. (1992) Purification, cloning, and molecular characterization of a high molecular weight hemorrhagic metalloprotease, jararhagin, from Bothrops jararaca venom. Insights into the disintegrin gene family. *J Biol Chem*, **267,** 22869.

355. Wolfsberg T.G. & White J.M. (1996) ADAMs in fertilization and development. *Dev Biol*, **180,** 389.

356. Almeida E.A., Huovila A.P., Sutherland A.E., Stephens L.E., Calarco P.G., Shaw L.M., Mercurio A.M., Sonnenberg A., Primakoff P., Myles D.G. & et al. (1995) Mouse egg integrin alpha 6 beta 1 functions as a sperm receptor. *Cell*, **81,** 1095.

357. Myles D.G. & Primakoff P. (1997) Why did the sperm cross the cumulus? To get to the oocyte. Functions of the sperm surface proteins PH-20 and fertilin in arriving at, and fusing with, the egg. *Biol Reprod*, **56,** 320.

358. Carroll D.J., Dikegoros E., Koppel D.E. & Cowan A.E. (1995) Surface expression of the pre-beta subunit of fertilin is regulated at a post-translational level in guinea pig spermatids. *Dev Biol*, **168,** 429.

359. Fambrough D., Pan D., Rubin G.M. & Goodman C.S. (1996) The cell surface metalloprotease/disintegrin Kuzbanian is required for axonal extension in Drosophila. *Proc Natl Acad Sci U S A*, **93,** 13233.

360. Rooke J., Pan D., Xu T. & Rubin G.M. (1996) KUZ, a conserved metalloprotease-disintegrin protein with two roles in Drosophila neurogenesis. *Science*, **273,** 1227.

361. Peschon J.J., Slack J.L., Reddy P., Stocking K.L., Sunnarborg S.W., Lee D.C., Russell W.E., Castner B.J., Johnson R.S., Fitzner J.N., Boyce R.W., Nelson N., Kozlosky C.J., Wolfson M.F., Rauch C.T., Cerretti D.P., Paxton

R.J., March C.J. & Black R.A. (1998) An essential role for ectodomain shedding in mammalian development. *Science*, **282,** 1281.

362. Qi H., Rand M.D., Wu X., Sestan N., Wang W., Rakic P., Xu T. & Artavanis-Tsakonas S. (1999) Processing of the notch ligand delta by the metalloprotease Kuzbanian. *Science*, **283,** 91.

363. Emi M., Katagiri T., Harada Y., Saito H., Inazawa J., Ito I., Kasumi F. & Nakamura Y. (1993) A novel metalloprotease/disintegrin-like gene at 17q21.3 is somatically rearranged in two primary breast cancers. *Nat Genet*, **5,** 151.

364. Kuno K., Kanada N., Nakashima E., Fujiki F., Ichimura F. & Matsushima K. (1997) Molecular cloning of a gene encoding a new type of metalloproteinase-disintegrin family protein with thrombospondin motifs as an inflammation associated gene. *J Biol Chem*, **272,** 556.

365. Yavari R., Adida C., Bray-Ward P., Brines M. & Xu T. (1998) Human metalloprotease-disintegrin Kuzbanian regulates sympathoadrenal cell fate in development and neoplasia. *Hum Mol Genet*, **7,** 1161.

366. Tortorella M.D., Burn T.C., Pratta M.A., Abbaszade I., Hollis J.M., Liu R., Rosenfeld S.A., Copeland R.A., Decicco C.P., Wynn R., Rockwell A., Yang F., Duke J.L., Solomon K., George H., Bruckner R., Nagase H., Itoh Y., Ellis D.M., Ross H., Wiswall B.H., Murphy K., Hillman M.C., Jr., Hollis G.F., Arner E.C. & et al. (1999) Purification and cloning of aggrecanase-1: a member of the ADAMTS family of proteins. *Science*, **284,** 1664.

367. Yagami-Hiromasa T., Sato T., Kurisaki T., Kamijo K., Nabeshima Y. & Fujisawa-Sehara A. (1995) A metalloprotease-disintegrin participating in myoblast fusion. *Nature*, **377,** 652.

368. Gilpin B.J., Loechel F., Mattei M.G., Engvall E., Albrechtsen R. & Wewer U.M. (1998) A novel, secreted form of human ADAM 12 (meltrin alpha) provokes myogenesis in vivo. *J Biol Chem*, **273,** 157.

369. Stocker W., Grams F., Baumann U., Reinemer P., Gomis-Ruth F.X., McKay D.B. & Bode W. (1995) The metzincins--topological and sequential relations between the astacins, adamalysins, serralysins, and matrixins (collagenases) define a superfamily of zinc-peptidases. *Protein Sci*, **4,** 823.

370. Blobel C.P., Wolfsberg T.G., Turck C.W., Myles D.G., Primakoff P. & White J.M. (1992) A potential fusion peptide and an integrin ligand domain in a protein active in sperm-egg fusion. *Nature*, **356,** 248.

371. White J.M. (1990) Viral and cellular membrane fusion proteins. *Annu Rev Physiol*, **52,** 675.

372. Eto K., Huet C., Tarui T., Kupriyanov S., Liu H.Z., Puzon-McLaughlin W., Zhang X.P., Sheppard D., Engvall E. & Takada Y. (2002) Functional classification of ADAMs based on a conserved motif for binding to integrin alpha 9beta 1: implications for sperm-egg binding and other cell interactions. *J Biol Chem*, **277,** 17804.

373. Eto K., Puzon-McLaughlin W., Sheppard D., Sehara-Fujisawa A., Zhang X.P. & Takada Y. (2000) RGD-independent binding of integrin alpha9beta1 to the ADAM-12 and -15 disintegrin domains mediates cell-cell interaction. *J Biol Chem*, **275,** 34922.

374. Iba K., Albrechtsen R., Gilpin B., Frohlich C., Loechel F., Zolkiewska A., Ishiguro K., Kojima T., Liu W., Langford J.K., Sanderson R.D., Brakebusch C., Fassler R. & Wewer U.M. (2000) The cysteine-rich domain of human ADAM 12 supports cell adhesion through syndecans and triggers signaling

events that lead to beta1 integrin-dependent cell spreading. *J Cell Biol*, **149,** 1143.

375. Iba K., Albrechtsen R., Gilpin B.J., Loechel F. & Wewer U.M. (1999) Cysteine-rich domain of human ADAM 12 (meltrin alpha) supports tumor cell adhesion. *Am J Pathol*, **154,** 1489.

376. Landolt-Marticorena C., Williams K.A., Deber C.M. & Reithmeier R.A. (1993) Non-random distribution of amino acids in the transmembrane segments of human type I single span membrane proteins. *J Mol Biol*, **229,** 602.

377. Mori S., Tanaka M., Nanba D., Nishiwaki E., Ishiguro H., Higashiyama S. & Matsuura N. (2003) PACSIN3 binds ADAM12/meltrin alpha and up-regulates ectodomain shedding of heparin-binding epidermal growth factor-like growth factor. *J Biol Chem*, **278,** 46029.

378. Loechel F., Gilpin B.J., Engvall E., Albrechtsen R. & Wewer U.M. (1998) Human ADAM 12 (meltrin alpha) is an active metalloprotease. *J Biol Chem*, **273,** 16993.

379. Loechel F., Overgaard M.T., Oxvig C., Albrechtsen R. & Wewer U.M. (1999) Regulation of human ADAM 12 protease by the prodomain. Evidence for a functional cysteine switch. *J Biol Chem*, **274,** 13427.

380. Nakayama K. (1997) Furin: a mammalian subtilisin/Kex2p-like endoprotease involved in processing of a wide variety of precursor proteins. *Biochem J*, **327 (Pt 3),** 625.

381. Abe E., Mocharla H., Yamate T., Taguchi Y. & Manolagas S.C. (1999) Meltrin-alpha, a fusion protein involved in multinucleated giant cell and osteoclast formation. *Calcif Tissue Int*, **64,** 508.

382. Borneman A., Kuschel R. & Fujisawa-Sehara A. (2000) Analysis for transcript expression of meltrin alpha in normal, regenerating, and denervated rat muscle. *J Muscle Res Cell Motil*, **21,** 475.

383. Galliano M.F., Huet C., Frygelius J., Polgren A., Wewer U.M. & Engvall E. (2000) Binding of ADAM12, a marker of skeletal muscle regeneration, to the muscle-specific actin-binding protein, alpha -actinin-2, is required for myoblast fusion. *J Biol Chem*, **275,** 13933.

384. Karkkainen I., Rybnikova E., Pelto-Huikko M. & Huovila A.P. (2000) Metalloprotease-disintegrin (ADAM) genes are widely and differentially expressed in the adult CNS. *Mol Cell Neurosci*, **15,** 547.

385. Cao Y., Zhao Z., Gruszczynska-Biegala J. & Zolkiewska A. (2003) Role of metalloprotease disintegrin ADAM12 in determination of quiescent reserve cells during myogenic differentiation in vitro. *Mol Cell Biol*, **23,** 6725.

386. Kronqvist P., Kawaguchi N., Albrechtsen R., Xu X., Schroder H.D., Moghadaszadeh B., Nielsen F.C., Frohlich C., Engvall E. & Wewer U.M. (2002) ADAM12 alleviates the skeletal muscle pathology in mdx dystrophic mice. *Am J Pathol*, **161,** 1535.

387. Kawaguchi N., Xu X., Tajima R., Kronqvist P., Sundberg C., Loechel F., Albrechtsen R. & Wewer U.M. (2002) ADAM 12 protease induces adipogenesis in transgenic mice. *Am J Pathol*, **160,** 1895.

388. Cornelius P., MacDougald O.A. & Lane M.D. (1994) Regulation of adipocyte development. *Annu Rev Nutr*, **14,** 99.

389. Gregoire F.M., Smas C.M. & Sul H.S. (1998) Understanding adipocyte differentiation. *Physiol Rev*, **78,** 783.

390. Kawaguchi N., Sundberg C., Kveiborg M., Moghadaszadeh B., Asmar M., Dietrich N., Thodeti C.K., Nielsen F.C., Moller P., Mercurio A.M., Albrechtsen R. & Wewer U.M. (2003) ADAM12 induces actin cytoskeleton and extracellular matrix reorganization during early adipocyte differentiation by regulating beta1 integrin function. *J Cell Sci*, **116,** 3893.

391. Asakura M., Kitakaze M., Takashima S., Liao Y., Ishikura F., Yoshinaka T., Ohmoto H., Node K., Yoshino K., Ishiguro H., Asanuma H., Sanada S., Matsumura Y., Takeda H., Beppu S., Tada M., Hori M. & Higashiyama S. (2002) Cardiac hypertrophy is inhibited by antagonism of ADAM12 processing of HB-EGF: metalloproteinase inhibitors as a new therapy. *Nat Med*, **8,** 35.

392. Higashiyama S., Lau K., Besner G.E., Abraham J.A. & Klagsbrun M. (1992) Structure of heparin-binding EGF-like growth factor. Multiple forms, primary structure, and glycosylation of the mature protein. *J Biol Chem*, **267,** 6205.

393. Matsumoto H., Nagasaka T., Hattori A., Rogi T., Tsuruoka N., Mizutani S. & Tsujimoto M. (2001) Expression of placental leucine aminopeptidase/oxytocinase in neuronal cells and its action on neuronal peptides. *Eur J Biochem*, **268,** 3259.

394. Rogi T., Tsujimoto M., Nakazato H., Mizutani S. & Tomoda Y. (1996) Human placental leucine aminopeptidase/oxytocinase. A new member of type II membrane-spanning zinc metallopeptidase family. *J Biol Chem*, **271,** 56.

395. Laustsen P.G., Rasmussen T.E., Petersen K., Pedraza-Diaz S., Moestrup S.K., Gliemann J., Sottrup-Jensen L. & Kristensen T. (1997) The complete amino acid sequence of human placental oxytocinase. *Biochim Biophys Acta*, **1352,** 1.

396. Ito N., Nomura S., Iwase A., Ito T., Kikkawa F., Tsujimoto M., Ishiura S. & Mizutani S. (2004) ADAMs, a disintegrin and metalloproteinases, mediate shedding of oxytocinase. *Biochem Biophys Res Commun*, **314,** 1008.

397. Shi Z., Xu W., Loechel F., Wewer U.M. & Murphy L.J. (2000) ADAM 12, a disintegrin metalloprotease, interacts with insulin-like growth factor-binding protein-3. *J Biol Chem*, **275,** 18574.

398. Ferry R.J., Jr., Katz L.E., Grimberg A., Cohen P. & Weinzimer S.A. (1999) Cellular actions of insulin-like growth factor binding proteins. *Horm Metab Res*, **31,** 192.

399. Rajkumar K., Modric T. & Murphy L.J. (1999) Impaired adipogenesis in insulin-like growth factor binding protein-1 transgenic mice. *J Endocrinol*, **162,** 457.

400. Modric T., Silha J.V., Shi Z., Gui Y., Suwanichkul A., Durham S.K., Powell D.R. & Murphy L.J. (2001) Phenotypic manifestations of insulin-like growth factor-binding protein-3 overexpression in transgenic mice. *Endocrinology*, **142,** 1958.

401. Laigaard J., Sorensen T., Frohlich C., Pedersen B.N., Christiansen M., Schiott K., Uldbjerg N., Albrechtsen R., Clausen H.V., Ottesen B. & Wewer U.M. (2003) ADAM12: a novel first-trimester maternal serum marker for Down syndrome. *Prenat Diagn*, **23,** 1086.

402. Asai M., Hattori C., Szabo B., Sasagawa N., Maruyama K., Tanuma S. & Ishiura S. (2003) Putative function of ADAM9, ADAM10, and ADAM17 as APP alpha-secretase. *Biochem Biophys Res Commun*, **301,** 231.

403. Fedorova L. & Fedorov A. (2003) Introns in gene evolution. *Genetica*, **118,** 123.

404. Duan J., Wainwright M.S., Comeron J.M., Saitou N., Sanders A.R., Gelernter J. & Gejman P.V. (2003) Synonymous mutations in the human dopamine receptor D2 (DRD2) affect mRNA stability and synthesis of the receptor. *Hum Mol Genet*, **12,** 205.

405. Bernstein H.G., Keilhoff G., Bukowska A., Ziegeler A., Funke S., Dobrowolny H., Kanakis D., Bogerts B. & Lendeckel U. (2004) ADAM (a disintegrin and metalloprotease) 12 is expressed in rat and human brain and localized to oligodendrocytes. *J Neurosci Res*, **75,** 353.

406. Nakagawa T., Sasahara M., Hayase Y., Haneda M., Yasuda H., Kikkawa R., Higashiyama S. & Hazama F. (1998) Neuronal and glial expression of heparin-binding EGF-like growth factor in central nervous system of prenatal and early-postnatal rat. *Brain Res Dev Brain Res*, **108,** 263.

407. Du Y. & Dreyfus C.F. (2002) Oligodendrocytes as providers of growth factors. *J Neurosci Res*, **68,** 647.

408. Kornblum H.I., Zurcher S.D., Werb Z., Derynck R. & Seroogy K.B. (1999) Multiple trophic actions of heparin-binding epidermal growth factor (HB-EGF) in the central nervous system. *Eur J Neurosci*, **11,** 3236.

409. Farkas L.M. & Krieglstein K. (2002) Heparin-binding epidermal growth factor-like growth factor (HB-EGF) regulates survival of midbrain dopaminergic neurons. *J Neural Transm*, **109,** 267.

410. Jin K., Mao X.O., Sun Y., Xie L., Jin L., Nishi E., Klagsbrun M. & Greenberg D.A. (2002) Heparin-binding epidermal growth factor-like growth factor: hypoxia-inducible expression in vitro and stimulation of neurogenesis in vitro and in vivo. *J Neurosci*, **22,** 5365.

411. Bartzokis G. (2004) Age-related myelin breakdown: a developmental model of cognitive decline and Alzheimer's disease. *Neurobiol Aging*, **25,** 5.

412. Grantham R. (1974) Amino acid difference formula to help explain protein evolution. *Science*, **185,** 862.

413. Li W.H., Wu C.I. & Luo C.C. (1984) Nonrandomness of point mutation as reflected in nucleotide substitutions in pseudogenes and its evolutionary implications. *J Mol Evol*, **21,** 58.